HIGH COMPRESSION RATIO TURBO GASOLINE ENGINE OPERATION USING ALCOHOL ENHANCEMENT

FINAL REPORT

U.S. DOE funded project DE-EE0005444

Massachusetts Institute of Technology
Sloan Automotive Laboratory
Cambridge, MA

Principal Investigator:	**Professor John B. Heywood**
Authors:	**Young Suk Jo, Raymond Lewis, Leslie Bromberg, John Heywood**
Project Duration:	**September 30, 2011 to October 1, 2015**

January 29, 2016

Executive Summary

Project Objectives

The overall objective of this project was to quantify the potential for improving the performance and efficiency of gasoline engine technology by use of alcohols to suppress knock. Knock-free operation is obtained by direct injection of a second "anti-knock" fuel such as ethanol, which suppresses knock when, with gasoline fuel, knock would occur. Suppressing knock enables increased turbocharging, engine downsizing, and use of higher compression ratios throughout the engine's operating map. This project combined engine testing and simulation to define knock onset conditions, with different mixtures of gasoline and alcohol, and with this information quantify the potential for improving the efficiency of turbocharged gasoline spark-ignition engines, and the on-vehicle fuel consumption reductions that could then be realized.

The more focused objectives of this project were therefore to:

- Determine engine efficiency with aggressive turbocharging and downsizing and high compression ratio (up to a compression ratio of 13.5:1) over the engine's operating range.
- Determine the knock limits of a turbocharged and downsized engine as a function of engine speed and load.
- Determine the amount of the knock-suppressing alcohol fuel consumed, through the use of various alcohol-gasoline and alcohol-water gasoline blends, for different driving cycles, relative to the gasoline consumed.
- Determine implications of using alcohol-boosted engines, with their higher efficiency operation, in both light-duty and medium-duty vehicle sectors.

Research Approach

This project was carried out by Professor John Heywood and his research team in the Sloan Automotive Laboratory at M.I.T. to explore the practicality of aggressively improving engine efficiency through use of alcohol-enhanced, boosted, high compression ratio engines, and determine the performance and fuel consumption potential of such knock-free gasoline engine

technology. We performed engine tests using various anti-knock fuel blends and used computational models to explore knock-free high-cylinder-pressure engine operation, and thus determine the alcohol fuel requirements over a wide range of engine conditions. The engine-in-vehicle simulation tool Autonomie was utilized to quantify the benefits of highly-boosted turbocharged, high compression ratio engines for light-duty and medium-duty vehicles in various driving cycles. This highly boosted, high compression ratio knock-free gasoline engine approach is realized by direct injection of alcohol (ethanol, methanol, alcohol-water mixtures) when knock with gasoline fuel would occur. Both an externally filled high-octane-fuel tank system, and an on-board fuel separation system fueled with a standard E10 gasoline blend are considered for practical realization of such dual-fuel engine operation.

The project (in Phase I) initially focused on experiments with the Sloan Automotive Labs' turbocharged direct-injection GM Ecotec gasoline engine test facility, carrying out engine tests to generate the experimental data needed to produce engine performance maps and knock onset contours with a range of knock-suppressing fuels. The computer simulation tools used for engine combustion analysis (GT-Power), and for knock-onset calculations (CHEMKIN), were used to interpret and expand the experimental database. These simulations were used to generate performance maps with knock onset limits for engine designs with higher compression ratios and boost levels. In Phase II of the program, we extended and refined these engine performance maps, so they could be used to generate engine-in-vehicle fuel economy results with the different knock-suppressing fuels (ethanol/gasoline or methanol/gasoline blends). A parallel higher-pressure engine-testing program at Cummins, with gasoline and gasoline-ethanol blends at compression ratio of 9.5 and 11.5, was carried out. A comparison of the two data sets showed similar performance of the knock suppressing fuels. In Phase III, the engine octane requirements from low to high-engine loads at various speeds were determined, primarily using PRF fuel blends. This allowed engine performance maps with octane requirement contours superposed to be generated. Additional engine-in-vehicle simulations were carried out to determine the average and distribution of the engine's fuel octane requirement over the standard U.S. driving cycles for both light-duty and medium-duty vehicle applications. A process-based model for an on-board fuel separation system was developed and used in engine-plus-separator vehicle simulations to quantify the fuel economy benefits of this approach. Finally, the fuel economy benefits and costs

of the two dual-fuel approaches examined here, that use the high octane rating of ethanol (or methanol) appropriately blended or mixed with gasoline to suppress knock, were assessed and compared. The two approaches are: (a) Use of two tanks (a larger one for gasoline and smaller one for the high alcohol content knock-suppressing fuel) filled separately, externally; and (b) Use of an on-board fuel separator system to split the single fuel put on board into higher and lower octane streams. Finally, the benefits of dual fuel system are quantified using an engine-in-vehicle simulation.

Project Findings

1. This work has helped develop a broader understanding of turbocharged gasoline-engine performance maps. These are significantly more complex than naturally-aspirated engine maps. The additional complexities include: wide-open-throttle definition; incorporation of maximum pressure constraints; fuel octane requirements and knock onset limits over the full performance map; effects of spark retard (negative impacts are less than in NA engines); the compression-ratio/boost/downsizing/reduced friction trade-offs. We have added to the available knowledge base in these areas.

2. The knock-suppressing potential of ethanol and methanol gasoline blends has been quantified, as has that of ethanol plus water. It is the combination of the chemical octane rating of the fuel plus the evaporative cooling impact of the fuel (that with direct injection is substantial) that is important.

3. Our work on knock-onset calculation methodology has identified the assumptions that have previously caused discrepancies between experiments and calculations. These have been resolved. This chemical-kinetic-based modeling methodology for predicting knock onset, coupled with use of pressure data from the fastest 10 or so percent of the engine's operating cycles, has been validated.

4. We have quantified the effects of higher compression ratios (13:1 is a sensible objective), and high boost, on turbocharged engine performance and efficiency of our "alcohol enhanced" knock-suppressed engine concept. Raising boost (to a BMEP of 3000 kPa) with engine

downsizing (while maintaining performance) has much greater impact than raising compression ratios above about 13:1.

5. The high-pressure operation, engine-testing program at Cummins, with gasoline and gasoline-ethanol blends at a compression ratio of 9.5 and 13.0, has been completed. Fuels used were gasoline, E30, E85, E100. This high-pressure larger-cylinder engine data was compared with MIT-generated data in terms of efficiency and knock onset. The trends are similar.

6. Our engine-in-vehicle simulations, with high compression ratio, high boost, and 50 percent downsizing, indicate that 25 to 30 percent (for urban and highway driving cycles) and 15 percent (for the more aggressive US06 cycle) miles per gallon increases—at essentially the same vehicle acceleration performance—using this ethanol knock-suppressed high compression ratio, high boost, turbocharged engine concept, relative to a current naturally-aspirated gasoline engine, in a standard passenger car, are realizable. Medium-duty truck simulations show comparable improvements, though these decrease as vehicle payload increases. These results relate to the two tank, dual fuel, with both tanks filled externally, approach.

7. Work by others (Exxon-Mobil, Corning, Toyota; and by Honda) has indicated the potential for on-board gasoline (E10) separation into a higher-octane stream (10-20% of the overall fuel volume, two-thirds of the ethanol) and lower octane stream, using membrane "pervaporation" technology. We developed a phenomenological model for such an on-board fuel separation system, and used it with our engine model for vehicle simulations. Engine tests were carried out to determine the engine's octane requirements at low, mid, and high loads, at several engine speeds. The vehicle fuel economy benefits with this on-board fuel separation approach (with standard E10 gasoline as the external-fill fuel) were closely comparable to the results obtained with the two-tank, two external-fill fuel approach. The operating parameter space available with on-board fuel separation is more flexible in that it can accommodate a range of driving needs and levels of aggressiveness.

8. Our cost estimates (additional to an equivalent standard turbocharged direct-injection gasoline engine vehicle) are: (a) For the two fuel tanks, each with external fill, approach, $40-45; (b) On-board fuel separation (with two fuel/tanks, for the separated higher and lower octane fuel streams), $80-85.

9. Overall, we conclude that using the high octane quality of ethanol more effectively in either of these two ways (two tanks both with external fill; on-board fuel separator with two tanks, standard E10 gasoline fill) offers a 15-30 percent improvement in vehicle mpg (in both light and medium-duty applications) relative to naturally-aspirated engine vehicles, and about half that, 7-15 percent improvement, relative to gasoline turbocharged DI engines. These are significant benefits and the application of this technology should be further explored.

A more detailed summary of our technical findings is presented in the Summary and Conclusions section of the report, and the three attached SAE technical papers we have authored at the end of this report.

Contents

1. Introduction

Internal combustion engines with Otto cycles have been developed for over 150 years, and the efficiencies have increased from less than 5% to above 30% (depending on the engine type, adopted technologies, operating conditions, and fuels used). However, increasing the efficiency of the engines is still an important task for the automotive industry due to increasing energy consumption and environmental problems worldwide.

According to the United States' Department of Transportation, about 28% of total U.S. energy in is consumed in the transportation sector, and among the transportation sector, about 62% of energy is consumed by light-duty vehicles as shown in the Figure 1-1 [1, 2]. Since spark ignition (SI) engines comprise over 90% of the light duty vehicles sold in the United States, about 16% of the U.S. energy is consumed by light duty vehicles equipped with SI engine. Therefore increasing SI engine efficiency is crucial in reducing the U.S. energy consumption and greenhouse gas emissions [3].

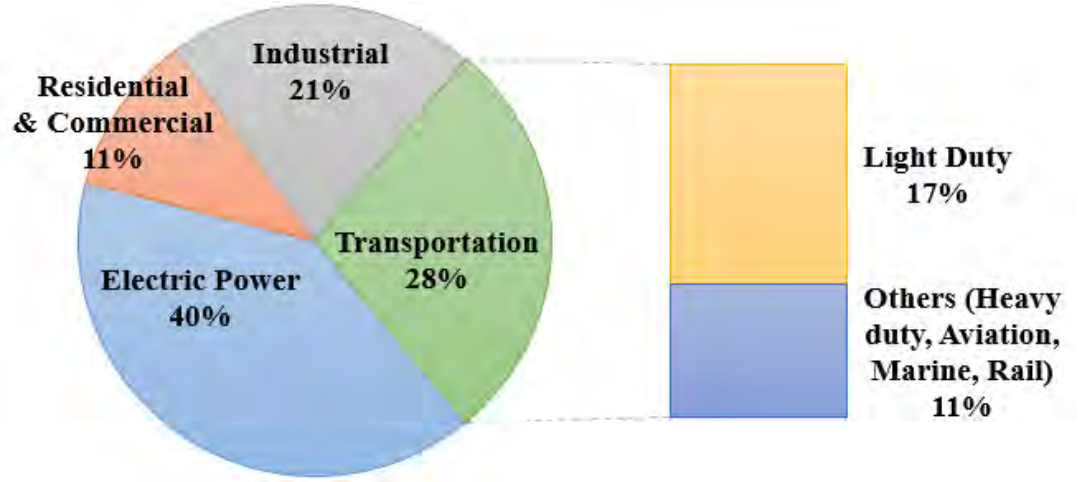

Figure 1-1: U.S. energy consumption by sector in 2014. Transportation sector is divided to show the portion of the energy consumed by Light duty vehicles

1.1 Motivation

The Environmental Protection Agency (EPA) has set an average fuel economy target for passenger cars and light duty trucks (fleet-wide) to be achieved by 2025: 54.5 miles per gallon

(MPG), equivalent to 163 g/mi of CO2 emission levels [4]. Since SI engines comprise large portion of the light duty vehicles sold in the United States (more than 90%), automakers are focusing on increasing the SI engine efficiencies [3]. Widely adopted methods for increasing the SI engine efficiency considered in this research are downsizing, turbocharging, and increasing the compression ratio. As shown in Figure 1-2, turbo-downsizing, in particular, is showing a significant increase in market share among passenger cars; the production share of gasoline turbocharged passenger vehicles has increased from 3% in 2010 to 16% in 2014 [5]. Along with turbo-downsizing, Gasoline Direct Injection (GDI) technologies are widely adopted as well due to its charge cooling effects and improved efficiencies at low load operations.

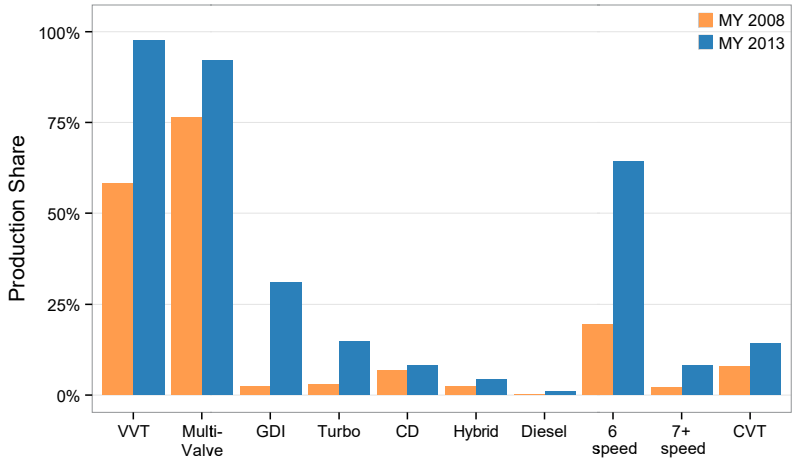

Figure 1-2: Engine technology profiles and their production shares. GDI and Turbocharger show a significant growth in the production share from Model Year (MY) 2008. Acronyms are variable valve timing (VVT), cylinder deactivation (CD), continuously variable transmission (CVT).

Much research has been done on the effect of downsizing on engine efficiency. Turbo-downsizing increases the average engine brake efficiency by shifting the engines' operating regions to where parasitic losses (such as pumping, friction, and heat transfer) are relatively low [6, 7, 8]. Smith and Cheng at MIT have utilized a cycle simulation model and concluded that part-load pumping, friction, and heat transfer losses decreased about 25%, 10%, and 4% respectively with reduction of the cylinder displaced volume by 100cc [9]. The current authors' previous work has found that the engine brake efficiency increases to 33% by increasing the engine load up to just half of the maximum torque in a turbocharged engine [10]. Figure 1-3 shows a substantial decrease in brake specific fuel consumption with increasing load on the engine map; above 500 g/kWh to around 300 g/kWh by changing load from 3 bar brake mean

effective pressure (BMEP) to 10 bar BMEP. This steep decrease in fuel consumption at part-load allows downsizing to reduce fuel consumption significantly.

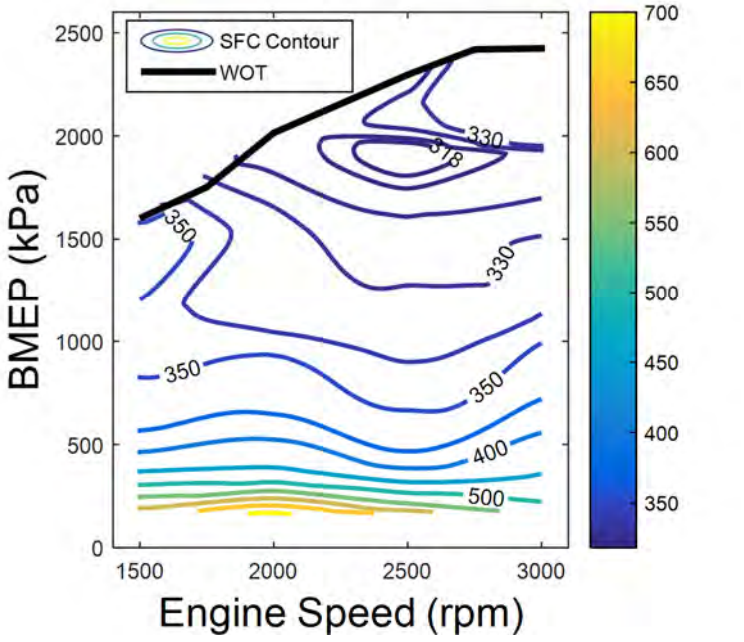

Figure 1-3: Brake specific fuel consumption contour (g/kWh) overlaid on the performance map of the test engine using E85 fuel.

It is also well known that increasing the compression ratio increases engine efficiency. Even though the compression work increases with increased compression ratio, the expansion work increase is much higher, which gives a net benefit in the work output [6]. Considering the ideal gas constant-volume combustion cycle, the gross indicated efficiency of the engine is related to the compression ratio by the equation below.

$$\eta_{f,ig} = 1 - \frac{1}{r_c^{\gamma-1}}$$

where $\eta_{f,ig}$, r_c, γ represent the indicated gross fuel conversion efficiency, compression ratio, and the specific heat ratio, respectively [6]. Based on this model explaining the fundamental relationship between compression ratio and efficiency, many researchers have done engine experiments or simulations to understand the effect of increasing compression ratio on engine efficiency. Gerty and Heywood at MIT estimated the efficiency gain with increased compression ratio by a cycle-simulation [11]. For a naturally aspirated (NA) engine, efficiency increased about 5% by increasing a compression ratio from 10 to 13 as shown in Figure 1-3.

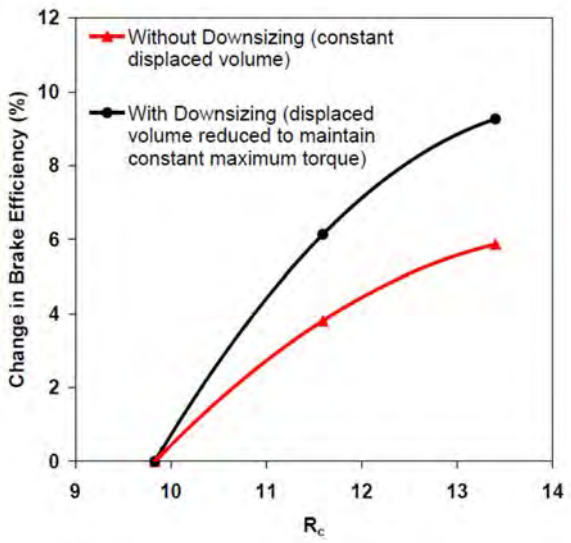

Figure 1-4: Efficiency gain with compression ratio change [11]

Recent studies conducted at MIT by Smith, Heywood, and Cheng carefully analyzed data sets generated by other researchers along with their own results and quantified the incremental efficiency gain with increasing compression ratio: on average, efficiency increased by about 5% by increasing a compression ratio from 10:1 to 14:1 with a diminishing return beyond that [7]. Stein, House, and Leone and others from Ford Motor Company have constructed a graph showing efficiency change with increasing compression ratio for different baseline compression ratios [12].

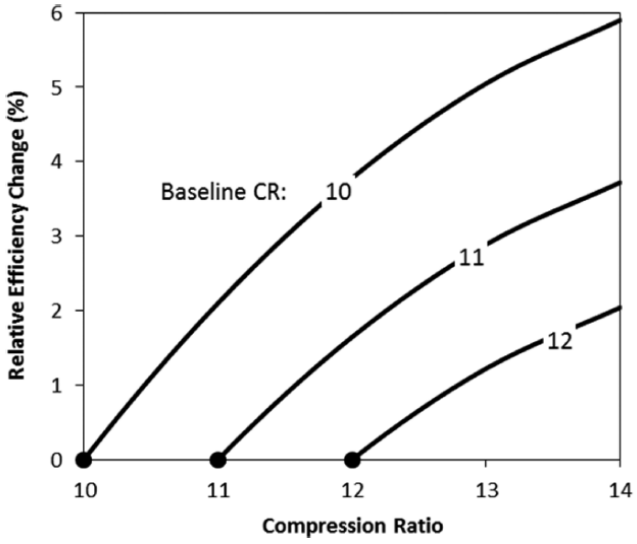

Figure 1-5: Relative efficiency change from increased compression ratio for three baseline compression ratios. A graph constructed by Leone, et al using data reported in Smith, et al [7, 12].

Previous research show the benefits of turbo-downsizing and increasing a compression ratio. Depending on the types of the technologies applied, modern spark engines' compression ratios range from about 9:1 to 13:1 [13, 14]. However, turbo-downsizing and increasing compression ratio result in higher in-cylinder pressures and temperatures, which increase the likelihood of engine knock. DI engines tend to have higher compression ratios than PFI engines, and TC engines adopt lower compression ratios than NA engines; both due to knocking.

Knock is an abnormal combustion phenomenon which is caused by an autoignition of a local region of the end gas in the SI engine. Strong pressure waves are caused by a sharp increase in local pressure and temperature generated by a spontaneous release of chemical energy [6]. Severe knock can destroy the engine hardware, so modern engines are equipped with knock sensors which automatically retard the spark timing to avoid knock. However, spark retard decreases efficiencies of the engine, as the engine no longer operates at the optimal spark timing [15]. Also, a previous paper by the current authors has shown that the efficiency reduction with spark retard is especially larger at highly boosted engine loads due to turbocharger feedback effects on intake manifold air pressure (MAP) [10]. Even with knock sensors, the potential of turbo-downsizing and increasing the compression ratio are limited by knock. This research explores ways to suppress knock without compromising efficiency by much.

1.2 Background and Previous Work

Probability of occurrence and severity of knock are both functions of fuel characteristics and the engine's operating conditions. If a fuel tends to auto-ignite faster than other fuels at a constant pressure and temperature, the fuel tends to knock more frequently and severely than other fuels. As engine runs in lower speeds and higher loads (higher in-cylinder temperatures and pressures), it tends to knock more and severe for a given fuel. Therefore, knock can be avoided by two methods: changing engine's operating conditions or by using fuels with high knock resistance.

Engine Knock

In a spark ignition engine, fuel-air mixtures are combusted by a spark generated by a spark plug on the top of the cylinder head. In a normal combustion scenario, the flame front generated from the spark plug propagates throughout the combustion chamber. However, in case of high

pressure and temperature, auto-ignition occurs in front of the flame front. This phenomenon is called engine knock as mentioned in a previous section, which might cause a serious damage to the engine hardware block. Therefore, it is important to suppress knock to avoid possible engine failure. Figure 1-6 illustrates the difference between normal combustion and knocking cases. For the knocking case shown on the right in Figure 1-6, auto-ignition occurs in front of the flame generated by a spark.

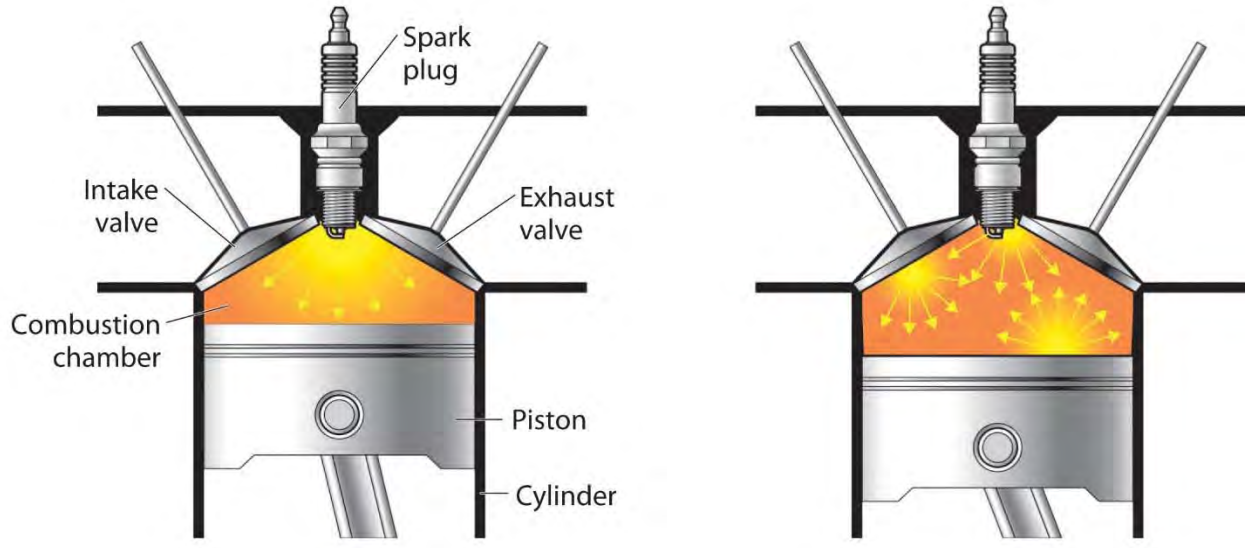

Figure 1-6: Normal combustion (left) and knocking (right). A spark generated flame propagates through the combustion chamber for normal combustion while high in-cylinder pressure and temperature leading to an auto-ignition of fuel-air mixture in the knocking case [16].

Avoiding knock is possible both by changing the operating conditions and by using high octane fuels. Spark retard and exhaust gas recirculation (EGR) are the most common ways to avoid knock by decreasing temperature or pressure levels inside the cylinder. However, both strategies require some compromising, such as engine efficiency or performance in return of reduced chances of knock. A straightforward but expensive way to reduce knock is to use high octane fuels. Fuel's anti-knock property is quantified by a number called octane rating.

Octane Rating: Anti-knock Measure

Octane rating (or octane index) is a number rating that quantifies a certain fuels' resistance to knock. The higher the number, the better the fuel resists knock. It is determined by two standard test methods, RON (Research Octane Number) and MON (Motor Octane Number) tests. Both tests are done using a single cylinder CFR (Cooperative Fuel Research) engine with continuously

variable compression ratios. The RON test is done at the engine speed of 600 rpm with 52 ºC intake air temperature, and the MON test is done at the engine speed of 900 rpm with an intake mixture temperature of 149 ºC. Due to this difference, RON correlates better with low-speed, and mild-knocking conditions while MON correlates best with high-speed and high-temperature knocking conditions.

RON and MON of a given fuel are determined by running the fuel in a CFR engine with specified test procedures from American Society for Testing and Materials (ASTM) method D2699/D2700. [17, 18] The octane number is then determined by comparing results with those of pure Primary Reference Fuel (PRF) blends (isooctane and n-heptane blends). If the fuel shows same knocking characteristics with 80 % isooctane and 20% n-heptane using RON test conditions, then the fuel's RON is 80 (same for MON test). Most real world fuels have different RON and MON values. Generally, most fuels have a lower value for MON than RON. The difference between RON and MON is called as a sensitivity of a fuel, i.e., S = RON-MON

Depending on the weighting method with two tests, octane index of a fuel can be determined. Anti-knock index (AKI) is the most common number seen in U.S. gas stations where octane number is determined by taking an average of RON and MON test number. Then, octane index (OI) can be defined as below.

$$OI = RON - K * S$$

where S is sensitivity and K is a K value. AKI is when octane index is calculated with K = 0.5.

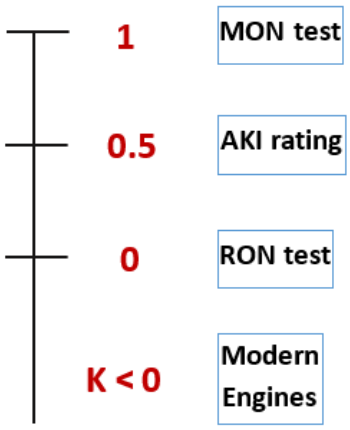

Figure 1-7: Linear weighting of RON and MON using K values. K = 1, 0.5, and 0 each indicates MON test, AKI rating, and RON test.

It has been found that K value is becoming less than 0.5 or even negative, as shown in Figure 1-7, meaning that MON test is becoming outdated for modern engines [19, 20, 21]. It has been also found that sensitive fuels show better anti-knock characteristics, but it is out of scope of this research as some fuels tested were sensitive while other fuels weren't. Only RON will be used in this research to describe the anti-knock capability of fuels for consistency.

Ethanol Fuel

An effective way to avoid knock without compromising efficiency of the engine is to use a high octane fuel such as E85. Ethanol has a much higher chemical or inherent octane number than gasoline (RON of 107 compared to 91-99 for gasoline). Also, ethanol has a better knock suppression characteristics than gasoline due to its evaporative cooling effect when injected directly into the cylinder [22]. Kasseris and Heywood at MIT quantified that gasoline and E85 each increase the effective octane number of a given fuel by 5 and 18 by charge cooling effects with direct injection (DI) [23]. Effective octane number with increasing volumetric ethanol contents are shown in Figure 1-8.

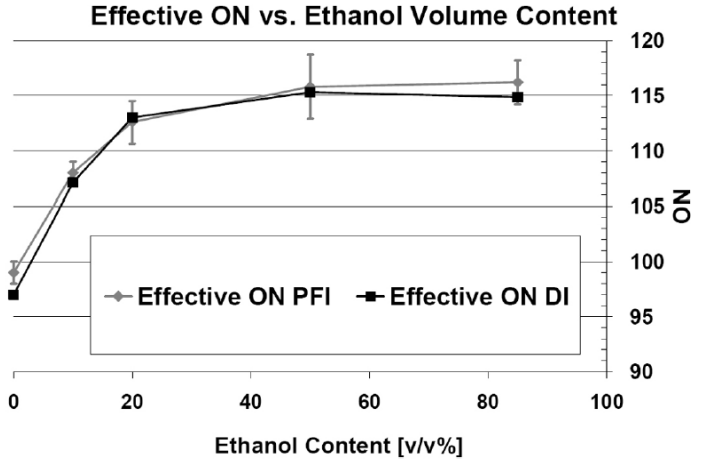

Figure 1-8: An effective octane number vs volumetric ethanol content.

There are already production vehicles which can take E85 as a fuel. Flex fuel vehicles, vehicles that can run on any mixtures of gasoline and ethanol up to 85% of ethanol, are already common in Brazil (about 88% of light duty vehicles) and are available in the United States as well [24]. However, the fuel efficiency of these vehicles is not much better than vehicles that run with a conventional gasoline. Their need to operate on gasoline as well as E85 limits their

potential to fully utilize E85's high octane rating. (Note that the energy content of E85 is about two-thirds that of gasoline, affecting the fuel economy measures, which is miles per gallon) [25]. Also, high octane fuel is not required in much of the engine performance map where knock is not a problem. Another issue with high ethanol content fuel is an on-going discussions about ethanol's output-to-input energy ratio and the land usage changes caused by corn production for fuel [26, 27, 28]. Therefore, even with the impacts of positive potential of using ethanol on a large scale, the use of ethanol in a vehicle has to be optimized due to limited supply and low energy content.

Octane On Demand

One way of optimizing the ethanol usage is by implementing an Octane on Demand (OOD) system. OOD is a way of providing the appropriate octane fuel to the engine when the engine requires it. One approach is a dual fuel injection where sufficiently high octane fuel (e.g., E85) is injected from a separate tank only when the regular gasoline is knock limited. Many studies were conducted with various engine configurations, injection strategies, and different fuels. Considering an emerging infrastructure for E85 fuel, currently the most practical approach would be a combination of regular gasoline and E85. E85 has an inherently high chemical octane number, and its evaporative cooling effects enhance knock suppression capability when used with the direct injection [29, 30]. Bromberg, Cohn and Heywood at MIT first suggested an approach of using E85 and gasoline to benefit from outstanding knock suppression characteristics of ethanol while optimizing the use [31, 32, 33]. Stein, House, and Leone from Ford Motor Company have found that the dual fuel approach using E85 and a regular gasoline allows more engine downsizing, higher compression ratio, and engine down-speeding, which make the SI engine significantly more efficient in normal driving. Also, they found that the ethanol replaces more gallons of gasoline by making the engine operate in a more efficient region with increased knock suppression capacity [25]. However, the dual fuel application requires the ethanol tank to be refilled regularly (but not as frequently as the gasoline tank).

To resolve the refilling issue, on board fuel separation (OBS) system has been suggested. OBS is a thermally driven system that separates conventional gasolines (with 10% ethanol content in more than 96% of gasolines in U.S [34]) into higher and lower octane streams. Partridge, Weissman, Ueda, et al from Exxon, Toyota, and Corning have developed a membrane

separation system. They estimated about an 8% increase in the fuel economy with OBS system installed. This increase comes from higher compression ratio (13:1) and knock suppression synergy of gasoline-ethanol blends with DI [35]. Figure 1-9 below shows the effect of OBS system on the fuel economy. Net fuel economy gain was calculated by combining benefits of higher compression ratio/downsizing and fuel economy penalty of fuel pump and injector power consumption. Exxon's study claims that only about 20% of normal driving requires high octane fuel, and about 2-4 liter tank for high RON stream would be sufficient. They also emphasized that the technology has a great potential when used with DI technology due to knock suppression synergy. Another important potential is reduced startup emissions with the higher volatility low RON fuels produced by OBS system (35% decrease in nonmethane hydrocarbon (NMHC) on startup).

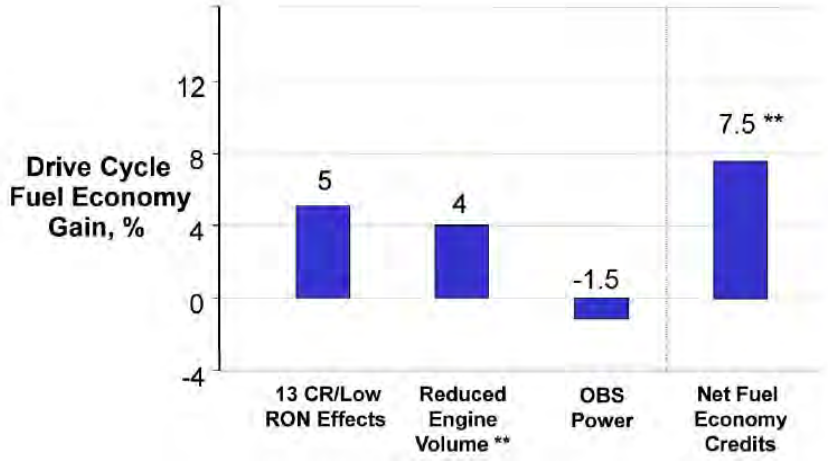

Figure 1-9: OBS fuel economy credits in Japan 10.15 mode (Figure Copyright to [35]).

A recent study done by Kuzuoka, Kurotani, Chishima, et al from Honda estimated about a 27% gain in the fuel economy using their OBS system, which comes from both downsizing and higher compression ratio [36]. They used DI for gasoline and port fuel injection (PFI) for ethanol to benefit from charge cooling effects of DI gasoline for a large fraction of the driving cycle. Three different engine map configurations with different spark retard strategies and transmission control were compared to see the effect on fuel economy and fraction of ethanol consumed. The results are shown in Figure 1-10 below.

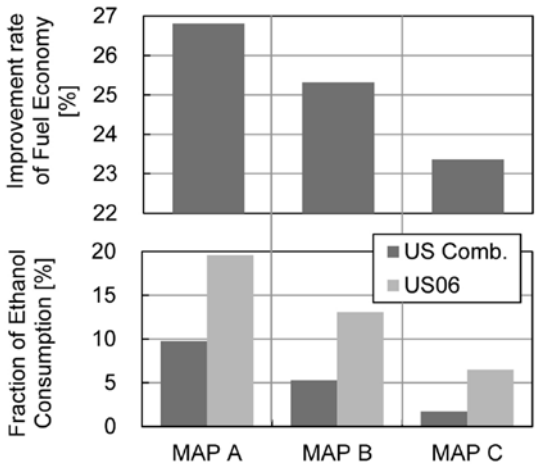

Figure 1-10: Improvement rates of fuel economy and ethanol consumption with different engine calibration strategies (Figure Copyright to [36]).

For the application of the OOD system, understanding the octane requirement of the engine itself and the driving patterns are important. Both Exxon et al. and Honda have developed an octane requirement map of their own. Chang, Viollet, Alzubail, et al. from Saudi Aramco have constructed an octane requirement map using a single cylinder engine with fuel blends as low as 61 RON [37]. They also carried out vehicle simulations to estimate the octane requirements of the single cylinder engine in the standard U.S. driving cycles. Even though there are rising interests in OOD applications, there is still a lot of engine experiments and vehicle simulation work to be conducted for deeper understanding of the implications of such systems on vehicle.

2. Research Objective and Methodology

The main objective of my research is to understand combustion phenomenon, knock limits, and octane requirements of a turbocharged spark ignition engine, and to evaluate the impacts of those variables on the engine efficiency and vehicle fuel economy. Engine experiments of different fuel blends and engine-in-vehicle simulation tool were utilized to achieve the analyses. This chapter will focus on the detailed objectives of experiments and simulation, research methodologies, and experimental and simulation apparatus adopted.

2.1 Research Objective

For an effective use of fuel octane in a turbocharged gasoline engine, the octane requirement has to be defined thoroughly. The octane requirement can be a requirement of an engine itself at various operating conditions, or the requirement of a vehicle at various driving conditions. Here, the octane requirement is first defined as the lowest RON of the fuel that is required to run the engine at a given operating point without knock. To quantify octane requirement, knock limits of a test engine has been determined by testing various fuels with a wide range of RON. By utilizing a large amount of fuel combustion data over a wide range of engine speed and load, the combustion, cycle-by-cycle variation, and knocking characteristics of different fuel blends were analyzed. Then, this information was adopted in an engine-in-vehicle simulation to estimate the octane requirements of vehicles in driving cycles. Finally, OOD systems were compared by system modelling and benefits assessment. Below are the list of questions to be answered throughout this research.

<u>What are the combustion characteristics of a turbocharged SI engine?</u>

- How does the efficiency change with engine speed, load, and combustion phasing with piston motion?
- How does the coefficient of variation (CoV) of NIMEP change with engine operating conditions and fuels?

<u>What is the octane requirement of an engine?</u>

- How can the octane requirement of a TC SI engine be defined?
- How can the fuel octane be optimized?

What is the octane requirement of a vehicle?

- What are the effects of engine configuration (turbocharging, downsizing, increased compression ratios) and engine operating conditions on the octane requirement?
- What are the effects of vehicle configurations (vehicle type and weight) and driving cycles on the octane requirement?
- What is the effect of optimal use of fuel octane on the engine efficiency?

How do different OOD scenarios compare?

- How does actual fuel consumption change with different engines and vehicle configurations?
- How does fuel separation rate change with system operating parameters?
- What is the effect of optimal use of fuel octane on vehicle fuel economy?
- What are the advantages and disadvantages of each system?

Research objectives were established to find answers to the above questions. Below are the list of research objectives.

1. Analyze combustion characteristics of a TC SI engine: Find effects of engine operating parameters on the engine efficiency and analyze cycle-by-cycle variations of SI engine combustion.

2. Understand the octane requirement of a TC SI engine: Define the octane requirement of a TC SI engine over a wide range of operating range.

3. Quantify the octane requirement of various driving cycles: Analyze the effect of engine configuration, driving cycle characteristics, and vehicle configuration on the octane requirement, and calculate the benefits of octane utilization on the engine efficiency and fuel economy.

4. Assess benefits of OOD system: Compare TC and NA, different compression ratios, spark retard strategies, fueling strategies (two tank/ OBS) in terms of engine efficiency and fuel economy benefits.

2.2 Research Methodology

Engine experiments, GT-power simulation, drive cycle simulation, and system level modelling were done together to achieve the research goals listed in a previous section. To define the octane requirements of a turbocharged spark ignition engine, engine experiments were conducted using fuel blends with research octane number ranging from 0 to 102. Combustion characteristics of various fuels were analyzed using pressure data collected in a wide range of engine operating variables (engine speed, load, and combustion phasing). For a given RON fuel, knock limits were defined at a range of engine speeds and loads. Based on knock limits determined by testing different fuel blends, an octane requirement map was constructed. Then drive cycle simulations were conducted to obtain the operating points on the octane requirement map. Based on the operating points calculated from the driving cycle simulation, octane requirements and ethanol consumption of over the drive cycles were calculated, for different driving cycles. The schematic diagram of a methodology is shown in Figure 2-1 below.

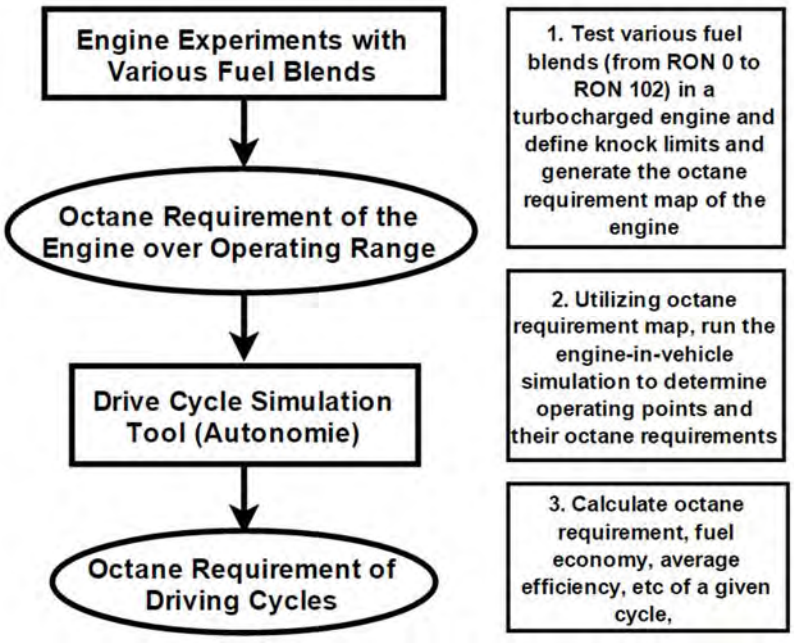

Figure 2-1: Schematics explaining how engine experiments and engine-in-vehicle simulation were utilized to get the octane requirements of the engine over its operating range, and those of the driving cycles.

Engine and Fuels Experiments

The engine experiments were conducted to superimpose knock limits of various fuel blends on the performance map efficiency contours. First, brake efficiencies of the engine were measured using E85 (85% ethanol and 15% 91 RON gasoline) fuel so that the efficiencies could be measured always at maximum brake torque timing without knocking. It has been determined that the efficiency is not dependent on the fuel, as long as it is at MBT timing. Then, knock limits of the various fuel blends were tested.

Gasoline-ethanol fuel blends were utilized to get octane requirements at the higher loads on the performance map. Octane ratings of the fuel blends were determined based on the fuel octane number tests conducted by Anderson, Leone, et al [38, 39]. The research grade gasoline with 91 RON from Gage Products was utilized as the base gasoline for gasoline-ethanol blends. This was done so that 10% ethanol added to the base gasoline would result in 96 RON fuel, which has a similar octane rating to the recommended fuel of the engine [40]. Then, PRF blends were tested to analyze the octane requirements in the lower load parts of the performance map. Even though modern gasolines have a sensitivity of 8-10, research grade gasoline with a very low octane is not available. Therefore, isooctane and n-heptane fuel blends were prepared to obtain a complete fuel octane test range from 0 RON to 100 RON. The exact test matrix for engine experiments will be given in a later section.

Vehicle and GT-Power Simulation

Displaced volume change with turbo-downsizing, spark retard strategies, compression ratio increase, and vehicle types are interesting variables for analyzing performance of dual fuel applications. However, the effects of those variables on engine efficiency, drive cycle fuel economy, and ethanol consumption in dual fuel applications are not well quantified. Also, it is not easy to do a complete parametric studies as changing engine geometries (compression ratio, displacement volume) and loading them on a vehicle for dynamometer tests take tremendous amounts of time and other resources. Still, it is important to estimate the ethanol consumption in many different scenarios before actually producing engines for dual fuel applications.

Ethanol consumption in dual fuel applications is a function of many variables: engine speed and load, driving aggressiveness, acceleration, spark retard, boost level, compression ratio, etc. However, the actual quantification of the ethanol requirement in a dual fuel applications for different engine configurations has not been done yet. Engines with various downsizing/boost levels, spark retard strategies, and compression ratios and vehicle type were generated using engine experiments and GT-Power simulation in order to simulate the performance of the engine beyond the limits of our engine experimental setup. After benchmarking the model to the experimental results, it was possible to generate performance maps of the engine for different boost levels, compression ratios, and spark retard strategies. To keep the engine's performance in a vehicle constant, turbocharger's boost levels were chosen so that the corresponding engine displacement volumes would result in the same maximum torque output (230 Nm, which is the maximum torque of Camry's base engine model). By comparing the brake fuel conversion efficiency estimated from GT-Power to that from engine experiments, it was possible to confirm the fidelity of the engine model [10] Maximum torque is only one of the requirements, as other issues are also important to assure similar "drivability". However, maximum torque is a rough guide useful in the tradeoff studies in this work.

Then those engines are loaded on the engine-in-vehicle simulation tool Autonomie to estimate the average engine efficiency, fuel economy, and ethanol consumption for the standard U.S. driving cycles. Vehicle models, boost levels (downsizing levels), and spark retard strategies were changed to analyze the effects of these variables on the octane requirement of a vehicle. By changing 5 variables (4 downsized engine volumes, 3 compression ratios, 3 spark retard scenarios, 3 driving cycles, and 2 vehicle types), total of 216 cases were compared. The exact test matrix for vehicle simulation will be given in a later section.

2.2 Research Tools

In this section, engine used for the experiments, experimental system setups, and driving cycle simulation tool will be introduced.

Test Engine

A General Motors Ecotec Generation II engine, or Ecotec LNF, was used to acquire experimental data. This four cylinder (2L engine displaced volume), turbocharged (twin turbo), direct injected engine was first sold in 2007. A picture of the engine is shown in Figure 2-2 below.

Figure 2-2: A General Motors Ecotec Generation II engine (Ecotec LNF)

Dual independent cam phasing is operated by Engine Control Unit (ECU) based on the calibration map designed for maximum fuel conversion efficiency. The engine geometries listed in Table 2-1 are similar to those of recent versions of LNF (LTG) except that compression ratio was raised to 9.5:1. LNF engine tested is representative of an entire class of four cylinder turbocharged engines as geometries of turbocharged engines in the same class are not significantly different from those of the LNF engine used for the experiments.

Table 2-1: Engine Specifications

Displaced Volume	1998 cc
Cylinders	In-line 4 Cylinders
Stroke	86 mm
Bore	86 mm
Connecting Rod	145.5 mm
Compression Ratio	9.2 : 1
Maximum Torque	353 Nm (2500 rpm ~)
Maximum Power	194 kW (at 5300 rpm)

Turbocharger	Twin-scroll
Fuel Injection & Ignition	Direct Injected Spark
Valve Timing	Dual Independent Cam Phasing

Experimental System

Intake air, fuel injection, exhaust, and cooling systems were designed to help the engine experiments run reliably and repeatable as shown in Figure 2-3. Detailed configurations of the surrounding systems will be discussed in this section.

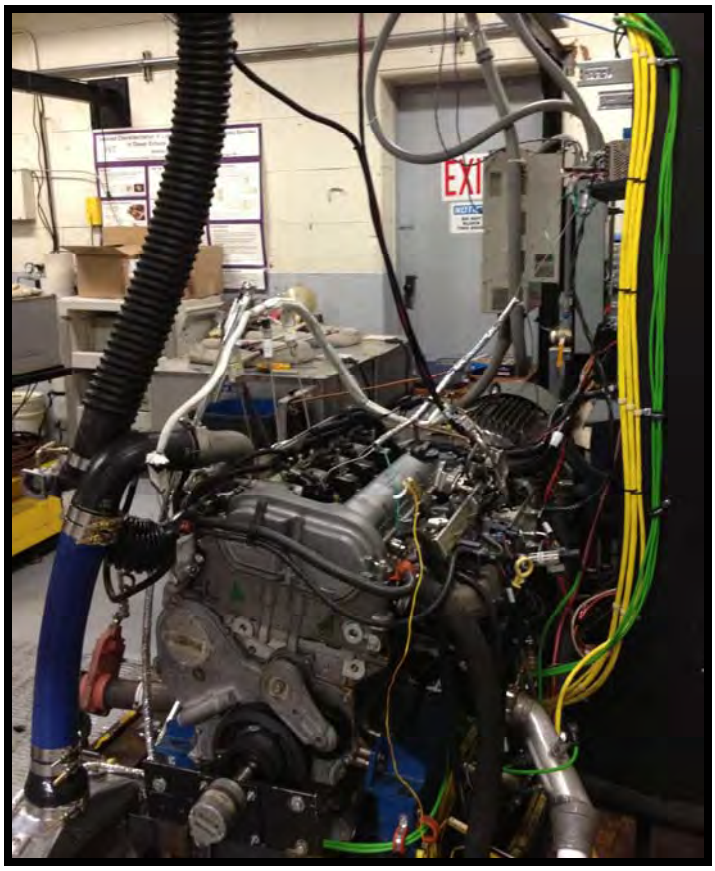

Figure 2-3: A picture of the actual experimental system. The engine and surrounding systems (intake, exhaust, turbocharging, intercooler, data acquisition) are shown in the picture.

Intake air system

Through a conical air filter, fresh air enters the engine passing through a turbine air flow meter (IMAC Systems Quantometer SZ-250) and a 41.6 L damping tank. Then, the air passes through a hot-film mass air-flow meter and into the compressor of the turbocharging unit. Then, the air is cooled by a water-to-air intercooler, which is connected to the city water supply. The flow rate of

the city water supply was adjusted by a system of vales so dyno system gets enough water supply. Then, cooled air is reheated by a process air heater (Sylvania SureHeat 074728 10kW). The air temperature is maintained at 30 ºC throughout the experiments by a PID controller integrated in the heating system. The actual pictures of the intake system components and locations of the sensors are shown in Figure 2-4.

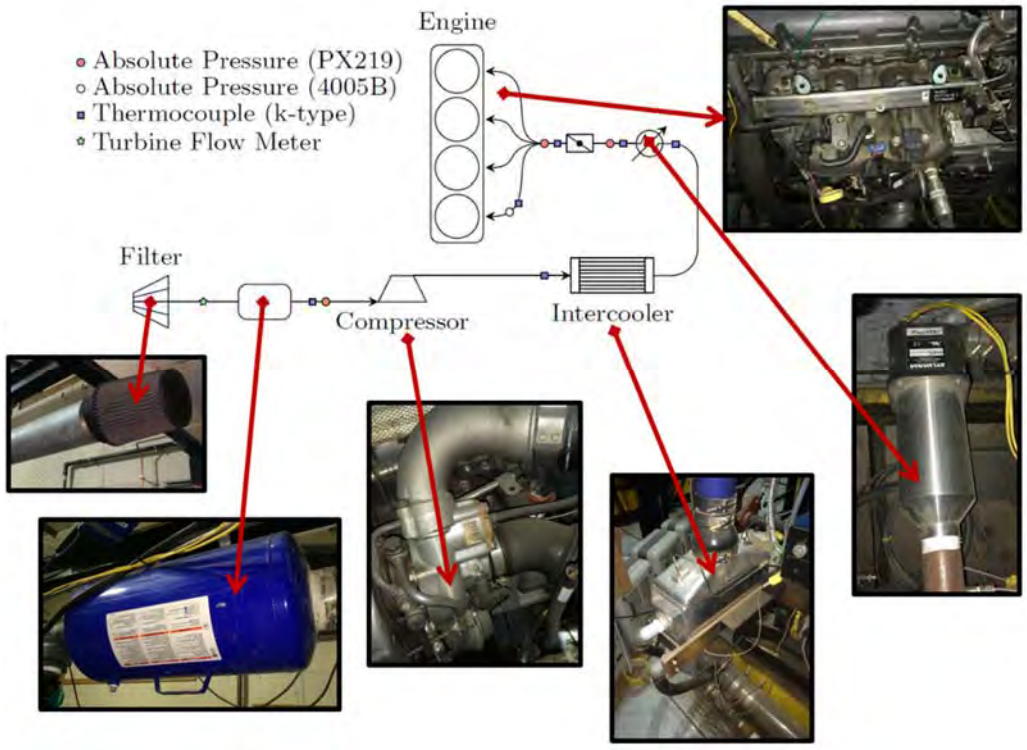

Figure 2-4: Positions of sensors in the intake air path and the pictures of the actual system components. From the upper right corner in clockwise direction, intake manifold with manifold pressure sensors, air heater, air-to-water intercooler, compressor, damping tank, and conical air filter. The schematic diagram in the middle is taken from a thesis by Jake McKenzie [41], who has used the same engine system.

Then, the air with a constant temperature passes through the throttle which is controlled by the ECU, which is controlled by a computer console with an engine calibration software called INCA. Various temperature and pressure sensors are installed through the entire intake air path. Temperatures are measured by k-type (chromel-alumel) thermocouples, and airflow pressures are measured by solid state diaphragm type absolute pressure transducers (Omega PX219) and a high speed miniature piezoresistive absolute pressure sensor (Kistler 4005B) with a piezoresistive amplifier (Kistler 4618A0). Kistler's MAP pressure sensor is used for pegging

the in-cylinder pressure measurements. Also, factory supplied temperature and pressure sensors were maintained on the engine system and connected to ECU.

Fuel injection system

The test engine has a high pressure direct injection system with a retrofitted port fuel injection system (which is not utilized for this research). The direct injection system installed on the LNF engine is shown in Figure 2-5.

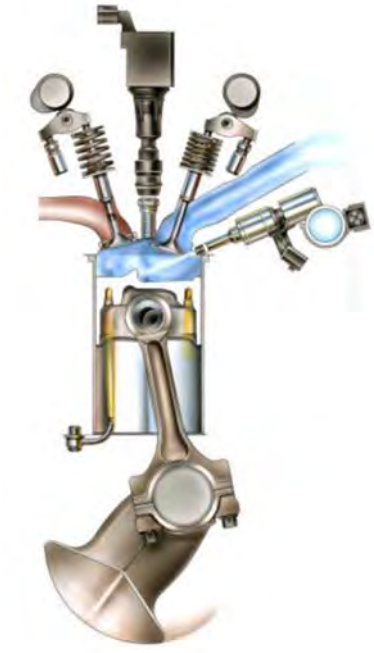

Figure 2-5: A diagram of the direct injection system on the LNF. Blue stream is intake air while red stream is exhaust. Image © General Motors.

Fuels are supplied by two outside tanks: one tank for Haltermann HF0437 (which is EPA Tier III reference fuel) and another tank for gasoline-ethanol blends or Primary Reference Fuel blends. Fuel specifications used for the experiments will be given in a later section and included in the appendix as well. Depending on the fuels used, the fuel is drawn from a pathway chosen by the control panel shown in figure 2-6. The fuel lines were designed so that the common fuel lines are as short as possible to make the purging of the system easy. After passing through the common fuel line driven by a low pressure pumps, fuels are fed into a small damping reservoir (approximately 100 ml) by a high pressure fuel pump driven by the camshaft.

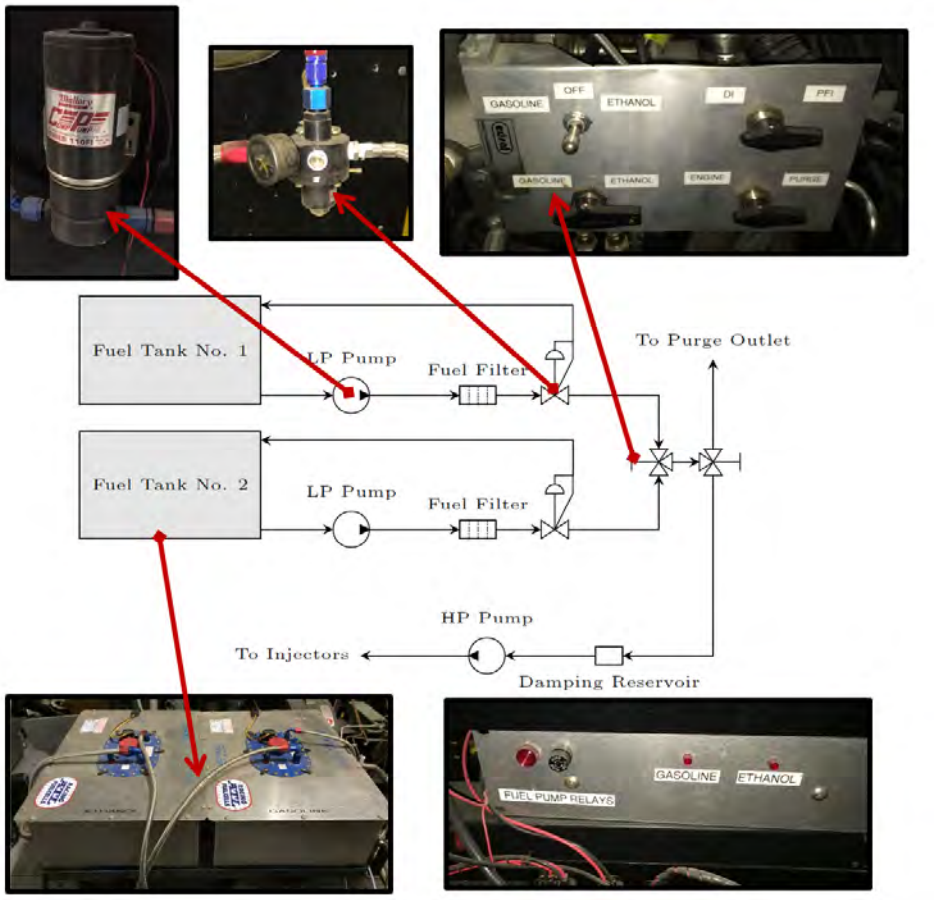

Figure 2-6: A schematic diagram of the fuel supply system with pictures of the actual system components. From upper right corner in clockwise direction, fuel path control panel, pressure regulator, low pressure fuel pump, two 15 gallons fuel tank, and fuel pump power relay. The schematic diagram in the middle is taken from a thesis by Jake McKenzie [41], who has used the same engine system.

To calculate the mass of the fuel injected into the cylinder using fuel rail pressure and injection duration controlled by the ECU, a calibration procedure was developed. Fuel was collected in a flask while the engine is operating at a constant injector pulse width and fuel rail pressure. Then, the weight of the fuel was measured every 150 seconds over a 15 minutes test. Then, this procedure was repeated for a range of fuel rail pressure and injection pulse width to create a fuel rate calibration map.

Turbocharger and Exhaust System

Exhaust streams from four cylinders are combined into two streams; exhaust runners of cylinder one and four meet upstream of the turbocharger flange, and exhaust runners of cylinder two and three are combined as well before feeding into the turbocharger. Then, the twin-scroll

turbocharger is fed each stream separately with appropriate scrolling of the flow. Turbine housing is integrated with a wastegate which is actuated by an external solenoid controlled by the ECU (shown in Figure 2-7). Base boost is called when there is no solenoid valve actuation, so as much flow is bypassed through the wastegate. To increase the boost pressure beyond the base boost, the actuation duty cycle of the solenoid has to be raised to hold the wastegate closed. Wastegate duty cycles were varied from 0% (base boost) to 100% (maximum boost) depending on the desired engine loads.

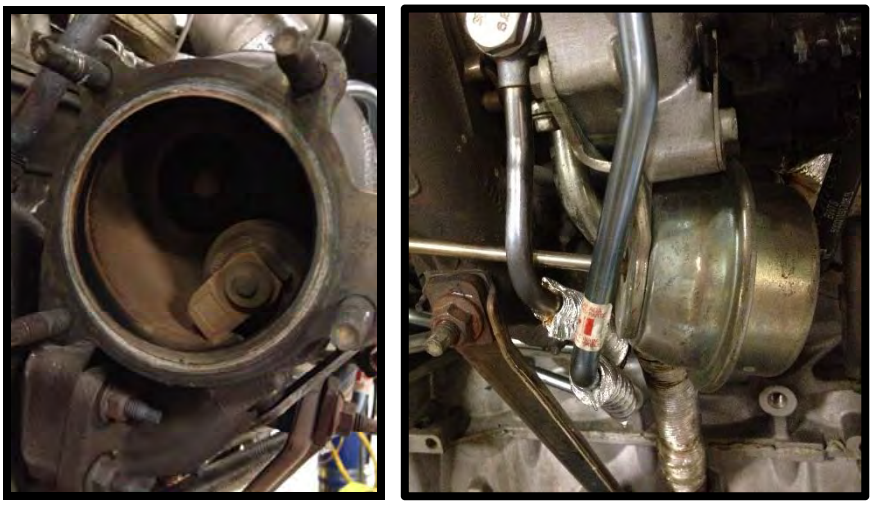

Figure 2-7: A turbocharger housing and a wastegate with catalyst removed (left) and a wastegate actuator with an external solenoid controlled by ECU (right).

Like in the intake system, temperature and pressure sensors were installed in the exhaust system to keep the system operating below the hardware limit (turbine inlet temperature of 950 ºC). Two wide band oxygen sensors (Bosch LSU 4.2) are installed to provide measurements to the ECU and to the data acquisition system. The sensors are connected to ETAS UEGO controller, which creates a voltage that is proportional to the air-fuel equivalence ratio entered on the controller. After passing through the oxygen sensors, three way catalyst is installed. Then, a gate valve was installed to simulate the back pressure of an exhaust system and a muffler.

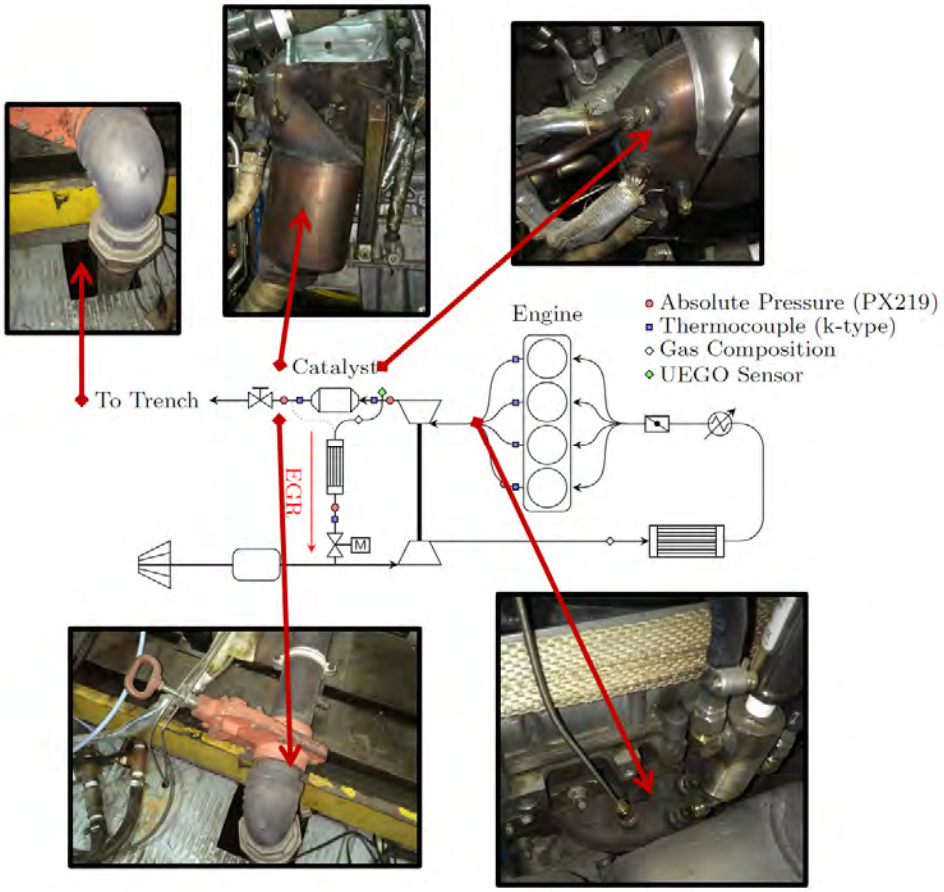

Figure 2-8: Positions of the sensors in the exhaust path and the pictures of the actual system components. From upper right corner in clockwise direction, UEGO sensor on a catalyst housing, catalyst housing with catalyst inside, exhaust trench, gate valve, and exhaust manifold. The schematic diagram in the middle is taken from a thesis by Jake McKenzie [41], who has used the same engine system.

Engine Cooling system

The engine coolant system is filled with a blend of ethylene glycol and distilled water. An external centrifugal pump is used to pump the coolant mixture through the engine. A coolant-to-water intercooler cools the coolant going back into the reservoir by city water, and an electrical heater is used to heat the coolant in case of cold start. A coolant temperature controller is used to maintain the coolant temperature in the tank at 80 ºC with fluctuations less than 1 ºC. A schematic diagram of the system and the actual pictures of the system components are shown in Figure 2-9.

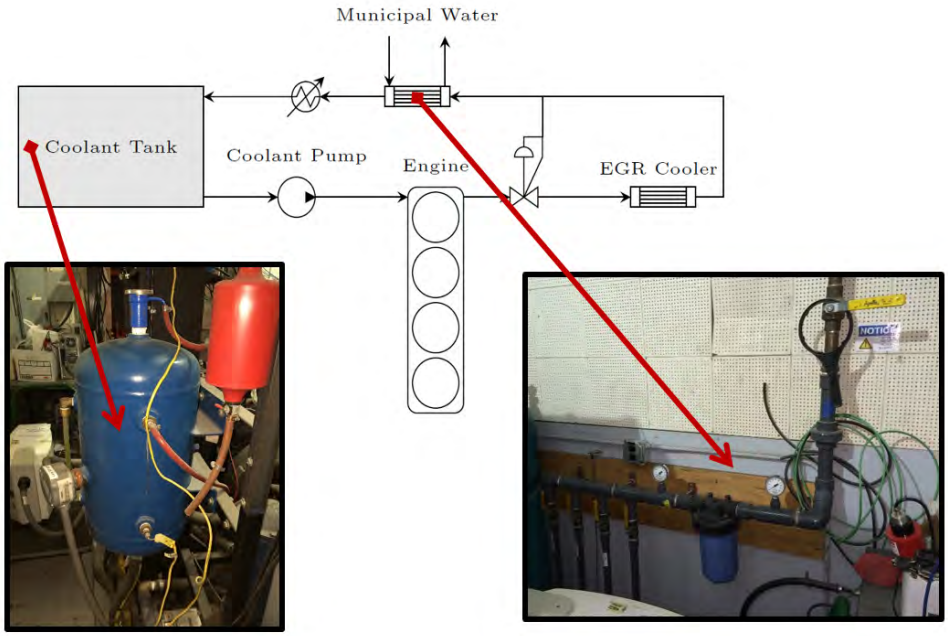

Figure 2-9: A schematic diagram of the engine coolant system with pictures of the actual system components; a coolant tank (left) and city water supply with a filter. The schematic diagram on the top is taken from a thesis by Jake McKenzie [41], who has used the same engine system.

System Control, Data Acquisition, and Processing

Components used to control the engine and data acquisition methods will be discussed in this section.

Engine speed and load control

The engine test system has dynamometer and electric motor which assists the engine to operate reliably. An electric motor is used as a starter motor to run the engine without combustion. A 40 hp electric motor (Baldor Electric Inverter Drive Motor) is used, which is controlled by a variable speed motor controller (Yaskawa Varispeed F7). At the starting of the engine, motor was run so the engine speed is at 1200 rpm, which is not significantly higher than normal idling speed of the engine. Dynamometer is connected to the flywheel by a flexible coupling as shown in Figure 2-10, and it controls engine speed or load by absorbing and dissipating power produced by the engine.

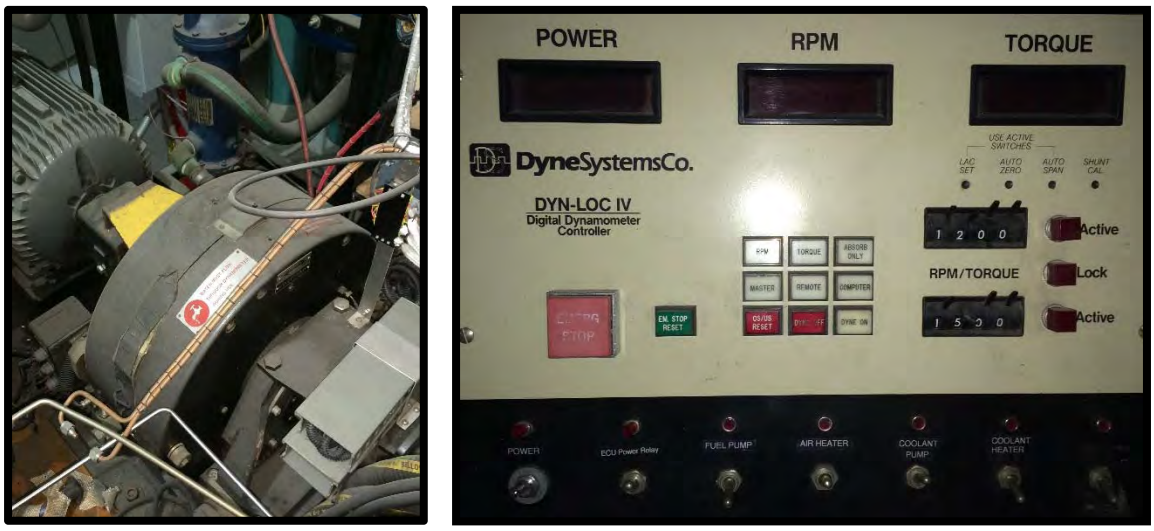

Figure 2-10: Pictures of a 40 hp electric motor (Baldor Electric Inverter Drive Motor) with an eddy current dynamometer (SAJ SE150) connected to the flywheel by a flexible coupling on the left and Dyne systems Dyn-Loc IV on the right.

The dynamometer used is eddy-current type, and it is rated up to 150 kW and 500 Nm of load (SAJ SE150). Rated power limited the range of engine speed and load that can be tested by the current engine. Dynamometer is connected to Dyne Systems Dyn-Loc IV, as shown in Figure 2-10, which controls either the engine speed or engine load to stay constant in case of engine running with combustion. Torque is measured by a strain gauge based load cell which was calibrated by a procedure suggested in a manual provided by a manufacturer. City water is supplied to cool the dynamometer system.

Engine operation control

The engine is controlled by communicating to ECU (Bosch ETKP 4.0) by a data communication interface (ETAS ES591.1) which connects ECU to a computer workstation with an ECU calibration software (ETAS INCA 6.2). The software reads and is able to control all the actuators and electrical systems on the engine (such as spark timing, valve timing, throttle, fuel injection pressure/pulse width, etc.) except for the engine speed which is controlled by the dynamometer, ignition system, and fuel delivery system. Ignition system and fuel delivery system were connected directly to the main control panel so the firing of the engine can be controlled easily (shown in Figure 2-11).

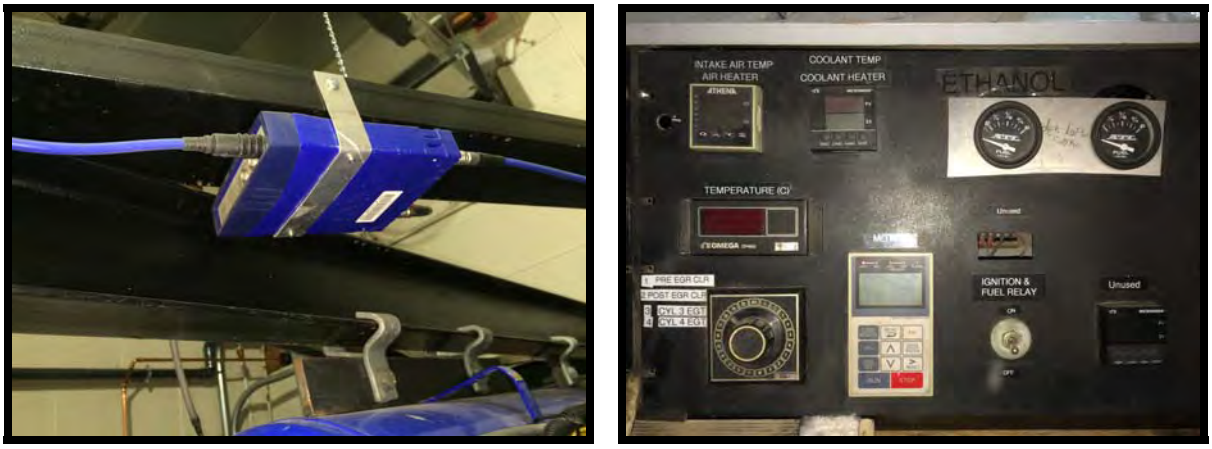

Figure 2-11: Pictures of a data communication interface (ETAS ES591.1) on the left and the main control panel capable of controlling intake air temperature, coolant temperature, electric motor, ignition on the right.

In-cylinder pressure measurements

Piezoelectric cylinder pressure transducers (Kistler 6125A) were used to measure in-cylinder pressures in cylinder one and three. Sensors were located between the intake and exhaust valves on the cylinder head component as shown in Figure 2-12. Piezoelectric sensors produce charge output which is converted to a voltage output by a charge amplifier module (Kistler 5010b). The cylinder pressure transducers and charge amplifiers were calibrated using a hydraulic dead-weight tester with the sensor heated at 100 ºC.

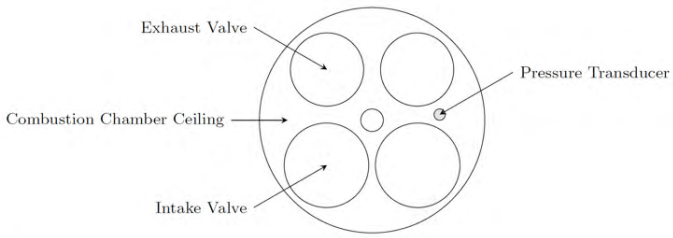

Figure 2-12: A diagram of the cylinder head of a single cylinder with a pressure transducer located between intake and exhaust valves (taken from a thesis by Jake McKenzie [41], who has used the same

engine system.) and the actual pictures of in-cylinder pressure transducers installed on cylinder one and three (silver wiring) on the left and charge amplifier modules (Kistler 5010b) on the right.

The crankshaft was connected to an incremental optical quadrature encoder (BEI H25) which provides 360 pulses per revolution. Custom made processing circuit was retrofitted so quadrature signal is decoded. The first channel from the decoder provides signal every 0.25º while the second channel gives a signal whenever crankshaft is at bottom dead center (BDC) position. Top deal center (TDC) sensor (AVL TDC Sensor 428) was utilized to align the piston and crankshaft at TDC.

Data Acquisition and Processing System

Sensors are connected to a National Instruments' modular data acquisition system (NI cDAQ 9188) which sends data via Ethernet to a computer workstation with LabVIEW installed. The module is shown in Figure 2-13. There are eight slots on the modular data acquisition system (DAQ), and several analog input modules (5x NI 9215), thermocouple input modules (NI 9213), and digital input-output ports (NI 9401 and NI 9402) were outfitted on the system (shown in Figure 2-13). On a workstation, LabVIEW code was configured to collect data for 100 engine cycles for every 0.25º of crank angle. Then, some analog data were collected for 100 cycles with a sampling rate at 100 kHz. Some of the engine control variables (spark timing, valve timing, fuel pressure, and injection duration) were also imported in LabVIEW by utilizing a data communication interface between ETAS INCA and NI LabVIEW using the ASAM-3MC protocol.

The data acquisition system gives a wide range of information on the LabVIEW user interface. It shows the most recently relayed in-cylinder pressures of cylinder 1 and 3, and also proceeding nine cycles with decreasing opacity in color, therefore showing 10 pressure traces in total. Using these traces, pressure-volume diagrams were also constructed. Load metrics such as BMEP, net indicated mean effective pressure (NIMEP), and gross indicated mean effective pressure (GIMEP) were also calculated on the user interface. The air-to-fuel equivalence ratio, fuel delivery rate, emissions, and various readings from temperature sensors were also displayed as well. New data output format was developed so that the data is collected in binary format which is the same format used by LabVIEW to store data in computer memory. Therefore, data could be stored quickly without losing data due to memory overrun.

Figure 2-13: A picture of data acquisition system with temperature sensor wires, a modular data acquisition system, ETAS UEGO, Kistler 5010b, power relay, etc.

Engine-in Vehicle and GT-power Simulation

The engine-in-vehicle simulation tool Autonomie was utilized to connect the operating points on the engine map for the different driving cycles. With a given vehicle model, Autonomie runs a vehicle model in a given driving schedule and estimates the fuel consumption and emissions over the time. A vehicle model can be constructed on the Autonomie, and engine configuration can be changed before feeding into the model. Then, the Autonomie runs a given driving cycle and determines the operating points on the engine map. This allows to analyze the impacts of vehicle models, boost levels (downsizing levels), and spark retard strategies on fuel economy, operating points, etc., therefore allowing a wide range of parametric studies.

GT-power is a simulation package specifically designed for the combustion study of internal combustion engines. A model of the engine was provided by GM, and it was used to get results for conditions beyond the capability of engine experiments. Utilizing GT-power model of the engine, several engine performance maps could be generated by changing boost conditions and engine geometries (such as engine displaced volume and compression ratio). For accurate

simulation results, engine experimental results were benchmarked to find the right coefficient for heat transfer, combustion efficiency, charge cooling models of GT-power model of the engine.

3. Combustion Characteristics of a TC SI Engine

In this chapter, combustion characteristics of a TC SI engine will be analyzed with focus on performance map and cycle by cycle variability.

3.1 Performance map of a TC SI engine

Different from naturally aspirated spark ignition engine, turbocharged engines have unique operating characteristics on their own. Those include WOT limits, peak pressure limits, turbocharger operating limits, intake MAP feedback effects, etc. Most of the characteristics were analyzed and documented in the author's Master's degree thesis [42], but those will be reviewed here briefly as a performance map is one of the main pieces of this project. The performance map of the engine shows engine fuel consumption over the range of speeds and loads. Fuel consumption can be provided in terms of the fuel conversion efficiency based on the lower heating value of the fuel. By constructing the performance map, general trends in fuel consumption can be analyzed.

Operating characteristics and limits of a TC engine

Wide open throttle (WOT) of a naturally-aspirated engine is well defined as an operating condition where the throttle position is fully open. In a TC engine, boost level not only changes with throttle position but also with wastegate actuator position. As engine load and speed increase, the turbocharger spools up and the wastegate opens to moderate the amount of boost created by the turbocharger. When throttle position alone reaches its maximum open position and the wastegate is fully open, the boost condition is called baseboost. From the baseboost condition, the wastegate can be closed to decrease the amount of exhaust bypassing the turbine in order to increase the amount of boost. The condition when wastegate actuator is at its full effort to close the wastegate is defined as the WOT limit of the TC engine.

Other than WOT limit, there are hardware limits. In the experiments the peak in-cylinder pressure was limited to less than 100 bars, to minimize the risk of damaging the head gasket. In-

cylinder peak pressure approaches 100 bar at NIMEP of 2000 kPa. At higher loads the spark was retarded to keep the peak in-cylinder pressure below 100 bar. Also, turbine inlet temperature was limited to 980 ºC, which puts limitations on the engine load and spark retard.

There is an intake MAP feedback effects in a TC engine as intake MAP is affected by a compressor which is coupled with a turbine, which depends on the exhaust gas temperature and pressure. Figure 3-1 shows the manifold pressure as a function of spark retard for several positions of the wastegate of the turbocharger. The manifold pressure increases with increasing spark retard for fixed positions of the throttle and the wastegate valve. The torque loss with spark retard decreases as the boost level increases because the amount of fuel injected increases along with increasing amount of air while air-to-fuel is fixed at the stoichiometric ratio. In an NA engine, the efficiency change with spark timing change is only a function of the torque output. However, in a TC engine, the fuel flow rate also changes along with MAP at the fixed fuel-to-air ratio.

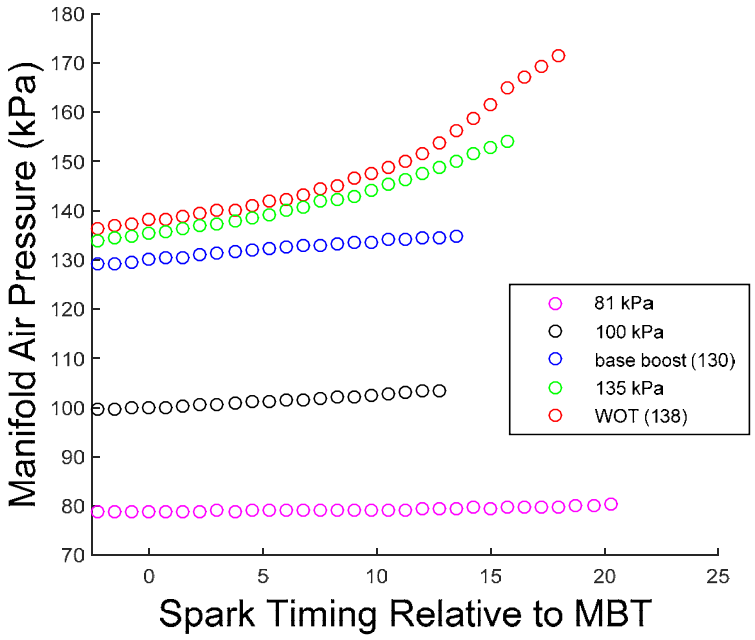

Figure 3-1: Manifold air pressures of spark sweeps measured at different boost levels at 1500 rpm. Manifold air pressure in the legend is measured at MBT timing.

For TC engines, since both fuel flow rate and torque output change with spark timing, MBT timing was no longer the maximum efficiency timing. It can be seen from Figure 3-2 that the maximum efficiency spark timing is actually slightly advanced from MBT timing.

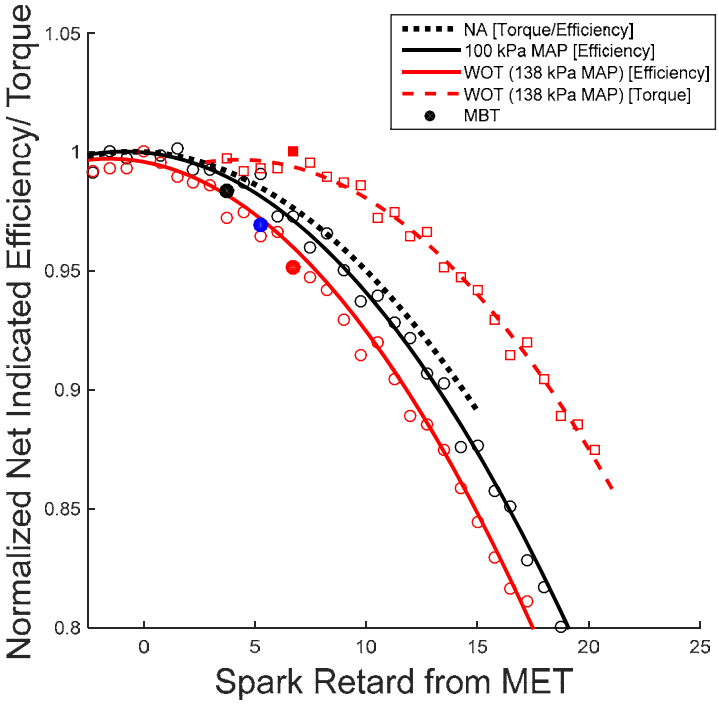

Figure 3-2: Normalized efficiency vs. spark timing with respect to maximum efficiency timing (MET). 0 CAD refers to the maximum efficiency timings.

The gap gets larger with higher boost levels since MAP change with spark retard is more significant at higher boost. At WOT, red filled marker shows that about 5% of efficiency can be improved by advancing the spark timing about 7 CAD from MBT to MET. Under high boost conditions, either a significant amount of spark retard or mixture enrichment is required to suppress knock. They all deteriorate the efficiency, and the efficiency degradation with spark retard is significantly worse for a TC engine at high boost conditions. Therefore, knock suppression at high load would increase the efficiency of the turbocharged engine significantly because it allows spark timing to be much closer to maximum efficiency timing. When generating an efficiency contour of the engine, all of the operating characteristics explained here have to be considered carefully as engine performance is limited by those characteristics.

Generating an efficiency contour

To generate the performance map of the GM engine, experiments were done over the full range of loads at engine speeds from 1500 rpm to 3000 rpm. This speed range tested was chosen since it is where the engine is mostly operated in normal driving cycles. At a given speed, testing points were determined such that MAP is fixed at low, medium, and high levels. This effectively

provides data at close to constant BMEP levels, as BMEP scales closely with intake MAP. Since the engine was tested over a wide range of loads and speeds, the valve timing calibrations given by GM was used. At each test point, spark sweeps were done to determine the MBT spark timing. Brake torque and fuel flow rates were measured at MBT timing to calculate fuel consumption and fuel conversion efficiency of the engine at each operating point. Fuel conversion efficiency was calculated using:

$$\eta_{f,b} = \frac{\text{Torque} * \text{engine speed}}{\dot{m}_{fuel} * LHV_f} \tag{3.1}$$

Similarly, specific fuel consumption can be calculated.

$$\text{sfc} = \frac{\dot{m}_{fuel}}{\text{Power}} \tag{3.2}$$

The first set of experiments was done to compare the brake fuel conversion efficiencies of RON 96 and E85 fuel in the knock-free region, shown in Figure 1-3.

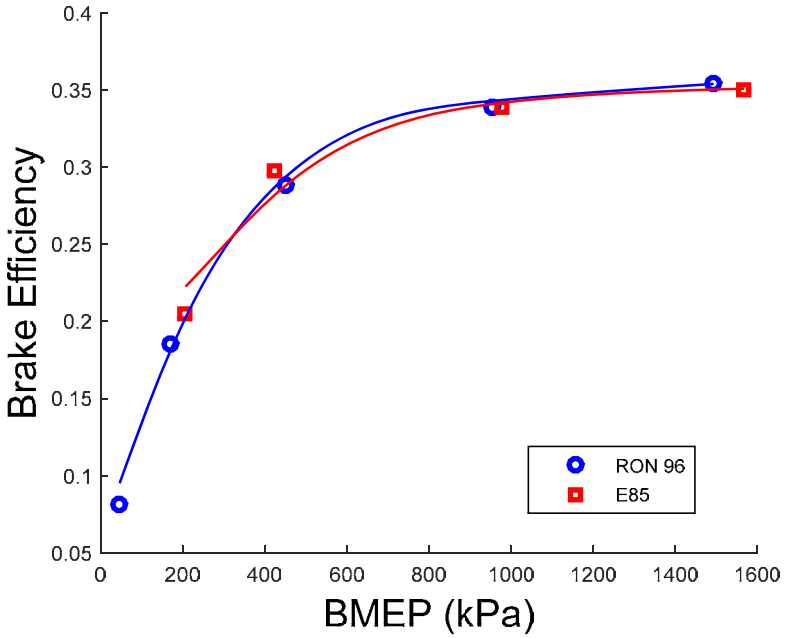

Figure 3-3: Brake fuel conversion efficiencies for RON 96 and E85 fuel at 2500 rpm in knock free region. Blue curve and red curve denotes RON96 and E85 fuels respectively.

The efficiencies for the two fuels as a function of BMEP are comparable: it is concluded that brake fuel conversion efficiency at fixed speed and load does not differ significantly between the two fuels considered. Even though the lower heating value of ethanol is 30 percent lower than that of gasoline, the lower heating values of their stoichiometric mixtures are almost the same because the air-to-fuel ratio of ethanol is 9, while that of gasoline is around 14.6. The denominator in equation (3.1) can be rewritten as

$$\dot{m}_{fuel} * LHV_f = \dot{m}_{air} * (F/A) * LHV_f \tag{3.3}$$

where $(F/A) * LHV_f$ for E85 is 2.96 MJ/kg and for gasoline is 2.95 MJ/kg. Therefore, for a fixed speed and load, the theoretical fuel conversion efficiencies of two fuels are similar as long as the air flow rates are not significantly different. Based on this observation, E85 is used to measure efficiencies of the engine to avoid effects of knock on the efficiency. Figure 3-4 shows the brake fuel conversion efficiency map of the engine based on the lower heating value of the fuel.

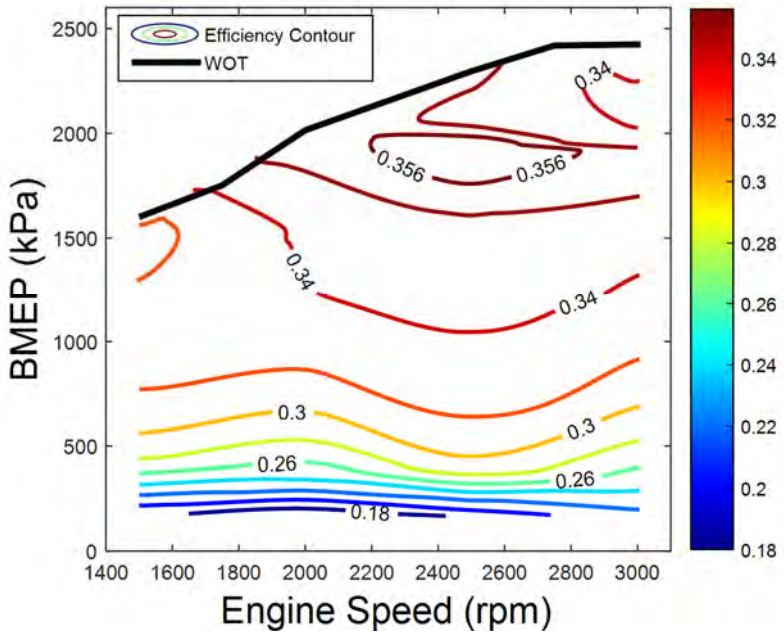

Figure 3-4: Brake fuel conversion efficiency contour of the engine using E85 fuel. A black line is WOT, colored lines are efficiency contours, and color bar on the right side illustrates efficiency value at different colors.

To obtain contours of constant fuel consumptions and engine efficiencies over the engine operating map, brake specific fuel consumption and brake fuel conversion efficiencies were interpolated over the tested ranges of BMEP and engine speed. Two-dimensional cubic interpolations were done to generate interpolated data sets. To avoid knock, E85 was used to generate the efficiency contours. Figures 3-4 show that the engine is the most efficient around 2500 rpm as seen by deepening contour lines around 2500 rpm. The general trend is that the engine gets more efficient as the load increases, but there is a diminishing return. As BMEP increases from very light load to around 1100 kPa, the efficiency increase is relatively large since the relative impact of pumping work is larger at a lower load. However, pumping work reduction has little impact from 1000 kPa onward, where the turbocharger starts to generate boost.

Around 3000 rpm, efficiency contour lines curve upwards, indicating decreasing efficiency compared to the same load at slower speeds. This trend can be explained by the increase in mechanical friction and in pumping work at higher speeds. Around 2000 kPa BMEP at 2500 rpm, efficiency starts to decrease slightly as the load is increased until WOT operation. Spark timing had to be retarded to maintain in-cylinder peak pressure below 100 bar, and the loss in torque with spark retard resulted in a slight reduction in efficiencies in that region. Other than in-cylinder peak pressure, spark timing had to be retarded for different fuels to avoid knock. To analyze in which part of the map knock limits the use of a specific fuel, engine experiments were performed using different ethanol-gasoline blends. Knock limit results will be presented in later sections in more detail.

3.2 Cycle-by-cycle variations of a TC SI engine

One of the many strategies used to avoid knock is to retard the spark timing. This lowers the overall in-cylinder pressure, therefore increasing knock limits. However, with spark retard, spark ignition engine exhibits a significant cycle by cycle variations increase. Cycle by cycle (CBC) variations of in-cylinder pressure can lead to drivability issues, fuel consumption increase [43], and engine out emissions variability issues [44, 45]. Since spark ignition engine operations are limited by the extremes cycles within the variations, it is important to understand the variations.

Sources of CBC variations

Many studies have been conducted to find the sources of cyclic variations. Keck and Heywood suggest that the CBC variations in the flame growth rate and location of kernel at early stage of combustion are the major causes of CBC variations in in-cylinder pressure [46]. It is also suggested that the mixture uniformity in the vicinity of spark plug plays an important role. Using a high speed photography, Soltau concluded that variations in the time period between a spark and a formation of stable flame front causes variations in the combustion period [47]. Distortion and wrinkling of the flame front by turbulence also generates CBC variations. Patterson measured hot-wire velocity in the combustion chamber of a motored engine and concluded that the mixture velocity variations near the spark plug at ignition causes the CBC variations of the combustion process [48]. Extending on this work, Barton, et al tried to find a connection between the gas motion near the spark plug at the time of ignition and CBC variations in the pressures. With a developed model, they have found a correlation of 0.975 between the standard deviation of the velocity and the angle of occurrence of maximum in-cylinder pressure [49].

Since variations in the early stage of combustion affect the overall combustion variability, it is important to understand how pressure variability develops over the course of combustion. Among many factors causing cycle-by-cycle variations, combustion related parameters provide the most useful insights unless cycle-by-cycle variations are visually analyzed on an optical bench as done by Rashidi [50]. It is well known that the lower burning rates during start of combustion result in lower maximum in-cylinder pressure [51]. Averette found that there are variations in the time after ignition required for in-cylinder pressure to reach the pressure above the compression pressure [52]. Soltau concluded that there is a variation on the flame development period while variation was little on the flame propagation period [48]. These studies all suggest that the development of pressure variations strongly depends on the early stage of combustion as well.

Pressure variations analysis

Cyclic variations can be measured in many different ways depending on the parameters of interest (such as pressure, rate of pressure change, and mass fraction burnt related parameters), but the most common measure is COV of IEMP, which is defined as below.

$$\mathrm{COV}_{imep} = \frac{\sigma_{imep}}{imep} x100 \tag{3.4}$$

where COV_{imep} is coefficient of variation of IMEP, σ_{imep} is a standard deviation of measured IMEP of cycles, $imep$ is the average IMEP of cycle IMEP values. Since IMEP is directly connected to torque output of the engine, variability of IMEP directly relates to the drivability issues. Well known trends of COV_{imep} is that it increases with retarded spark timing, lower engine loads, leaner mixture, and slower burning fuels.

To better understand how pressure variations cause variations in COV_{imep}, COV of in-cylinder pressures of 100 cycles at a given range of crank angle degrees were analyzed. Some previous studies have done a similar analysis. Zervas has calculated COV of the in-cylinder pressure on each crank angle for a number of cycles using a natural gas fueled SI engine operating under lean conditions. It is suggested that the integral of COV curve in the combustion region is a good criterion for the quantification of the cycle dispersion [53]. The study did analyze the effects of spark timing, but engine speed and load effects were not analyzed fully, and data points were limited. Using Zervas's method, Samuel et al has compared COV of throttle body injection (TBI) and Gasoline Direct Injection GDI engines. The study concluded that COV of NIMEP of TBI engines are lower than that of GDI engine [54]. This study explores effect of fuel injection system, engine speed, engine load on COV but does not mention or explore the effect of combustion phasing. Combustion phasing is one of the most important factor that determines the cyclic variability of the engine. In this section of report, general trends of COV of NIMEP are explored. Then, the effects of engine operating parameters and fuels on COV will be analyzed in a systematic way.

Spark sweep results

Spark sweep results for a wide range of operating loads and various fuel blends are considered here. A range of operating points of interest were determined so that it encompasses the most driven region on the engine map. Also, fuel blends were chosen so they don't knock at the operating conditions tested and provide full range of spark sweep. Below is a test matrix showing the variables.

Table 3-1: COV experiments test matrix

Engine Speed (RPM)	1500 and 2000
Engine Load (intake MAP in absolute bar)	0.8~1.5
Total number of operating points	26 spark sweeps 600 steady-state operating points 60,000 cycles in total
Fuels	RON 96 standard research gasoline Isooctane E85, E50, M10, EW15 (15% of water mixed with E85)

Figure 3-5 shows how COV of NIMEP changes with spark timing and CA50 timing. Ethanol blends generally show lower COV than gasoline fuels.

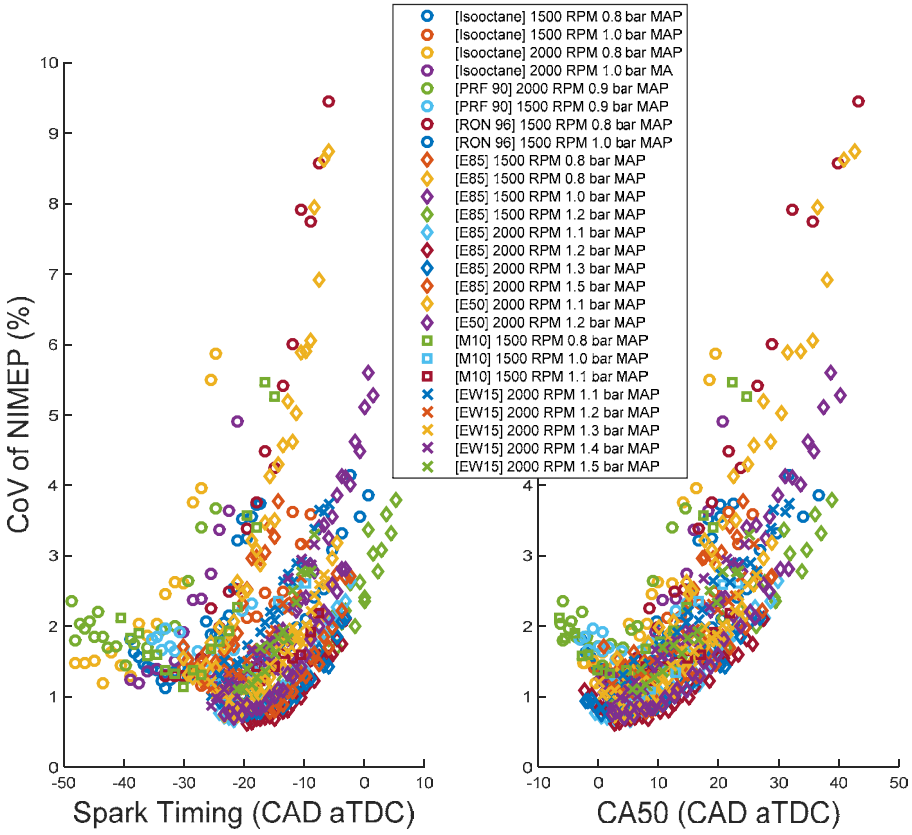

Figure 3-5: COV of NIMEP vs. spark timing (left) and vs. CA50 timing (right). Different fuel blends are marked with different marker, and different operating points were colored differently within a given marker group. Circle, diamond, square, and x markers each represent gasoline fuels, ethanol-gasoline blends, M10, EW15 fuels.

General trend shows increasing COV with retarded spark timing, which is well known already. Since different fuels were tested at wide range of engine speed and load, COV are dispersed. To get the general trend better, MBT timings are aligned at 0 on x-axis in Figure 3-6. Figure 3-6 exhibits slightly better collapse results, but it still has dispersion across y-axis. This dispersion is normalized in 3-7, so y-axis in 3-7 shows percent increase in COV with spark retard.

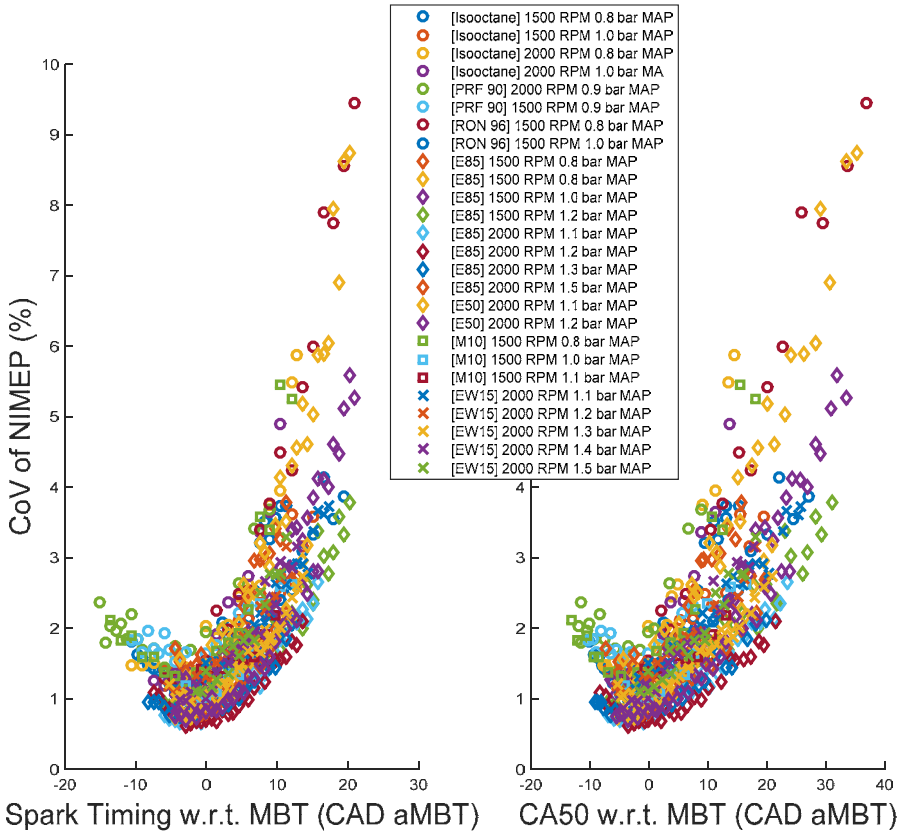

Figure 3-6: COV of NIMEP vs. spark timing w.r.t. MBT timing (left) and vs. CA50 timing (right). Different fuel blends are marked with different marker, and different operating points were colored differently within a given marker group. Circle, diamond, square, and x markers each represent gasoline fuels, ethanol-gasoline blends, M10, EW15 fuels.

By looking at the general trend of COV of NIMEP shown in 3-7, it is found that the minimum COV is located slightly before MBT timing (about 3~4 CAD before). In the range tested, it seems like that the general shape of the normalized COV curve seems to be independent of fuels, engine load, and engine speed. It can be concluded that the main parameter changing the COV seems to be the combustion phasing, as COV change with spark timing is larger than COV

dispersion in y-direction of Figure 3-6. To further analyze the effect of engine speed and engine loads, spark sweep results were plotted for few cases.

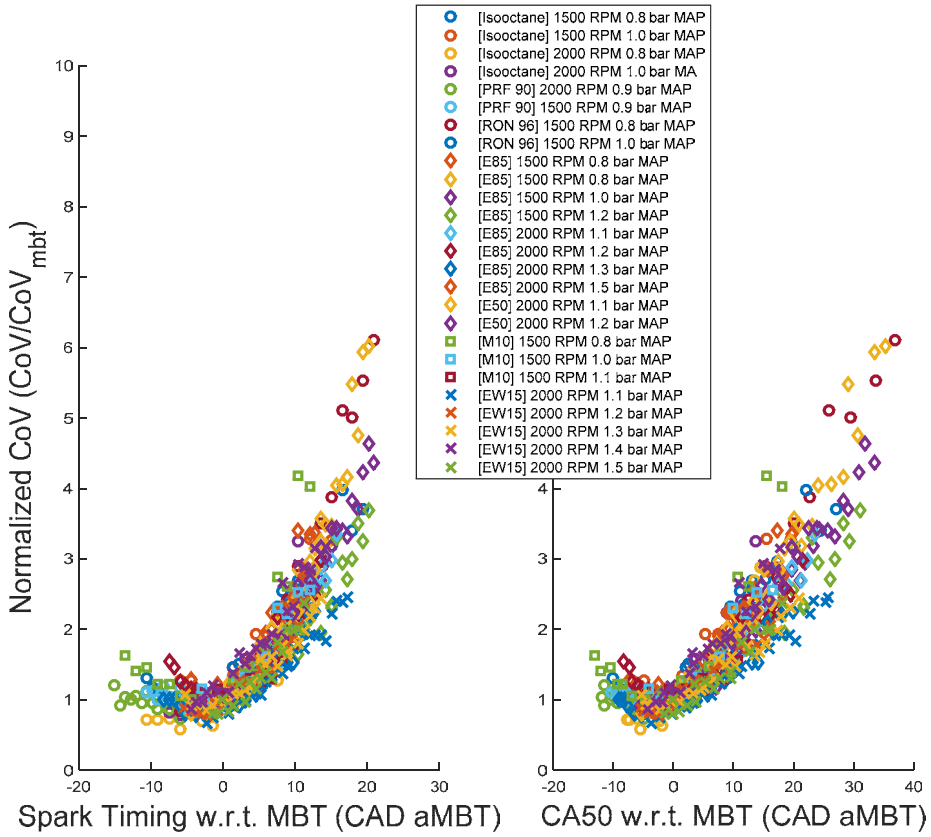

Figure 3-7: Normalized COV of NIMEP at MBT vs. spark timing w.r.t. MBT timing (left) and vs. CA50 timing (right). Different fuel blends are marked with different marker, and different operating points were colored differently within a given marker group. Circle, diamond, square, and x markers each represent gasoline fuels, ethanol-gasoline blends, M10, EW15 fuels.

Figure 3-8 shows COV curves of isooctane fuel tested at three engine speeds. It shows that the higher speed results in higher COV. One of the possible reasons is due to increased turbulent velocity at higher speeds which might cause larger variability. The gap between speeds also increases with spark retard, mainly because combustion duration increase with spark retard is larger at higher speeds. Figure 3-9 shows COV change with engine load. With less residual, engine runs with less variability at higher loads, and it is well shown in the trend below. COV drops down below 1% for boosted cases.

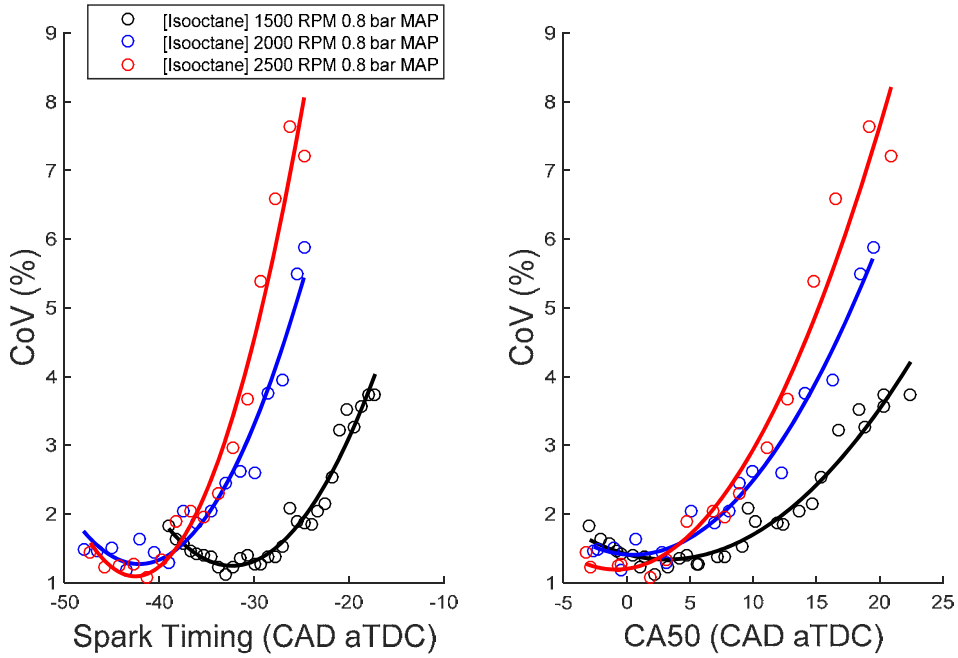

Figure 3-8: COV vs. spark timing (left) and CA50 timing (right). A black, blue, and red line each denote engine speed 1500 rpm, 2000 rpm, and 3000 rpm tested at 0.8 abs bar intake MAP using isooctane.

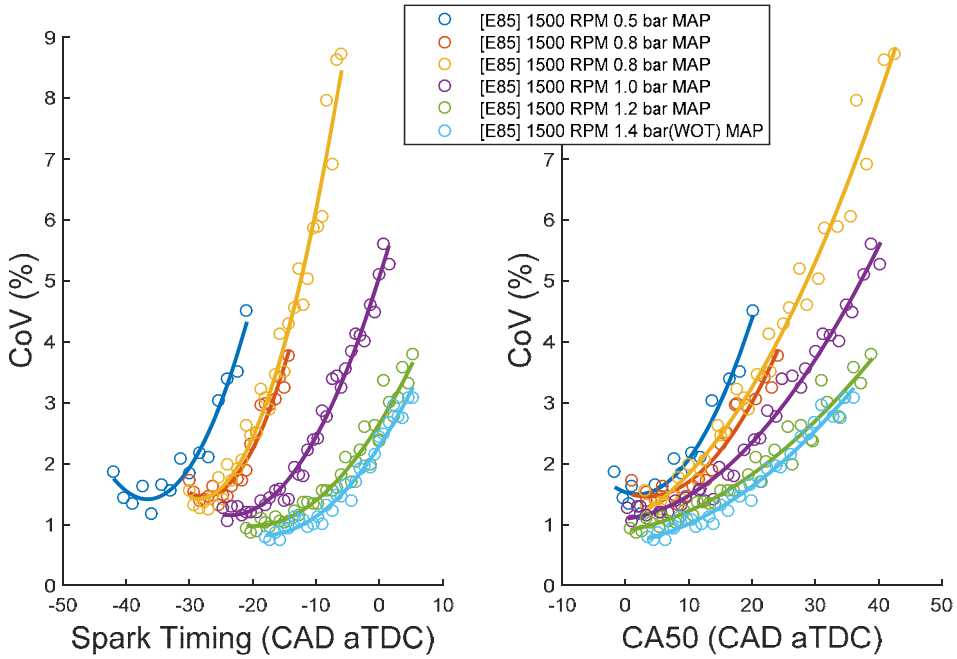

Figure 3-9: COV vs. spark timing (left) and CA50 timing (right). E85 fuel was tested at 1500 rpm for different loads which are denoted by different colors.

To further analyze the effects of engine load on COV, burn durations were plotted in Figure 3-10 and 3-11. Figure 3-10 and 3-11 each are burn duration results of isooctane tested at 0.4 and 1.0 bar absolute MAP respectively.

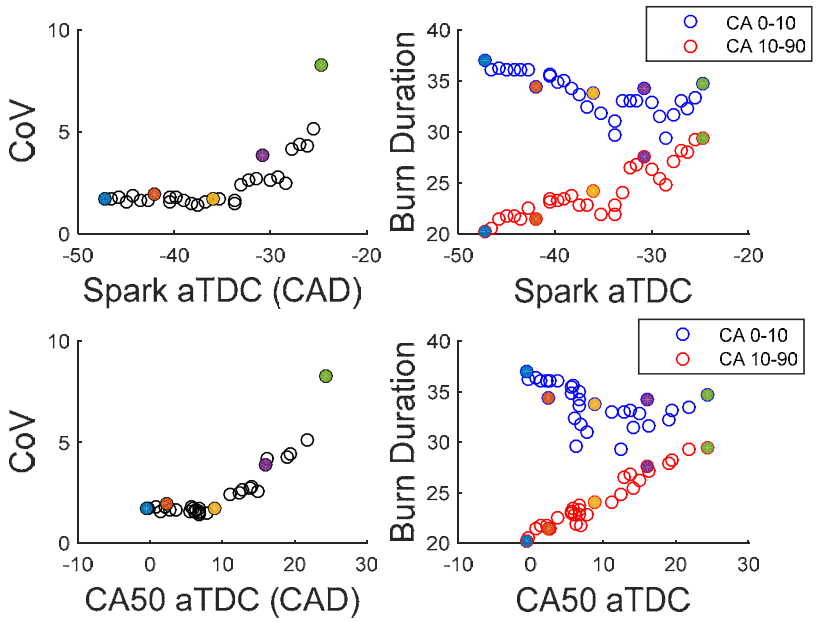

Figure 3-10: COV (left) and burn duration (right) plotted against spark timing (top) and CA50 (bottom), Isooctane tested at 1500 rpm and 0.4 abs bar MAP.

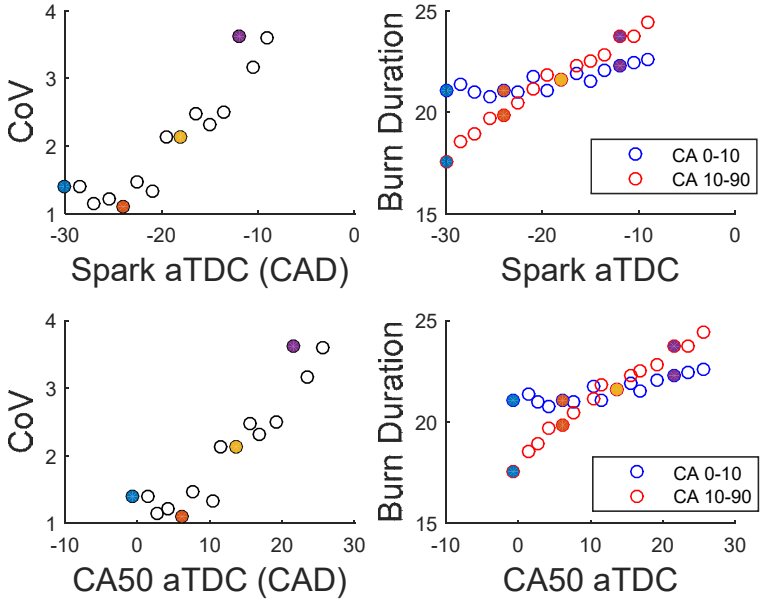

Figure 3-11: COV (left) and burn duration (right) plotted against spark timing (top) and CA50 (bottom). Isooctane tested at 1500 rpm and 1.0 abs bar MAP.

With about 15 CAD spark retard from MBT timing, COV increased from 2 to 4%, and CA10-90 burn duration increased from 23 to 28 CAD in low load case. With about 15 CAD spark retard from MBT timing, COV increased from 1 to 3.5%, andCA10-90 burn duration increased from 22 to 25 CAD for low load case. Burn duration increase with retard is less significant at high load, which leads to lower COV. To see the effect of engine speed and burn duration on COV, burn durations were plotted for isooctane tested at 2500 rpm and 1.0 bar absolute MAP in Figure 3-12.

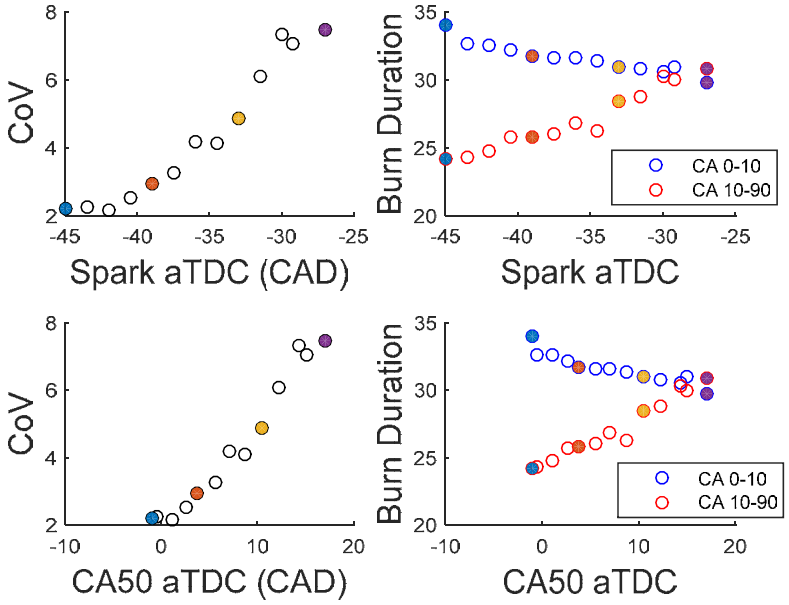

Figure 3-12: COV (left) and burn duration (right) plotted against spark timing (top) and CA50 (bottom). Isooctane tested at 2500 rpm and 1.0 abs bar MAP.

For 2500 rpm case, COV increased from 2 to 7% with about 12 CAD spark retard from MBT timing, and CA10-90 burn duration increased from 26 to 30. Compared to Figure 3-11, burn duration is longer for higher engine speed as there is less time for a given CAD.

Cycle by cycle variation of a pressure traces

Studying a general trend in COV of NIMEP with engine operating condition, it was found that spark timing affects COV of NIMEP the most (in terms of magnitude) among the other variables considered. Therefore, in-depth analysis will be done on the effect of spark timing on COV of NIMEP. Figure 1-13 shows an example of a spark sweep results of the engine running at 1500 rpm and 0.4 bar absolute MAP with isooctane fuel. NIEMP vs. Spark timing result shows a well-

known trend of engine work output change with spark retard. There is an optimal spark timing where the engine work output is maximum: retarding from the optimal timing reduces the overall pressure level while advancing from the optimal timing increases heat transfer losses. Among tested spark timing points, four points are analyzed in Figure 3-14~17.

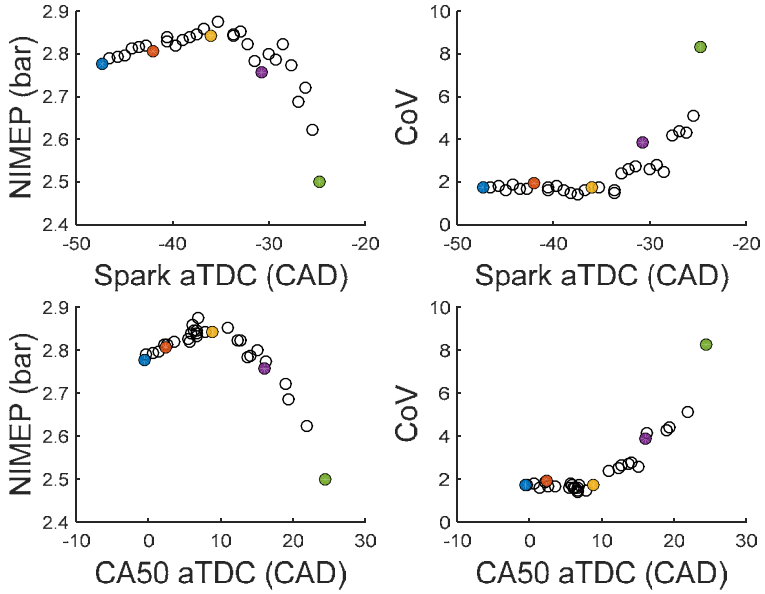

Figure 3-13: NIMEP (left) and COV (right) plotted against spark timing (top) and CA50 (bottom). Isooctane tested at 1500 rpm and 0.4 abs bar MAP. Colors points are to be analyzed in depth.

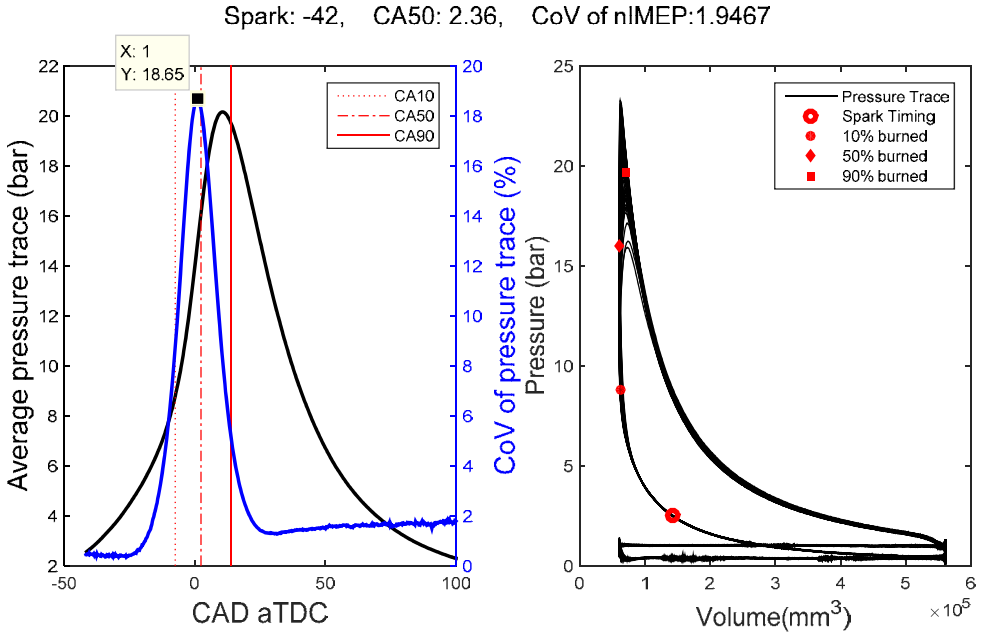

Figure 3-14: Average pressure trace and COV of pressure traces vs. CAD on left and 100 cycles of pressure traces vs. combustion chamber volume on right. The average CA10, CA50, and CA90 timings

are indicated on both graphs with red lines and markers. Spark timing at -42 CAD aTDC with Isooctane tested at 1500 rpm and 0.4 abs bar MAP.

Figure 3-14 shows the average pressure trace and COV of pressure trace at each CAD on the left graph and 100 pressure cycles plotted against the combustion chamber volume on the right. The shape of the blue curve shows that there is still a significant CBC variation on local pressure data even when COV of NIMEP is little. Figure 3-15 shows MBT timing (6 CAD retarded from Figure 3-14 case). On MBT timing case, the shape of the blue curve did not change much. Zervas also found in his research that the shape of the blue curve is somewhat universal [53].

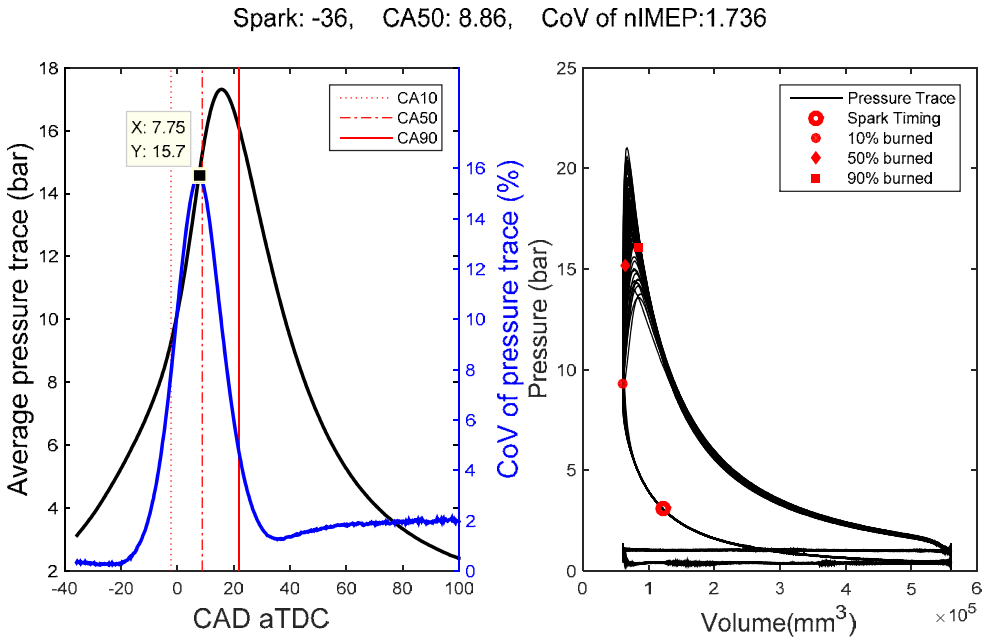

Figure 3-15: Average pressure trace and COV of pressure traces vs. CAD on left and 100 cycles of pressure traces vs. combustion chamber volume on right. The average CA10, CA50, and CA90 timings are indicated on both graphs with red lines and markers. Spark timing at -36 CAD aTDC with Isooctane tested at 1500 rpm and 0.4 abs bar MAP.

To confirm this, more analysis is done on spark timing much retarded from MBT timing in Figure 3-16 and 3-17. Blue curves in Figure 3-16 and 3-17 still have similar shape as previous cases.

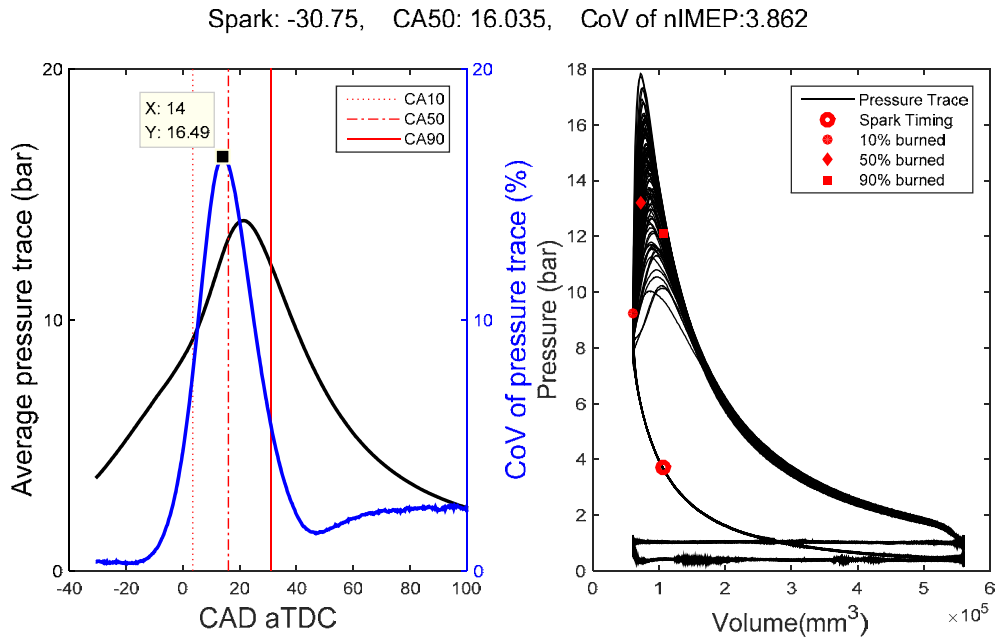

Figure 3-16: Average pressure trace and COV of pressure traces vs. CAD on left and 100 cycles of pressure traces vs. combustion chamber volume on right. The average CA10, CA50, and CA90 timings are indicated on both graphs with red lines and markers. Spark timing at -30.75 CAD aTDC with Isooctane tested at 1500 rpm and 0.4 abs bar MAP.

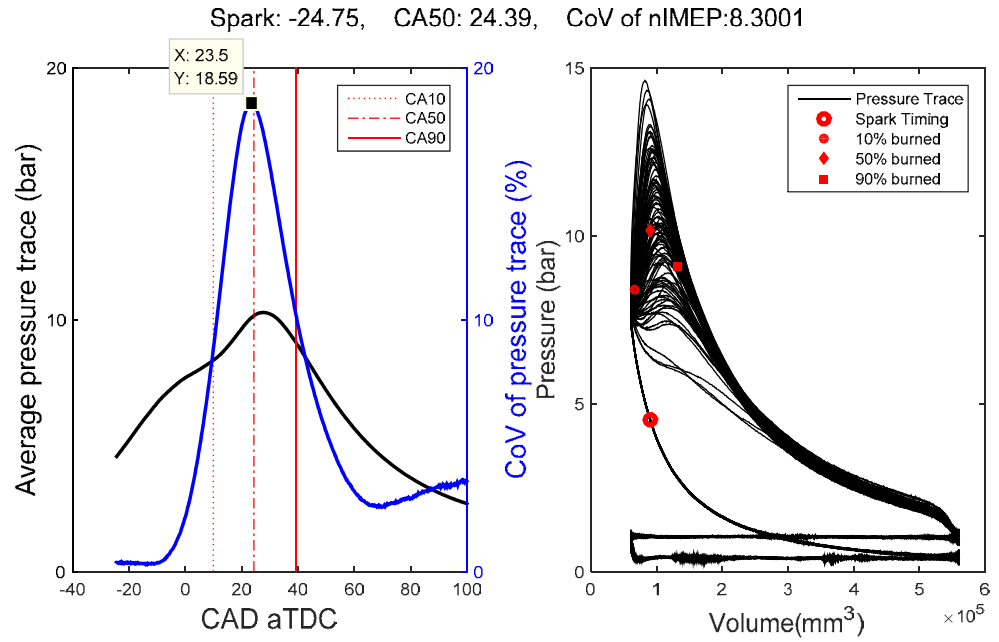

Figure 3-17: Average pressure trace and COV of pressure traces vs. CAD on left and 100 cycles of pressure traces vs. combustion chamber volume on right. The average CA10, CA50, and CA90 timings are indicated on both graphs with red lines and markers. Spark timing at -24.75 CAD aTDC with Isooctane tested at 1500 rpm and 0.4 abs bar MAP.

One difference is that the curve is widened in x-axis, meaning that the range of pressure variations are becoming longer as combustion phasing is retarded. Retarding from MBT timing, COV of NIEMP starts to increase significantly. It can be inferred that the phasing of blue curve triggers the variations in the shape of the PV (Pressure-volume) diagram. Pressure variations exist in cases where COV of NIMEP is low, but they don't vary the shape of PV diagram much as variations occur in a region where vertical changes don't affect the shape of PV diagram much (a region close to TDC where volume is little).

By looking at many different cases, the general shapes of the COV of pressure traces are very similar no matter the engine load, engine speed, and most importantly spark timing. Even at very low COV of NIEMP, there are still variations in cylinder pressures. COV of NIEMP can be visualized by looking at the dispersion of the area of the PV diagram. It is found that the dispersion of the area of the PV diagram is caused by the phasing of the blue curve and piston motion. Therefore, it can be concluded that COV of NIMEP is a strong function of the burn duration and the position of the maximum COV of pressure trace with respect to TDC. COV of NIMEP is caused by the phasing of pressure variations with piston motion, not by the magnitude of the cylinder pressure variations. It is also notable that the peak of the blue curve is always at around the average CA50 timing (2~3 CAD before). This large pressure variation around CA50 timing might be attributed to the large burn rate changes caused around CA50 timing. Flame front reaches close to the combustion chamber wall at CA50 timing due to much lower density of burned gas than that of unburned gas. Whether the flame front touches the wall or not could result in significant differences in the burn velocities as burn rate is proportional to the flame area (and velocity). However, more study is required to fully understand the reason behind the specific magnitudes of the coefficient of variations of in-cylinder pressures.

To find the equation of the general shape of the COV of pressure traces, COV of pressure traces were plotted for different spark timings. Among three COV of pressure trace graphs in Figure 3-18, COV is normalized w.r.t. mean of maximum COV curve and CAD is normalized by the burn duration on the right graph. This normalizing method shows a very nice clustered graphs.

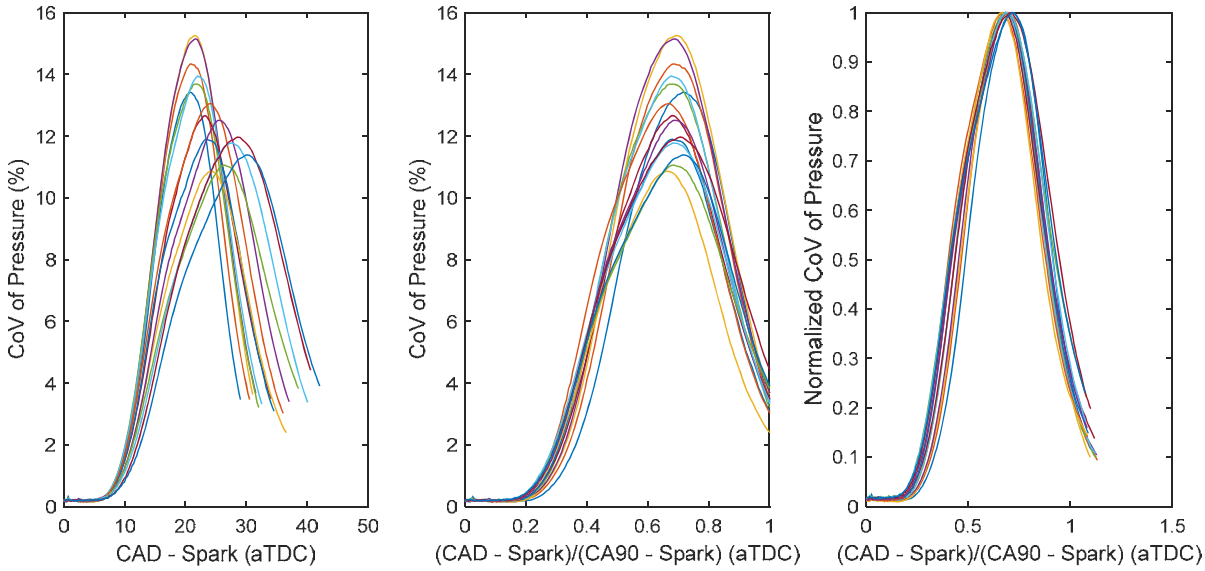

Figure 3-18: COV of cylinder pressure traces vs. CAD w.r.t. spark timing (left), normalized combustion duration (medium), and normalized COV of cylinder pressure traces vs. normalized combustion duration (right). E85 tested at 2000 rpm and 1.1 abs bar MAP.

Figure 3-19 shows the right graph in Figure 3-18 with better resolutions, and a 2nd order Gaussian model was fitted.

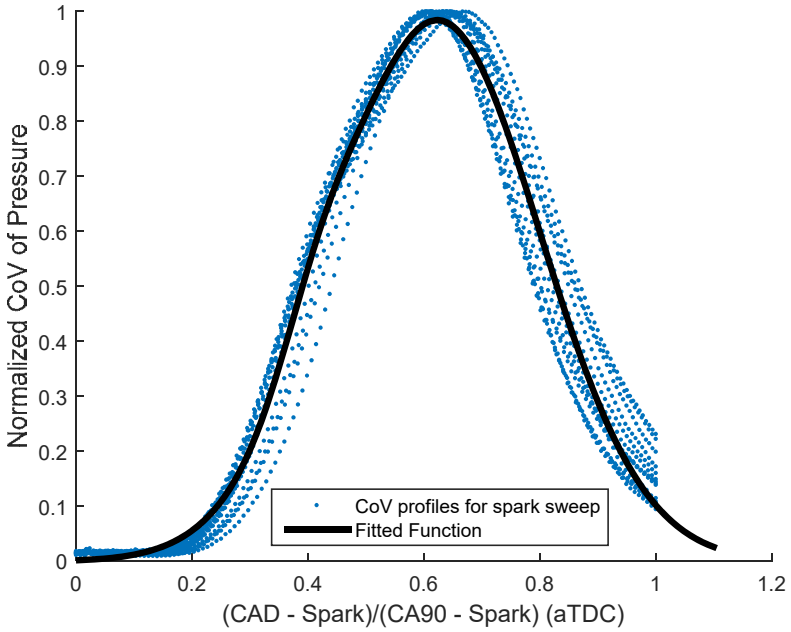

Figure 3-19: Normalized COV of cylinder pressure traces vs. normalized combustion duration (blue dots) with best fitting curve (black line). E85 tested at 2000 rpm and 1.1 abs bar MAP.

Using this general shape function, it is possible to estimate PV shape variations. The attempts were made to predict maximum and minimum NIMEP for a given average pressure traces for a spark sweep. Figure 3-20 shows the spark sweep results.

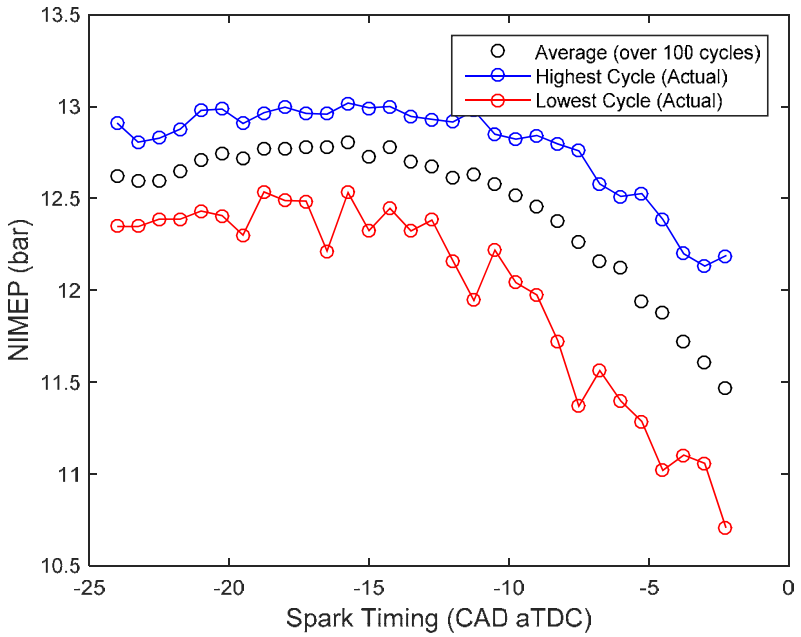

Figure 3-20: NIMEP vs. Spark timing of E85 tested at 2000 rpm and 1.1 abs bar MAP. Black, blue, and red dots denote the average NIMEP over 100 cycles, highest NIMEP among 100 cycles, and lowest NIMEP among 100 cycles respectively.

Using COV of pressure variations, a standard deviation was calculated backwards, knowing the average of pressure traces. Then looking at the distribution of NIEMP, it was possible to estimate the lowest and highest NIMEPs only using the mean pressure profile as shown in Figure 3-21. The model estimates the maximum and minimum NIMEP well, but the estimation does not work with advanced timings relative to MBT; the model calculates variations to go to zero. It was because the model estimates maximum and minimum NIMEP by estimating PV diagram change during the combustion duration (from spark to CA90 timing) only. As shown in previous graphs (from 3-14 to 3-17), in-cylinder variations affect the area variations of PV diagram less with advanced spark timing. Therefore with very advanced timing, the model assumes there is no variation in the area while there is a variation due to pressure variations in the later parts of the expansion stroke. More work has to be done to include effects of in-cylinder variations during the latter part of the expansion stroke.

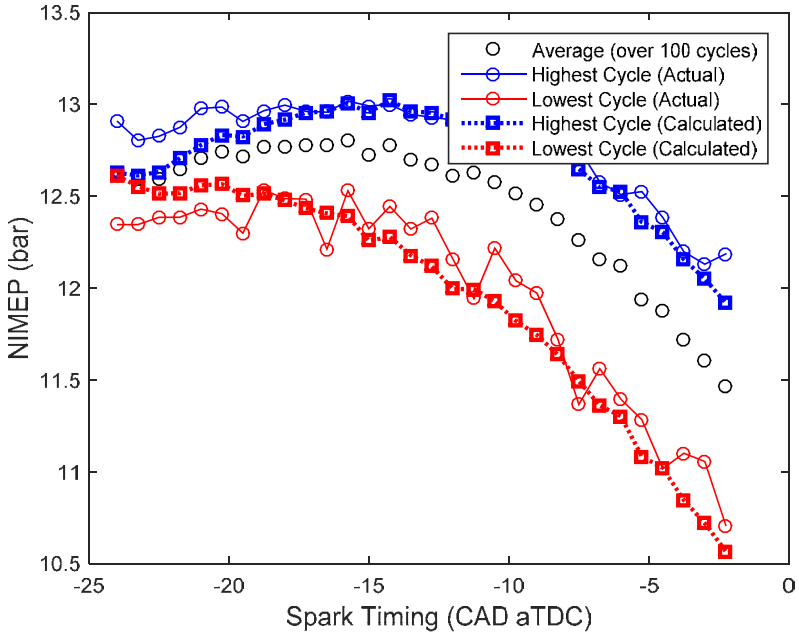

Figure 3-21: NIMEP vs. Spark timing of E85 tested at 2000 rpm and 1.1 abs bar MAP. Black, blue, and red dots denote the average NIMEP over 100 cycles, highest NIMEP among 100 cycles, and lowest NIMEP among 100 cycles respectively. Dark colors represent simulated results.

4. Understanding Octane Requirements

The engine experiments were conducted to superimpose knock limits of various fuel blends on the performance map efficiency contours. First, brake efficiencies of the engine were measured using E85 (85% ethanol and 15% 91 RON gasoline) fuel so that the efficiencies could be measured always at MBT timing without knocking. Then, knock limits of various fuel blends in Table 2 were tested.

Table 4-1: Fuel blends test matrix

PRF Blends	PRF 100 (100% isooctane), PRF90 (90% isooctane and 10% n-heptane), PRF85, PRF80, PRF75, PRF65, PRF50, PRF25, PRF 0 (100% n-heptane)
Gasoline-ethanol Blends	E0 (91 RON gasoline), E10 (90% 91 RON gasoline with 10% ethanol), E20, E25, E85
Engine Speed (RPM)	1500, 2000, 2500, 3000
Engine Load	Full range (0.3 bar MAP to Wide Open Throttle, WOT)

To quantify the octane requirements of a production turbocharged engine over a wide operating range, engine experiments are done with 14 different fuel blends (PRF blends and gasoline-ethanol blends, properties listed on Table 4-2) using a turbocharged engine to construct the octane requirement map even at very low loads that have not previously been explored. The GT-Power simulation and a drive cycle simulation tool called Autonomie (developed by Argonne national lab) were utilized to run 135 simulations to analyze how the octane requirements of driving cycles change with cycle characteristics, levels of downsizing, and spark retard strategies.

Table 4-2: Properties of the gasoline-ethanol blends tested

Fuels Tested	Gasoline (RON 91)	E10	E20	E50	E85	Ethanol (E100)	Methanol (M100)
LHV (MJ/kg)	43.3	41.7	40	36	31	27	20
HoV (kJ/kg)	~350	N/A	N/A	N/A	N/A	840	1103
A/F ratio	14.6	14	13.5	11.7	9.8	9	6.5
RON	90.5	95	99	105	107.8	108	107

4.1 Definition of Knock Limits

The knock characteristics of the engine depend on many variables: engine speed, engine load, intake temperature, spark timing, etc. Therefore, the octane requirements of the engine has to be defined on a three-dimensional map (like an engine performance map) rather than by a single value. This section will discuss how the octane requirement map was generated for the production turbocharged spark-ignition engine used. To produce the map, knock limits of various fuel has to be defined thoroughly.

MBT CA50 determination

For a given fuel at a given engine speed, engine load was increased up to the point where the spark timing has to be retarded from MBT timing to prevent knock onset. That point was called the knock limit (or knock limited engine load) of the fuel at that fixed engine speed. To accurately determine the knock limit, it was necessary to understand how MBT timing changes with engine load or speed and to determine the knock-limited spark advance (KLSA) timing of a fuel.

By doing a spark sweep, it is not easy to accurately determine MBT timing only by definition. MBT timing is when the torque output is maximum, but torque output (or indicated work output) does not vary much with spark timing around the MBT point. A method was developed to be consistent in defining the MBT timing. Ayala, Gerty, and Heywood, at MIT, have done spark sweeps for a range of engine speeds, loads, compression ratios, and different fuels. They developed a general equation that well correlated NIMEP and Crank Angle of 50% burn point (CA50) as shown below [15].

$$\frac{\text{NIMEP}}{\text{NIMEP}_{\text{MBT}}} = 1 - 0.168[\left(1 + 0.0044(\theta_{CA50} - \theta_{CA50,MBT})^2\right)^{0.5} - 1] \tag{4.1}$$

Since Equation (4.1) can be applied to a wide range of loads, speeds, and fuels, the equation was utilized to find the best fit MBT point. For each spark timing, the equation was fitted assuming that the point is the MBT. Then the mean squared error (MSE) between the fitted curve and the actual NIMEP values was calculated using the equation (4.2) below:

$$\text{MSE} = \frac{1}{n}\sum_{i=1}^{n}(NIMEP_{actual} - NIMEP_{expected})^2 \tag{4.2}$$

where n is the number of spark sweep points, $NIMEP_{actual}$ is the experimentally measured NIEMP, and $NIMEP_{expected}$ is the expected NIMEP calculated from Equation 1. Figure 4-1 shows the actual spark sweep results and which MBT point gives the best fit to the known spark sweep trends.

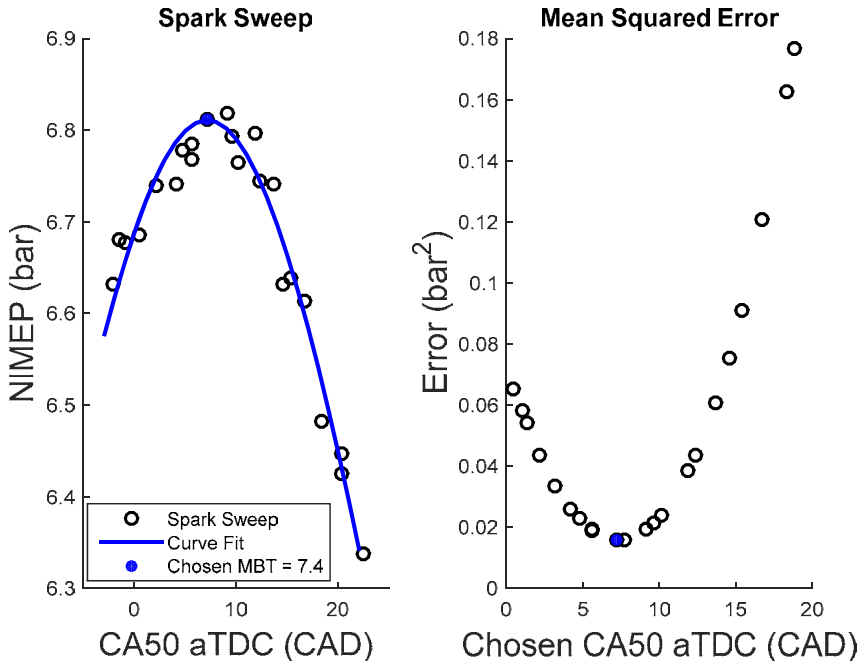

Figure 4-1: A spark sweep results (NIMEP vs CA50 timing) at 1500 rpm around 6.8 bar NIMEP. An MSE was calculated for each point, and the best fitting MBT CA50 timing (with the lowest error) was determined to be at 7.4 CAD aTDC in this case. The blue curve is a graph drawn assuming that the chosen point is MBT timing.

The point with the least MSE is the best candidate for MBT timing as it fits the known trend the best. In this case, MBT timing of 7.4 Crank Angle Degree (CAD) after Top Dead Center (aTDC) gives the least MSE, and the blue curve is a good fit to the spark sweep results. This methodology was used for about 50 sets of complete spark sweeps without knock. Then the results were analyzed to see if there is any significant trend of MBT timing with respect to engine speed or load. It was found that the MBT CA50 timing does not change much with load, but it changes moderately with engine speed. The correlation between MBT CA50 timing and engine speed is shown in Figure 4-2. MBT CA50 timing changes from 9.3 CAD aTDC to 7.3 CAD aTDC when the engine speed changed from 1500 rpm to 3000 rpm.

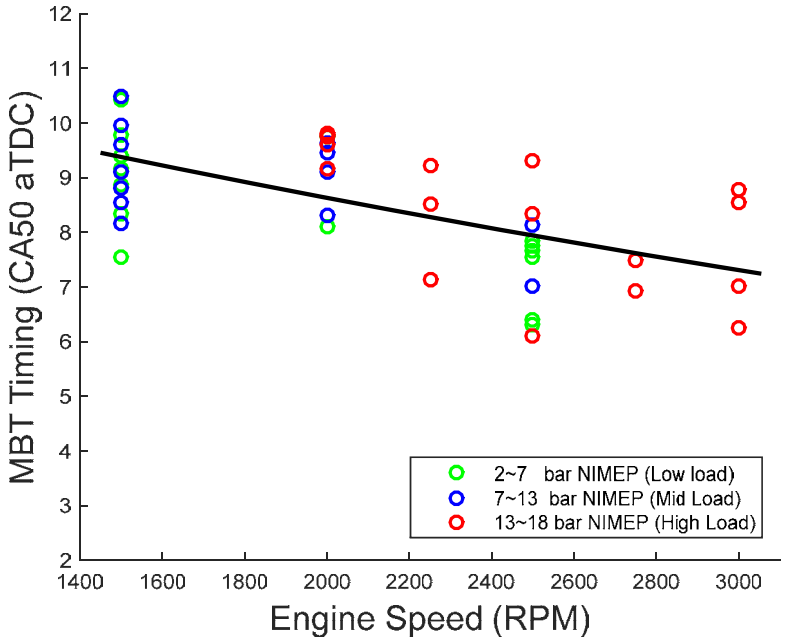

Figure 4-2: A collection of MBT timings in CA50 aTDC vs engine speeds in RPM. Data points are color-coded by three different load intervals. The black line shows the best fitting line across the data points.

Knock limited spark advance boundaries

After tightly defining the MBT timing of a spark sweep, knock limited BMEP were determined along with KLSA lines. Figure 4 shows KLSA of PRF75 (75% isooctane and 25% n-heptane) fuel at three different speeds. For fixed speeds, four sets of spark sweeps were done at different engine loads. For each spark sweep, spark timing was advanced until knock onset (defined below), and this specific timing was defined as a KLSA timing.

Pressure traces of 100 cycles were collected for each spark timing, and high-pass filtered pressure traces were analyzed to determine a knock intensity (maximum peak to peak pressure oscillation). The operating point was said to be knocking when it satisfies two conditions; 1) it had a maximum knock intensity (KI) more than 2 bar, and 2) 10% or more cycles have more than 1 bar KI. Using this standard, a KLSA boundary was generated by fitting a curve to KLSA timing points determined at various loads. In Figure 4-3, the engine can be operated without knock below the KLSA boundary, while knocking occurs above the boundary line.

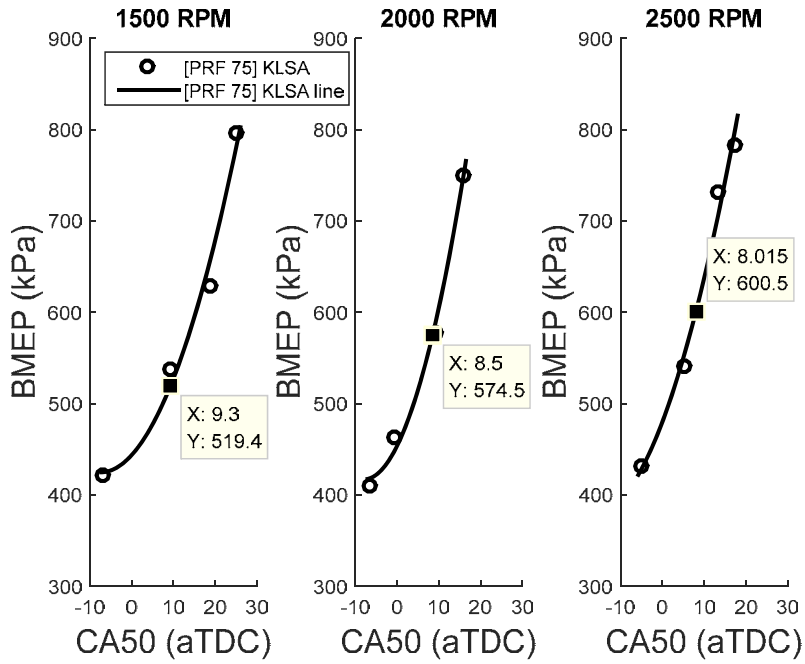

Figure 4-3: Knock limited spark advance timing of PRF 75 (75% isooctane and 25% n-heptane) at three different speeds. For each speed, 4 sets of spark sweeps are done to find the knock limited spark advance timing at different loads. Points with a data-tips (text boxes) represent the knock limits at MBT timing.

Once MBT CA50 timings are known for different speeds, knock limits can be found easily. MBT timing cannot be achieved above 520 kPa BMEP at 1500 rpm, so the knock limited BMEP of PRF75 fuel at 1500 rpm is 520 kPa. As engine speed increases, knock limited BMEP increases slightly, but not by much. This procedure was applied to all 14 fuels tested (both PRF blends and gasoline-ethanol blends). Results at 1500 rpm are shown in Figure 4-4 (results at other engine speeds are shown in Figure 4-5 and 4-6). KLSA boundaries were generated in terms of BMEP, NIMEP, and GIMEP.

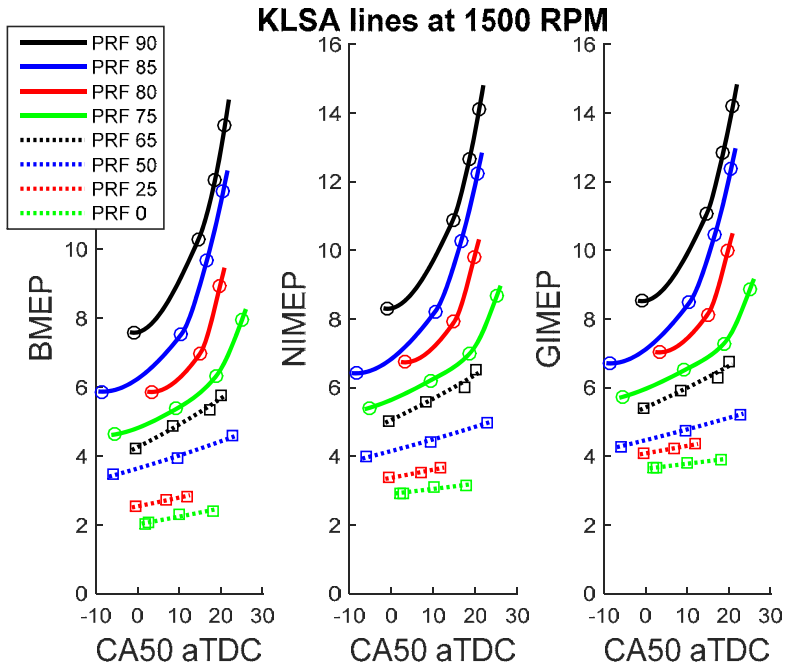

Figure 4-4: Knock limited spark advance timing of PRF 0 (100% n-heptane) through PRF 90 (90% isooctane and 10% n-heptane) at 1500 rpm. For each fuel, KLSA boundaries were generated for BMEP, NIMEP, and GIMEP.

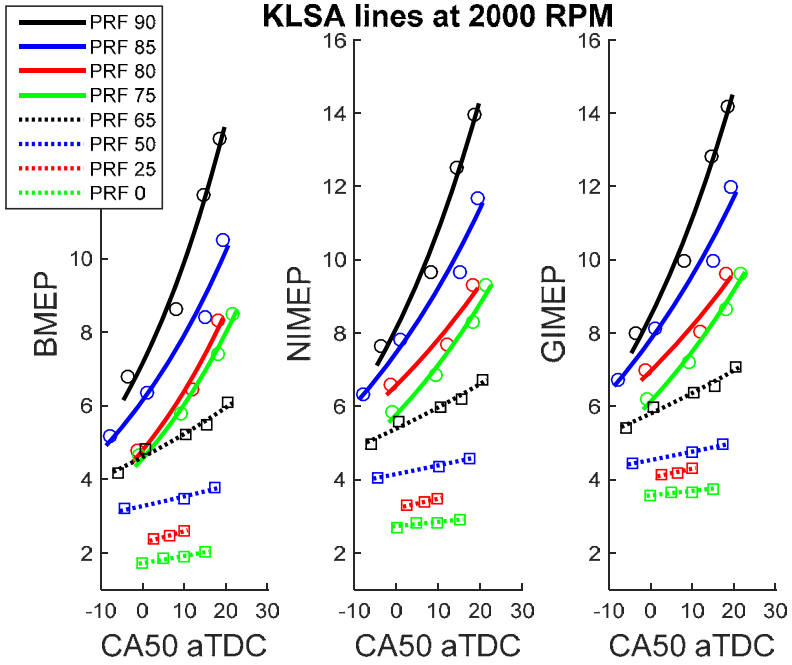

Figure 4-5: Knock limited spark advance timing of PRF 0 (100% n-heptane) through PRF 90 (90% isooctane and 10% n-heptane) at 2000 rpm. For each fuel, KLSA boundaries were generated for BMEP, NIMEP, and GIMEP.

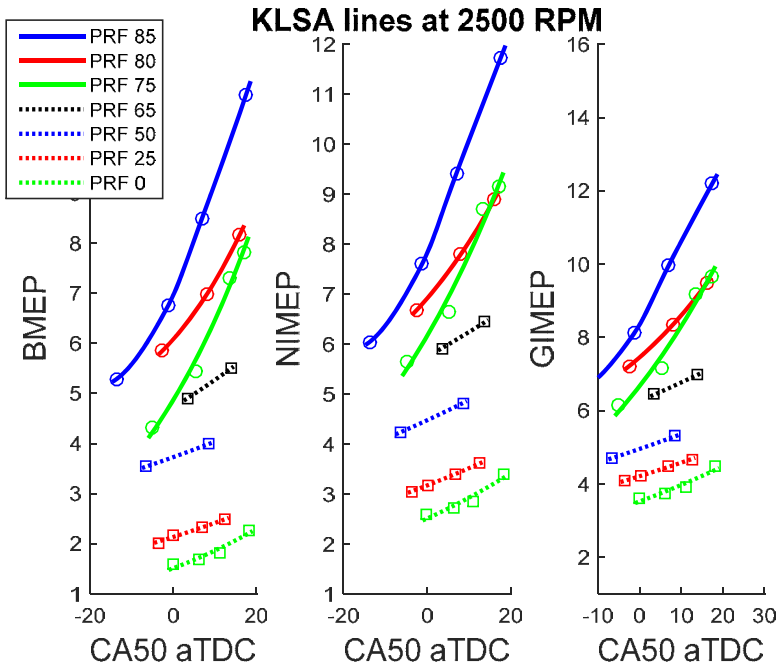

Figure 4-6: Knock limited spark advance timing of PRF 0 (100% n-heptane) through PRF 90 (90% isooctane and 10% n-heptane) at 2500 rpm. For each fuel, KLSA boundaries were generated for BMEP, NIMEP, and GIMEP.

BMEP is the engine work output normalized by the displaced volume. Removing friction effects from BMEP results in slightly higher knock limit for NIMEP. Then, excluding pumping work from NIMEP shows the highest knock limits for GIMEP. However, the knock limit increase, from BMEP to GIMEP, is smaller at higher loads (7.6 to 8.5 bar for PRF90 while 2.0 to 3.7 bar for PRF0). This is because relative effects of pumping and friction get lower as the engine load increases. Utilizing knock limited spark advance lines of different octane rating fuels, knock limits of the engine at different speeds and loads can be constructed. The combined results will be shown in the section 4.3.

Effect of spark retard, engine speed, and valve timing

Spark timing effects

It is well known that the knock limits (or knock limited engine loads) increase with spark retard. The knock limit increase with spark retard is higher for high octane fuels than for low octane fuel. With 18 CAD retard in CA50 timing, the knock limit increased by 4.5 bar BMEP for PRF90,

while it increased only 0.4 bar BMEP for PRF0. In this research, the phrase 'knock limit increase' means that knock is less constraining, as the knock limit refers to knock limited engine load. Visually, the KLSA curve becomes much steeper with increasing retard at higher loads than at lower loads. Because a pressure drop is higher with spark retards at higher loads than at lower loads, it can be inferred that the spark retard becomes more effective in suppressing knock at higher loads. Figure 4-7 shows how, with increasing retard, the average peak pressure drops at different engine loads. Retarding 10 CAD from MBT timing, peak pressure only dropped about 8 bar at a light load (0.4 bar MAP), while it dropped about 25 bar at a high load (1.2 bar MAP).

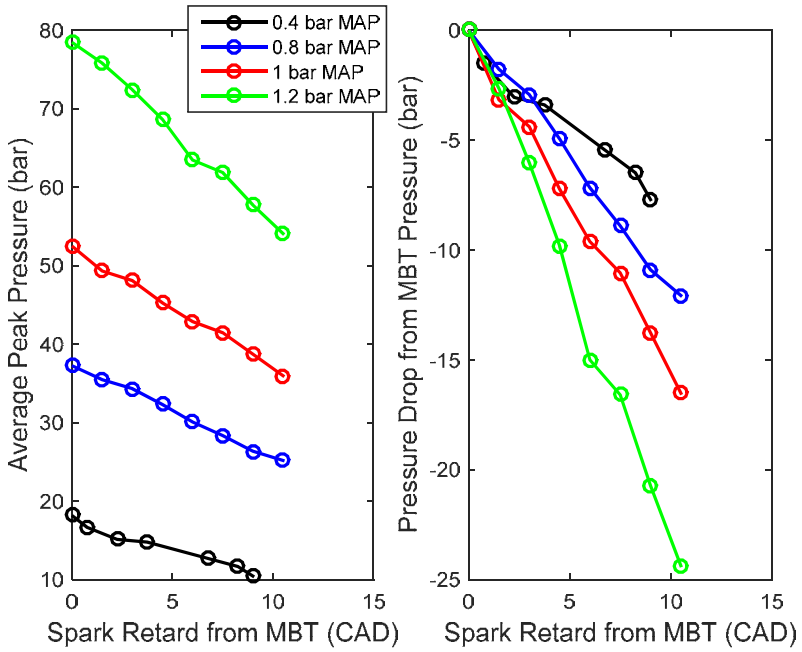

Figure 4-7: Average peak pressure change with spark timing at 1500 rpm. Left graph shows the actual peak pressure, and the right graph shows the relative drop of the peak pressure with spark retard.

Engine speed effects

It is generally expected that the engine tends to knock less at higher speeds since time available for autoignition is shorter, reducing chances of knock. Therefore, it is understood that knock limits increase with engine speeds. However, knock limits in BMEP do not increase as much as expected. To explain this phenomenon, two operating points (1500 rpm and 2500 rpm at 5.5 bar BMEP) with knocking conditions are considered as shown below in Table 4-3. A fuel used for the engine test is PRF75.

Table 4-3: Knocking conditions comparison for 1500 rpm and 2500 rpm

	1500 rpm	**2500 rpm**
BMEP	5.4 bar	5.5 bar
Average Knock Onset Time	0.0056 sec	0.0038 sec
Maximum Knock Intensity	2.04	2.64
Knock Frequency	0.11	0.11
Spark Timing	-32.25 aTDC	-42 aTDC
Peak Pressure	34.9 bar	39.5 bar

Both cases are chosen so that both operating points are at a comparable BMEP level with similar knocking characteristics in terms of knock intensity and knock frequency. To check if knocking characteristics are similar, the actual pressure profiles of knocking cycles are plotted in Figure 4-8. Since knock frequency is 0.11 for both cases, and data of 100 cycles are collected, and each figure contains knocking pressure traces of eleven cycles.

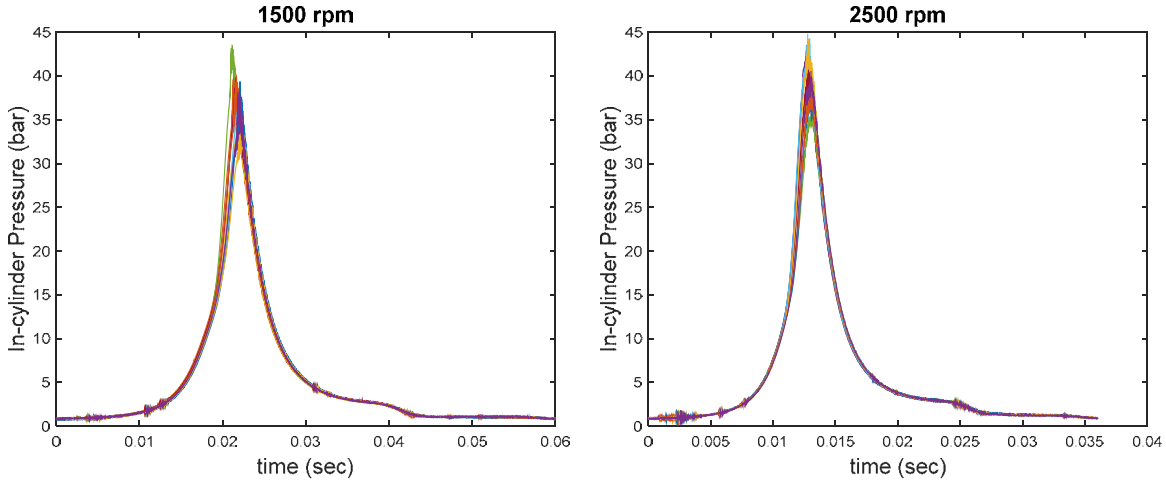

Figure 4-8: In-cylinder pressure traces of knocking cycles of the engine running at 1500 rpm (left) and 2500 rpm (right)

As it can be seen from Figure 4-8 and from peak pressure values shown in Table 4-3, one important difference is that in-cylinder peak pressure is higher at 2500 rpm than at 1500 rpm regardless of the comparable BMEP level. This is due to higher friction losses at higher engine speeds: in-cylinder pressure has to be higher at higher speed to result in the same BMEP as in lower speed. Higher engine speed case shows generally higher pressure in the compression stoke

than lower engine speed case as shown in Figure 4-9, which would influence the temperature level inside the cylinder. Therefore, with higher pressure and temperature levels, ignition delay time would be shorter at higher speeds. This would lead to knock in reduced time at higher speeds.

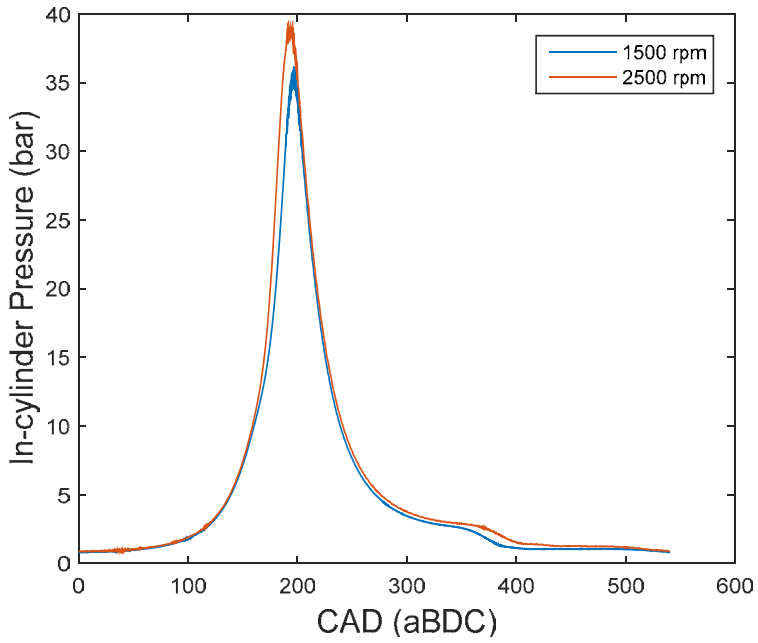

Figure 4-9: Averaged pressure profiles of knocking cycles for two cases shown in Figure 4-8.

Intake valve close timing effects

Intake valve close (IVC) timing affects pressure and temperature of the mixture at the beginning of the mixture compression as effective compression starts with IVC. Therefore, IVC timing affects the overall pressure and temperature of the mixture during the compression process. Later IVC timing gives lower pressure and temperature, therefore increasing knock limits. Exhaust valve timings were kept at a fixed position at a given engine load and speed. Therefore, valve overlap decreased with later IVC timing due to later intake valve opening. To quantify the knock suppression capacity, a set of experiments were conducted as shown in Table 4-4.

Table 4-4: Test matrix of IVC timing experiments

Fuel	E10 (RON91 base)
Speed	2000 rpm
Load	1.0,1.1,1.2,1.3 bar MAP (0.1 bar increments)
Spark Timing	Spark sweep
Valve timing	IVC: 10 to 60 CA aBDC (10 CA increments) Exhaust valve: follow GM's calibration map, (valve closing of 20~25 CAD aTDC depending on the engine speed and load).

E10 fuel was chosen so it represents the premium gasoline that is required by manufacturer of the engine tested. At 6 different IVC timings, knock limits were determined by finding KLSA at various engine loads. Figure 4-10 shows knock intensity and knock frequency change with spark advance at 6 different IVC timings. Both knock intensity and knock frequency increase with spark advance. With later IVC timings, knock intensity and knock frequency increase with spark advance is less, as effective compression ratios are lower. Knock suppression capability of later IVC timing becomes substantial after 40 aBDC (after Bottom Dead Center).

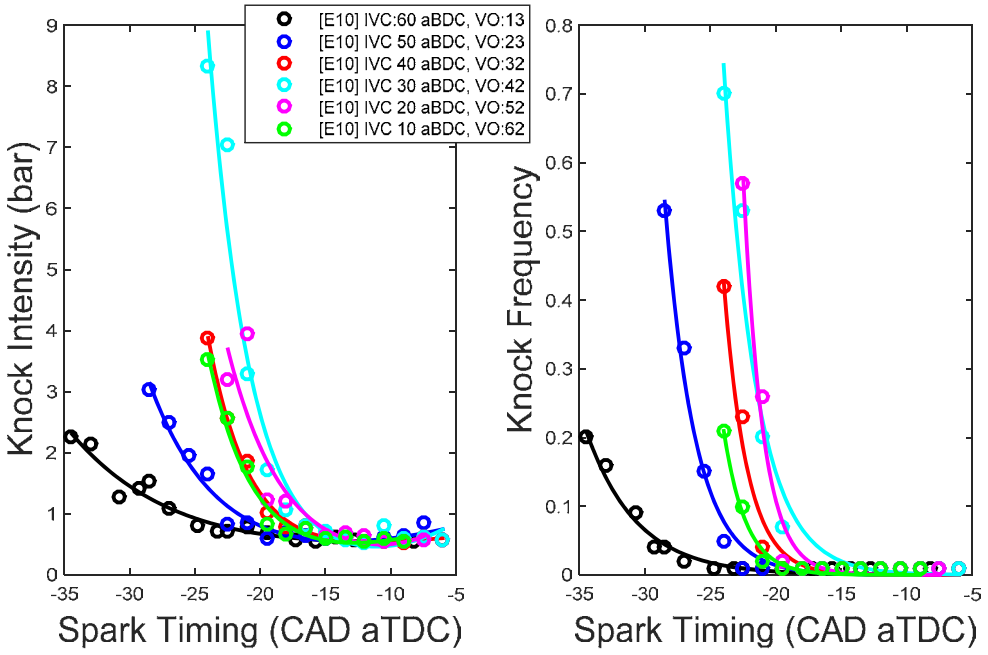

Figure 4-10: Knock intensity and knock frequency of spark sweeps at different IVC timings. Different IVCs are noted by different colors. All the spark sweeps are done at 1.0 bar intake MAP at 2000 rpm.

Utilizing results shown in Figure 4-10 for four different engine loads, knock limited spark advance timings could be determined for different IVC timings. Figure 4-11 shows four sets of spark sweep results with a fixed IVC timing at 60 CAD aBDC. The same graph can be generated at different IVC timing (from 10 CAD aBDC to 60 CAD a BDC), and knock limited BMEP at MBT timing can be found as done in Figure 4-4. Then, knock limited BMEP at different IVC timings could be determined, which could be translated as knock suppression capability of later IVC timings. Results are shown in Figure 4-12.

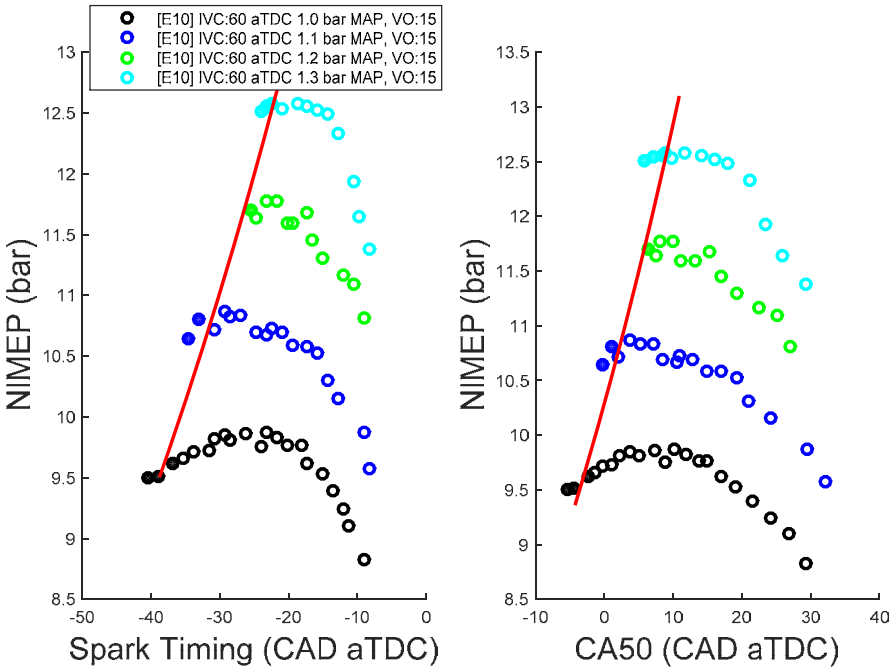

Figure 4-11: Knock limited spark advance in terms of spark timing (left) and CA50 timing (right) at IVC of 60 CAD aBDC

Changing IVC timing from 10 CAD aBDC to 60 CAD aBDC increases knock limits from 10 bar to 13.5 bar in NIMEP. This effect is similar as increasing octane of a fuel from 90.5 to 96.5 RON. One interesting feature of this result is that knock limits do not increase much by changing IVC from 10 to 20 CAD aBDC. This is expected as volume change is not significant in this region. However, more analysis should be done in the future to figure out why knock limits do not change significantly from 50 CAD aBDC to 60 CAD aBDC. Possible reasons are the amount of residuals and the effect of valve lift. Also note the effective compression ratio calculated for different IVC timings. In this case, the effective compression ratio only accounts for the initial compression volume change incurred by a late intake valve closing.

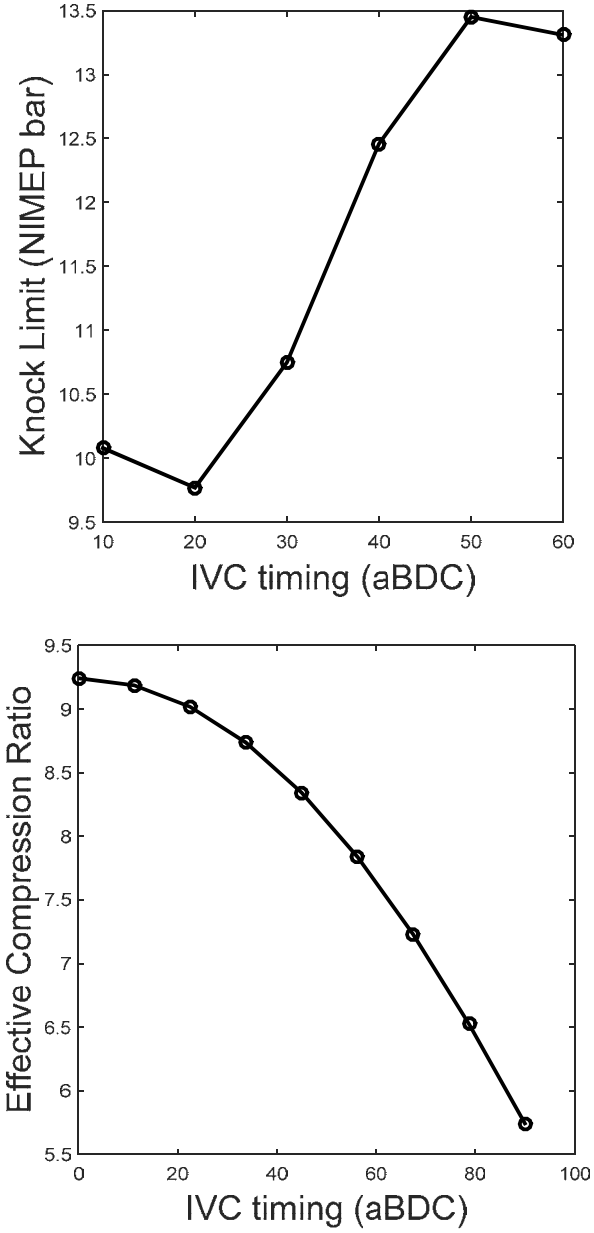

Figure 4-12: Knock limits at MBT timing vs IVC timings, fuel tested is E10 (right) and the effective compression ratio vs IVC timings

4.2 Knock Limits at Higher Compression Ratios

Knock limits explored above are determined at a compression ratio of 9.2:1. As mentioned in Chapter 2, GT-Power model of the engine was used to simulate performance of the engine at different geometries which include different compression ratios. Also, engine experiments were conducted by Cummins as a part of DOE program that the current research project was involved.

Higher compression ratio engine experiments

Cummins has done engine experiments using a single-cylinder test engine with 107mm bore and 124mm stroke giving a 1.1 liter displacement volume. The table below shows the test variables and their tested range.

Table 4-5: Cummins Test Matrix

Configurations	**Tested Range**
Compression Ratio	9.5 and 13
Speed	1500 and 2500 rpm
Ethanol Fraction	0, 85%, 100% 30% only at 13 CR
MAP	0.4, 0.5, 0.6, ... In bar

In this section, results of gasoline, E30, and E85 fuels tested on 13:1 compression ratio engine will be presented. Figure 4-13 shows a set of spark sweeps done using gasoline fuel at 1500 rpm. By finding knock onset points of spark sweeps done at different loads, it is possible to find the knock limited spark advance timing. On the right side of Figure 4-13, net indicated thermal efficiency (NTE) is plotted. NTE increases with a diminishing return as engine load increases, and efficiency stays almost constant above 0.6 bar MAP due to knock limits.

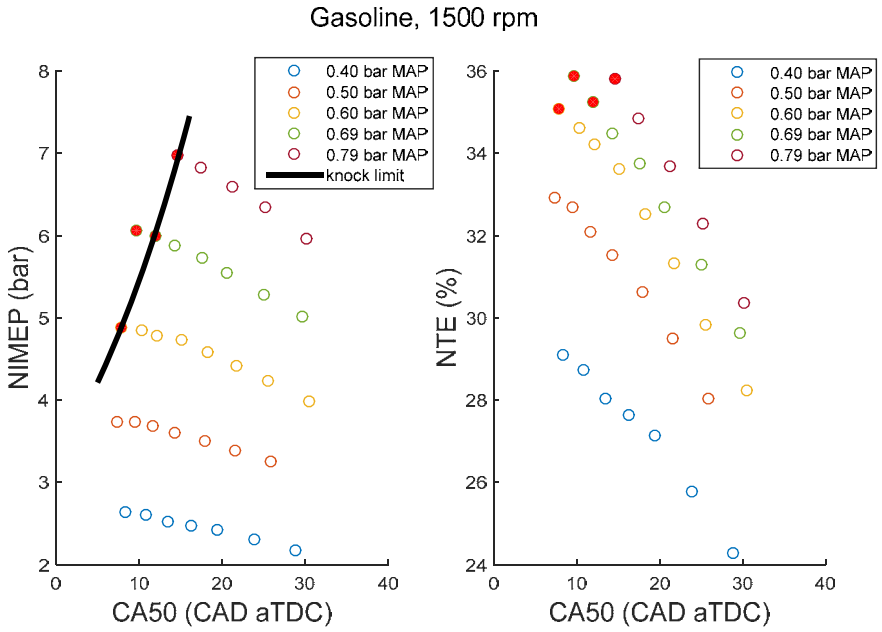

Figure 4-13: Spark sweep results at 1500 RPM using gasoline with engine configuration of 13:1 compression ratio. Each color represents a set of spark sweep at a fixed MAP, and the MAP was changed in the increment of 0.1 bar. NIEMP vs CA50 timing (left) and Net indicated efficiency vs. CA50 timing (right). Knocking points are noted by filled markers.

Figure 4-14 and 4-15 shows the same results as in Figure 4-13 but with E30 and E85, respectively. It can be clearly seen that the knock boundaries are higher than gasoline case.

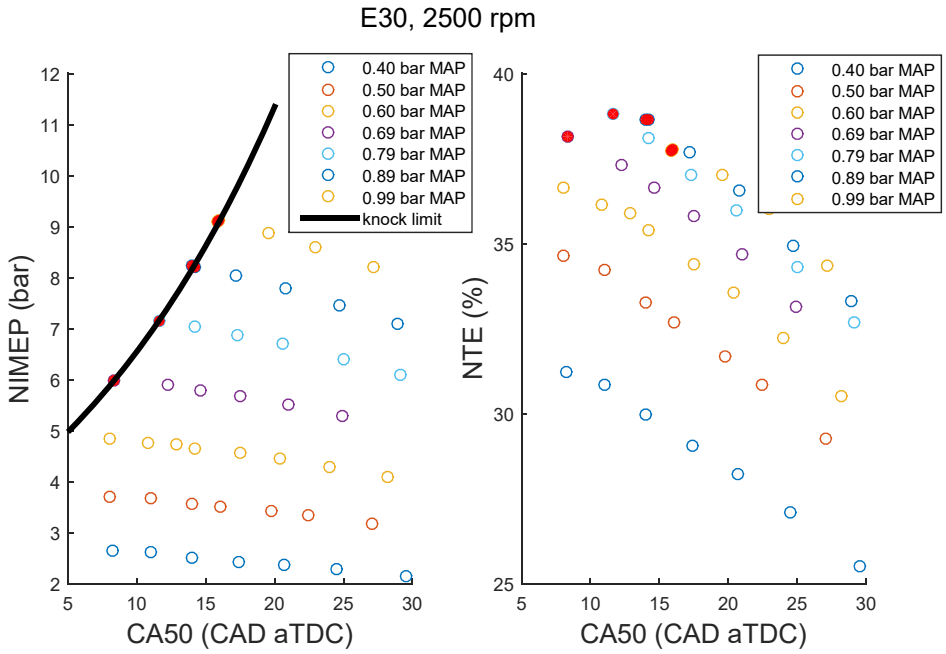

Figure 4-14: Spark sweep results at 2500 RPM using E30 with engine configuration of 13:1 compression ratio. Each color represents a set of spark sweep at a fixed MAP, and the MAP was changed in the increment of 0.1 bar. NIEMP vs CA50 timing (left) and Net indicated efficiency vs. CA50 timing (right). Knocking points are noted by filled markers.

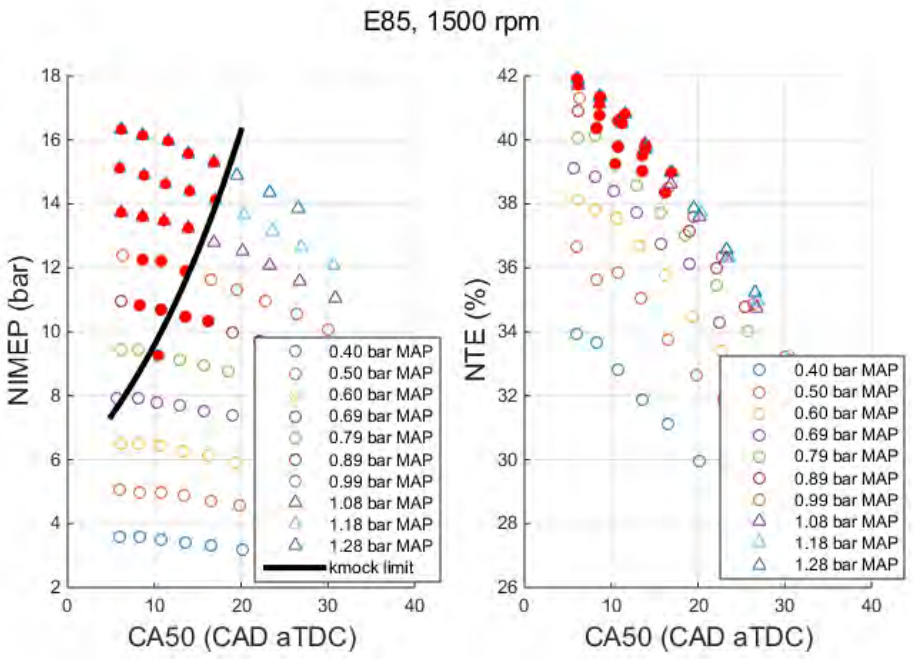

Figure 4-15: Spark sweep results at 1500 RPM using E85 with engine configuration of 13:1 compression ratio. Each color represents a set of spark sweep at a fixed MAP, and the MAP was changed in the increment of 0.1 bar. NIEMP vs CA50 timing (left) and Net indicated efficiency vs. CA50 timing (right). Knocking points are noted by filled markers.

Also, efficiencies also increased up to 37% for E30 compared to 35% of gasoline. This is mainly due to knock suppression of ethanol at higher loads. E85 shows the highest efficiencies of 38% with much higher knock limits. Then, spark sweep results are utilized to plot efficiencies at MBT timing at different loads. Figure 4-16~18 show efficiency at MBT timing vs engine loads for two compression ratios for fuels shown in previous figures. For a constant load, efficiency is higher at higher compression ratio, but knock limit is lower at higher compression ratio. Knock limits increase with higher ethanol contents, and efficiency increases accordingly (E85 at 13:1 compression ratio reaches efficiency close to 40% around 9 bar NIMEP).

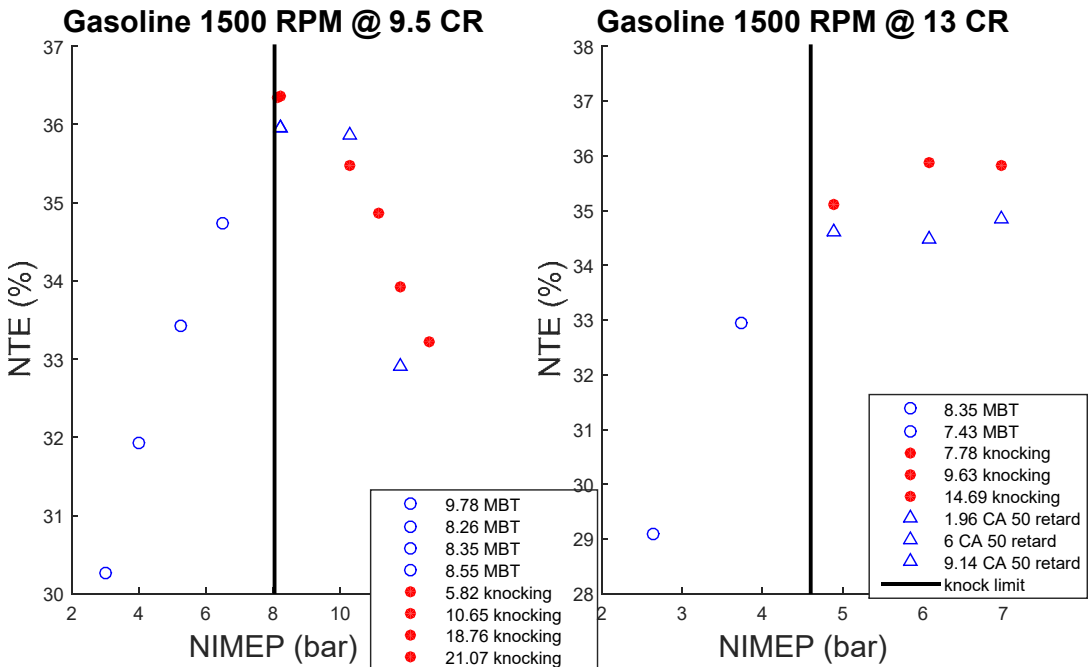

Figure 4-16: Net indicated thermal efficiency vs engine load in NIMEP for two compression ratios, 9.5:1 on the left and 13:1 on the right. Un-filled markers indicate MBT timings, filled red markers indicate knock onset, and black line is knock limited engine load in NIMEP. Tested fuel is gasoline.

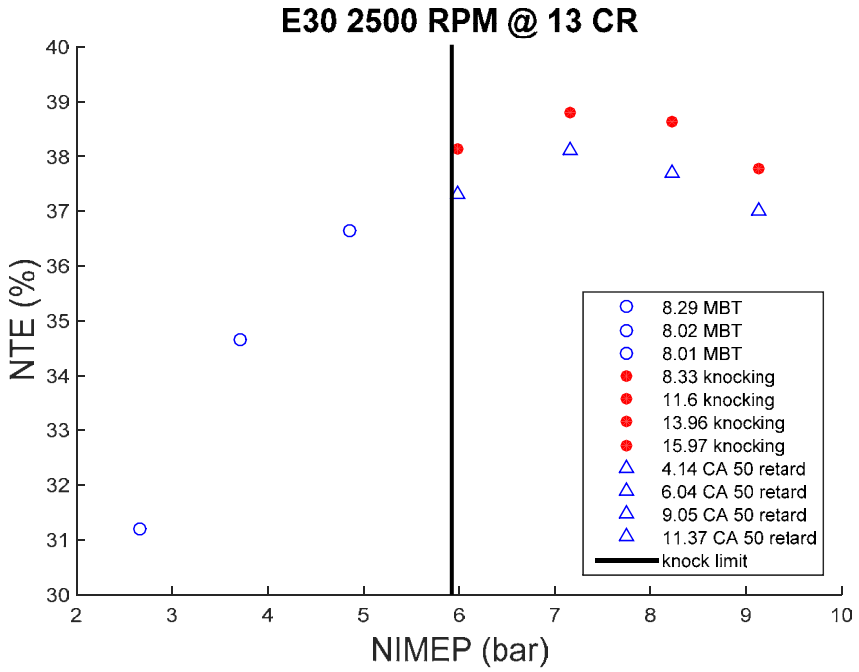

Figure 4-17: Net indicated thermal efficiency vs engine load in NIMEP for two compression ratios, 9.5:1 on the left and 13:1 on the right. Un-filled markers indicate MBT timings, filled red markers indicate knock onset, and black line is knock limited engine load in NIMEP. Tested fuel is E30.

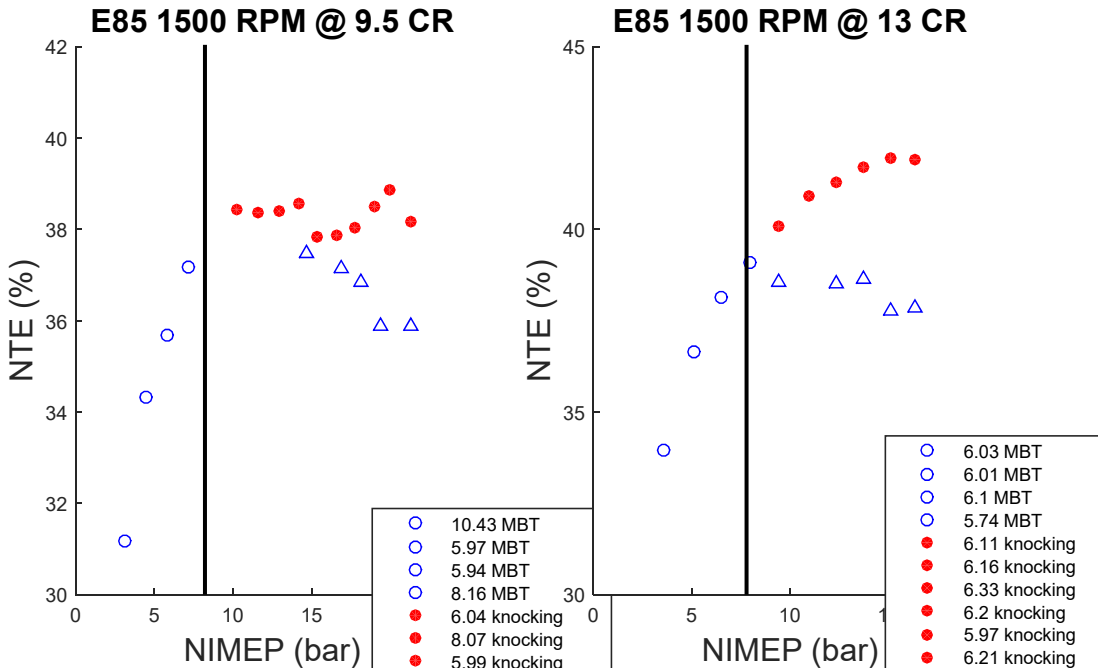

Figure 4-18: Net indicated thermal efficiency vs engine load in NIMEP for two compression ratios, 9.5:1 on the left and 13:1 on the right. Un-filled markers indicate MBT timings, filled red markers indicate knock onset, and black line is knock limited engine load in NIMEP. Tested fuel is E85.

Autoignition Integral for knock onset determination

To find the knock onset point using pressure and temperature profiles calculated from GT-Power model of the engine, it is assumed that the autoignition reaction can be modeled as a one–step Arrhenius reaction with a time constant τ. At each point in the cycle the reaction can be said to progress by an amount equal to $\int \frac{\mathrm{dt}}{\tau}$. Knock onset (KO) can be said to occur when the value of the integral reaches 1. In these sets of calculations the integration is carried out through the time at the peak pressure because at low speeds knock onset occurs at peak pressure.

$$\int_{IVC}^{KO} \frac{dt}{\tau} = 1 \tag{4.4}$$

The correlation used in this paper is as follows. [55]

$$\tau = 17.68\left(\frac{\mathrm{ON}}{100}\right)^{3.402} \mathrm{p}^{-1.7} \exp\left(\frac{3800}{\mathrm{T}}\right) \tag{4.5}$$

Here τ is in milliseconds, ON is the effective octane number, p is the in-cylinder pressure in bars and T is the temperature of the unburned mixture in Kelvin. GT-Power was used to calculate the ethanol requirement to suppress knock at each point by using the knock integral approach at each speed tested. This was done by using a PID controller to force the value of the autoignition integral to reach one by adjusting the throttle and wastegate in the simulation accordingly for a given fuel blend. To generate an upper bound on the knock onset lines, the bounds of the integral were set from the time of IVC to that of peak pressure. For each fuel tested a knock onset line was determined from GT-Power and superimposed on the performance map.

Equation (4.5) was used to solve for the octane number for experimentally determined knock conditions; the results are shown in Table 4-6, which also includes results from a previous study [39]. Here the effective octane number appears consistently higher than the previous results. The difference could be broken down into two components, the evaporative cooling octane number and the engine to engine differences.

Evaporative octane number benefit is the increase in the effective octane number due to charge cooling during fuel evaporation. In direct injection, the fuel is injected into the cylinder as a liquid and evaporates, therefore reducing the temperature of the mixture due to the fuel's latent heat of vaporization. This has the effect of improving the knock resistant properties of the fuel, an effect that is quantified using octane numbers. Here it is assumed that the benefit due to evaporative cooling benefit is 7 for gasoline and 20 for ethanol, numbers based on a previous study [23]. Those results are compared in Table 4-6. An additional factor is the difference between the current engine test operating conditions and those in the CFR test engine used to determine the gasoline RON, which could be up to two octane numbers. These two effects could account for the difference between current and previous studies.

Table 4-6: Effective octane number calculated from experimental pressure and simulated temperature profiles.

Fuel	**Effective Octane Number**	**Research Octane Number [39]**	**Variations due to Evaporative Octane Number**
RON 91	91	91	-
RON 96	97	96	-
E10	100	95	8.3
E20	105	99	9.6
E25	111	100	10

At low speeds, knock limit of simulation matches well to that of engine experiment when integral bound is at peak pressure. However, comparing simulation to experiment, it was determined that the knock limit is less dependent on speed than that calculated by the simulation. It was found out that the reason for this behavior is that at higher speeds knock onset occurs after peak pressure occurs. The autoignition integral upper bound was adjusted to consider cases where knock could occur after peak pressure. By extending the integral upper bound from peak pressure to 5 CAD after peak pressure, knock limited BMEP decreased from 1200 kPa to 800 kPa at 2000 rpm. Results including the 5 CAD increase in the upper bound of the integral are shown in Figure 4-19.

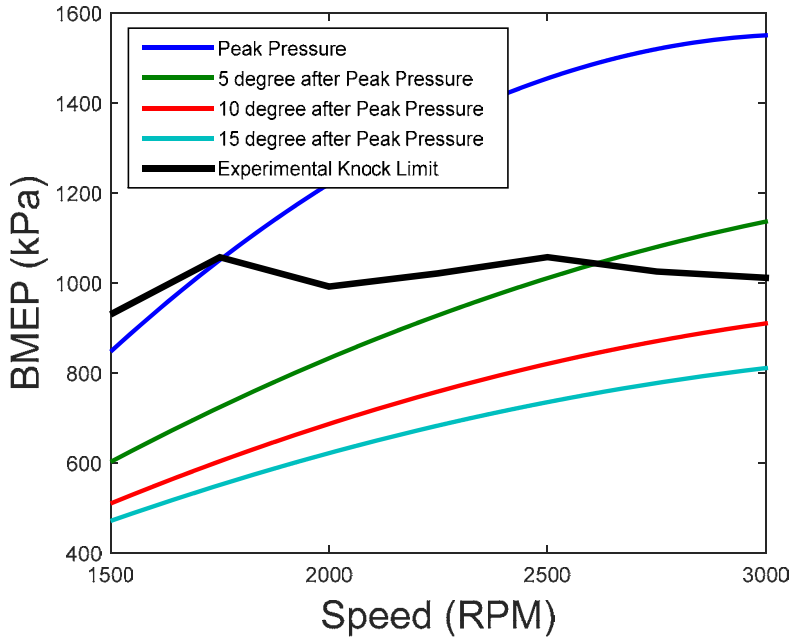

Figure 4-19: Change of knock limits in BMEP with knock onset occurring at different points with respect to the location of a peak in-cylinder pressure. A black line is knock limits determined by engine experiments while other colors represent simulation results with different integral bounds.

4.3 Octane Requirement Map

Using the knock limits of the 14 different octane fuels at 4 different engine speeds, it was possible to generate the octane requirement map. Knowing the octane number of the fuel required to suppress knock at various speeds and loads, 3-dimensional interpolation was done to generate the octane requirement surface.

The octane requirement map

The octane requirement map was mainly based on the knock limits over-imposed on the performance map of the engine. Figure 4-20 shows knock limits, in-cylinder peak pressure limits, and WOT limits over-imposed on the efficiency contour of the engine. Instead of using efficiency as a z-axis, RON limit values can be used as a z-axis to construct an octane requirement contour rather than an efficiency contour.

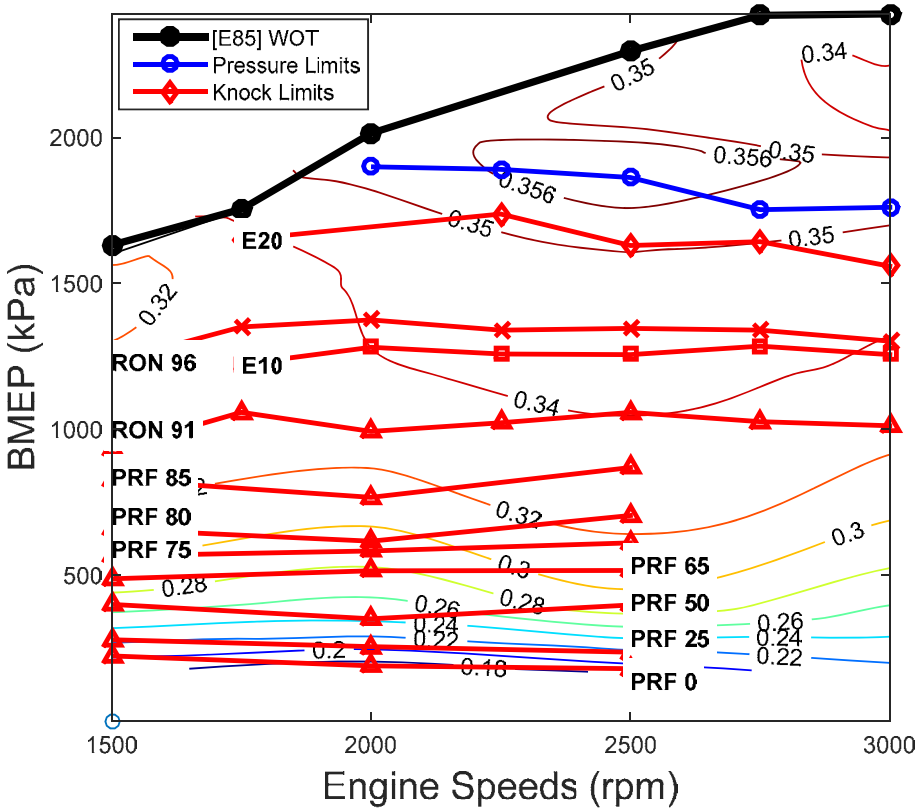

Figure 4-20: Knock limits (red line), in-cylinder peak pressure limits (blue line), and wide open throttle limits (black line) imposed on the efficiency contour. Knock limits of different fuel blends are noted by a text box. MBT operation at every point except above pressure limits.

A 2-dimensional version with contours is shown in Figure 4-21. The black dashed line is the WOT limit, the maximum BMEP achievable by maximum turbocharger boost, and the blue dashed line is the peak pressure limit; above the blue line, spark timing has to be retarded not because of knock but because of the hardware (in-cylinder peak pressure) limitations.

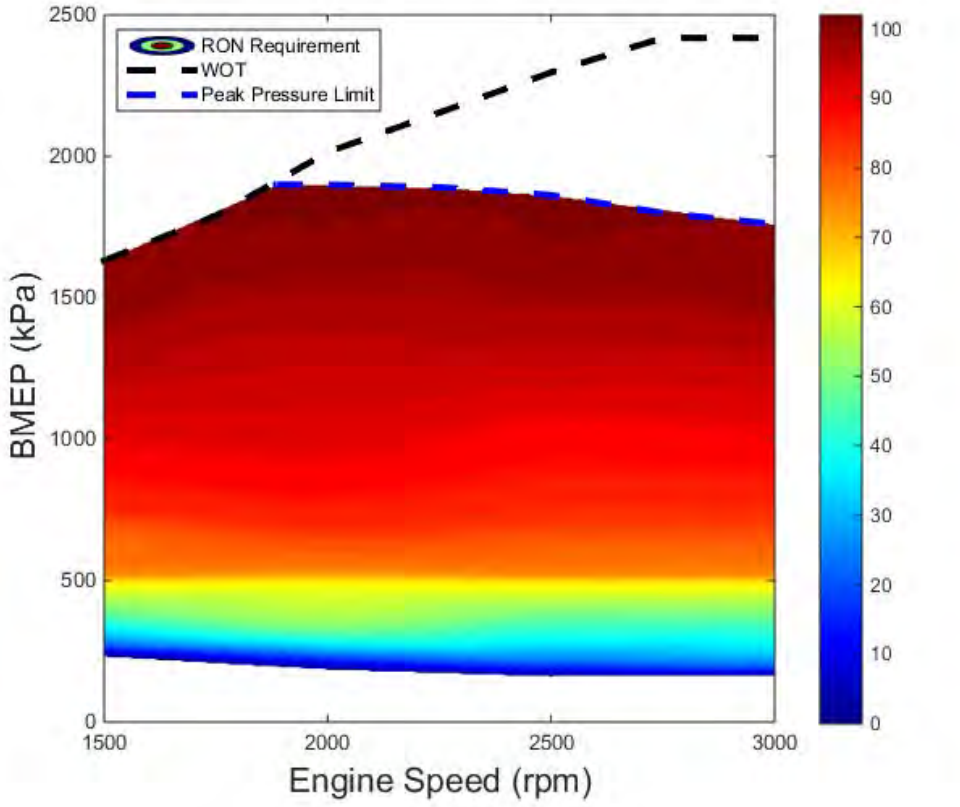

Figure 4-21: Octane requirement map with WOT and peak pressure limits. The 3-dimensional surface was translated to a 2-dimensional octane requirement contour with color codes. Colors and the corresponding octane numbers are shown in the bar next to the map.

From the octane requirement contours, which RON fuel is required at a given load can be determined. For example at 500 kPa BMEP at 2000 rpm, about 65 RON fuel is good enough for the engine to operate at MBT timing. However, above 500 kPa BMEP, higher octane fuel has to be used or spark timing has to be retarded. Looking at the color of the map, the majority of the map is in red (above 75 RON) while the region below 600 kPa contains the majority of the other colors. To better understand this, RON requirements were plotted against engine load (BMEP) in Figure 4-22.

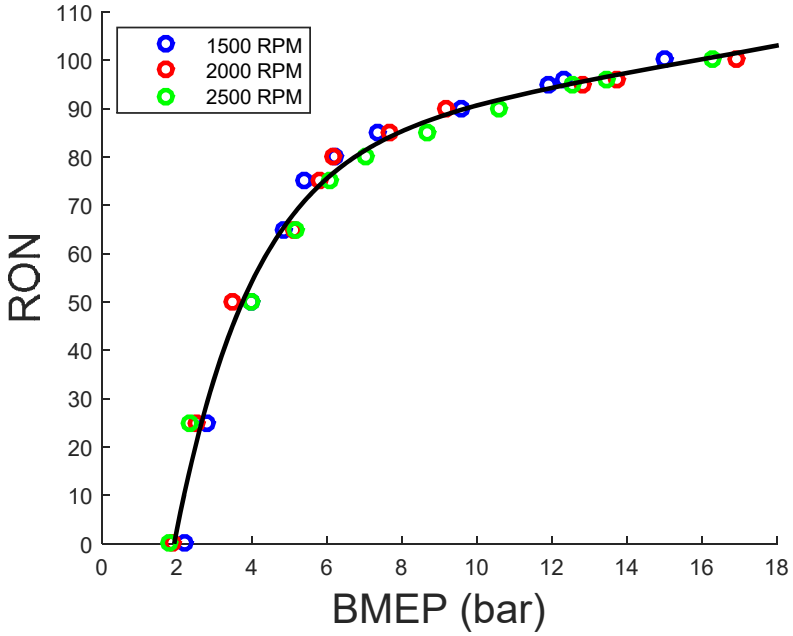

Figure 4-22: Knock limits (RON) vs engine load (BMEP). Different speeds were indicated with different colors

Increasing RON from 0 to 50 gives only a 2 bar BMEP increase in the knock limits while increasing RON from 50 to 100 gives a 16 bar increase in knock limits. Since pressure levels increase almost linearly with BMEP, the shape of the graph suggests that the knock suppression capability increases non-linearly as isooctane contents increase. This can also be verified by considering the autoignition integral equation developed by Douaud and Eyzat as shown in Equation (4.5). Even though Douaud and Eyzat formulated this equation by testing PRFs whose octane numbers range from 80 to 100, Equation (4.5) show that the ignition delay time increases with octane number raised to the power 3.4. At very light loads, there is additional difficulty of very large residuals, which could depress the required RON to avoid knock. At higher BMEP, the residuals are substantially decreased.

Octane requirement and load metrics

It is thought that knock limits increase with engine speed as there is less time for autoignition to develop. However, knock limits in terms of BMEP do not increase much with increasing speeds as mentioned in a previous section. This is because in-cylinder pressure levels increase with increasing speed at a constant BMEP: constant BMEP does not necessarily correspond to a constant in-cylinder pressure level. In addition, at constant BMEP and increased engine speed,

the engine generates more power and the cylinder walls are hotter. The left figure in Figure 9 shows that at 5 bar BMEP, the average in-cylinder peak pressure increases from 30 bar to almost 40 bar. This is because higher in-cylinder pressures are required at faster engine speeds to overcome higher friction losses. This is confirmed by the right hand graphs in Figure 4-23. At a constant GIMEP, pressure levels do not change much with engine speed since mechanical friction effects are not included. Figure 4-24 shows how knock limits change with different engine work output measures.

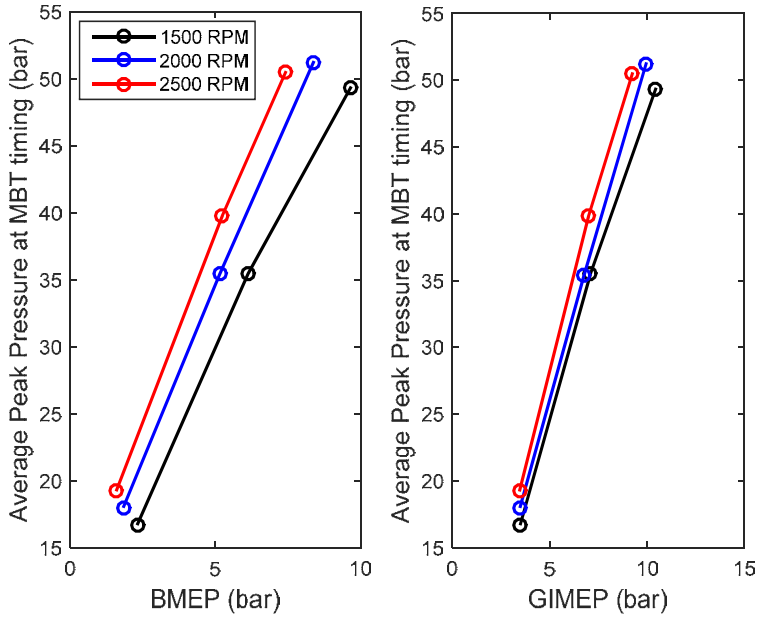

Figure 4-23: Average peak pressure at MBT timing for three engine speeds plotted against BMEP and GIMEP.

When expressed in GIMEP, knock limits generally increase with increasing speed since the effects of pumping and mechanical friction are not present. Adding pumping, the knock limits in NIMEP are decreased. Adding mechanical friction, the knock limits decrease with engine speed for very low octane fuels as relative impact of mechanical frictions is high at low loads.

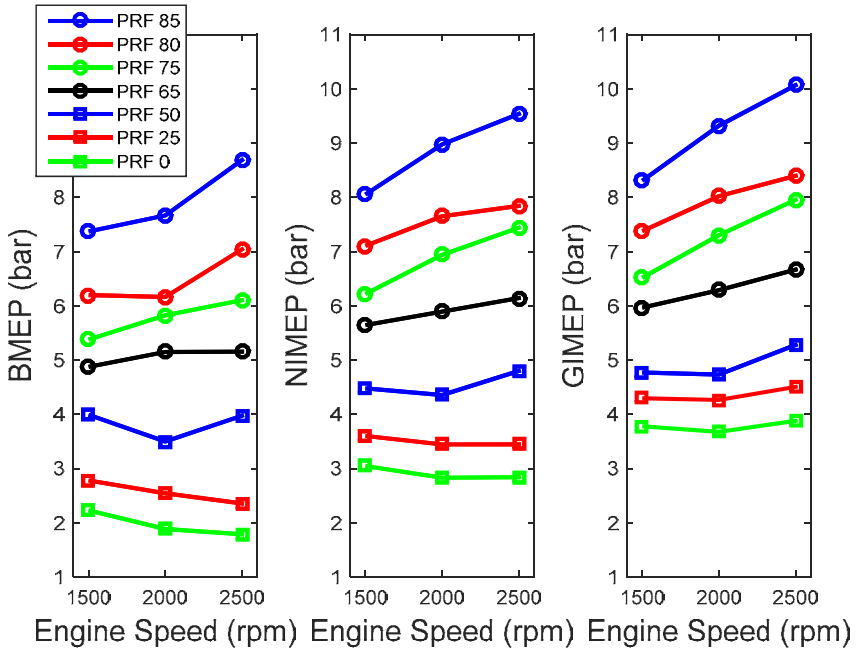

Figure 4-24: Knock limits in BMEP, NIMEP, and GIMEP vs engine speeds. Different fuels were indicated with different colors and marker shapes.

Knock Onset Calculations

We have developed a methodology for knock onset calculations, using the experimentally determined results in our MIT engine, at two different points and with two very different fuels.

The experimentally determined results in our MIT engine, at three different points, was first used to evaluate the performance with primary reference fuels. We have performed a large number of simulations with GTPower to evaluate the behavior, not of the average cycle (which does not knock), but for different individual cycles. There are substantial differences in the details of the pressure (and temperature) profiles for the cases investigated, even though the coefficient of variation of indicated mean equivalent pressure (COV of IMEP) are comparable. The residuals were not included in initial calculations, and we needed to develop the methodology to determine their level.

Table 4-7 shows the main parameters for three operating points, all of them at knocking conditions. The fuels used were primary reference fuels. Shown in the table are the type of fuel used, the maximum knocking intensity, frequency of knocking cycles (defined as knock intensity

> 1), the maximum and minimum peak pressures (over 100 cycles) and the mean standard deviation of the peak pressure.

The first column shows the results for operation at part load and 2500 rpm, using a PRF 80 fuel. There is a large spread of peak pressures, with a maximum peak pressure about twice that of the minimum pressure (over 100 cycles). The spread between the maximum peak pressure and minimum peak pressure is lower for the other engine conditions (at lighter loads).

Table 4-7: Characteristics of 3 points that have been evaluated

Fuel	PRF 80	PRF 0	PRF 0
Speed (rpm)	2500	1500	3000
NIMEP (bar)	8.91	3.16	2.57
BMEP (bar)	8.18	2.41	1.52
map (bar)	1	0.48	0.47
CoV (%)	4.09	3.5	2.1
Max knock Intensity	2.26	2.1	2
Knock Frequency	0.13	0.25	0.22
Peak pressure statistics over 100 cycles:			
Average peak pressure	36.2	19.8	20.6
max preak pressure (bar)	50.5	24.0	24.4
min peak pressure (bar)	25.2	15.2	16.5
Average deviation (bar)	4.9	1.7	1.5

Our assumption is that knocking occurs during the cycles with high peak pressure. Figure 4-25 shows the maximum knock intensity as a function of peak pressure for individual cycles, for all 100 cycles of engine data. Indeed, though there is substantially scatter, the figure indicates that as the peak pressure in a given cycle increases, the knocking intensity increases, suggesting a threshold-like behavior.

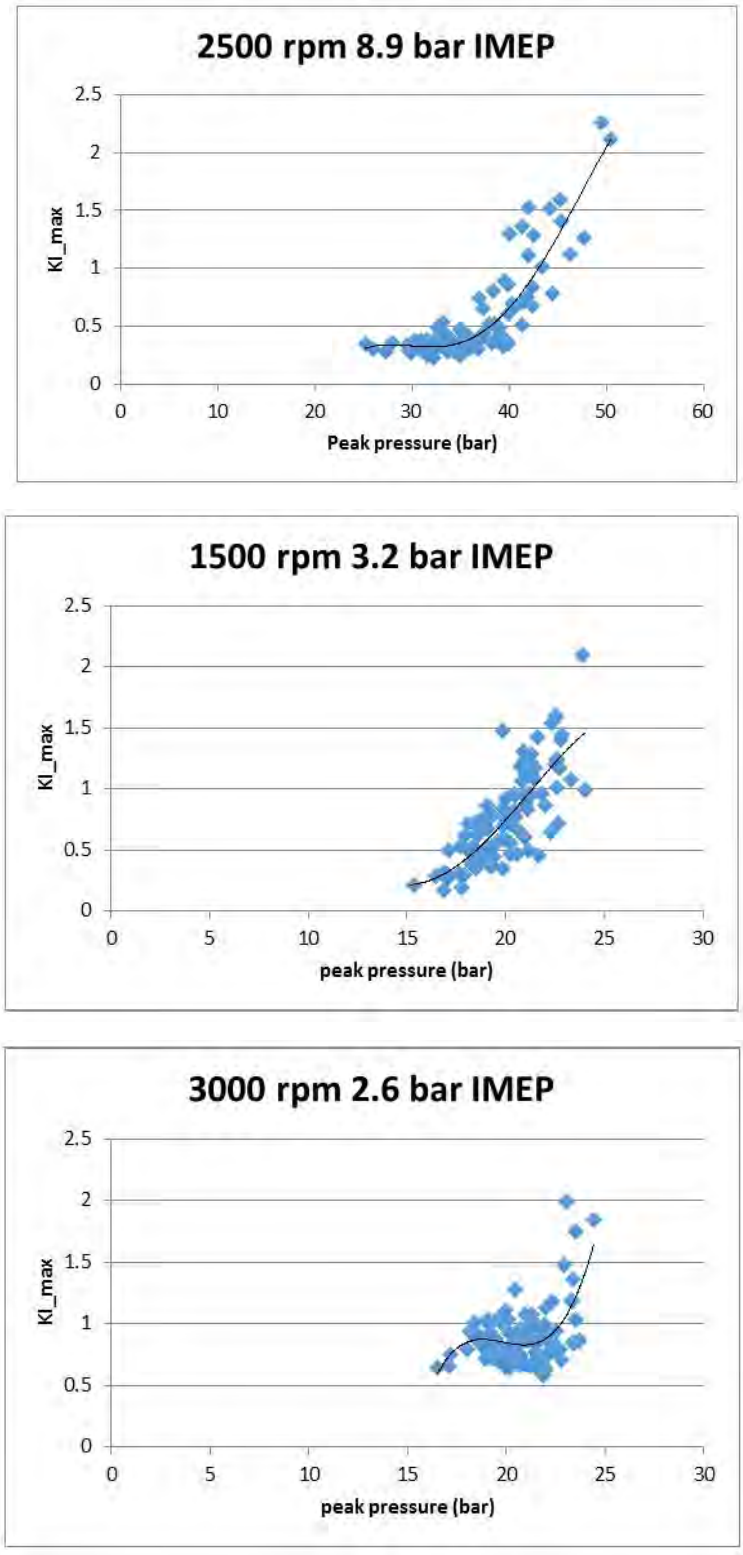

Figure 4-25: Knock intensity as a function of peak pressure for 100 cycles in our engine, for the three different conditions from Table AA

We have investigated, using GTPower, the engine operating conditions that are needed to provide the large spread of peak pressure. We need to investigate the impact of different combustion phasing on the temperature for the cycles, in order to perform autoignition calculations, as shown in previous report for other conditions and other fuels. In the simulation, we have adjusted the engine conditions to simulate the engines operation. Then the combustion timing (CA50) is adjusted to determine the starting temperature for the chemical-kinetic calculations that will be presented during the next section.

Table 4-8: Engine simulation for 8.9 bar BMEP, 2500 rpm conditions

CA50	0	7	30
Peak pressure (bar)	58	50	29
residual mass fraction (SOC)	10%	10%	7.80%
Temperature at 20 CA BTDC	728	730	717
Pressure at 20 CA BTDC	13	13	13.9
Exhaust temp (K)	1162	1190	1370

Table 4-8 shows the results for the case with 8.9 bar BMEP and 2500 rpm. The combustion timing was varied in the simulations from 0 to 30 CA ATDC. Comparing with Table 4-7 it appears that the combustion timing for the maximum pressure cycle (50 bar) corresponds to a combustion timing of 7 CA ATDC. However, for the minimum peak pressure, the simulation indicates that extreme delayed combustion timing is needed, to about 30 CA ATDC (about 27 bar). It should be noted that the engine conditions needed for the chemical kinetics calculations (basically, the amount of residuals, shown in the table at Start of Cycle, SOC, and the temperature at 20 CA BTDC) do not change much as a function of the combustion timing. Thus, we can start the chemical kinetics calculations for this point at 730 K and 10% residuals. We will report on the calculations in the next section.

Table 4-9: Engine simulation for 2.4 bar BMEP, 1500 rpm conditions

CA50	0	7	15	30
Peak pressure (bar)	28	24	20	13.7
residual mass fraction (SOC)	35%	35%	35%	31%
Temperature at 20 CA BTDC	836	838	843	846
Pressure at 20 CA BTDC	8.3	8.3	8.3	8.6
Exhaust temp (K)	915	943	983	1096
Intake pressure (bar)	0.6	0.6	0.6	0.6
Intake temperature (K)	520	525	532	539

Similarly, Table 4-9 shows the results for 2.4 bar BMEP and 1500 rpm, a light load. Very delayed combustion is needed in order to match the low pressure of the extreme cycle (15 bar, in this case). As with the other results, the amount of residuals at the Start Of Cycle (SOC) (at IVC), is about constant, independent of combustion phasing.

Finally, Table 4-10 shows the results for the third case, at very light load and intermediate speeds. The residual mass fraction is lower than in the previous case; however, it is still fairly substantial. The level of residuals is not sensitive to the combustion timing, nor the temperature at 20 CA BTDC.

Table 4-10: Engine simulation for 1.5 bar BMEP, 3000 rpm conditions

CA50	0	10	20	30
Peak pressure (bar)	23	18	14	12
residual mass fraction (SOC)	26%	27%	25%	23%
Temperature at 20 CA BTDC	839	849	845	840
Pressure at 20 CA BTDC	6.4	6.1	6.4	6.8
Exhaust temp (K)	1096	1130	1193	1272
Intake pressure (bar)	0.48	0.46	0.48	0.51
Intake temperature (K)	518	534	530	524

Chemical kinetics calculations

We modeled engine operation a large number of simulations with GTPower for different individual cycles, and determined temperatures prior to combustion. The knock model and additional information from the experiment to determine whether the chemical kinetic can be

used to predict knock. We have confirmed that within a small temperature deviation, the chemical kinetics model in a real engine using primary reference fuels are accurate for predicting knock.

The main difference between these calculation and those that we performed initially is the use of the end-of-combustion (instead of peak pressure) when performing the knock calculations. We have determined the combustion phasing using experimental data. The time (in crank-angle degrees) to combustion 10% and 90% of the fuel (CA10 and CA90, respectively) are shown in Figure 4-26 and 4-27 for two engineoperating conditions, with two different fuels (PRF80 and PRF0, that is, n-heptane). Also shown in the figures are simple linear fits for CA90. It is interesting to note that the spread is similar on both the CA10 and CA90. As expected, as the combustion timing is retarded, the peak pressure decreases.

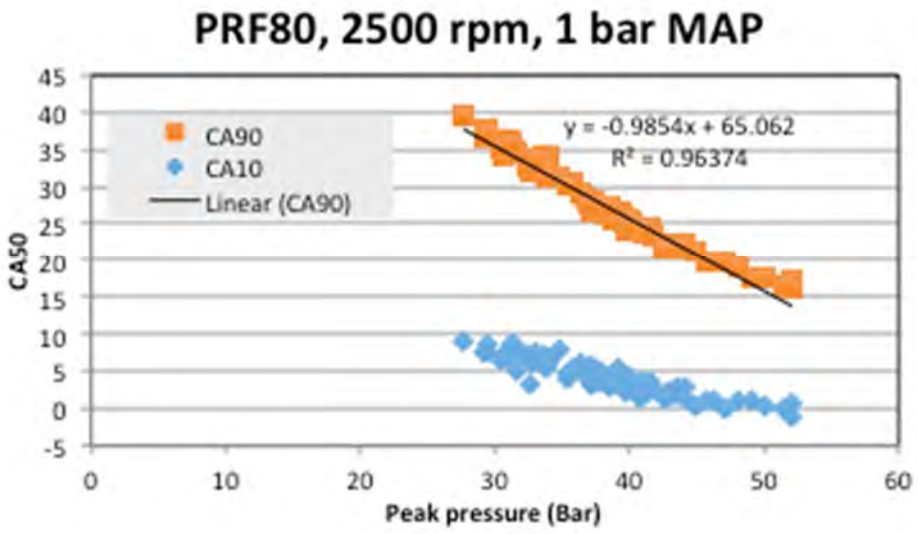

Figure 4-26: CA10 and CA90 for the ECOTEC engine running at 2500 rpm, 1 bar manifold air pressure, for 100 consecutive cycles of engine operating on PRF80.

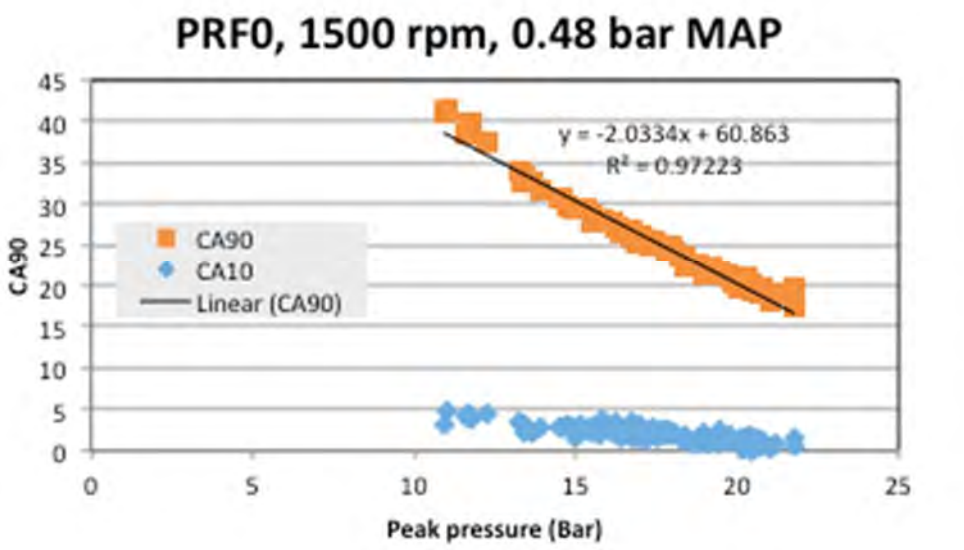

Figure 4-27: CA10 and CA90 for the ECOTEC engine running at 1500 rpm, 0.48 bar manifold air pressure, for 100 consecutive cycles of engine operating on PRF0.

The chemistry is calculated as a function of time using CHEMKIN in the unburnt air-fuel mixture using experimental pressure profiles, using the residuals estimated in the GTPower calculations described in the previous section. The CHEMKIN simulations assume an adiabatic unburnt air-fuel mixture, using the Mehr mechanism. If there is autoignition of the air-fuel mixture prior to CA90 timing, we assume that the model predicts knock. If it happens after, we assume that there is no knock. The region in between is considered the borderline knock condition, for a given operating point. As we can only estimate the temperature (not measured, only interpreted from the engine simulation), we vary the temperature. The CHEMKIN modeling at 20 CA before top dead center (prior to any combustion), and continue through CA90.

The knock conditions are determined from the results presented in the prior report. Only one condition, that at 2500 rpm and 1 bar MAP, is shown in Figure 4-28. The knocking pressure (corresponding to those cycles with Knock-Intensity, KI, > 1) is about 45 bar. For the conditions at 1500 rpm, the knocking pressure (i.e., KI > 1) is about 20 bar. In Figure 4-28, the unburnt temperature (at 20 CA BTDC) required for autoignition is shown for several cycles with different peak pressure. Also shown in Figure 4-28 is the corresponding CA90. For a temperature lower than that shown for a given peak pressure, there no autoignition, while for higher temperature, there is autoignition; the temperatures shown in Figure 4-28 correspond to

"borderline knock". For this case, for a peak pressure of 45 bar (KI > 1), the borderline temperature (at 20 CA BTDC) is about 775K. This temperature compares well with the one estimated from the model with GTPower, which estimates at temperature of about 745 K at 20 CA BTDC, independent of combustion timing. This degree of temperature non-uniformity on cylinder is expected at this time. Thus there is good agreement between the knock model predicting knocking conditions at this operating point.

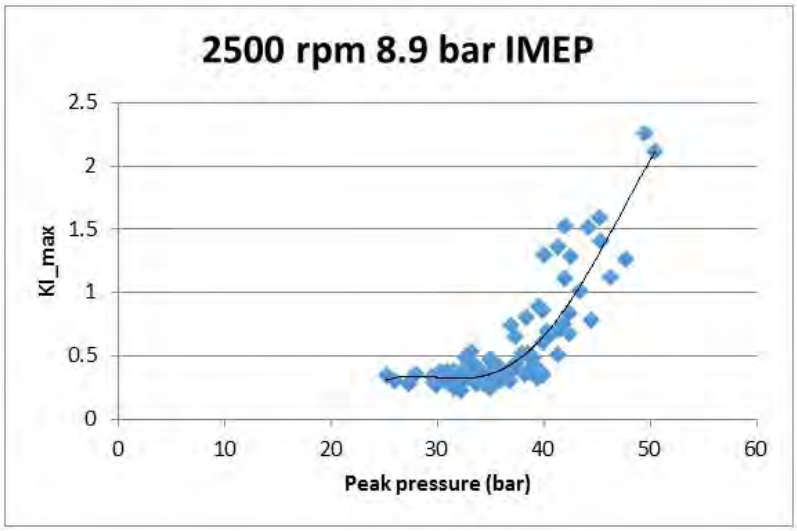

Figure 4-27: Knock intensity as a function of peak pressure for 100 cycles in our engine, for 2500 rpm and 1 bar MAP

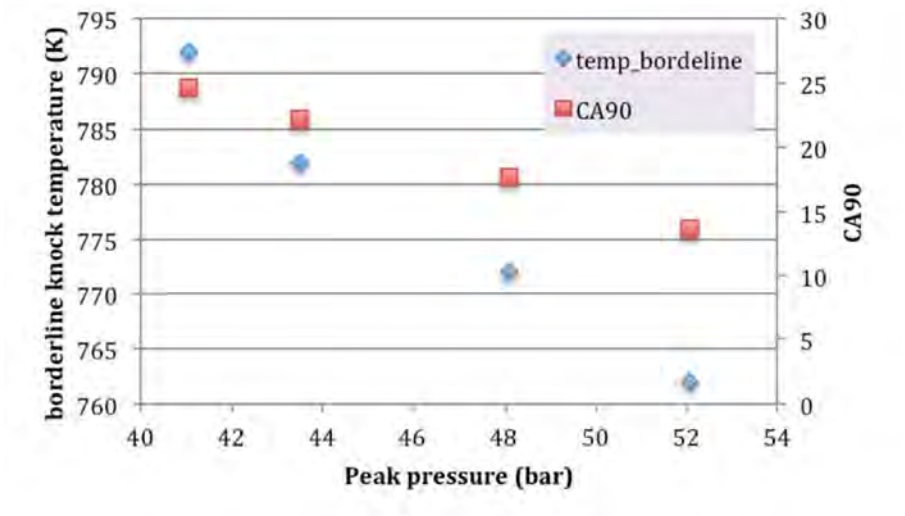

Figure 4-28: Borderline knock temperature (at 20 CA BTDC) vs peak pressure for 4 cycles in our engine with different peak pressure, for 2500 rpm and 1 bar MAP. Also shown is estimated CA90

We have repeated the process for the 1500 rpm case, with PRF0 and 0.48 bar MAP. The borderline knock temperatures and CA90 for 3 cycles are shown in Figure 4-29. The results presented in the previous quarterly report indicated that for this engine operating condition, the knocking pressure (that resulted in KI > 1) was about 20 bar. The borderline knock temperature (at 20 CA BTDC) for this operating point is about 840 bar. Figure 4-29 shows that borderline knock is about 840 K for 20 bar. Thus, very good agreement is achieved in this case.

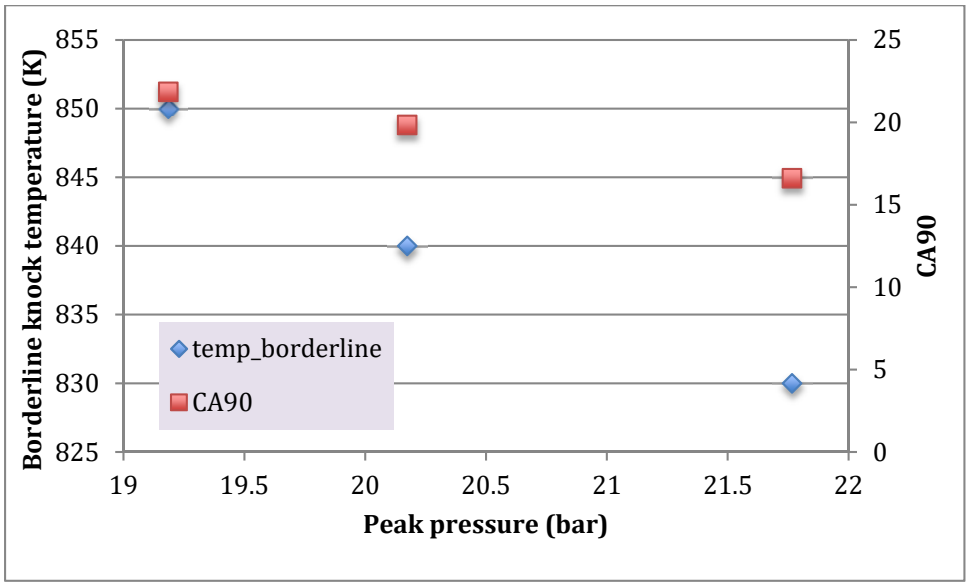

Figure 4-29: Same as Figure 4-28 for 1500 rpm and 0.48 bar MAP. Also shown is estimated CA9

In summary, we have confirmed that the chemical kinetic model agrees with experimental data on knock in the ECOTEC engine, operating at widely different operating points and with very different fuels. However, in order to achieve the required accuracy, means for estimating CA90 and peak pressure are needed. GT-Power can be used for determining the peak pressure, while CA90 needs to be inferred from similar engines. Our methodology for estimating knock onset in a given engine with a known octane number fuel, is therefore a useful tool for helping develop fuel management strategies for the dual-fuel approaches we have examined.

5. Octane Requirements of Driving Cycles

In the previous chapter, utilizing GT-power model (based on the experiment) of the engine, we generated several engine performance maps by changing boost conditions and engine displaced volumes. By comparing the simulation results to experimental results, it was possible to confirm the fidelity of the engine model. In this chapter the engine model is used in vehicle models.

The engine-in-vehicle simulation tool, Autonomie, was utilized to get the operating points on the engine map for various driving cycles. Vehicle models, boost levels (downsizing levels), and spark retard strategies were changed to analyze the effects of these variables on the octane requirement of a vehicle. Table 5-1 shows the variables changed in the vehicle simulation. Three vehicle models, 3 engine displaced volumes, 5 spark retard strategies, and 3 driving cycles gave 135 cases of vehicle simulation results.

Table 5-1: Variables changed for engine-in-vehicle simulation

Vehicle Models	2014 Toyota Camry LE, Ford F-550 XL (with no payload and half the payload) - 3 models
Displaced Volume (Turbo Boost Level)	2.5L ~ 1.25L (NA to 30%, 50% downsizing) - 3 cases
Spark Retard Strategies	0~12 CAD retards from MBT timing – 5 cases
Driving Cycles	UDDS, HWFET, US06

Three of the EPA's standard light-duty vehicle chassis dynamometer driving schedules were tested: Urban Dynamometer Driving Schedule (UDDS), Highway Fuel Economy Test Cycle (HWFET), and US06 Supplemental Federal Test Procedure (US06). UDDS, HWFET, and US06 represent city, highway, and aggressive (or more modern) driving conditions respectively. Detailed features of the three cycles are shown below in Table 5-2. Though the UDDS, HWFET, and US06 are known to overestimate real-world fuel consumption (by about 20%), these cycles were chosen as they are extensively used, and their characteristics are well known [56, 57]. Then, other standard driving conditions were tested (Federal Test Procedure (FTP), New York city driving, combined EPA, and standard European cycles).

Table 5-2: U.S. driving cycles tested [58]

Driving Cycles	UDDS	HWFET	US06
Duration (s)	1369	765	596
Distance (miles)	7.45	10.26	8.01
Average Speed (mph)	19.6	48.3	48.4
Maximum Speed (mph)	56.7	59.9	80.3
Maximum Acceleration (m/s^2)	1.48	1.43	3.78

A primary vehicle model chosen was Toyota's Camry, as it was the most popular passenger vehicle at the United States in 2014. Also, medium duty truck models were constructed to compare vehicle impacts on OOD applications. Specifications of vehicle models are given in Table 5-3. Different engine models were loaded on the vehicle model to study the effects of various parameters on a vehicle performance and ethanol consumption. A maximum torque was kept the same for all the performance maps so the vehicle has a similar acceleration capacity. Even though the maximum power varied slightly, all the performance maps tested showed closely comparable performance in terms of 0-60 mph acceleration times. Also, they were all able to follow the required speed profile of the driving cycles tested (none showed particular over-speed or under-speed relative to the given speed profile of the driving cycle.)

Table 5-3: Vehicle model and engine specifications [59, 60]

Vehicle Model	2014 Toyota Camry LE	2014 Ford F-550 XL
Vehicle Curb Weight / Payload	1470 kg / 136 kg according to EPA's Chassis dynamometer testing rule [61]	2958.8 kg (Class 5 truck with Gross Vehicle Weight Rating (GVWR) range of 16,001-19,500 lab) / 2603 kg, Average Loaded Vehicle Weight (ALVW)
Fuel Economy (city/highway)	25 / 35 mpg	No official values available

Engine Displacement Volume and Configuration	2.4 L, in-line 4 Cylinder	6.8 L, V10
Maximum Torque	230.5 Nm (at 4100 rpm)	619.6 Nm (at 3250 rpm)
Maximum Power	132.7 kW (at 6000 rpm)	269.9 kW (at 4750 rpm)

Figure 5-1 shows the operating points of UDDS cycle generated by Autonomie. In this case, the engine was 50% downsized from the naturally-aspirated engine. Since efficiency, octane requirement, and ethanol requirement of the engine at a given speed and load are known, various parameters can be calculated: average octane rating, engine brake efficiency, fuel economy, ethanol fraction, etc. Figure 5-2 and 5-3 respectively show the operating points of HWFET and US06.

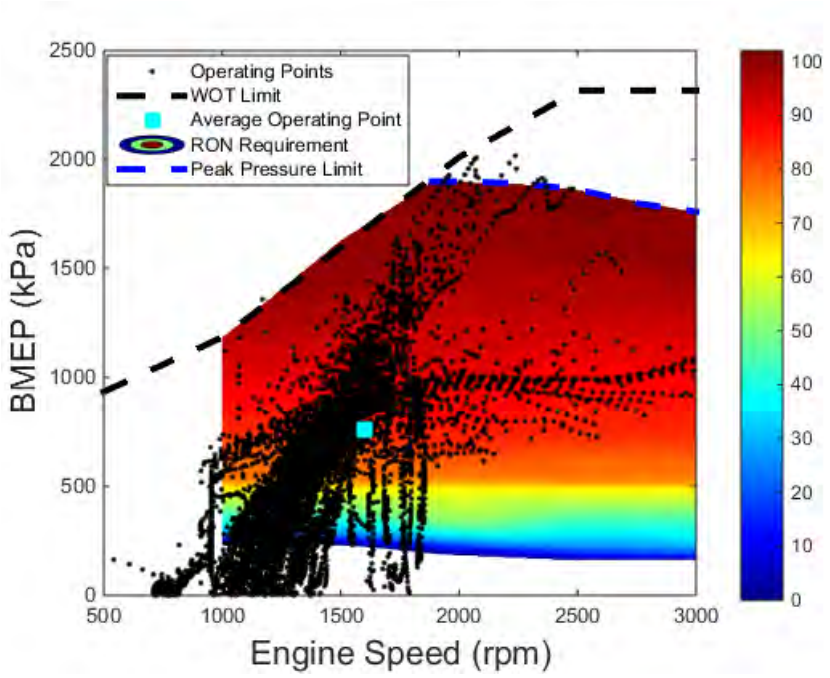

Figure 5-1: Operating points on generated from Autonomie over-imposed on the octane requirement map (50% downsized engine with a passenger vehicle run on UDDS cycle). The black points each represent 0.1s of operation at the specific speed/BMEP. The dashed black line and blue line are WOT limits and in-cylinder peak pressure limits respectively.

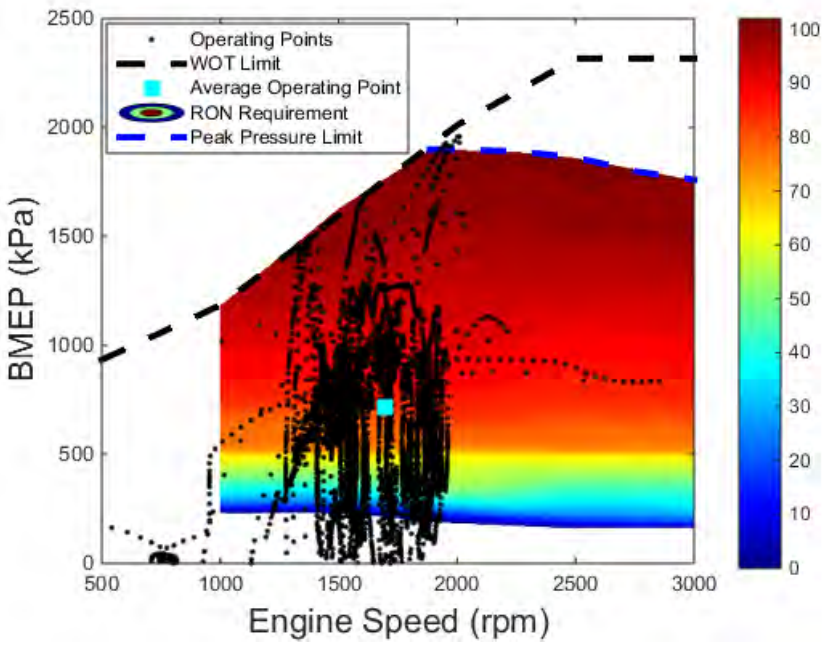

Figure 5-2: Operating points on generated from Autonomie over-imposed on the octane requirement map (50% downsized engine with a passenger vehicle run on HWFET cycle). The black points each represent 0.1s of operation at the specific speed/BMEP. The dashed black line and blue line are WOT limits and in-cylinder peak pressure limits respectively.

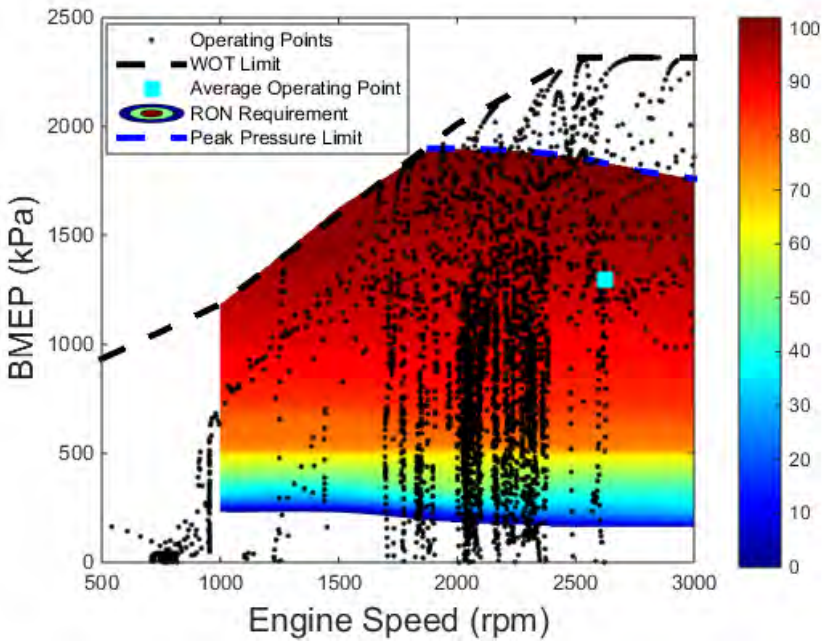

Figure 5-3: Operating points on generated from Autonomie over-imposed on the octane requirement map (50% downsized engine with a passenger vehicle run on US06 cycle). The black points each represent 0.1s of operation at the specific speed/BMEP. The dashed black line and blue line are WOT limits and in-cylinder peak pressure limits respectively.

5.1 Driving Cycle Effects

The actual distributions of fuel usage by RON were plotted for the 30% downsized engine. Figures 5-4~6 show the fuel octane consumption distribution for UDDS, HWFET, and US06 cycles respectively.

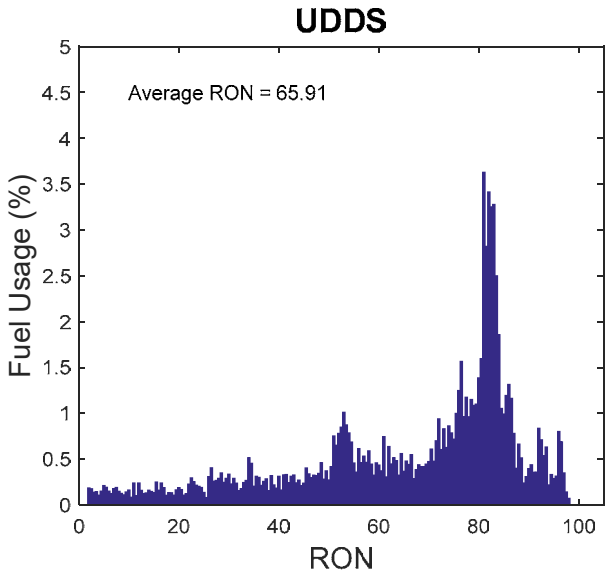

Figure 5-4: Fuel consumption distribution by RON of the fuel at UDDS cycle run by a passenger vehicle with 30% downsized engine.

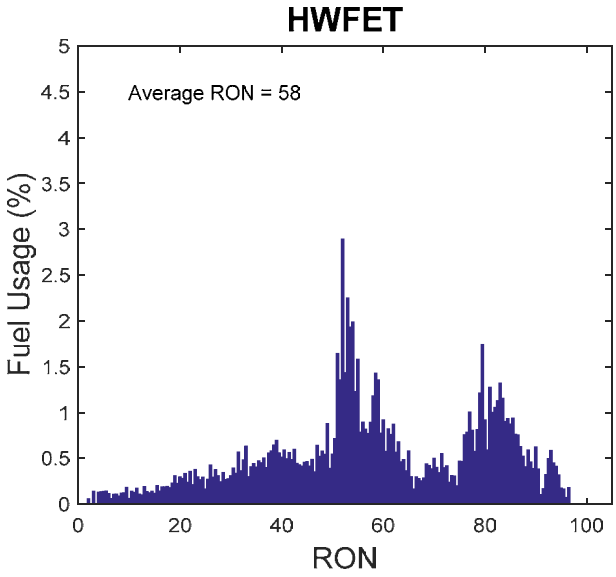

Figure 5-5: Fuel consumption distribution by RON of the fuel at HWFET cycle run by a passenger vehicle with 30% downsized engine.

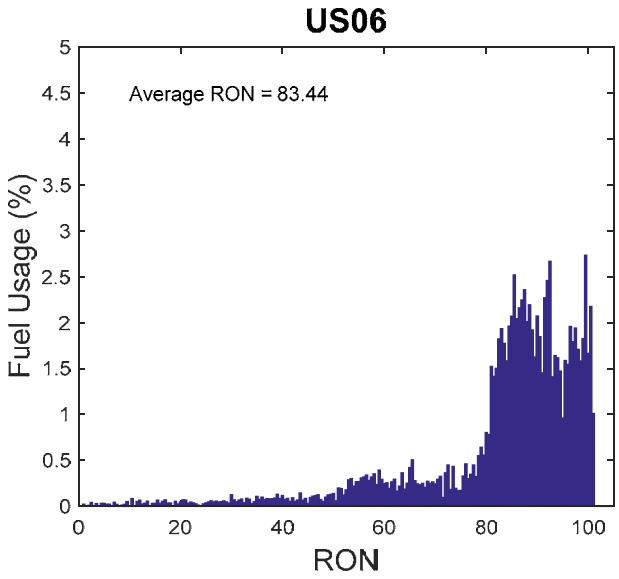

Figure 5-6: Fuel consumption distribution by RON of the fuel at US06 cycle run by a passenger vehicle with 30% downsized engine.

About 3.5% of the total fuel used to complete UDDS cycle, at MBT timing (without knock) was 80 RON. Since the engine test involved fuel RON ranging from 0 to 102 fuel (gasoline-ethanol blends are used above 91 RON), the distribution could be generated for the complete RON range. From the skewedness of the histograms, it is possible to correlate the octane usage and driving styles. For the UDDS cycle, though the average speed is lower than the HWFET cycle the maximum acceleration is higher, so high octane fuel usage is higher. HWFET cycle shows two peaks: the lower peak around 50 RON is due to high speed cruising while another peak around 80 RON is due to accelerations. Since US06 is the most aggressive driving cycle, it is skewed to the left the most. Average octane requirements were calculated by taking the weighted average of the distributions. The fuel usage distributions of other cycles are given in Figure 5-7 and Figure 5-8. A distribution of NYC cycle shows similar shape as that of UDDS, but with more acceleration peaks. European cycles also have their distinctive peaks.

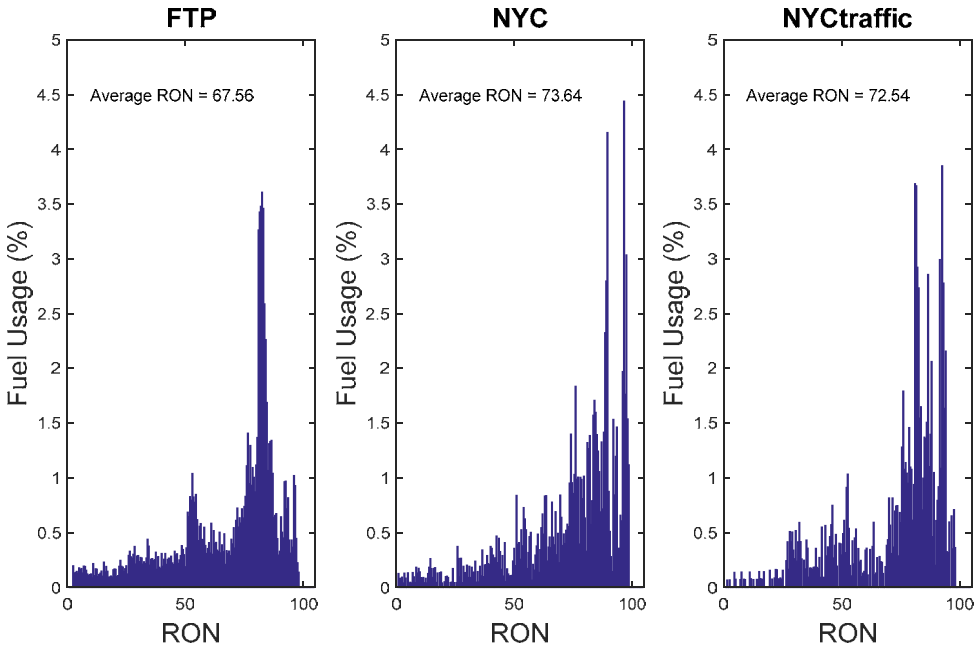

Figure 5-7: Fuel consumption distribution by RON of the fuel at FTP cycle (left), NYC cycle (middle), NYC traffic cycle (right) run by a passenger vehicle with 30% downsized engine

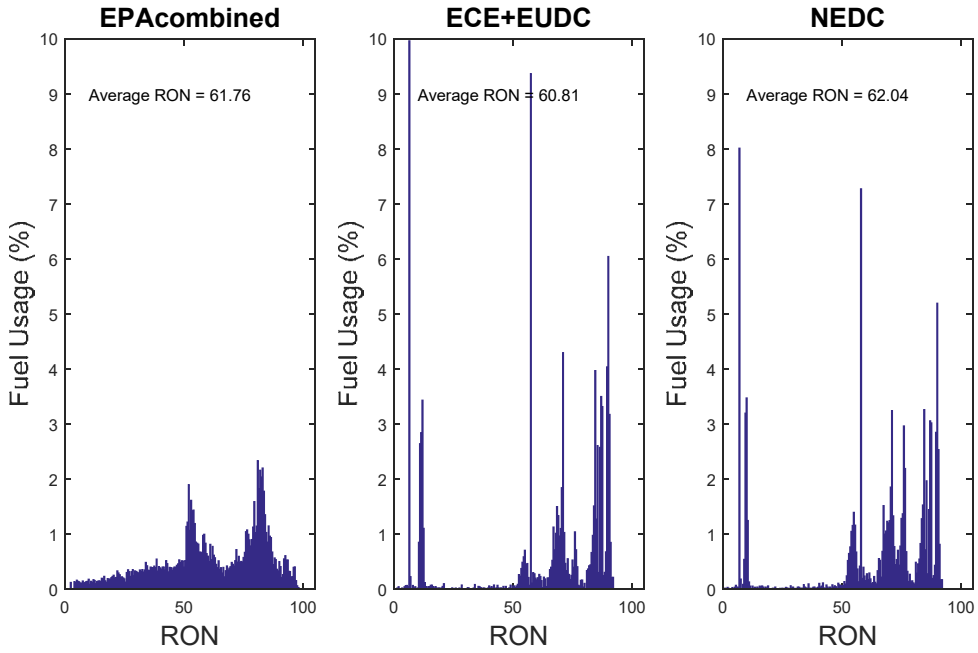

Figure 5-8: Fuel consumption distribution by RON of the fuel at EPA combined cycle (left), ECE (urban driving cycle) and Extra Urban Driving Cycle (EUDC) at the middle, New European Driving Cycle (NEDC) at the right run by a passenger vehicle with 30% downsized engine.

Vehicle speeds, acceleration, and the octane requirement were plotted in Figure 5-9 (for the US06 cycle) to see how the octane requirement changes during the drive cycles. The octane requirement is closely related to the vehicle acceleration. However, in the highway driving portion of the US06 (from 132 to 495 seconds) where accelerations are modest, octane requirements are still high. This is because engine is already operating at relatively high load at these high speeds, so modest acceleration shifts the operating load to where higher octane fuel is required. The octane requirement is both a function of the harshness of acceleration and load of the engine at the start of the acceleration.

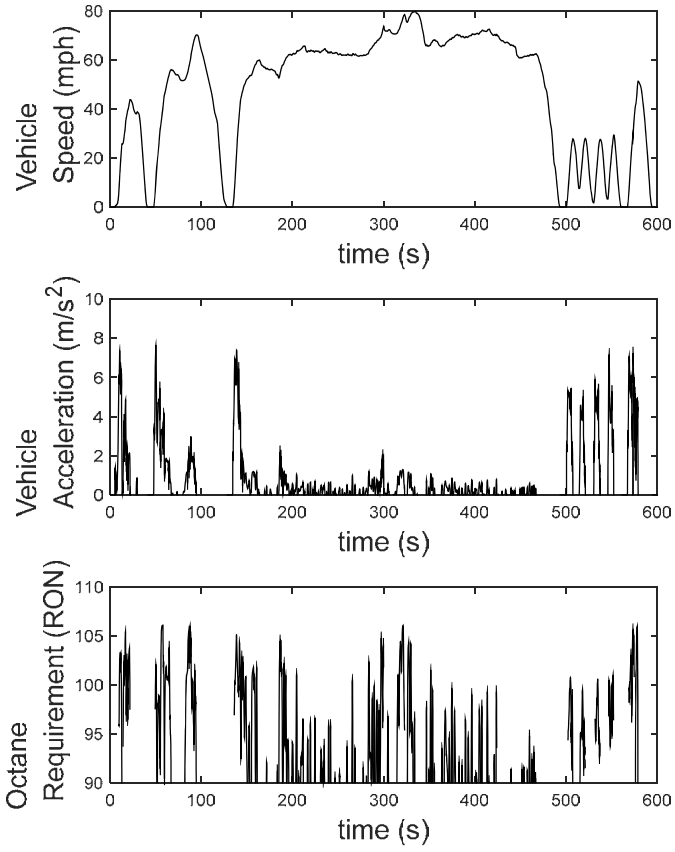

Figure 5-9: Vehicle speed, vehicle acceleration, and octane requirement plotted against the time in the US06 cycle run with a passenger vehicle.

5.2 Downsizing Effects

To see the effect of reduced displaced engine volume (the degree of downsizing) on the octane requirement and fuel economy, three engine performance maps were utilized: NA, 30% downsizing from NA, and 50% downsizing from NA. Figure 5-10 shows how the average operating BMEP changes with downsizing. Average operating BMEP was calculated by taking the weighted average BMEP of the cycle's operating points on the engine map (weighted by the amount of fuel used at each point).

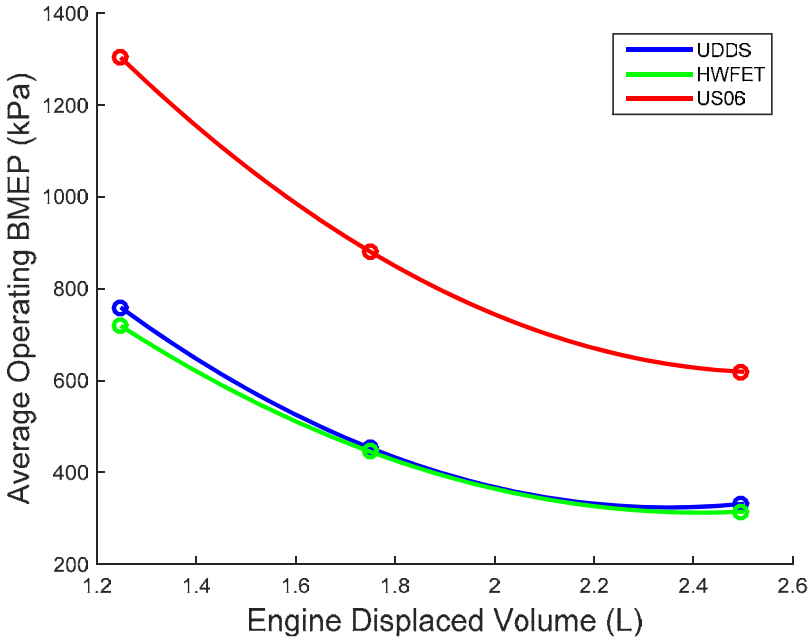

Figure 5-10: Average operating BMEP vs. engine displaced volume for three standard U.S. driving cycles (UDDS, HWFET, US06) run with a passenger vehicle. Spark timings were at MBT timing.

For the naturally-aspirated engine, average BMEP is about one fourth of the maximum BMEP (1100~1200 kPa) under UDDS and HWFET cycle conditions. For the US06 cycle, it is about half of the maximum BMEP. With 50% downsizing, the average operating BMEP is about one third of the maximum BMEP (2500 kPa) while it is still almost half for the US06 cycle. Then, to analyze how this operating region change affects the engine efficiency, the average engine brake efficiency is calculated using the equation below.

$$\text{Engine Brake Efficiency} = \frac{\text{Engine Power Out (W)}}{\text{Fuel Consumption Rate } \left(\frac{\text{kg}}{\text{s}}\right) * \text{LHV (J/kg)}}$$

(5.1)

Assuming the OOD applications (whether dual fuel or OBS) allow the engine to operate at MBT timing all the time, downsizing the engine greatly increases the average engine brake efficiency. Figure 5-11 shows 50% downsizing gives about a 29% increase in the average brake efficiency for the UDDS.

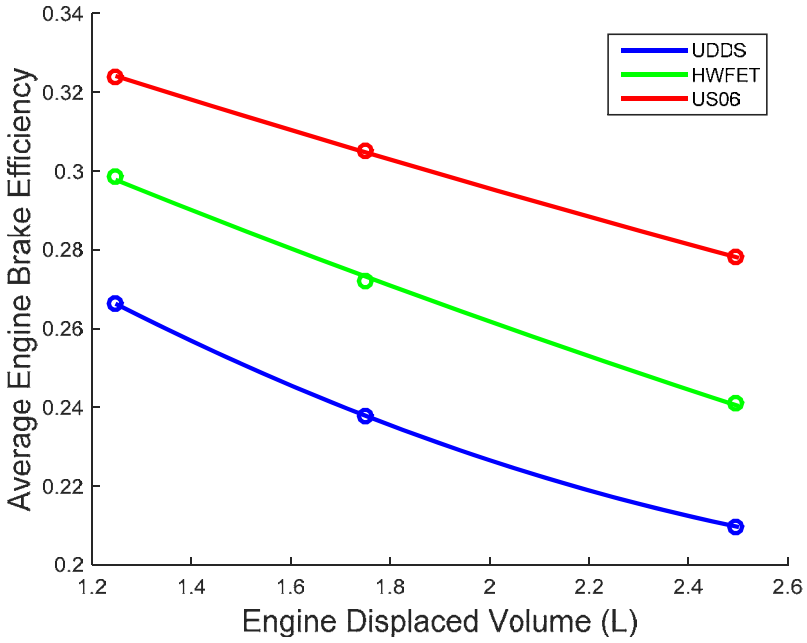

Figure 5-11: Average engine brake efficiency vs. engine displaced volume for three standard U.S. driving cycles (UDDS, HWFET, US06) run with a passenger vehicle. Spark timings were at MBT timing.

To check if the vehicle models and Autonomie give reliable results, the fuel economy was calculate in Figure 5-12.

Official fuel economy values were calculated using the equation below, following the EPA rule. The rule before 2008 was used for simplicity (new rule requires 3 additional cycles with a wider range of operating conditions.)

$$\mathrm{MPG}_{combined} = \frac{1}{\frac{0.55}{MPG_{UDDS}} + \frac{0.45}{MPG_{HWFET}}}$$

(5.2)

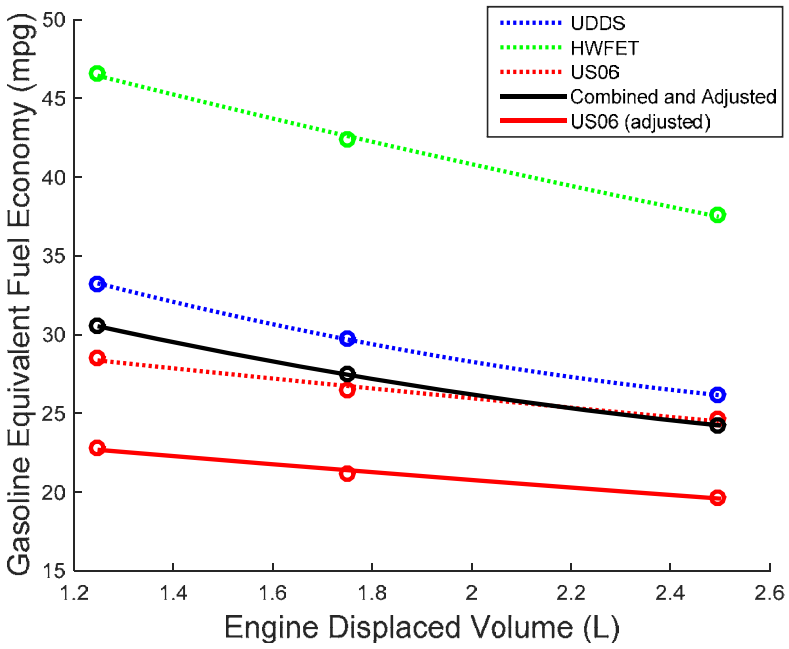

Figure 5-12: Gasoline equivalent fuel economy vs engine displaced volume for three standard U.S. driving cycles (UDDS, HWFET, US06) run with a passenger vehicle. Spark timings were at MBT timing. Dotted lines are the results from the engine-in-vehicle simulation, and solid lines are combined (UDDS and HWFET) and adjusted values. The fuel economy for the US06 cycle was just adjusted.

In Figure 5-12, the solid lines are the combined and adjusted values (Adjusted includes a 20% fuel economy reduction.) The Camry's official combined and adjusted fuel economy value is 29 miles per gallon, in the range of the expected fuel economy values represented by the black solid line. With further downsizing, fuel economy values increased with increased average engine brake efficiency. 50% downsizing resulted in 26% increase in fuel economy. Figure 5-13 shows the effect of downsizing on the octane requirement of different driving cycles.

Since it was assumed that enough ethanol is provided to allow operation of OOD application, it is important to see how the octane requirement changes with increased efficiencies. For all cycles, octane requirements increased with downsizing (and boosting). Naturally-aspirated engine gives the average octane requirement of 51, 41, and 71 RON for UDDS, HWFET, and US06 cycles, respectively. With 50% turbo-downsized engine, the average octane requirement increased to 88, 76, and 92 for UDDS, HWFET, and US06, respectively. For the US06 cycle, downsizing by 50% gives a 30% increase in the octane requirement (70.9 to 92.1 RON), 17% increase in the average engine brake efficiency (27.8 to 32.4%), and 16% increase in the fuel economy (24.6 to 28.5 mpg). It can be said that the higher octane requirement implies

higher octane utilization with the OOD system is equipped on the vehicle. Higher octane utilization means higher ethanol consumption.

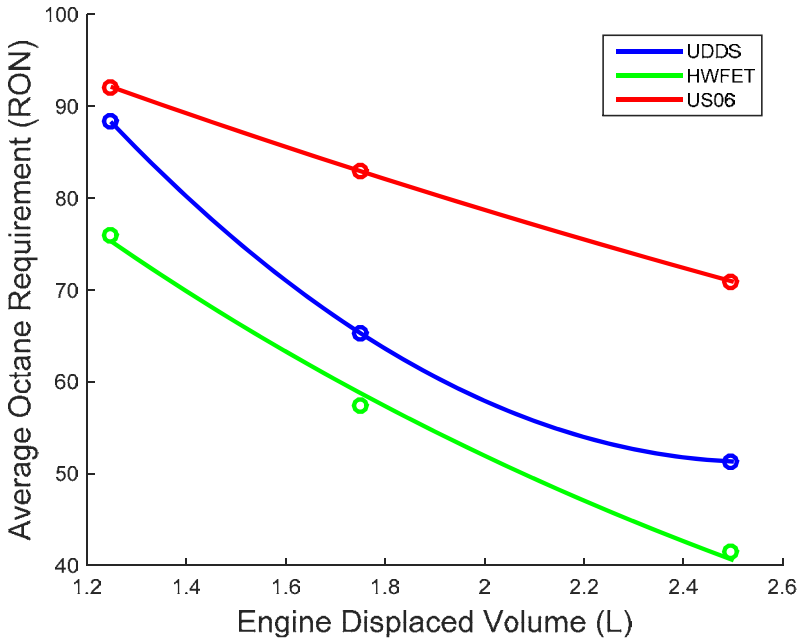

Figure 5-13: Average octane requirement vs. engine displaced volume for three standard U.S. driving cycles (UDDS, HWFET, US06) run with a passenger vehicle. Spark timings were kept at MBT timing.

Spark retard has a significant impact on the fuel octane requirement at all operating points on the engine performance map. A paper submitted for 2016 SAE congress examines the trade-offs involved with retarded combustion timing. The reduction in ethanol use with up to 5 CAD, and then up to 10 CAD of spark retard is significant. Applying up to 5 CAD retard, the reduction in test-cycle fuel economy from engine-in-vehicle simulations is modest as described in the next section.

5.3 Spark Retard Effects

Fractions of ethanol consumed for different driving cycles and downsizing levels are displaced in Figure 5-14. As mentioned in the previous section, the octane requirement increased about 30% for US06 cycle with 50% downsizing. This increase requires that about 12% of fuel consumed (by volume) has to be ethanol when combined with RON 91 gasoline. Depending on the high octane fuel blends utilized, fraction of high octane stream consumption would go up (14% for

dual fuel with E85 or 20% for OBS with a high octane stream of E60 [39]) because pure ethanol is barely used as a stand-alone fuel.

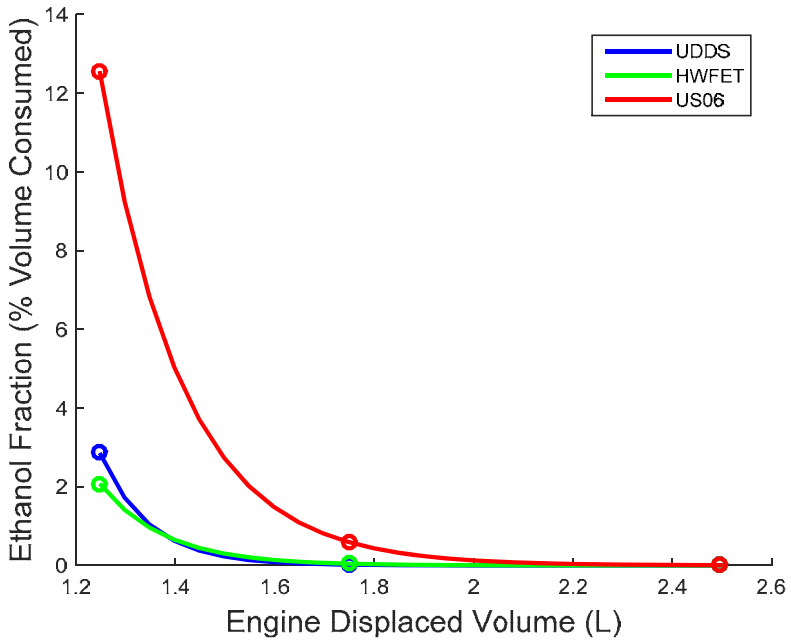

Figure 5-14: Ethanol fraction vs. engine displaced volume for three standard U.S. driving cycles (UDDS, HWFET, US06) run with a passenger vehicle. Spark timings were kept at MBT timing.

So far, we have considered cases where the engine is always operating at MBT timings. However spark timings can be retarded to reduce the amount of ethanol needed. Retarding the spark timing from MBT timing lowers in-cylinder pressures, thus reducing knock, but engine efficiencies would drop as the engine is not operated at the optimal timing. To analyze the effects of spark retard, a case with 50% downsizing in US06 cycle is considered (the 1.25L displacement case on the red line in Figure 5-14).

Spark retard was applied gradually for each scenario. For example, the 5 CAD retard case means that the engine's spark timing is gradually retarded by up to 5 CAD from the engine load where knocking starts with regular gasoline. When 5 CAD retard is not enough to suppress knock, ethanol is used to suppress knock further, while maintaining a 5 CAD retard. 0 CAD case means the MBT timing scenario as considered previously. Figure 5-15 shows that the ethanol fraction can be reduced from 12.5% down to 4% when up to 10 CAD of retard is allowed, giving 66% reduction in ethanol volume. However, the gasoline-equivalent fuel economy also drops by

10%. Since the fuel economy drop gets significantly worse after 5 CAD retard strategy, it would be the best to limit spark retard to 5 CAD or less.

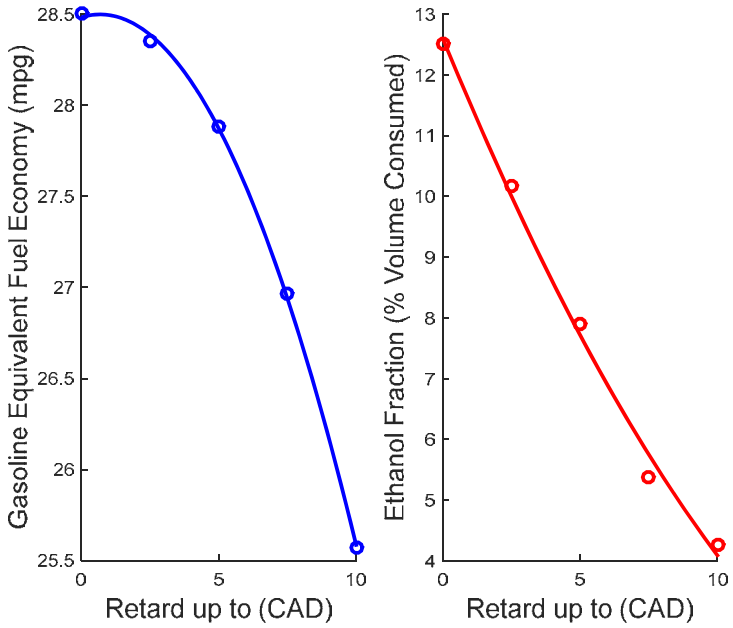

Figure 5-15: Fuel economy and ethanol fraction vs. spark retard strategies. 50% downsized engine run by a passenger vehicle at US06 cycle was considered.

5.4 Vehicle Effects

To examine how the vehicle type changes the octane requirement, a Ford F-550 model was developed. Vehicle specifications are presented in Table 5-3. Driving cycles were simulated using the vehicle model for two cases: one without any payload, and another with the average loaded vehicle weight (ALVW). Since maximum payload of F-550 is 5200 kg, 2600 kg of payload was added. Figure 22 shows the fuel economy values. With no payload, the combined fuel economy increases about 20% with 50% downsizing. According to the EPA's officials, EPA regulations do not require class 5 vehicles to be chassis tested for certification. Therefore, there is no official fuel economy value available for comparison. According to discussions at the user forum of the F-550, the average fuel economy of F-550's gasoline models range from 7 to 10 mpg. The combined fuel economy gets closer to the reported values for the case with ALVW as shown in Figure 5-17.

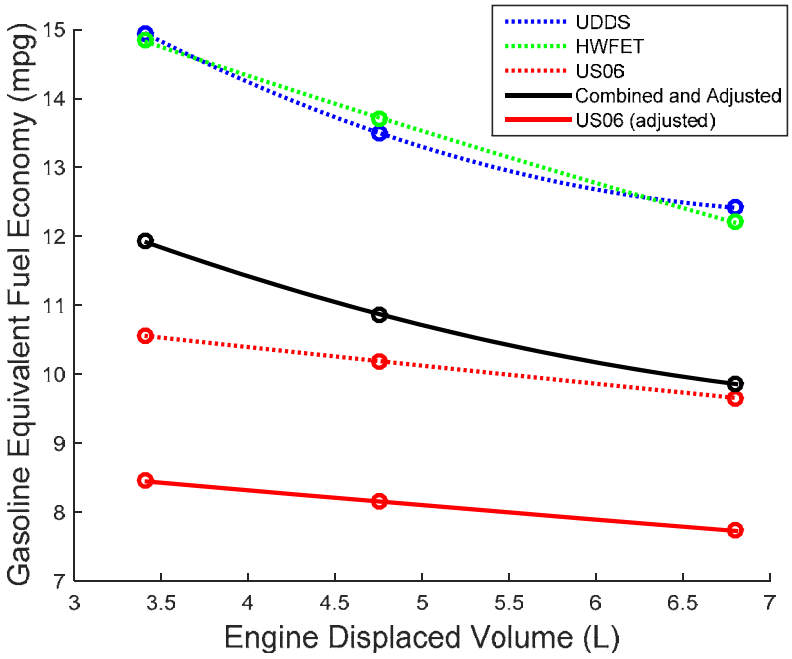

Figure 5-16: Gasoline equivalent fuel economy vs engine displaced volume for three standard U.S. driving cycles (UDDS, HWFET, US06) run with a medium duty truck. Spark timings were at MBT timing. Dotted lines are the results from the engine-in-vehicle simulation, and solid lines are combined (UDDS and HWFET) and adjusted values. The fuel economy for the US06 cycle was just adjusted. Only curb weight with no payload.

With half the payload, the fuel economy decreased: the combined fuel economy decreased by about 20% as shown in Figure 5-17. It is well known that aggressive driving cycles result in lower fuel economy. Adding weight to the vehicle effectively makes a given driving cycle more aggressive as more weight requires more acceleration/torque. Since curb weight of the F-550 is about 3000 kg, adding 2600 kg of payload would shift the operating points up on the engine map. Figure 5-18 compares the average operating BMEP for the case without and with payloads. It can be seen that the average BMEPs are always higher for the case with increased weight, which demands higher torque. Without payload, average BMEPs are similar to those of the passenger car case in Figure 5-10.

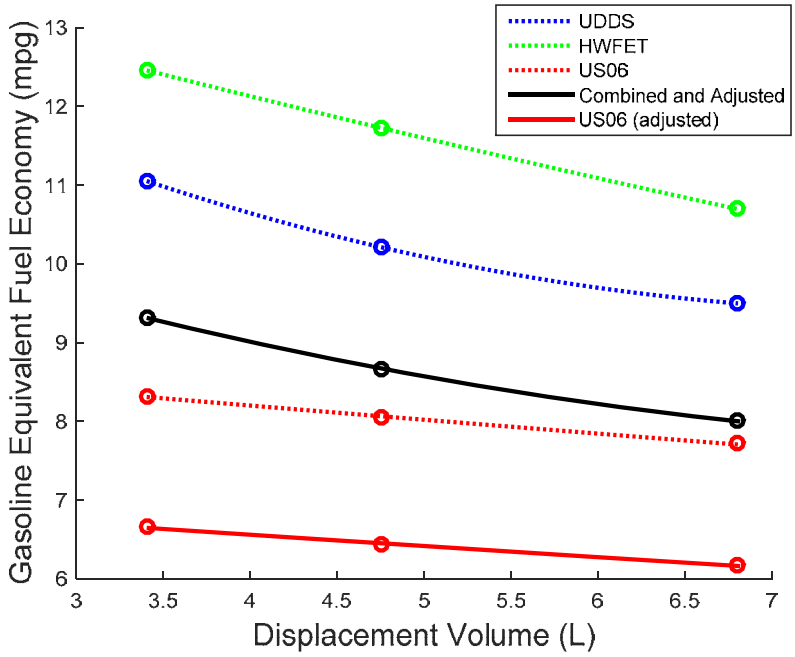

Figure 5-17: Gasoline equivalent fuel economy vs engine displaced volume for three standard U.S. driving cycles (UDDS, HWFET, US06) run with a medium duty truck. Spark timings were at MBT timing. Dotted lines are the results from the engine-in-vehicle simulation, and solid lines are combined (UDDS and HWFET) and adjusted values. The fuel economy for the US06 cycle was just adjusted. Curb weight with half the payload.

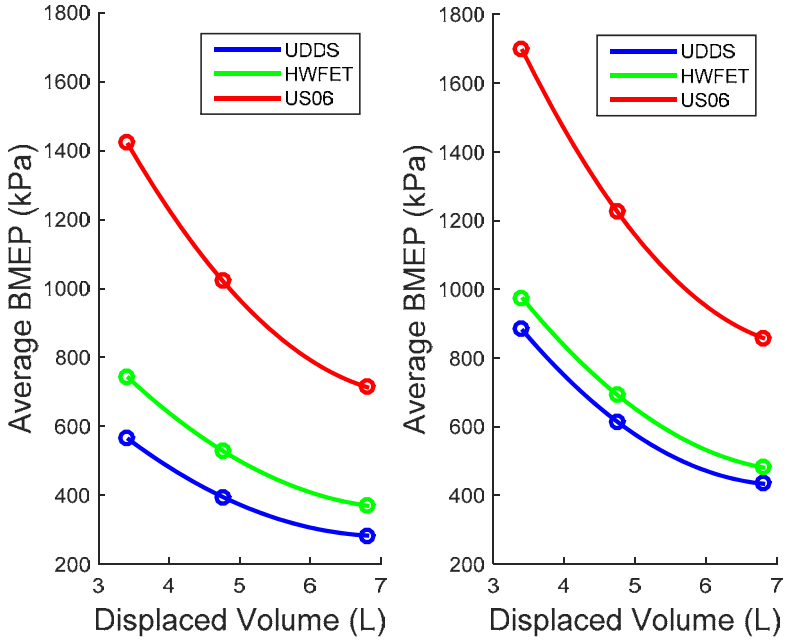

Figure 5-18: Average operating BMEP vs. engine displaced volume for three standard U.S. driving cycles (UDDS, HWFET, US06) run with a medium duty truck. Left graphs are without payload, and the right graphs are with half the payload (ALVW).

Figure 5-19 compares the average octane requirements for the cases without and with payloads. By adding a payload, the average octane requirements increased for the UDDS and HWFET cycles by about 15%, while it increased only 3% for the US06 cycle. Since the US06 is already an aggressive cycle, adding a payload did not increase the octane as much as for relatively less aggressive driving cycles. For both cases, octane requirements increased substantially with downsizing.

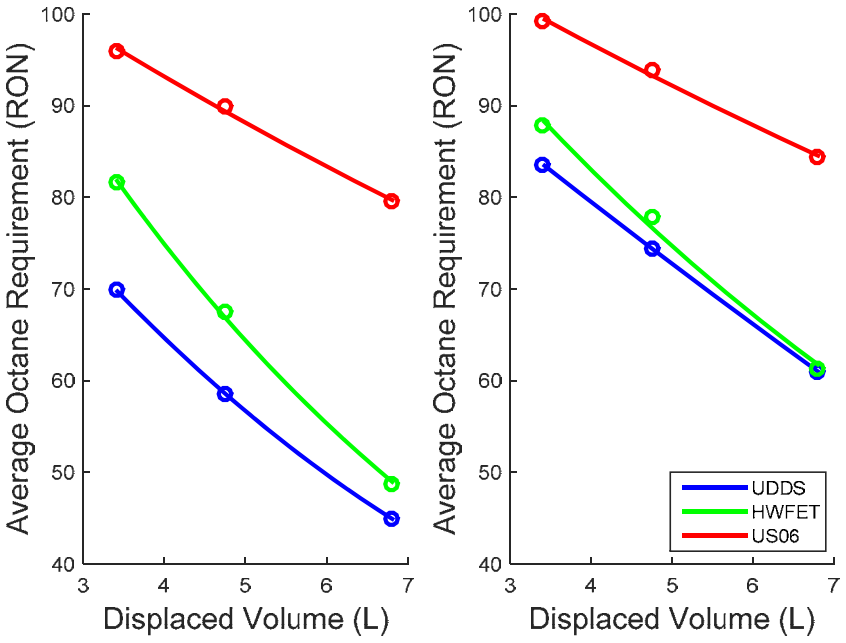

Figure 5-19: Average octane requirement vs. engine displaced volume for three standard U.S. driving cycles (UDDS, HWFET, US06) run with a medium duty truck. Left graphs are without payload, and the right graphs are with half the payload (ALVW).

Ethanol consumption for two cases are compared in Figure 5-20. Without payloads, the ethanol fraction increase is similar to that of the passenger vehicle case in Figure 5-14. However, the ethanol volume fraction increases greatly, even for UDDS and HWFET cycles, when the payload is added to the vehicle. By looking at the octane requirement increase and the ethanol fraction increase, it can be inferred that the payload is an important parameter that determines octane utilization. As the payload gets heavier, the vehicle can utilize octane effectively, so the fuel economy benefits increase. However, strategies involving a moderate amount of spark retard will have to be applied to reduce the amount of ethanol usage while not compromising the fuel economy too much. Similar behavior is observed in light duty vehicles that are towing.

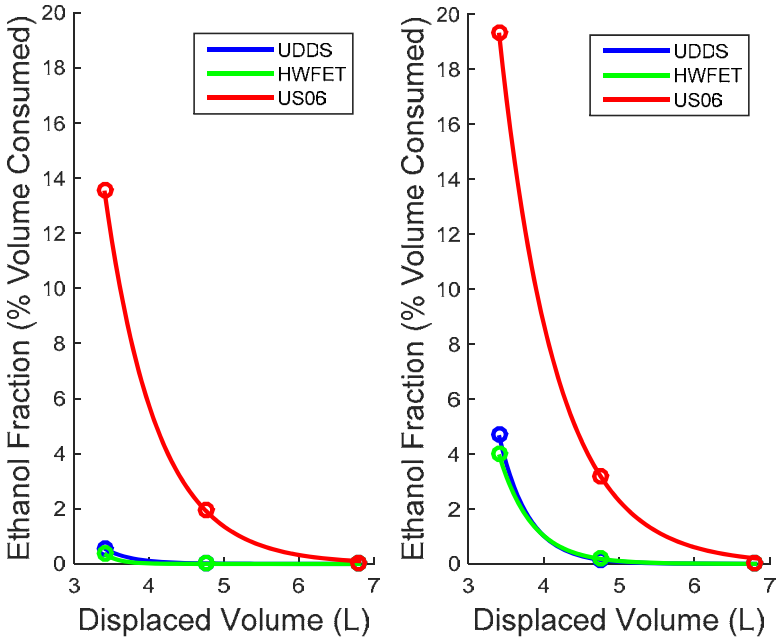

Figure 5-20: Ethanol fraction vs. engine displaced volume for three standard U.S. driving cycles (UDDS, HWFET, US06) run with a medium duty truck. Left graphs are without payload, and the right graphs are with half the payload (ALVW).

6. Dual Fuel Systems Modelling and Assessments

There are two practical applications that allow dual fuel operations of the engine: a two-tank system and an on-board fuel separation system. As explained in the very first chapter of this report, two systems each have advantages and disadvantages. The two-tank system is straightforward to model, assuming that the ethanol tank (for high octane fuels such as E85) can be filled up as necessary. However, modelling an on-board fuel separation system is not trivial, as it involves modelling the pervaporation process. In this chapter, a modelling tool for the fuel separation system will be presented, and advantages and disadvantages of the two alternatives for dual fuel injection will be discussed.

6.1 On-board separation system modelling

Based on the literature review and research, this system model is constructed as shown in Figure 6-1.

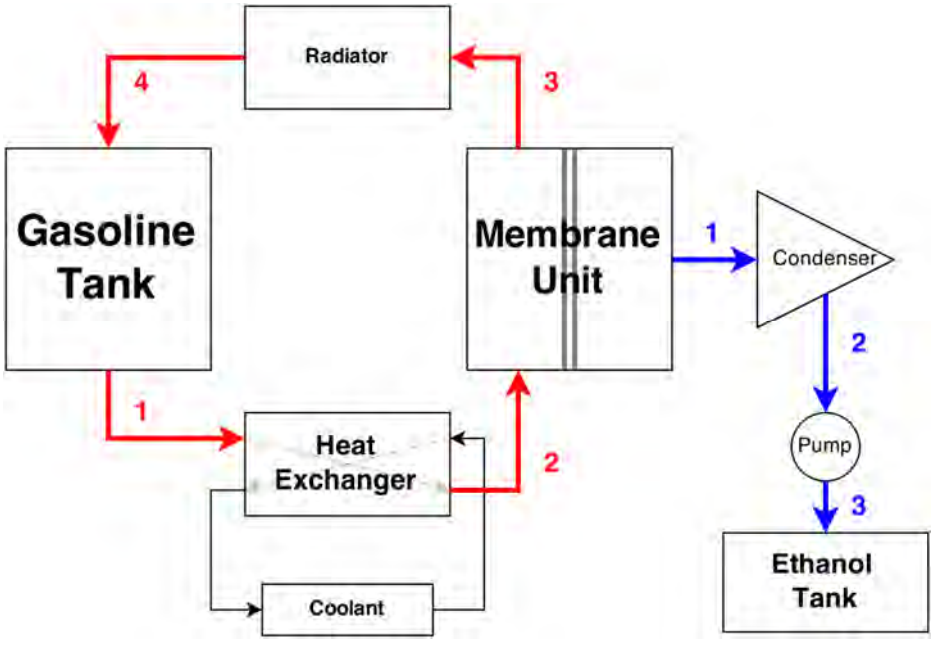

Figure 6-1: Schematic diagram of the on-board separation system model. System components are represented by a rectangle, a triangle, and a circle. Red and blue lines each denote low octane stream and high octane stream fuels. Low octane stream processes are pre-heating (1-2), membrane separation (2-3),

cooling (3-4), and mixing (4-1), and high octane stream processes are condensation (1-2) and pumping (2-3).

The on-board fuel separation system is a system that separates high octane fuel stream from the regular E10 gasoline sold in the U.S. Literature reviews of the existing systems are given in the first chapter of this report. Starting from the gasoline tank, E10 fuel is heated by a heat exchanger which has an engine coolant as a working fluid. Hence, the fuel can be heated up to 80 ºC, depending on the temperature of the coolant and the engine's operating conditions. Then the fuel is processed in the membrane unit, which separates ethanol. The remaining fuel is cooled down by a radiator, then goes back into the gasoline tank. The separated fuel is condensed, and then pumped into the ethanol tank for later use with knocking conditions. In this process, the most important piece to be modelled is the membrane separation unit.

Pervaporation process models

A pervaporation process is utilized in the membrane separation unit. Pervaporation is a combination of membrane permeation and evaporation [62]. The process separates mixtures of liquid by partial vaporization through a non-porous or a porous membrane. Pervaporation is one of the promising separation processes due to its low energy consumption, low investment cost, compactness. Therefore, it is suitable for fuel separation in a vehicle system that requires low energy and cost [63]. Figure 6-2 shows the process in a schematic diagram.

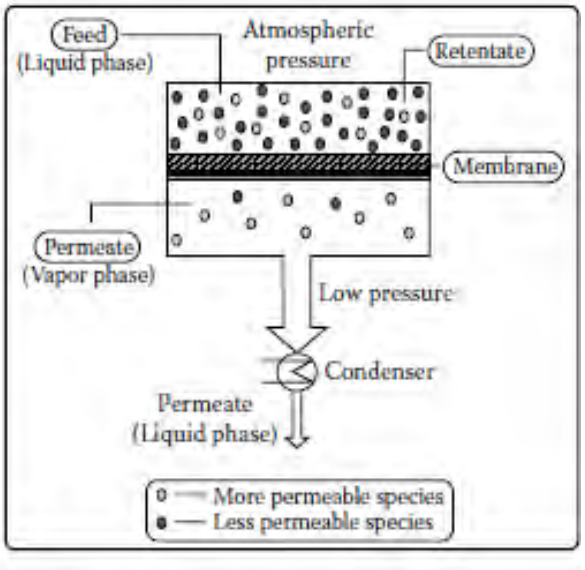

Figure 6-2: A schematic diagram explaining the process of pervaporation; the figure is taken from [62].

The driving force of the mass transport in pervaporation is the partial pressure difference of the permeate in the feed and permeate sides. Therefore, temperature and vacuum pressure on the permeate side are the important parameters determining the separation rate of the process. Pervaporation is governed by the polarity differences of feed components, and separation is carried out as the membrane has the ability to transport a certain component more easily than others. Based on the solution-diffusion model, the flux of a permeate component is given as

$$J = \frac{P}{l}(p_o - p_l) \tag{6.1}$$

where J is the flux, P is the permeability (which is the product of solubility and diffusivity), l is the membrane thickness, p_o is the partial vapor pressure of the permeate in the liquid feed, and p_l is the partial vapor pressure of the permeate in vapor.

There are many empirical, semi-empirical, and theoretical models of the pervaporation process. Most models have empirical features built in which support the model with experimental results. For the modelling of pervaporation for E10 fuel, a model called the pore flow model is chosen since pervaporation experiments could not be done due to limited resources. There are previous studies which have done experiments on ethanol-gasoline fuel blends and utilized the pore flow model to verify the results.

The pore flow model was introduced by Okada and Matsuura in 1991 [64]. The basic assumption is that the membrane can be seen as a bundle of straight cylindrical pores distributed on the surface layer of the membrane. A detailed look of a cylindrical pore is shown in Figure 6-3.

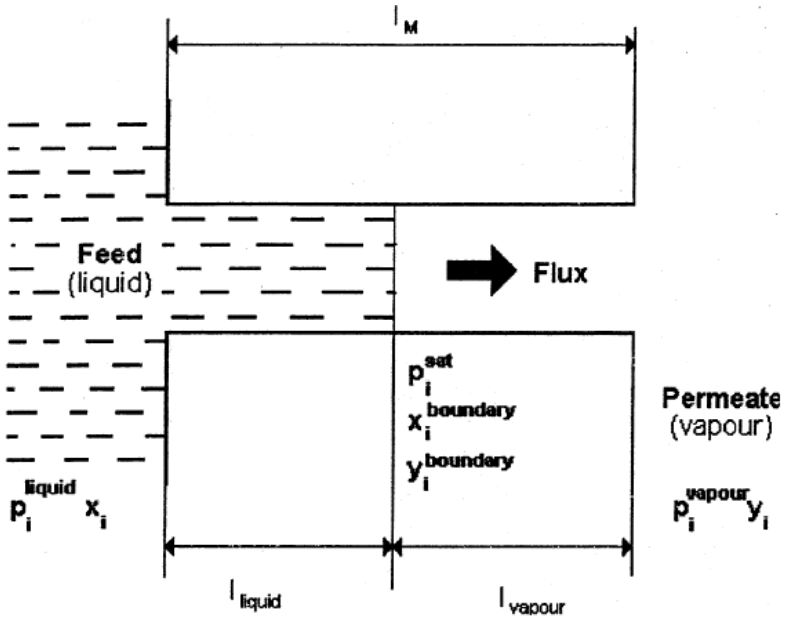

Figure 6-3: A description of the pore flow model; the figure is taken from [62]

The model considers the pervaporation process in a cylindrical pore as a combination of liquid and vapor transport, where liquid transport is by reverse osmosis and vapor transport is by membrane vapor separation. Then, there is a boundary between the liquid and vapor inside the pore. By Darcy's equation, liquid transport can be expressed as

$$\mathrm{J}_{liquid} = \frac{A^{Pore}}{l_{liquid}}(p^{liquid} - p^{sat}) \tag{6.2}$$

where A^{Pore} is a proportionality constant, l_{liquid} is the length of the liquid portion, p^{liquid} is the liquid pressure, and p^{sat} is the saturation pressure. Then, the vapor transport can be expressed as

$$\mathrm{J}_{vapor} = \frac{B^{Pore}}{l_{vapor}}(p^{sat} - p^{vapor}) \tag{6.3}$$

where B^{Pore} is a proportionality constant (defined by simplification of Henry's law and monolayer adsorption,), l_{vapor} is the length of the vapor portion, p^{sat} is the saturation pressure, and p^{vapor} is the vapor partial pressure. Assuming a steady state, liquid and vapor fluxes are

equal to the total fuel separation rate. Also, membrane thickness is equal to the sum of the length of the vapor portion and the liquid portion. Therefore, combining both equations, it is possible to calculate the total flow rate in terms of constants, membrane thickness, and partial pressures as below:

$$\mathrm{J} = \frac{A^{Pore}}{l_M}\left(p^{liquid} - p^{sat}\right) + \frac{B^{Pore}}{l_M}\left((p^{sat})^2 - (p^{vapor})^2\right) \tag{6.4}$$

where l_M is the membrane thickness. For binary mixtures, equation (6.4) can be simplified as below:

$$\mathrm{J}_i = \frac{B^{Pore}}{l_M}\left((p_i{}^{sat})^2 - (p_i{}^{vapor})^2\right)$$

$$\mathrm{J}_i = \frac{B^{Pore}}{l_M}\left((p_i{}^{sat})^2 - (p_i{}^{vapor})^2\right) \tag{6.5}$$

Using the equations (6.5) and known parameters of membranes from previous studies [65, 66], it was possible to estimate the separation rate of the ethanol-isooctane mixture. Saturation pressures are determined by Antoine equations, and vapor partial pressures are calculated assuming vapor liquid equilibrium at the liquid-vapor boundary. On the permeate side, partial pressures are determined based on the separation rate. Then, the ethanol fraction in the gasoline tank is determined assuming a well-stirred reactor with saturation partial pressure determined again by assuming vapor-liquid equilibrium. Therefore, the separation rate could be calculated iteratively and the ethanol fraction could be calculated in discrete time steps.

System model and parametric study

The fuel separation system model was utilized to simulate the ethanol separation rate of the system and the amount of ethanol left in the system. Figure 6-4 shows the separation rate vs. time. The high octane fuel stream separation rate is a function of an ethanol concentration on the feed side, the temperature of the heated fuel, the vacuum pressure in the permeate side, and the ethanol concentration in the permeate side. Therefore, the ethanol separation rate decreases as

the ethanol concentration in the feed side decreases, as separation goes on. Since a large portion of the fuel separated is ethanol, even though a small portion is still gasoline, the total separation rate decreases as well. The gasoline separation rate increases as the ethanol separation rate decreases.

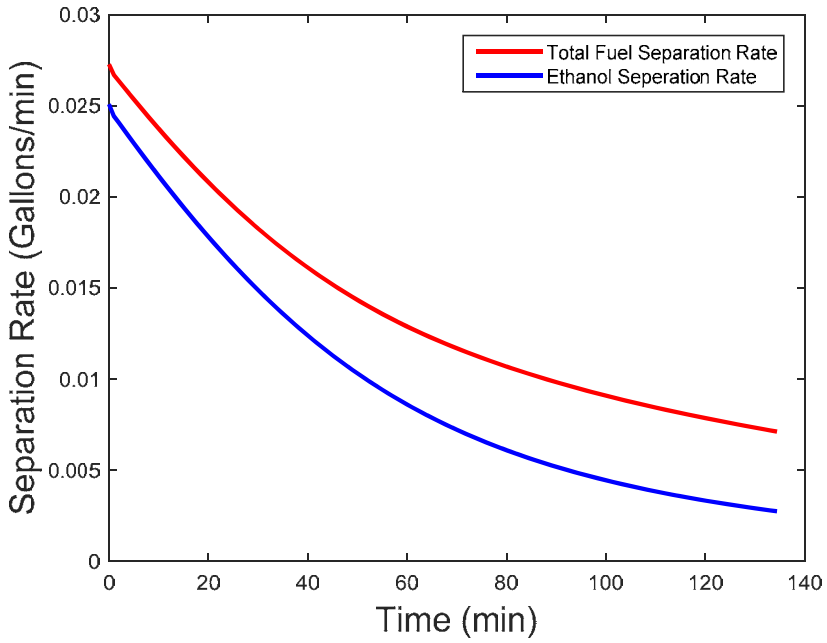

Figure 6-4: Separation rate of a pure ethanol (blue) and a total fuel flowrate (red) in gallons per minute vs. time in seconds

Based on the separation rate, the fuel contents in the gasoline tank and the ethanol tank can be calculated. Results are shown in Figure 6-5 and 6-6. Assuming that the gasoline tank holds 17 gallons and is filled up with E10 gasoline, the fuel contents in the gasoline tank are plotted. Ethanol and gasoline contents decrease with diminishing rate, and the ethanol fraction decreases with a diminishing rate as well. In the case of a study conducted by Honda, separation continued until the ethanol content in the main tank reached 2.5%. In this case, it took more than 100 minutes to complete that separation. In the opposite sense, the total amount of the fuel in the ethanol tank increases with a diminishing rate.

In Figure 6-6, the gap between the red and blue lines represents the amount of gasoline, which gradually increases as gasoline separation rate increases with time. The separation has to be stopped at some point before the gasoline is separated too much. Criteria for stopping the

separation would be the fuel tank capacity, ethanol fraction, separation rate, power consumption of the system, etc. As mentioned in a previous section, separation rates are a strong function of temperature since one of the important parameters is the saturation pressure.

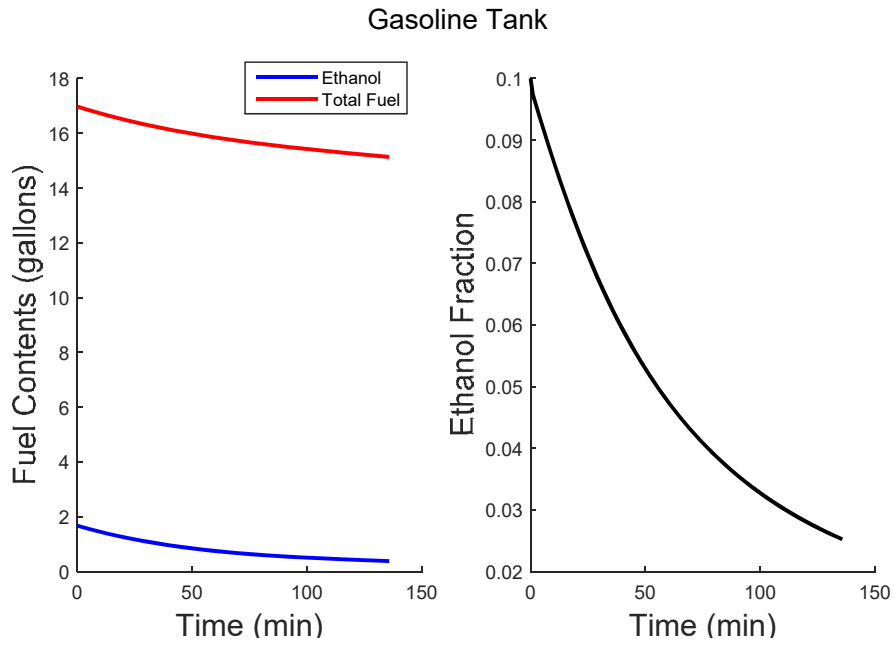

Figure 6-5: The amount of ethanol (blue) and total fuel (red) in gallons shown on the left graph and the ethanol fraction of the gasoline tank on the right graph.

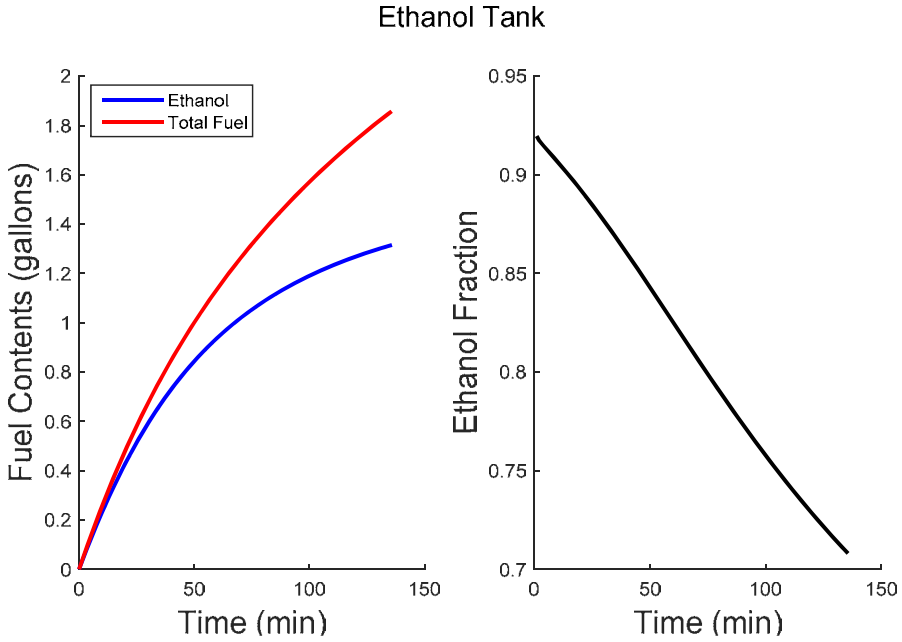

Figure 6-6: The amount of ethanol (blue) and total fuel (red) in gallons shown on the left graph and the ethanol fraction of the ethanol tank on the right graph.

Figure 6-7 and 6-8 show how much faster the separation can be done with a system higher temperature and separation rate with different fuel temperatures.

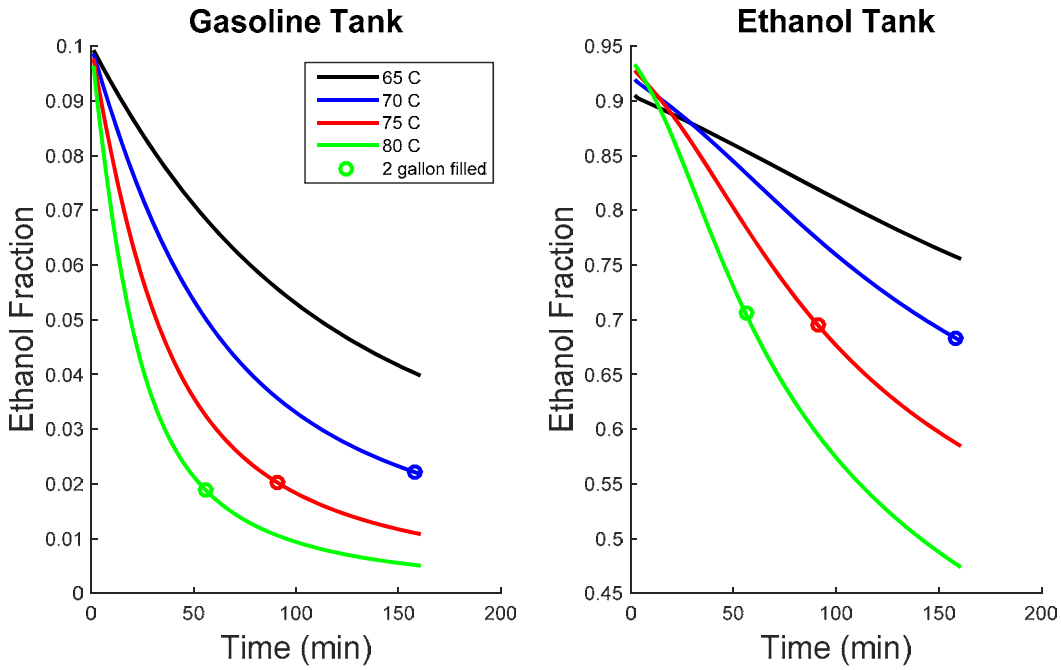

Figure 6-7: Ethanol fraction in the gasoline tank (left) and the ethanol tank (right) vs. time for different fuel temperatures. A marker in each temperature line denotes the point of filled ethanol tank.

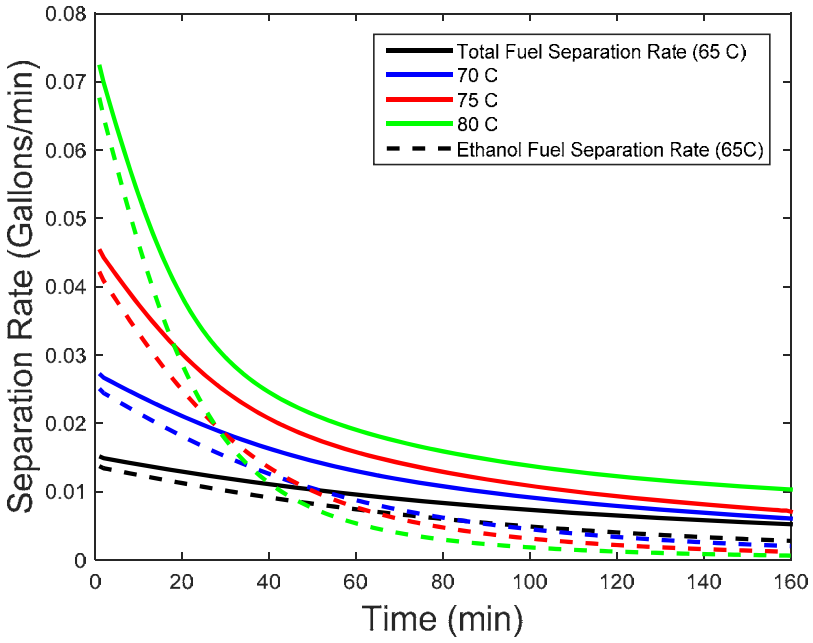

Figure 6-8: Fuel separation rate in gallons per minute vs. time in seconds. Solid lines are for total fuel while dotted lines are for ethanol.

It can be seen that the separation is much faster for higher temperatures as the difference between the saturation pressure on the feed side and the vacuum pressure on the permeate side is higher. By raising the fuel temperature by 10 ºC from 70 ºC, the separation time decreased by 1/3. This is because the separation rate at the beginning of the process is almost three times faster, as shown in Figure 6-8. However, as the separation rate is faster at the beginning, it diminishes faster as well due to the rapid change in ethanol concentration on the feed side. Another important parameter that can be controlled is the vacuum pressure. The lower the vacuum pressure, the faster the separation gets, as shown in Figure 6-9, but it requires more power consumption. The vacuum pressure slightly changes ethanol concentration at the start of the separation process.

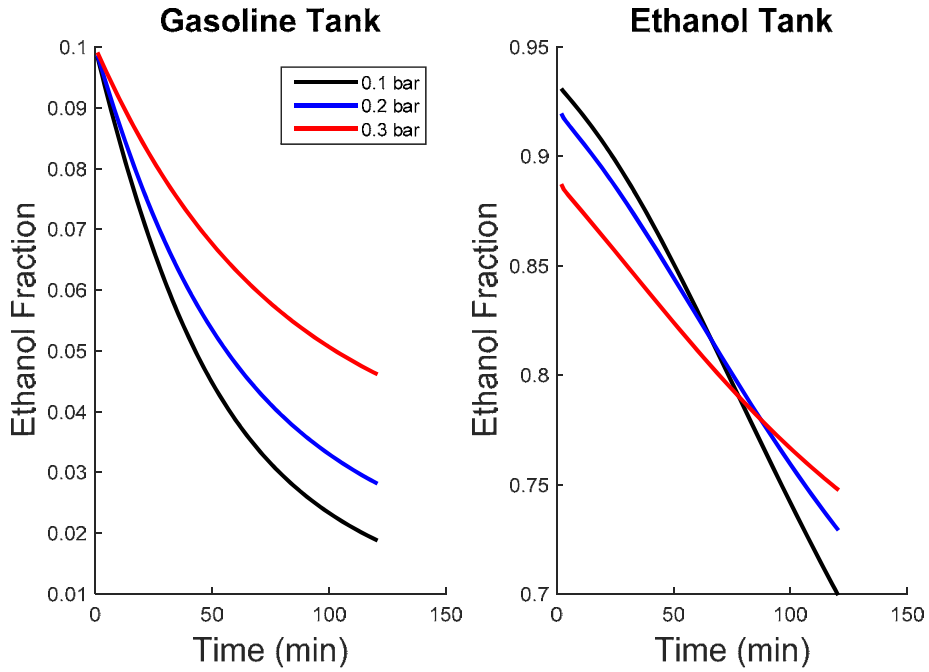

Figure 6-9: Ethanol fraction in the gasoline tank (left) and the ethanol tank (right) vs. time for different vacuum pressures.

Then, a parametric study is done to see the effect of fuel temperature and vacuum pressure on the time it takes to separate the fuel until the ethanol concentration in the main tank hits 2.5%, as shown in Figure 6-10. A three-dimensional map is constructed to visualize the effects of fuel temperature and vacuum pressure on the separation time (shown in Figure 6-10). To make the analysis easier, a two-dimensional contour was generated in Figure 6-11.

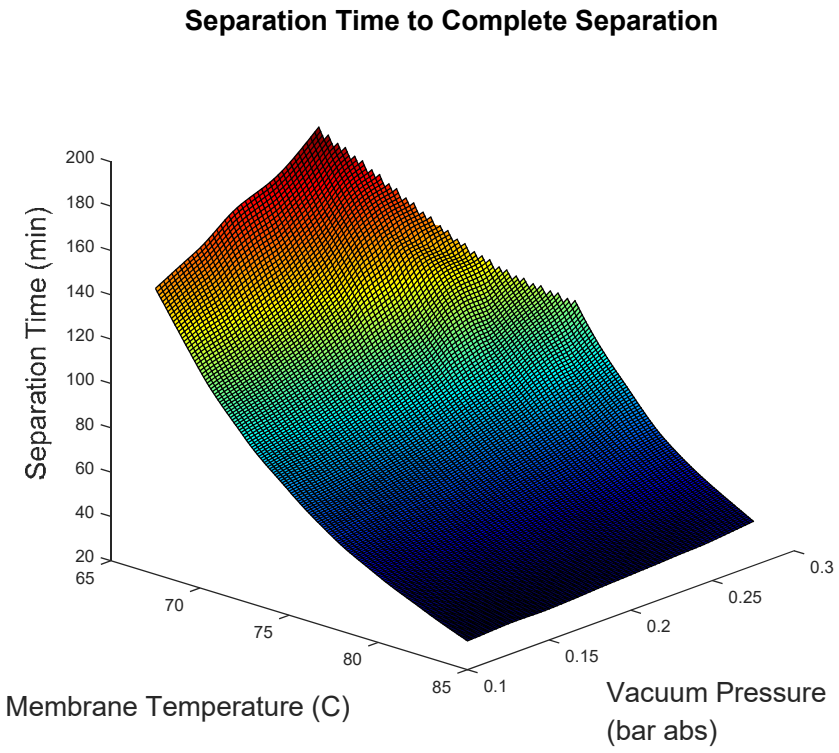

Figure 6-10: Separation time to complete the fuel separation vs. membrane temperature in Celsius and vacuum pressure in absolute bar. The surface is color-coded.

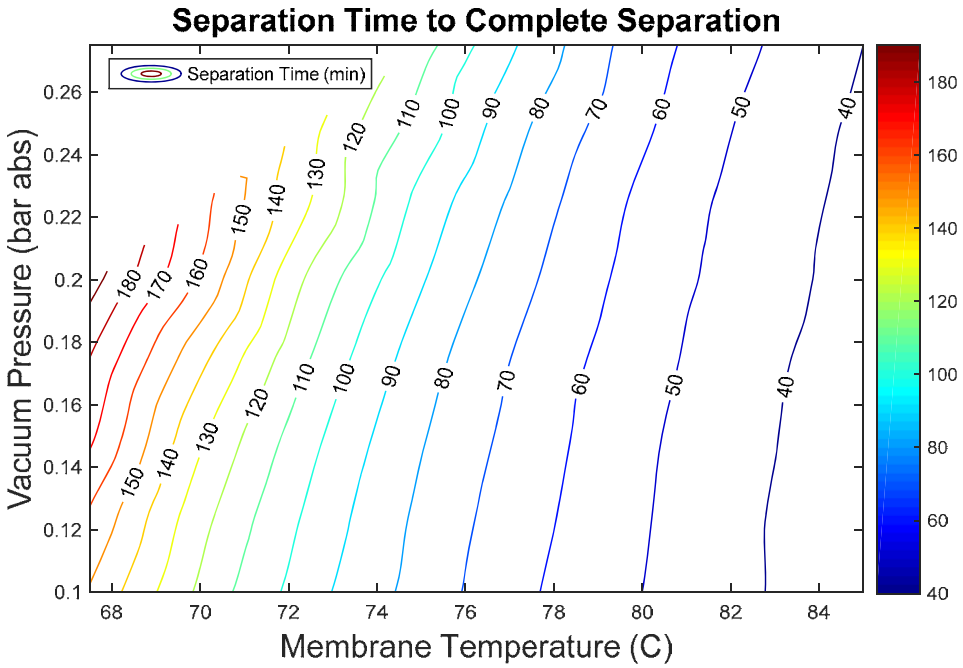

Figure 6-11: Separation time in minutes to complete the fuel separation vs. membrane temperature in Celsius and vacuum pressure in absolute bar. Contours are color-coded.

As analyzed before, separation is faster with higher fuel temperature and lower vacuum pressure. However, it can be seen that the fuel temperature effect dominates, so the vacuum pressure has to be kept at a moderate level so power consumption is not too high. Finally, simulation results are compared to performance of the actual system constructed by Honda. Honda's results assume 1/3 of the tank filled with E09 fuel, so the model was modified to match the initial conditions. The separation rate of the model is directly proportional to the membrane surface area. A membrane area is assumed to be 0.1 m^2, which is similar to the membrane area used in Exxon's paper [35]. Honda kept the fuel temperature at 70 ºC since it was easy to maintain with engine coolant, and there were no concerns about fuel boiling. Figure 6-12 shows the result of the comparison, and the ethanol fraction change with time matches well that of Honda's result.

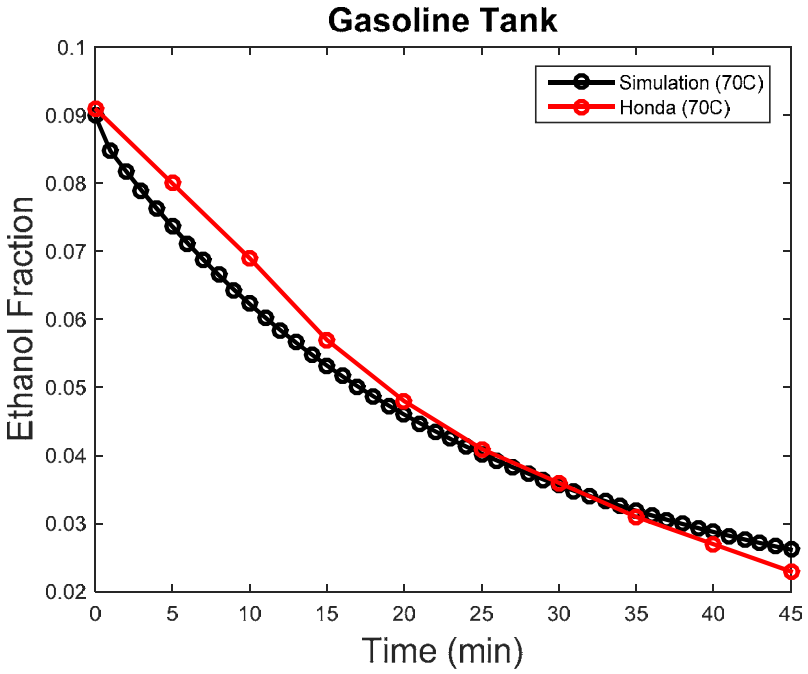

Figure 6-12: Ethanol fraction in the main tank vs. time in minutes. The black line with markers are simulated results, and the red line with markers is data taken from Honda's experimental results [36].

6.2 Ethanol consumption of a dual fuel system

In this section, ethanol consumption and fuel economy of various engine configurations will be presented. Results with four engine downsizing scenarios (one more than what was shown in an earlier section), different spark retard strategies, and three different compression ratios will be

presented for a passenger vehicle model. Most of the results are presented at a compression ratio at 11.5:1 since it is considered as a point beyond which efficiency benefits marginally decrease.

Displaced volume effects

Decreasing the engine's displaced volume while increasing a boost level to maintain maximum torque, the engine's performance remains similar to that of the original Camry's engine. Figure 6-13 and 6-14 show the results of the engine-in-vehicle simulation. Both maps were used to run the vehicle on the UDDS cycle, but the boost levels are different; Fig. 6-13 shows a naturally aspirated engine map (2.5 L) while Fig. 6-14 shows a downsized engine map (1.1 L) with 1 bar extra boost (2 bar absolute intake manifold air pressure) generated from the turbocharger. Compression ratio was 11.5:1 for both cases. Each black point means that the engine was run at that point for 0.1 second.

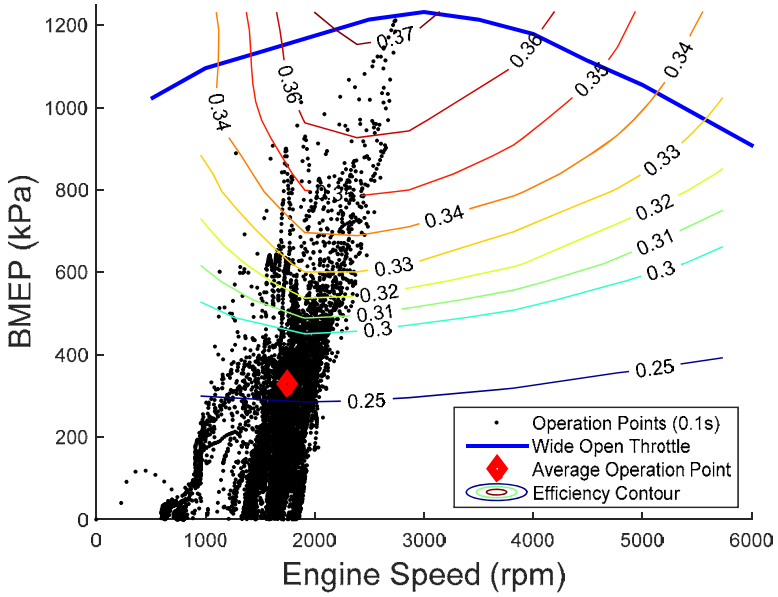

Figure 6-13: Operating points on the engine's performance map (2.5L NA engine with compression ratio of 11.5:1). Blue line is a wide open throttle limit, black points are operating points simulated from Autonomie over the UDDS cycle run with a passenger vehicle, a red square is the average operating point, and efficiency contours are in varying colors. Spark timings were kept at MBT timing.

To compare how the operating points shifted, the average operating point was determined. It can be seen that the average operating point in BMEP is much higher in the turbo-downsized engine though the torque outputs are the same. This makes the engine operate in a more efficient area on the engine map. The average operating point lies on the 26% brake engine efficiency for

NA engine, but it lies on the 35% for the turbo-downsized engine. However, this also makes the engine more prone to knock. Similar comparisons are done in HWFET and US06 cycles in Figure 6-15 and 6-16 respectively.

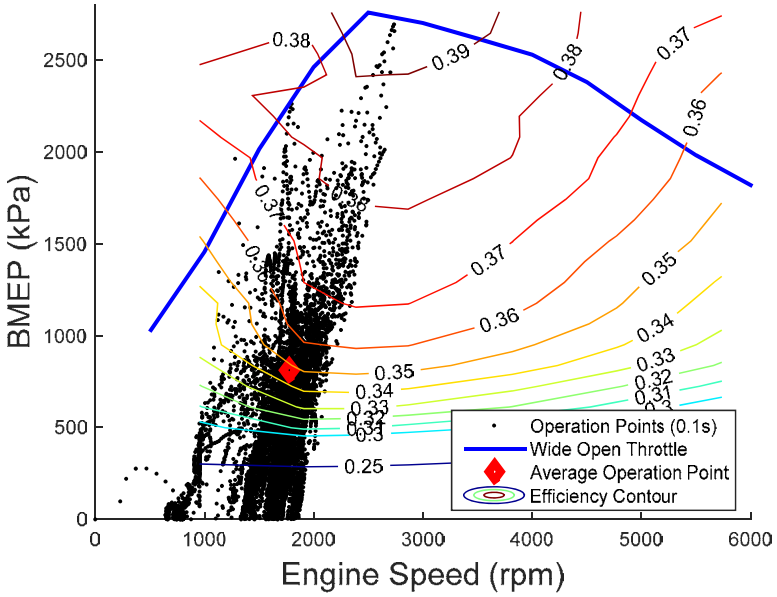

Figure 6-14: Operating points on the engine's performance map (1.1L turbo-downsized engine with compression ratio of 11.5:1). Blue line is wide open throttle limit, black points are operating points simulated from Autonomie over the UDDS cycle run with a passenger vehicle, red square is the average operating point, and efficiency contours are in varying colors. Spark timings were kept at MBT timing.

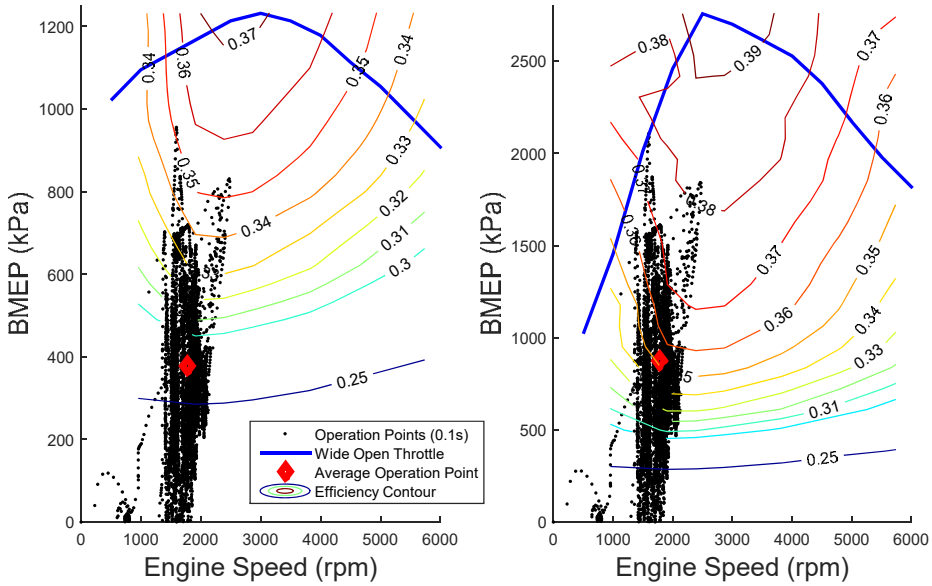

Figure 6-15: Operating points on the engine's performance map with a 2.5L NA engine (left) and 1.1L turbocharged engine (right) with compression ratio of 11.5:1. Blue line is wide open throttle limit, black

points are operating points simulated from Autonomie over the HWFET cycle, a red square is the average operating point, and efficiency contours are in varying colors. Spark timings were kept at MBT timing.

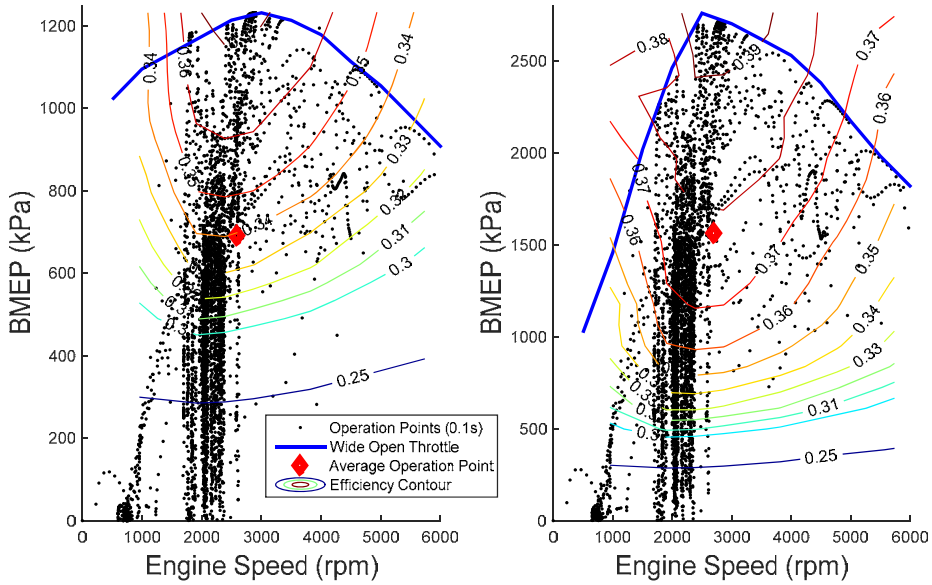

Figure 6-16: Operating points on the engine's performance map with a 2.5L NA engine (left) and 1.1L turbocharged engine (right) with compression ratio of 11.5:1. Blue line is wide open throttle limit, black points are operating points simulated from Autonomie over the US06 cycle, a red square is the average operating point, and efficiency contours are in varying colors. Spark timings were kept at MBT timing.

Figure 6-17 shows the effect of downsizing on the average brake efficiency for the UDDS cycle as the engine is operating on a more efficient region on the engine map. For each operating point, the engine brake efficiency is calculated by using the equation (5.1). The average engine brake efficiency was calculated for the three driving cycle in Figure 6-17. For all three cycles, downsizing the engine greatly increases the average engine brake efficiency. Downsizing the engine by 50% provides about a 30% increase in the average brake efficiency for the UDDS cycle. The US06 cycle shows a 15% increase with 50% downsizing, because in this cycle the engine is already operating in a higher efficiency region without downsizing. As a vehicle is driven in more aggressive cycle, the benefits of downsizing will decrease, and ethanol consumption increases substantially. As the average engine brake efficiency for the cycle increases, fuel economy also improves (shown in Figure 6-18).

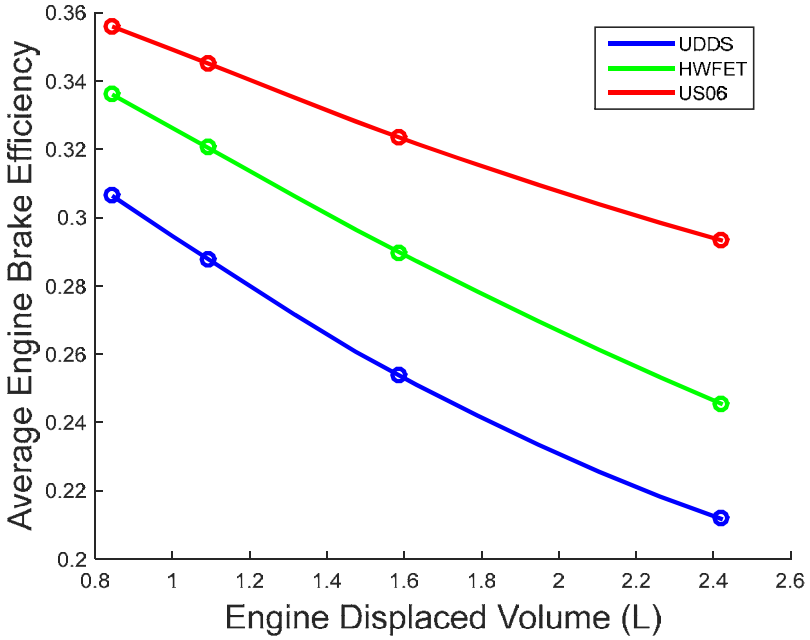

Figure 6-17: The average brake efficiency vs. engine displaced volume for three standard U.S. driving cycles run with a passenger vehicle. Compression ratio was at 11.5:1, and the spark timings were kept at MBT timing.

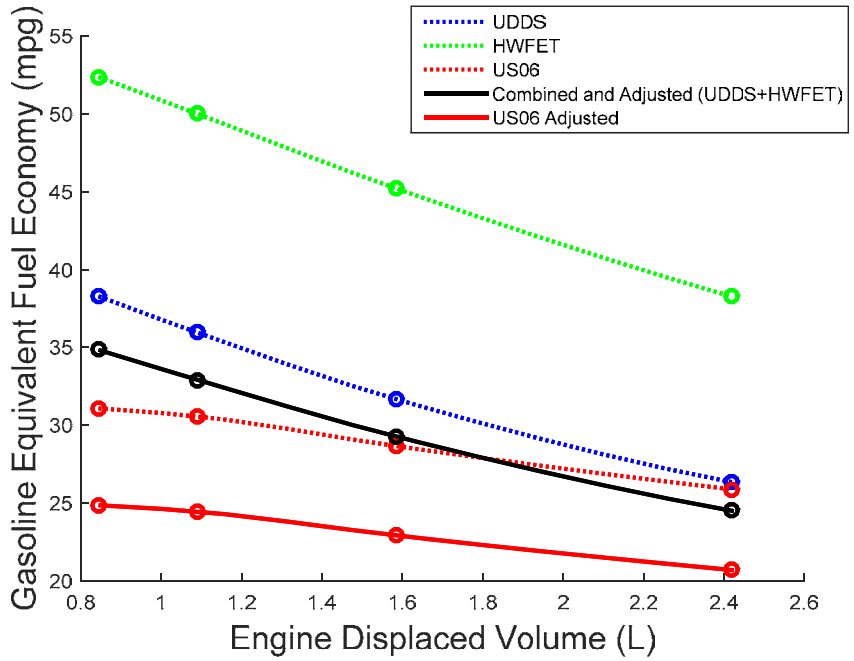

Figure 6-18: Gasoline equivalent fuel economy vs. engine displaced volume for three standard U.S. driving cycles run with a passenger vehicle. Dotted lines are the results from the engine-in-vehicle simulation, and solid lines are combined (UDDS and HWFET) and adjusted values. The fuel economy for the US06 cycle was just adjusted. Compression ratio was at 11.5:1, and the spark timings were kept at MBT timing.

Figure 6-18 shows that 50% downsizing increases the combined fuel economy from 25 mpg to 30 mpg, which is about a 20% increase. Engine brake efficiency increase and the fuel economy increase are not exactly the same, since transmission efficiency and gear ratios affect the fuel economy. Downsizing results in higher efficiency and fuel economy as shown in Fig. 6-17 and 6-18, but this benefit comes with a cost of increased ethanol consumption. Figure 6-19 shows the effect of downsizing on the ethanol requirements, with the engine operating at MBT spark timing. UDDS and HWFET require very little ethanol when the engine is naturally aspirated. However, 50% downsizing increases the ethanol fraction to 8~10%. This is worse for US06 as the ethanol fraction increases by almost 7 times with 50% downsizing. However, ethanol fraction can be reduced with a proper use of spark retard. This will be discussed in the next section.

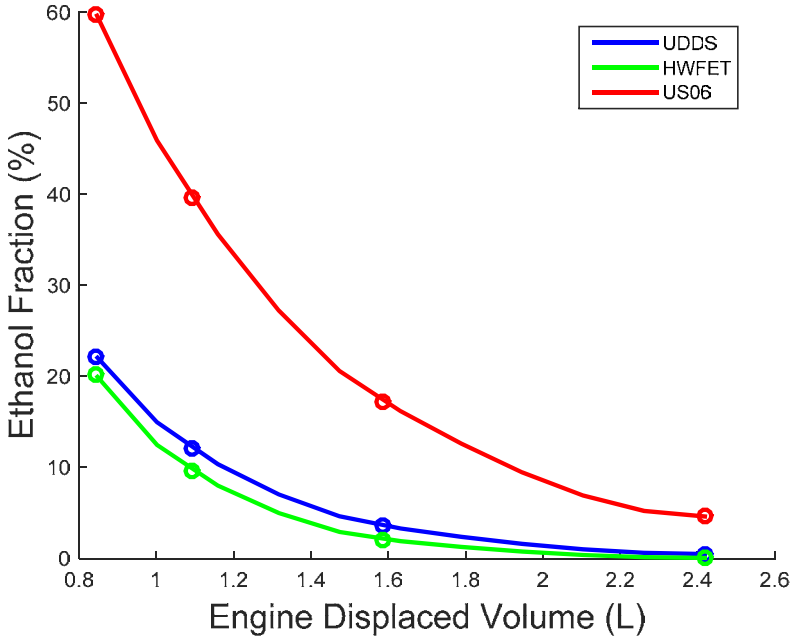

Figure 6-19: Ethanol fraction in percentage by volume vs. engine displaced volume for three standard U.S. driving cycles run with a passenger vehicle. Compression ratio was at 11.5:1, and the spark timings were kept at MBT timing.

Spark retard effects

By retarding the spark timing from MBT timing, the probability of knocking decreases due to lower in-cylinder pressures and temperatures, at the expense of reduced engine brake efficiencies. Therefore, spark retard can reduce the amount of ethanol required to suppress knock. Figure 6-20

shows the effect of spark retard on ethanol consumption. UDDS and US06 cycles were considered with 3 different retard scenarios. The first case is when the engine is run always at MBT timings with no spark retard. In the second case, the engine is allowed to retard the spark timing when needed up to 5 CAD from MBT timing, at the engine load where the knocking starts. After retarding by up to 5 CAD, ethanol is then used to suppress knock, while maintaining 5 CAD spark retard. Similarly in the last retard case, the engine is allowed to retard by up to 10 CAD from the engine load where knocking starts.

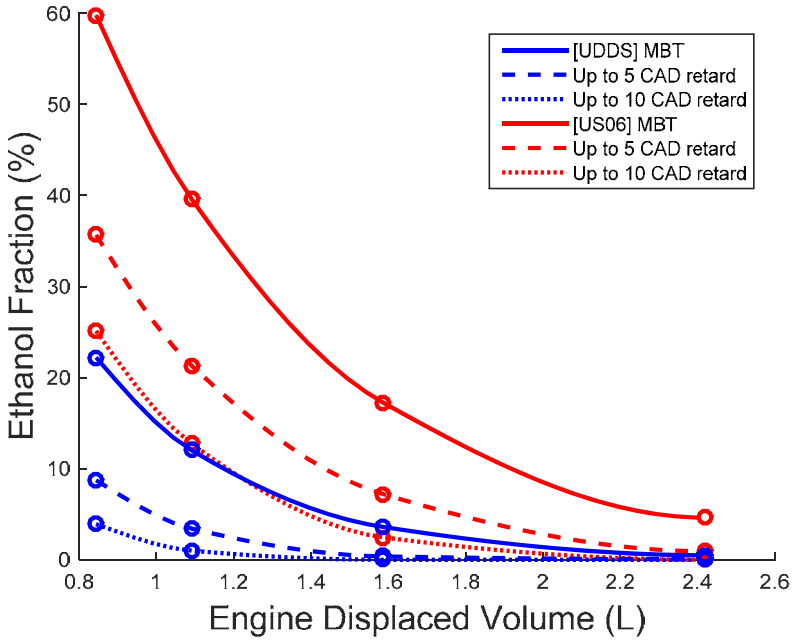

Figure 6-20: Ethanol fraction in percentage vs. engine displaced volume for UDDS (blue) and US06 (red) cycles run with a passenger vehicle. Dashed-lines represent the case with up to 5 CAD retard allowed, and dotted-lines represent the case with up to 10 CAD retard allowed. Compression ratio was at 11.5:1.

The engine brake efficiency and the fuel economy are shown in Figures 6-21 and 6-22 respectively. For US06 cycle, the ethanol fraction decreased from 33% to 9.7% at 1.2L displaced volume with up to 10 CAD retard, about a 70% reduction in ethanol requirement. The ethanol fraction decreased down to 1% for UDDS cycle. It can be seen that spark retard is effective in reducing the ethanol fraction. As mentioned above, in the NA engine (without downsizing) knock is avoided, without the need of ethanol. However, retarding the spark timing slightly reduces the engine brake efficiencies as the engine no longer operates at the optimal timing. Figure 6-21 shows the effect of spark retard on the engine brake efficiencies.

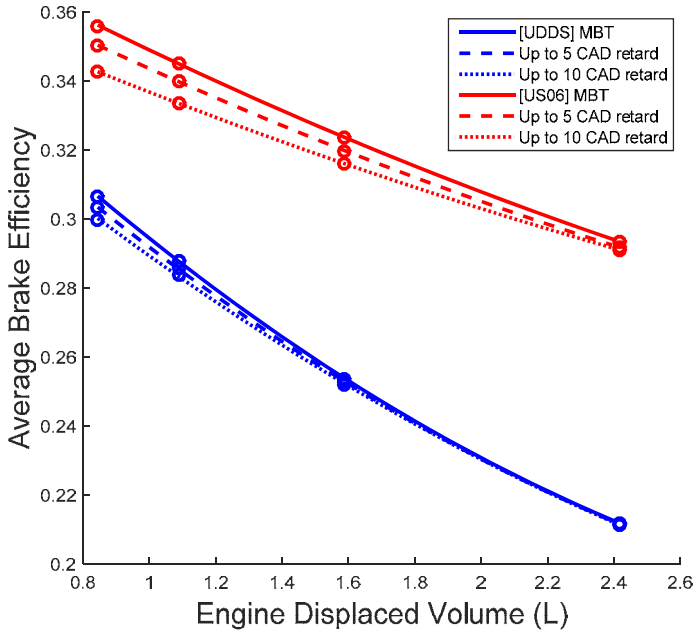

Figure 6-21: Average engine brake efficiency vs. engine displaced volume for UDDS (blue) and US06 (red) cycles run with a passenger vehicle. Dashed-lines represent the case with up to 5 CAD retard allowed, and dotted-lines represent the case with up to 10 CAD retard allowed. Compression ratio was at 11.5:1.

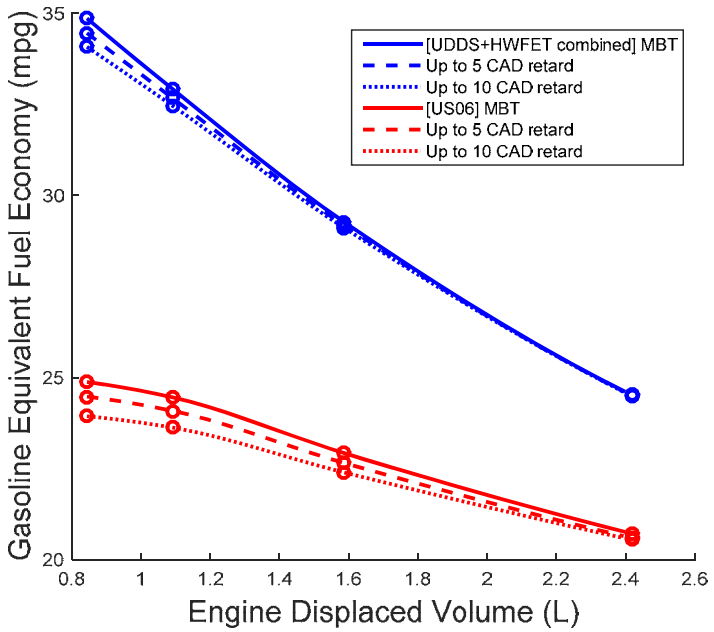

Figure 6-22: Gasoline equivalent fuel economy vs. engine displaced volume for UDDS (blue) and US06 (red) cycles run with a passenger vehicle. Dashed-lines represent the case with up to 5 CAD retard allowed, and dotted-lines represent the case with up to 10 CAD retard allowed. Compression ratio was at 11.5:1.

Engine brake efficiency dropped about 3% for a 1.2L displaced volume engine running the US06 cycle. Interestingly, fuel economy also decreased by about the same amount (3%). Though the efficiency and fuel economy drop seems little, it has to be noted that even with 10 CAD retard, 10% ethanol is required to complete the US06 cycle without knocking. To reduce the ethanol consumption further, more retard has to be applied, and the efficiency drops further [15]. Also, the efficiency drop with increasing spark retard is worse when the engine is boosted as shown previous work [10].

For the UDDS, spark retard does not affect the engine brake efficiencies or fuel economy much until a substantial downsizing (about 50%) is realized. This is because the engine operates in a region away from knock where spark retard is not required. As the engine is further downsized, the UDDS's operating region shifts up to where knock suppression is required. Spark retard is more effective in the highly downsized cases and with aggressive driving styles. Based on the ethanol fraction and spark retard effects analyzed, ethanol and gasoline consumption in 1000 miles are plotted in Figure 6-23~25. 6-23 is a case where the spark retard is not allowed at all, while 6-24 and 6-25 are cases where the spark retard is allowed up to 5 CAD and 10 CAD respectively.

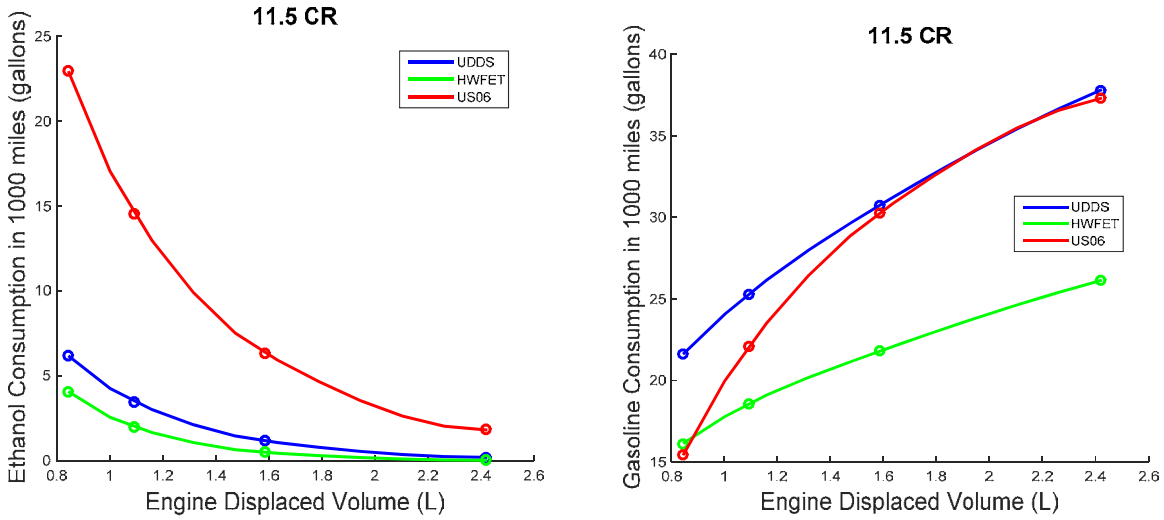

Figure 6-23: Ethanol consumption in 1000 miles (left) and gasoline consumption in 1000 miles (right) vs. engine displaced volume for three standard U.S. driving cycles run with a passenger vehicle. Spark timings were kept at MBT timing.

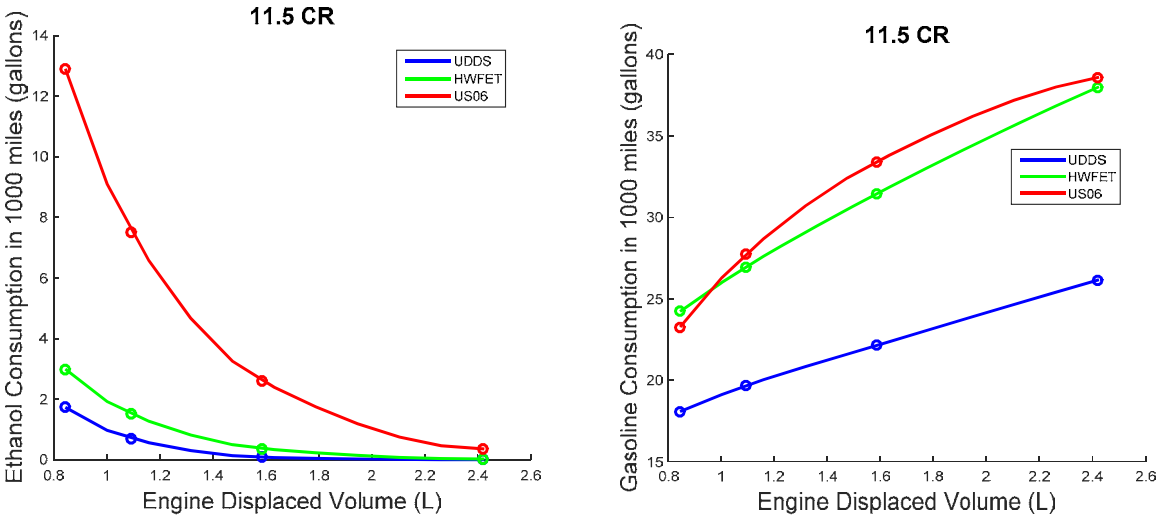

Figure 6-24: Ethanol consumption in 1000 miles (left) and gasoline consumption in 1000 miles (right) vs. engine displaced volume for three standard U.S. driving cycles run with a passenger vehicle. Up to 5 CAD retard allowed from MBT timing.

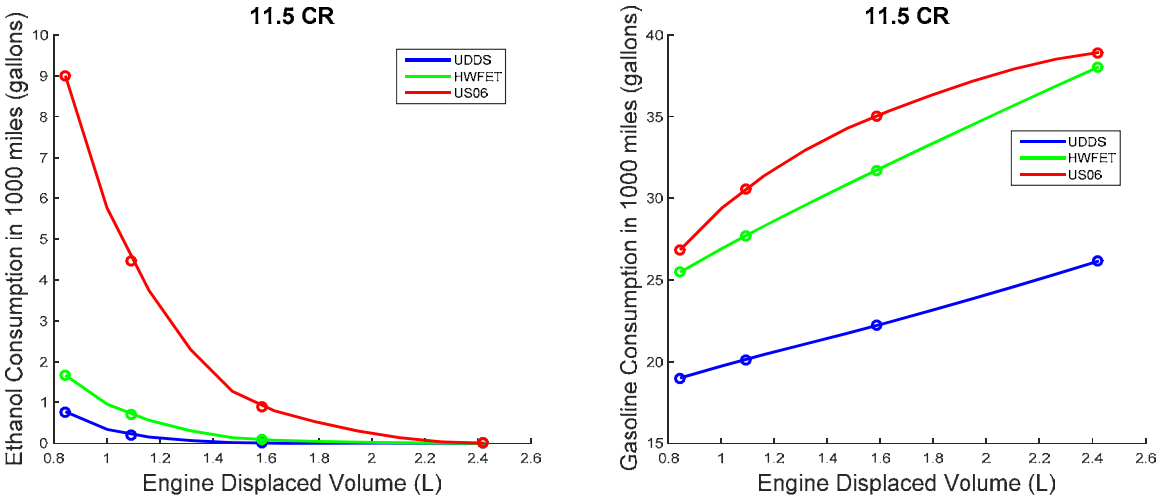

Figure 6-25: Ethanol consumption in 1000 miles (left) and gasoline consumption in 1000 miles (right) vs. engine displaced volume for three standard U.S. driving cycles run with a passenger vehicle. Up to 10 CAD retard allowed from MBT timing.

Shapes of the ethanol consumption graphs are similar to those of the ethanol fraction graphs. However, gasoline consumption shows increasing trends with diminishing manner as engine displaced volume increases. This is mainly due to exponentially decreasing ethanol requirement with less downsizing.

Compression ratio effects

All the results shown so far before were with a compression ratio of 11.5:1. To see the effect of compression ratio on the engine brake efficiencies, fuel economy, and ethanol fraction,

performance maps with two other compression ratios were considered (9.2:1 and 13:1). The average brake efficiencies are compared in Figure 6-26.

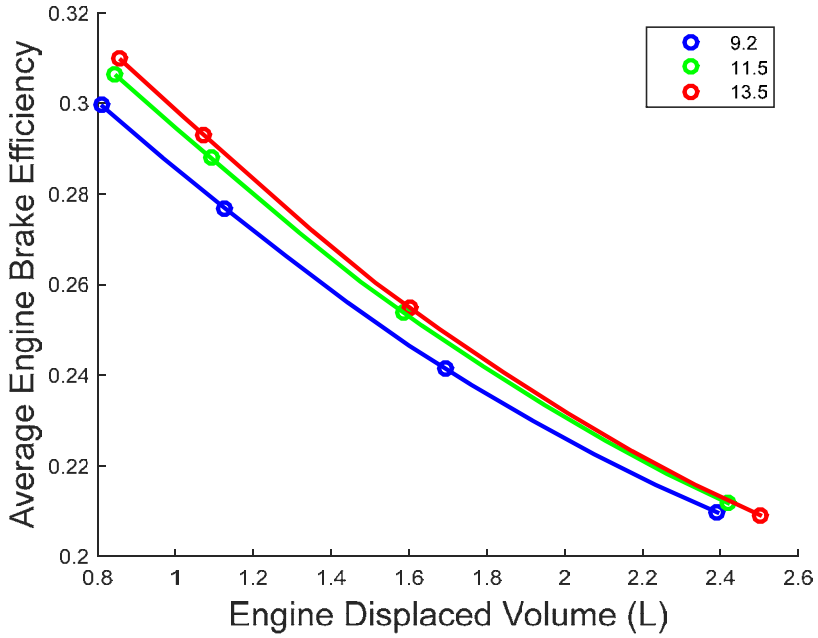

Figure 6-26: Average engine brake efficiency vs. engine displaced volume for UDDS cycle run with a passenger vehicle. Blue, green, and blue lines each represent 9.2:1, 11.5:1, and 13.5:1 compression ratios. Spark timings were kept at MBT timing.

For UDDS cycle with 50% downsized engine, the average engine brake efficiency increased about 3% by increasing a compression ratio from 9.2:1 to 11.5:1, while engine brake efficiency increased only about 1.5% by increasing compression ratio from 11.5:1 to 13.5:1. This decreasing marginal return in efficiency with increased compression ratio is well known from previous studies.

Figure 6-27 shows the engine brake efficiency change with different compression ratios for the US06 cycle. For this cycle with 50% downsized engine, the average engine brake efficiency increased about 4.5% by increasing a compression ratio from 9.2:1 to 11.5:1, while engine brake efficiency increased by about 3% by increasing compression ratio from 11.5:1 to 13.5:1. In a previous study by Smith et al., it was found that the efficiency increase with compression ratio is larger at higher loads [7, 10]. Since the engine operates at higher loads than in UDDS, the efficiency increase was higher in the US06 than in the UDDS cycle. Similar trends apply to fuel economy shown in Figure 6-28.

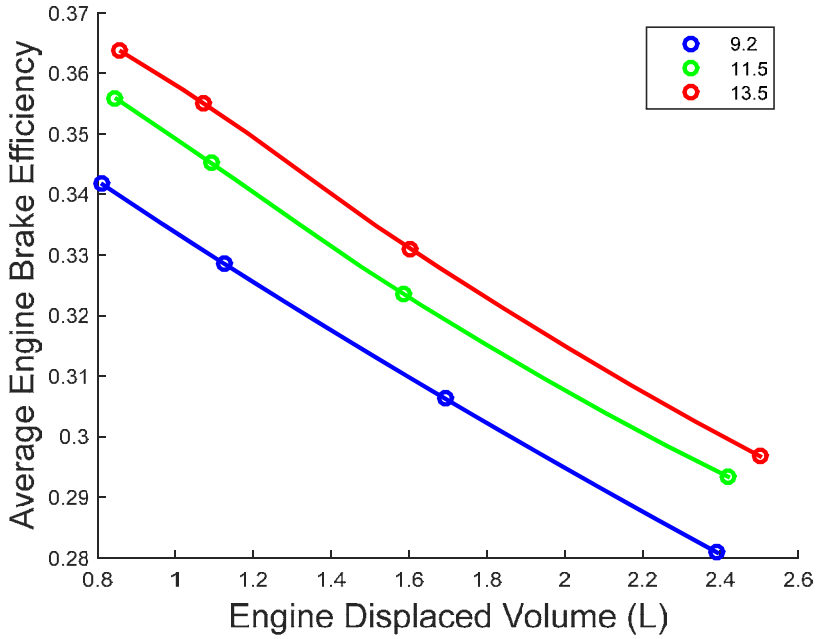

Figure 6-27: Average engine brake efficiency vs. engine displaced volume for US06 cycle run with a passenger vehicle. Blue, green, and blue lines represent 9.2:1, 11.5:1, and 13.5:1 compression ratios respectively. Spark timings were kept at MBT timing.

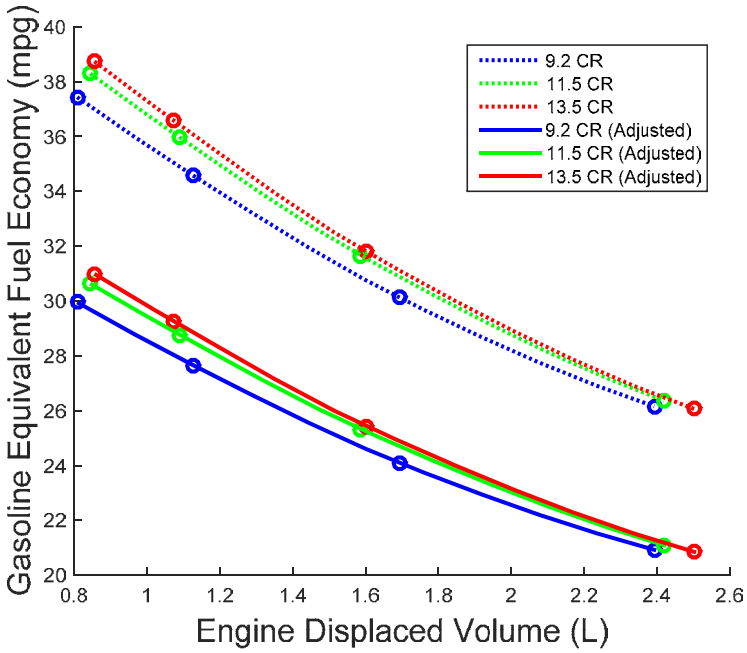

Figure 6-28: Fuel economy vs. engine displaced volume for UDDS cycle run with a passenger vehicle. Solid blue, green, and blue lines represent 9.2:1, 11.5:1, and 13.5:1 compression ratios respectively (dotted are unadjusted cycle simulation results). Spark timings were kept at MBT timing.

Figure 6-29 and 6-30 show the ethanol fraction consumed for different compression ratios at MBT for UDDS and US06 cycles respectively. For the UDDS cycle, downsizing increases ethanol consumption more with higher compression ratio than with lower compression ratio, because the engine is more knock limited at high loads with higher compression ratio than at lower compression ratio. As Figure 6-31 shows, more ethanol is required at higher compression ratio than at lower compression ratio. Since downsizing shifts the average operating load to higher BMEP, higher compression ratio results in a much higher increase in ethanol consumption than in the lower compression ratio case. This effect is less significant for US06 cycle where the average operation region is already quite high even for naturally-aspirated engines.

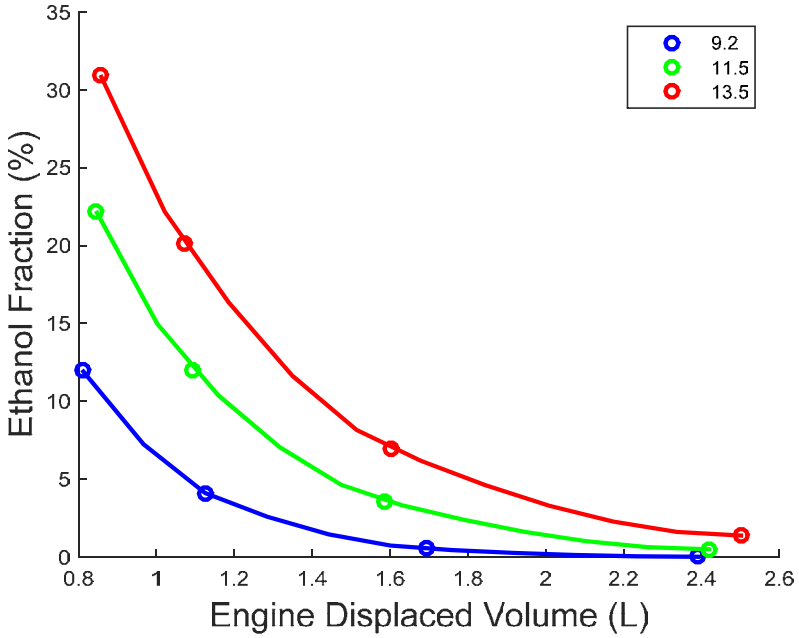

Figure 6-29: Ethanol fraction vs. engine displaced volume for UDDS cycle run with a passenger vehicle. Blue, green, and blue lines represent 9.2:1, 11.5:1, and 13.5:1 compression ratios respectively. Spark timings were kept at MBT timing.

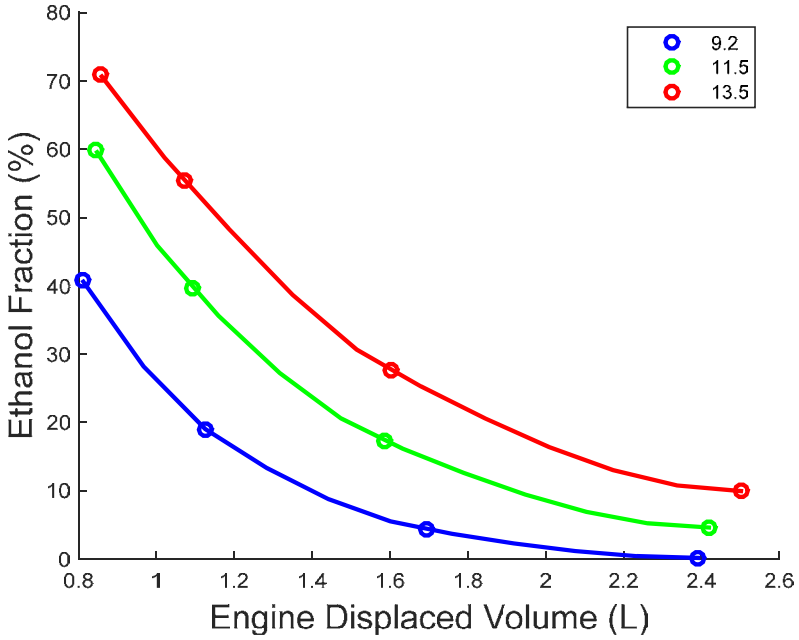

Figure 6-30: Ethanol fraction vs. engine displaced volume for US06 cycle run with a passenger vehicle. Blue, green, and blue lines represent 9.2:1, 11.5:1, and 13.5:1 compression ratios respectively. Spark timings were kept at MBT timing.

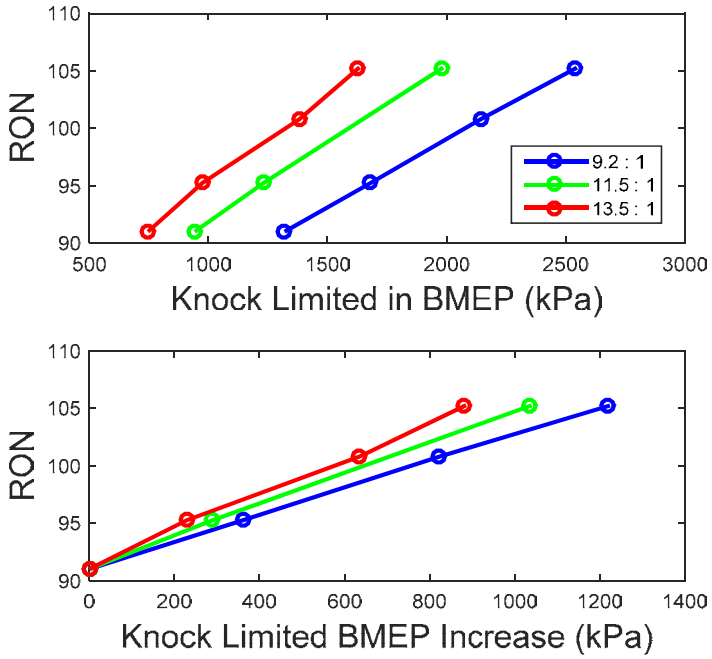

Figure 6-31: Octane requirement vs. knock limited BMEP (top) and knock limited BMEP increase (bottom). Blue, green, and blue lines represent 9.2:1, 11.5:1, and 13.5:1 compression ratios respectively. Spark timings were kept at MBT timing.

By looking at the average engine efficiency and ethanol fraction required for a given cycle at different compression ratios, it is possible to compare the effect of downsizing and compression ratio. Looking at 6-27 and 6-30 (results with US06 cycle), 2.5L NA engine with 13.5:1 CR has the same average engine brake efficiency as TC 1.9L engine with 9.2:1 CR, but ethanol fraction required is much higher for 13.5:1 CR, meaning that moderate downsizing is beneficial than raising compression ratio. Again, TC 0.8L engine with 9.2:1 CR and TC 1.4L engine with 13.5:1 CR have the same average engine brake efficiency while 9.2:1 engine has higher ethanol consumption. In this case, TC 1.2L 11.5:1 CR engine had the lowest ethanol consumption with the same average engine brake efficiency. The graph gives a good reference to compare the effect of turbocharging and compression ratio on the average engine brake efficiency and ethanol consumption, which makes a direct comparison possible.

With the same amount of BMEP increase, pressure levels would increase more with higher compression ratio than in lower compression ratio. Efficiency benefits of increasing compression ratio decreases above around 11.5:1 compression ratio while ethanol consumption increase substantially along with downsizing. Therefore, for this dual fuel approach, it is beneficial to keep the compression ratio reasonably high (not too high) and apply a moderate amount of spark retard to keep ethanol consumption low while not degrading efficiency much. Other miscellaneous trends are shown in Figure 6-32 and 6-33.

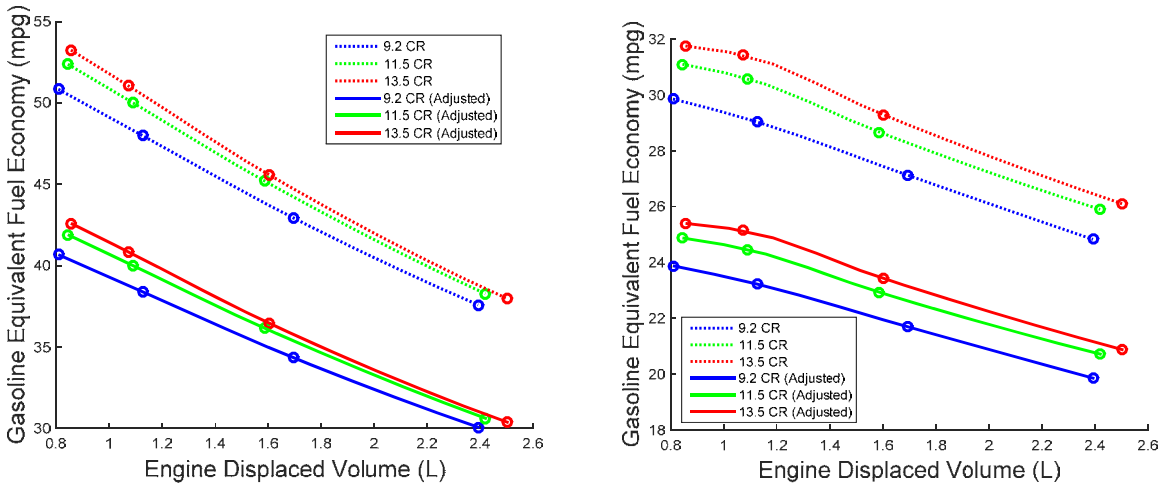

Figure 6-32: Gasoline equivalent fuel economy for HWFET cycle (left) and gasoline equivalent fuel economy for US06 cycle vs. engine displaced volume. Dotted lines are the results from the engine-in-

vehicle simulation run with a passenger vehicle, and solid lines are adjusted values. Compression ratio was at 11.5:1, and spark timings were kept at MBT timing.

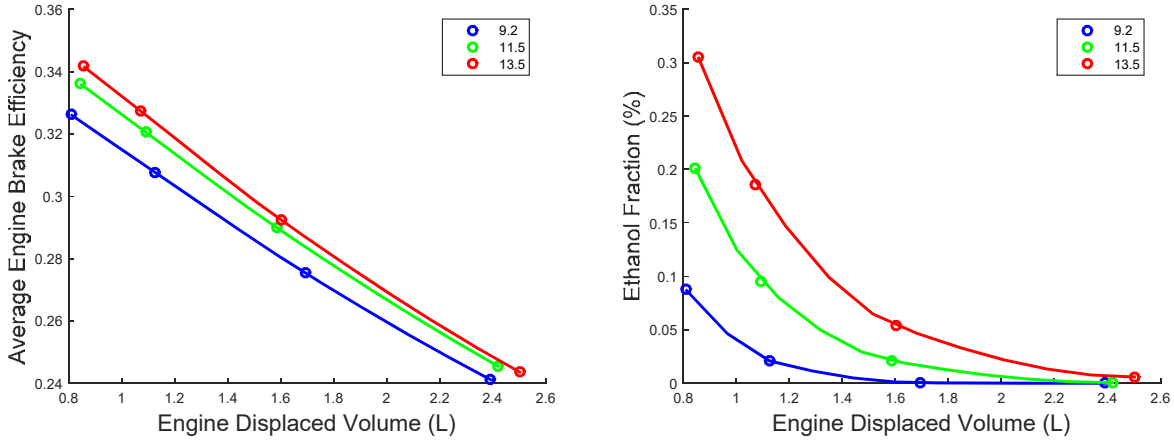

Figure 6-33: The average engine brake efficiency (left) and ethanol fraction (right) vs. engine displaced volume for HWFET cycle run with a passenger vehicle. Spark timings were kept at MBT timing.

Based on the analysis of compression ratio effects on the ethanol fraction, ethanol and gasoline consumption in 1000 miles are plotted in Figure 6-34~36. The results are similar as in Figures 6-23~25 but Figure 6-34~36 are results with different compression ratios at MBT timing. Figure 6-34, 6-35, and 6-36 respectively show gasoline and ethanol consumption for UDDS, HWFET, and US06 cycles, and they present results at different engine displaced volumes and different compression ratios.

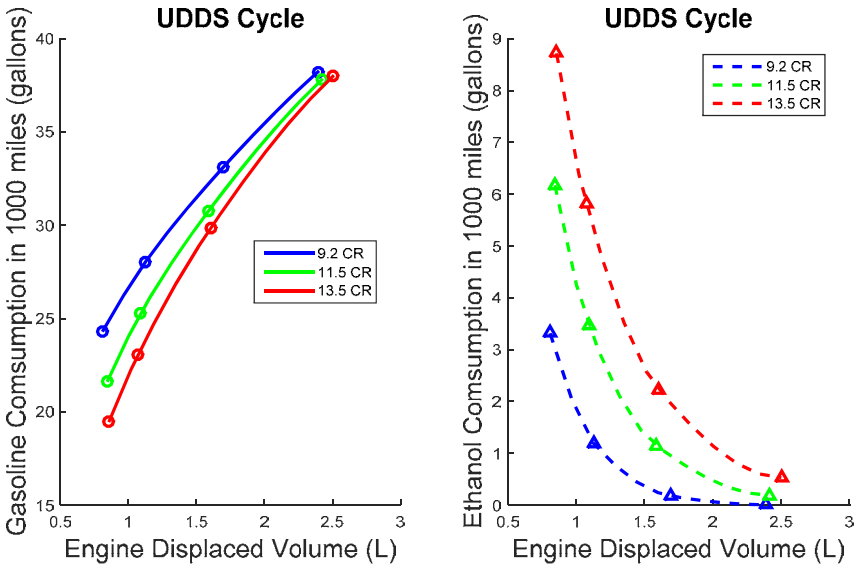

Figure 6-34: Gasoline consumption in 1000 miles (left) and ethanol consumption in 1000 miles (right) vs. engine displaced volume for UDDS cycle run with a passenger vehicle. Spark timings were kept at MBT timing.

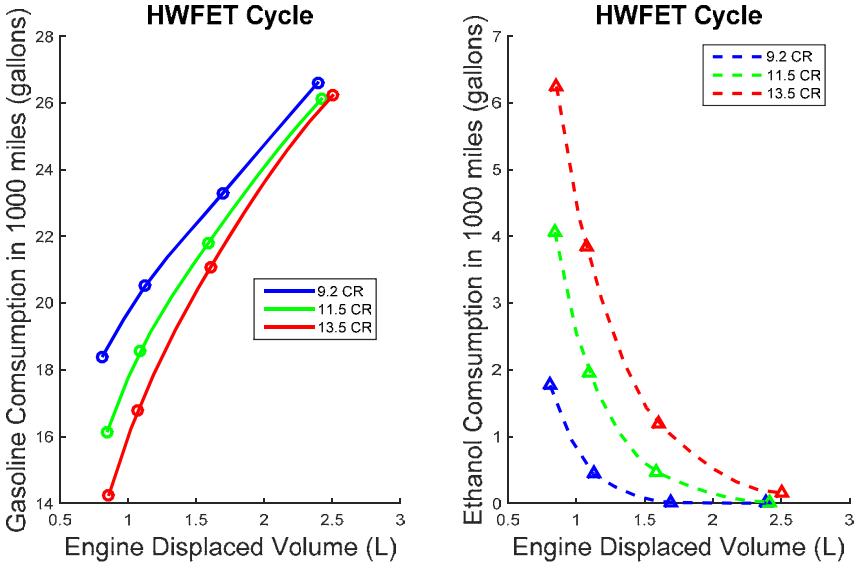

Figure 6-35: Gasoline consumption in 1000 miles (left) and ethanol consumption in 1000 miles (right) vs. engine displaced volume for HWFET cycle run with a passenger vehicle. Spark timings were kept at MBT timing.

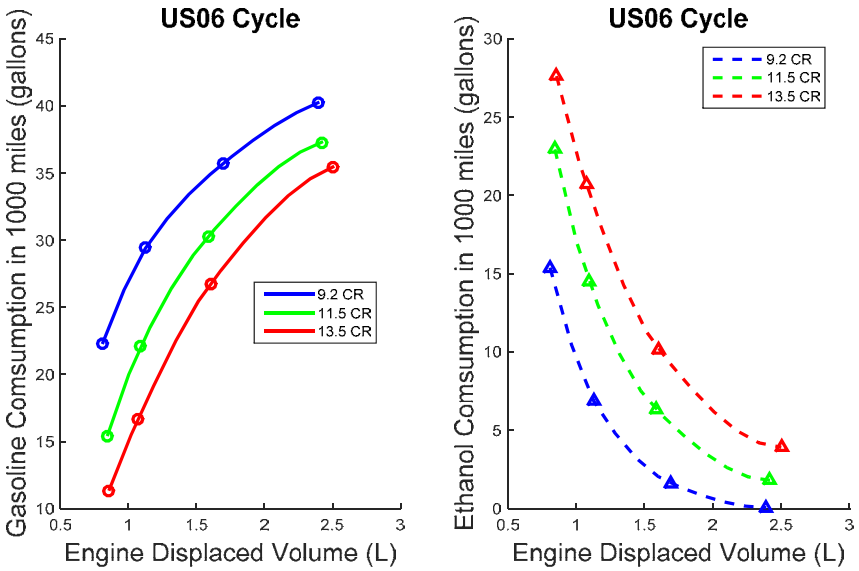

Figure 6-36: Gasoline consumption in 1000 miles (left) and ethanol consumption in 1000 miles (right) vs. engine displaced volume for US06 cycle run with a passenger vehicle. Spark timings were kept at MBT timing.

Like in Figure 6-23~24, shapes of the ethanol consumption graphs are similar to those of the ethanol fraction graphs. However, gasoline consumption shows increasing trends with diminishing manner as engine displaced volume increases. This again can be attributed to exponentially decreasing ethanol requirement with less downsizing.

6.3 Scenarios comparison

With a fuel separation system model and ethanol consumption results, it is possible to consider two OOD applications: two-tank and OBS. For two-tank system, refueling frequency of the ethanol tank is important while capability of completing a given cycle is important for OBS system. In this section, benefits and disadvantages of each system are discussed. All the cases discussed in this section is with results from the test engine with CR of 9.2:1.

Two-tank scenarios

For realistic estimation of the amount of high octane fuel consumption, ethanol fraction is converted to E85 consumption. This is because ethanol is barely used as a stand-alone fuel. Two vehicles (passenger and medium duty truck), three downsizing cases (NA, 30%, 50% downsizing), and five spark retard strategies are considered. Figure 6-37 shows the fuel

consumption of a passenger vehicle with three downsized engines running on the U.S. combined cycle and US06 cycle.

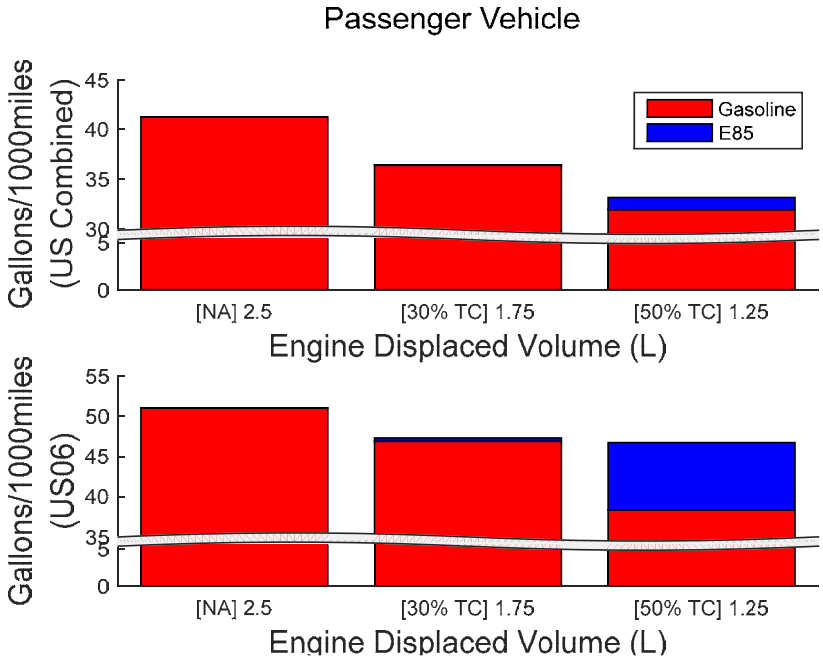

Figure 6-37: Fuel consumption per 1000 miles of a passenger vehicle with three downsized engines. In a bar graph, gasoline consumption is colored in red while E85 consumption is colored in blue. Results for U.S. combined cycle (on the top) and US06 cycle (on the bottom) are shown. All the engines operating at MBT timings.

For both cycles, total fuel consumption drops with downsizing of the engine since downsized engines run in a more efficient area on the engine map. However, that region is more knock limited, so E85 consumption increases as well. Due to a lower volumetric energy content of E85 (about 2/3 of that of gasoline), significant increase in ethanol consumption increases total fuel consumption greatly as shown for US06 case. However, this is because spark timings are kept always at MBT in this case. To see how spark retard can reduce the E85 consumption, 50% downsized engine running on US06 is considered in Figure 6-38.

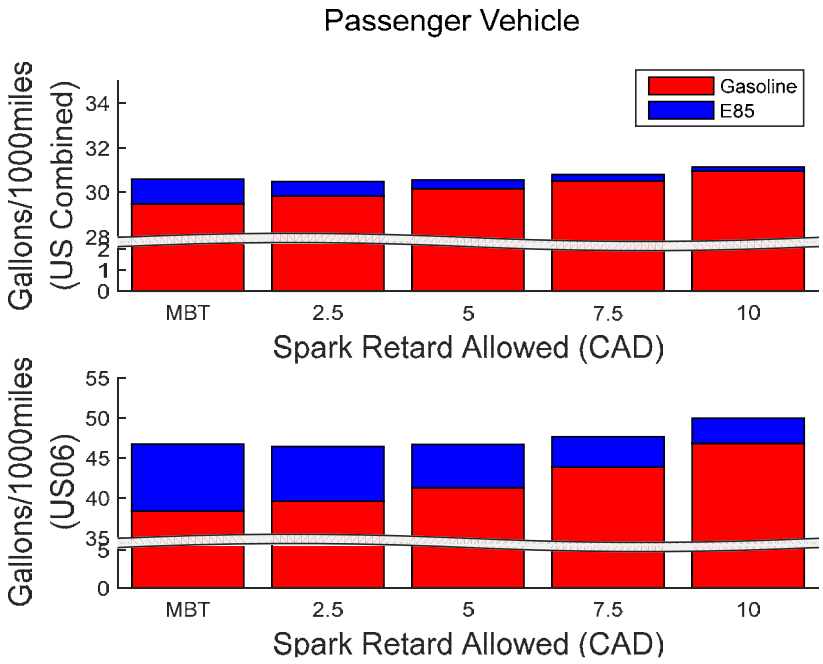

Figure 6-38: Fuel consumption per 1000 miles of a passenger vehicle with five different spark retard strategies on a 50% downsized engine. In a bar graph, gasoline consumption is colored in red while E85 consumption is colored in blue. Results for U.S. combined cycle (on the top) and US06 cycle (on the bottom) are shown.

Total fuel consumption increases with spark retards up to 10 CAD, but gasoline replaces ethanol effectively up to 5 CAD retard without increasing the total fuel consumption much. Up to 5 CAD retard allowed, total fuel consumption does not change much with decreasing E85 consumption. Therefore, moderate spark retard (up to 5 CAD) has to be applied for dual fuel applications. Similar analysis is done with medium duty truck in Figures 6-39 and 6-40. Results are similar, only the scale of volumetric fuel consumption is higher with lower fuel economy.

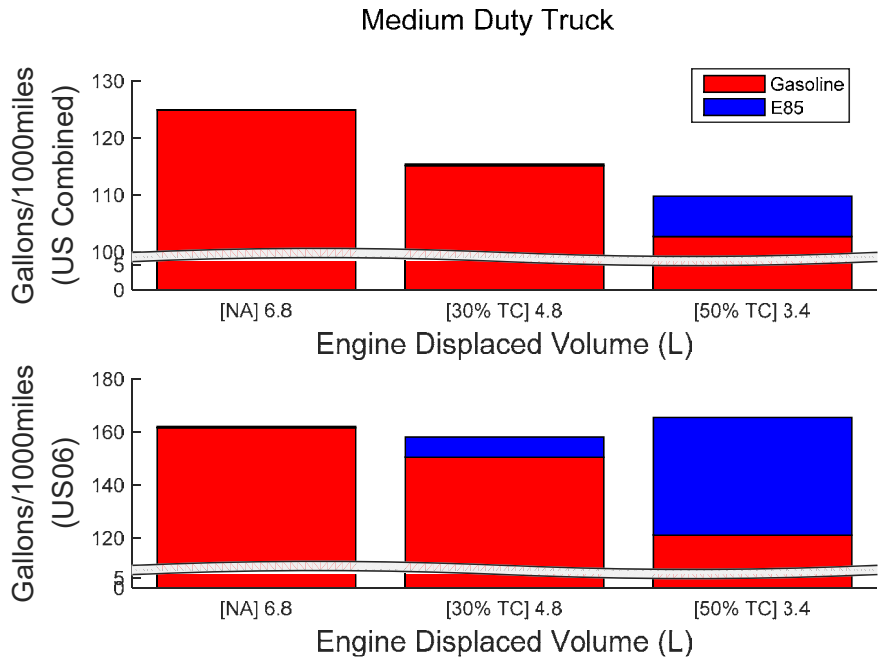

Figure 6-39: Fuel consumption per 1000 miles of a medium duty truck with three downsized engines. In a bar graph, gasoline consumption is colored in red while E85 consumption is colored in blue. Results for U.S. combined cycle (on the top) and US06 cycle (on the bottom) are shown. All the engines operating at MBT timings.

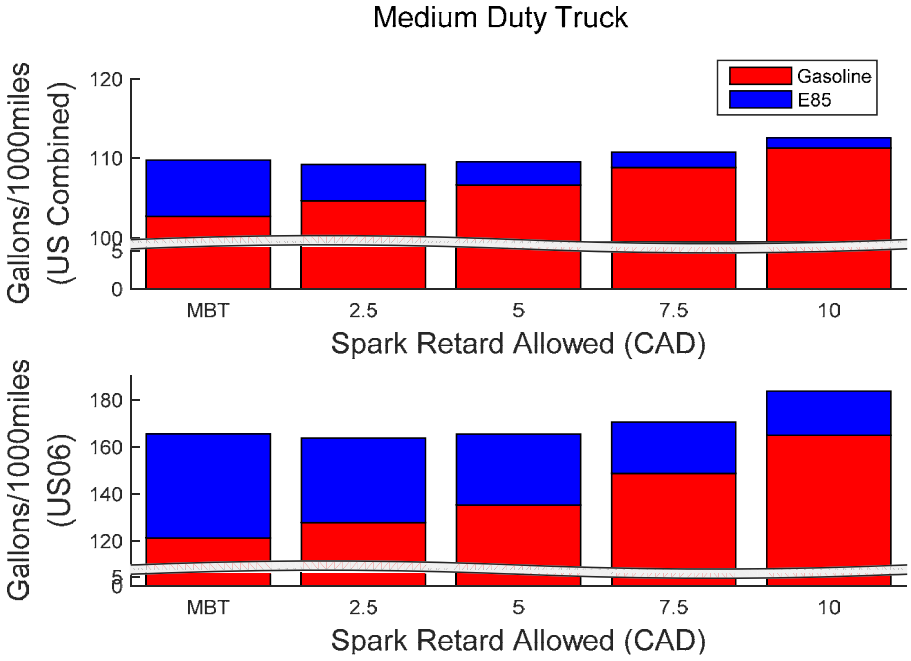

Figure 6-40: Fuel consumption per 1000 miles of a medium duty truck with five different spark retard strategies on a 50% downsized engine. In a bar graph, gasoline consumption is colored in red while E85 consumption is colored in blue. Results for U.S. combined cycle (on the top) and US06 cycle (on the bottom) are shown.

Based on the fuel consumption results, it is possible to calculate the leveraging ratios. A leveraging effect is when a gallon of high octane fuel (e.g. E85) replaces more than a gallon of gasoline. For example, 1 gallon of E85 replaces 9.8 gallons of gasoline for 30% downsized turbocharged engine when compared to naturally aspirated engine running the US06 cycle (therefore leveraging ratio of 9.8:1). This effect happens due to the fuel economy improvements by turbo-downsizing and knock suppression achieved by dual fuel injection. Table 6-1 shows leveraging ratios for two vehicles with different downsizing levels and driving cycles. As driving cycle or downsizing is more aggressive, leveraging ratio decreases with increased high octane fuel consumption.

Table 6-1: Leveraging ratios of downsized engines for passenger and medium duty truck, based on the naturally aspirated running at MBT

Drive Cycle	Downsizing	Passenger	Medium Duty Truck
U.S. Combined	**NA to 30%**	250.9 : 1	34.2 : 1
	NA to 50%	7.6 : 1	3.1 : 1
US06	**NA to 30%**	9.8 : 1	1.5 : 1
	NA to 50%	1.5 : 1	0.9 : 1

Knowing E85 consumption, refueling frequency of the ethanol tank can be calculated. Figure 6-41 and 6-42 shows how many times the ethanol tank has to be refueled for every gasoline tank refueling for US combined cycle and US06 cycle respectively. It was assumed that the gasoline and E85 tank sizes are 15 and 3 respectively (changing this numbers will change the refueling proportionality accordingly). With spark retard, refueling proportionality drops significantly, but one has to be mindful that the total fuel consumption starts to increase substantially beyond 5 CAD retard. Also, more frequent E85 tank refuels are required for severe driving cycle (US06 shown in 6-42) and vehicle loading (medium duty truck with half the payload).

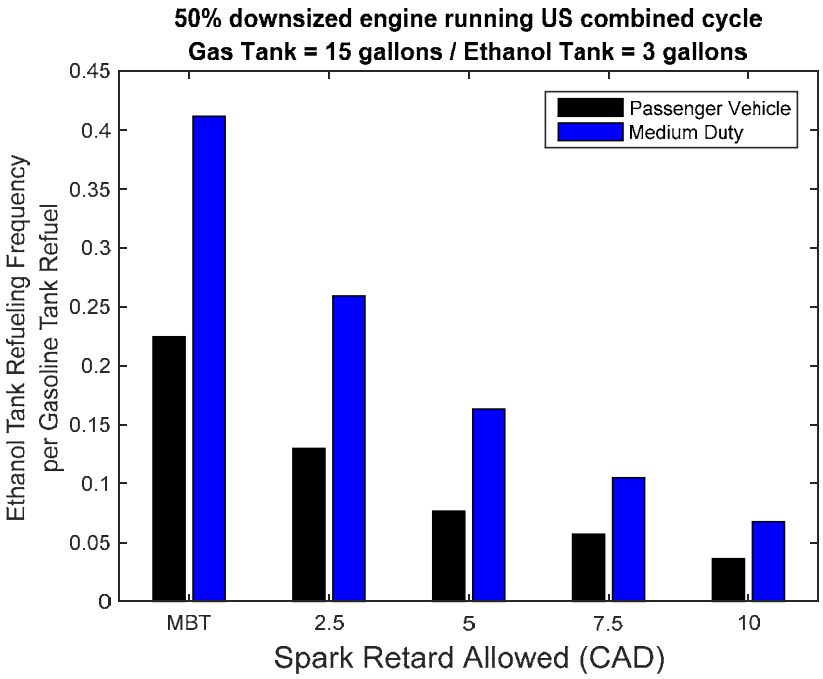

Figure 6-41: E85 tank refueling frequency per a gasoline tank refuel for various spark retard strategies for a 50% downsized engine running U.S. combined cycle. Black and blue bars each represent passenger vehicle and medium duty truck.

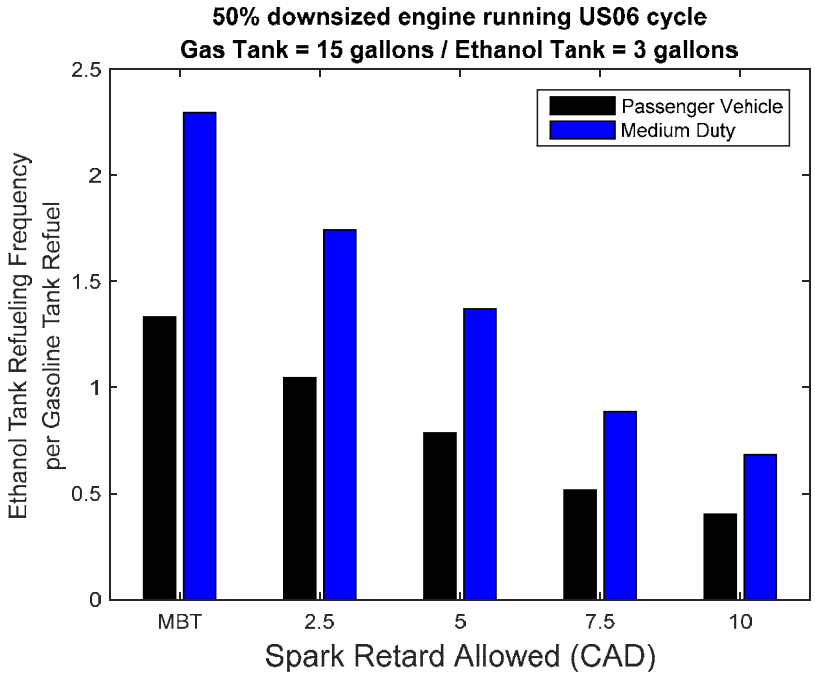

Figure 6-42: E85 tank refueling frequency per a gasoline tank refuel for various spark retard strategies for a 50% downsized engine running US06 cycle. Black and blue bars each represent passenger vehicle and medium duty truck.

On-board Separation Scenarios

To assess the on-board fuel separation system operations, some driving scenarios have to be assumed. Figure 6-43 shows the remaining fuels in each fuel tank in case of running U.S. combined and US06 cycles. 50% downsized engines with 9.2:1 compression ratio engine is considered for all the scenarios considered here (for both passenger car case and medium duty truck case). This driving scenario assumes that the two tanks are completely empty, and the main tank is filled up with E10 gasoline. Sizes of the main tank and the ethanol tank are assumed to be 15 gallons and 3 gallons. The tank capacities are chosen so the high octane tank can have some spare capacity in case of high octane fuel surplus. The main tank size was chosen so the total fuel capacity is close to Camry's tank size, which is about 17 gallons.

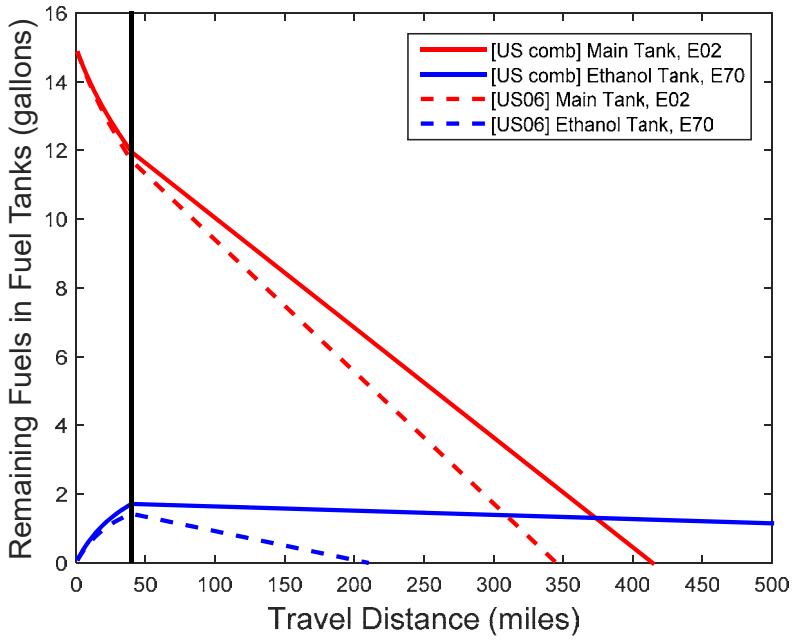

Figure 6-43: Remaining fuels in the main tank and the ethanol tank for a passenger vehicle equipped with a 50% downsized engine running at MBT timing. Red and blue lines represent the amount of fuel left in the main tank and the ethanol tank, respectively. Solid lines are U.S. Combined cycle and dashed lines are US06 cycle. Black line is when the fuel separation is complete.

At the start of the driving, about 1 hour (or 40 miles, averaging the three driving cycles) is required to completely separate the high octane fuel from the low octane fuel. It is shown that the fuel production rate is fast enough to let the engine operate with dual fuel strategy while the fuels are separating. After the fuel separation is complete, the vehicle runs like two-tank system

discussed before. For U.S. combined cycle, the high octane fuel remains when the main tank is empty. For US06 cycle, the high octane fuel is used up before the main tank is empty, so there is no way to operate the system dual fuel. From this point, excessive spark retard has to be applied with a single fuel approach, or fuel management system has to be present to apply spark retard beforehand.

Figure 6-44 shows the effect of spark retard on the US06 cycle. Driving range reduces down 7% and 18% with 5 CAD and 10 CAD retard respectively. However, spark retard up to 5 CAD maintains enough ethanol until the main tank is empty. Again, spark retard up to 5 CAD retard results in a reasonable compromising between fuel economy and the ethanol consumption. When spark retard is allowed or driving cycle is not aggressive, high octane fuel remains in the ethanol tank, and Figure 6-45 considers this case.

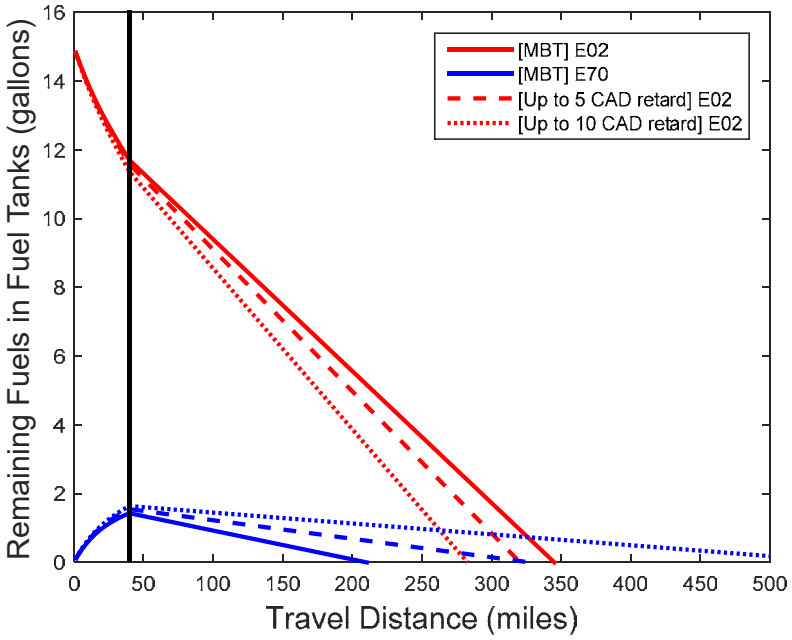

Figure 6-44: Remaining fuels in the main tank and the ethanol tank for a passenger vehicle equipped with a 50% downsized engine. Red and blue lines represent the amount of fuel left in the main tank and the ethanol tank, respectively. Solid, dashed, and dotted lines each represent MBT, up to 5 CAD, and up to 10 CAD retard allowed. Black line is when the fuel separation is complete.

Figure 6-45 below assumes a case where the vehicle runs first with U.S. Combined cycle, refuels the main tank, and then runs US06 cycle. After the car runs for 414 miles at MBT timing, there are still about 1.3 gallons of high octane fuel left in the ethanol tank. Since separation starts

with this remaining fuel, now there is enough fuel to finish the US06 cycle at MBT timing. This is why the ethanol tank has to be over-sized than the amount of high octane fuel separated from the full main tank.

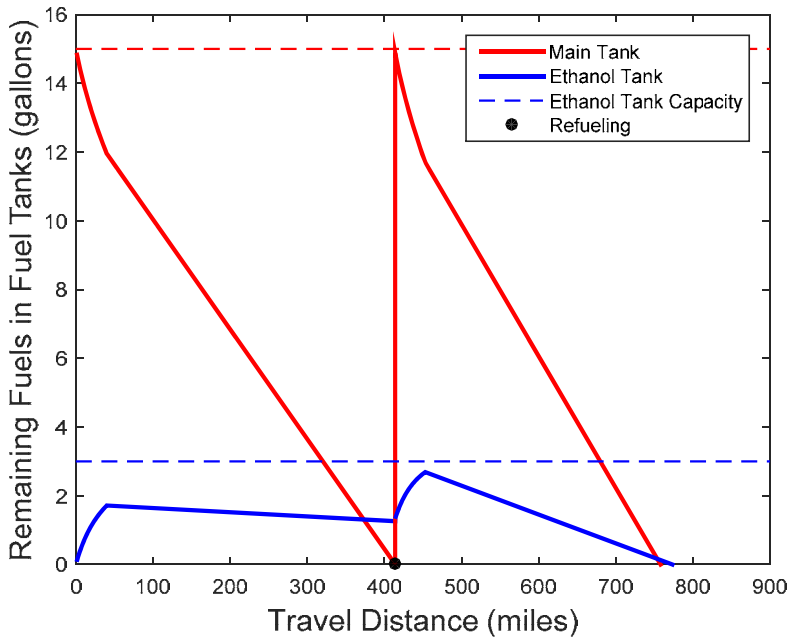

Figure 6-45: Remaining fuels in the main tank and the ethanol tank for a passenger vehicle equipped with a 50% downsized engine running at MBT timing. Red and blue lines represent the amount of fuel left in the main tank and the ethanol tank, respectively. Solid lines are U.S. Combined cycle and dashed lines are US06 cycle. Black line is when the fuel separation is complete.

The same results are shown for the medium duty truck with half the payload. As shown in earlier sections, medium duty truck with payload has much lower fuel economy and requires significantly higher amount of high octane fuel compared to the passenger vehicle. Figure 6-46 shows that the driving range is shorter than the passenger vehicle as expected. Ethanol tank runs out of the high octane fuel just after about 50 miles of driving after the fuel separation is complete. Similar to passenger vehicle's case, spark retard strategies are compared to reduce the high octane fuel requirements. More than 5 CAD retard is required to reach the driving range with dual fuel application as shown in Figure 6-47. Figure 6-48 suggests that high octane fuel is insufficient even after saving from a non-aggressive driving cycle. Hence, spark retard strategies have to be applied in this case.

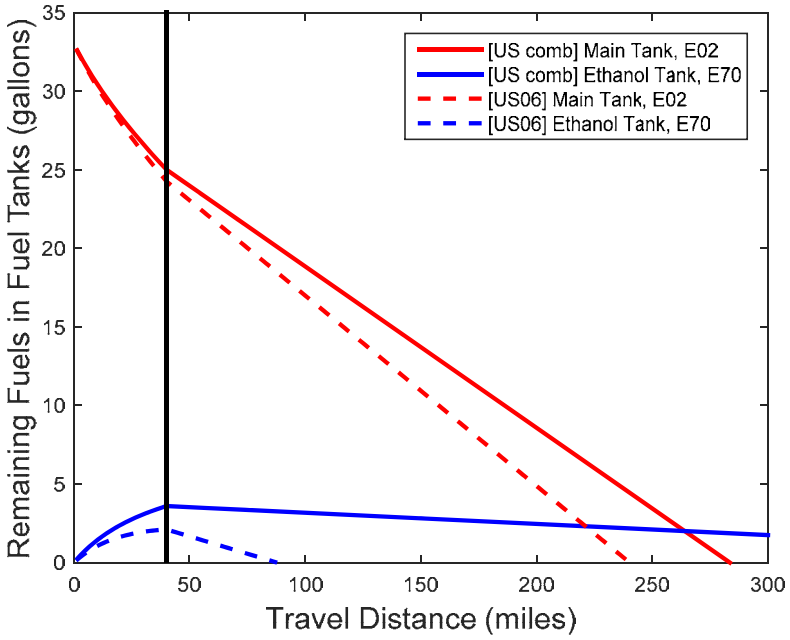

Figure 6-46: Remaining fuels in the main tank and the ethanol tank for a medium duty truck equipped with a 50% downsized engine running at MBT timing. Red and blue lines represent the amount of fuel left in the main tank and the ethanol tank, respectively. Solid lines are U.S. Combined cycle and dashed lines are US06 cycle. Black line is when the fuel separation is complete.

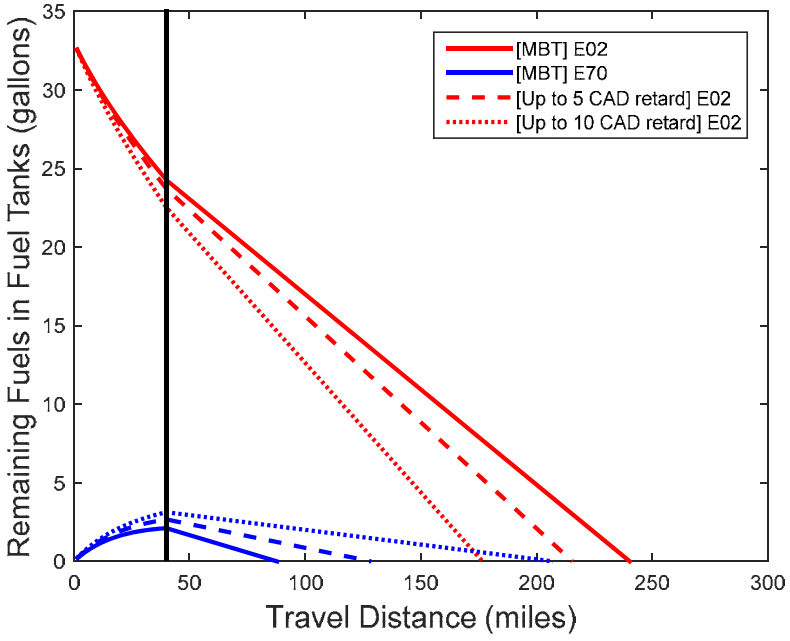

Figure 6-47: Remaining fuels in the main tank and the ethanol tank for a medium duty truck equipped with a 50% downsized engine. Red and blue lines represent the amount of fuel left in the main tank and the ethanol tank, respectively. Solid, dashed, and dotted lines each represent MBT, up to 5 CAD, and up to 10 CAD retard allowed. Black line is when the fuel separation is complete.

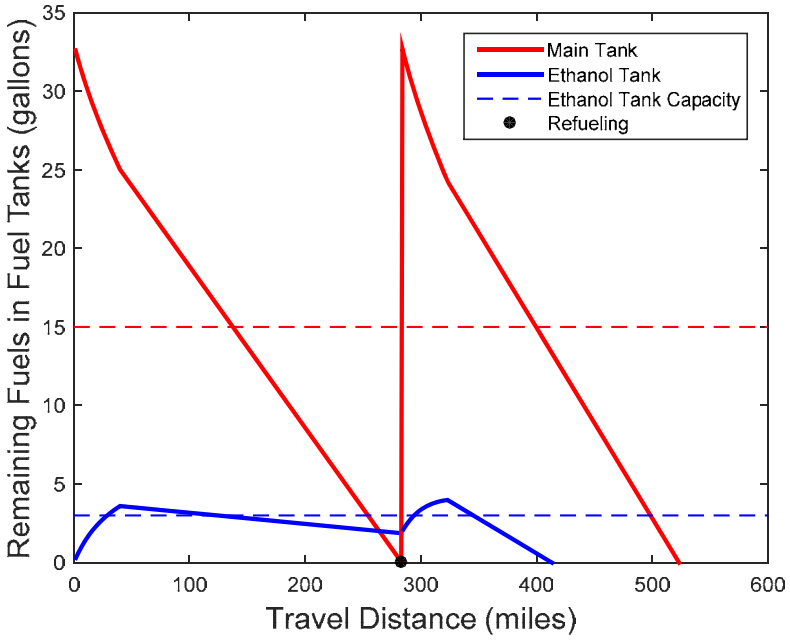

Figure 6-48: Remaining fuels in the main tank and the ethanol tank for a medium duty truck equipped with a 50% downsized engine running at MBT timing. Red and blue lines represent the amount of fuel left in the main tank and the ethanol tank, respectively. Solid lines are U.S. Combined cycle and dashed lines are US06 cycle. Black line is when the fuel separation is complete.

Another scenario is when the main tank is refueled before it is emptied. This will change the initial separation condition as ethanol contents of the main tank would be lower than E10 if there is E02 fuel remaining in the tank. In this case, separation time might be longer as ethanol separation rate is slower when ethanol contents in the feed side is lower as discussed in earlier sections. Membrane surface area, operating temperatures of the system, and vacuum pressures would have to be determined based on these various scenarios.

Cost analysis and system comparison

The additional costs of the two-tank external-fueling On-Board Separation (OBS) system were compared using published data on OEM costs. For the new elements, such as the membrane, comparable mass production components in the vehicle is used to estimate the cost by extrapolating cost to volume or area ratios. Since comparison of a turbo-downsized engine and naturally aspirated engines are well understood, turbo-downsized engine is set as a baseline cost. Turbocharged direct injection engines cost about $1500 more than naturally aspirated engines [67].

Using information from a report written by FEV on vehicle lightweighting, breakdown of the original equipment manufacturer (OEM) costs of the different components in a turbocharged direct injection engine (of Toyota Venza) could be determined. [68]. In Table 6-2 below, OEM costs of all the components required for two-tank and on-board fuel separation systems are listed.

Table 6-2: OEM costs of additional components required for two-tank and on-board fuel separation systems

	Baseline	**Two-tank**	**On-board Separation**
Fuel tanks	$ 64.4	$ 86.4	$ 86.4
Fuel pumps	$ 12.1	$ 24.1	$ 24.1
Fuel lines	$ 4	$ 8	$ 8
Fuel injectors (PFI)	0	$ 3	$ 3
Fuel vapor management subsystem	$ 8	$ 10	$ 10
Heat exchangers	0	0	$ 11
Vacuum pump	0	0	$ 12
Valves/ sensors	0	0	$ 2.3
Separator unit	0	0	$ 13.6
Additional Costs (compared to the baseline TC engine)	$ 0	$ 43.1	$ 82.2

Additional components are the secondary tank, an additional fuel pump (assuming that the original pump is alcohol resistant, which most automotive components are today), fuel lines, fuel injectors and a larger fuel canister for controlling parasitic emissions. Note that the report indicates that the cost of the PFI injectors (4 injectors) is about $3.01. The cost of the injectors to the OEM is thus about 2 orders of magnitude lower than the cost of an injector in the aftermarket. The additional total cost of the system is $43.11. A similar investigation is done for the OBS system. The cost of the membrane has been extrapolated from a similar high-volume system presently used, dialyzer membranes. The lifetime of the membrane is not known, but it could be an element that is replaced periodically, similar in cost to the oil filter. In addition, a control valve is required, as well as a sensor (a thermocouple). The vacuum required for the separation is not very high, about 0.3 bar. It is possible to create such a vacuum with a conventional fuel pump, pumping the condensed liquid. That is, the pump will not have gas flow

through it, but only liquid after condensation. A conventional fuel pump is used and the cost is also given.

The OOD systems are compared as below in Table 6-3. A passenger vehicle equipped with 50% downsized engine running the U.S. combined cycle with 5 CAD retard allowed is considered. With fully working dual fuel system, fuel economy improvement was over 25% for both systems. There might be a slight reduction in the fuel economy for OBS system due to slightly higher power requirements for the system operation. Exxon estimated about 1.5% decrease in the fuel economy with their system [35]. For two-tank system, refueling frequency is important as that directly impacts consumers. For the baseline case analyzed, high octane tank has to be refueled every 10 times of the main tank refueling. The OBS system had no problem of finishing U.S. combined cycle with up to 5 CAD spark retard allowed. However, the OBS requires a more complex system layout which might increase the manufacturing costs.

Table 6-3: Octane on Demand Systems Comparisons

	50% downsized engine running U.S. combined cycle with up to 5CAD retard allowed	
	Two-tank	**OBS**
Fuel Economy	**26% improvement** compared to a single fuel engine	**26% improvement** compared to a single fuel engine
High Octane Fuel Supply	Refueling frequency of 0.1	Supplies **enough** to finish the driving cycle
Extra Cost (Components)	~ **$43** Extra tank, fuel pumps, injectors, etc	~ **$82** Heat exchangers, vacuum pump, membrane unit, etc
System Complexity	Low	High (membrane unit control)
Consumer-side Impacts	High (refueling, second tank)	Low (no external refueling)

7. Summary and Conclusions

This research has investigated the combustion characteristics and knock limits of a commercially available turbocharged spark ignition engine. Effects of downsizing, retarding spark timing, increasing compression ratio, and vehicle type on dual fuel applications are analyzed. This section summarizes technical findings, discusses implications of the conducted research, and suggests future work.

Combustion Characteristics of a TC SI Engine

The operation limits of a turbocharged engine such as wide open throttle limits and in-cylinder peak pressure limits were explored and carefully defined. A turbocharged engine had unique characteristics such as spark retard and intake manifold air pressure feedback effects. The increased-boost feedback effect of a turbocharger due to spark retard is higher under a highly boosted condition. Due to the change of manifold air pressure with spark timing, maximum brake torque timing (at fixed throttle and wastegate positions) does not correspond to maximum efficiency timing for a turbocharged engine under highly boosted conditions. The torque reduction with spark retard is lower than that of an NA engine, but fuel consumption increased with spark retard with stoichiometric operation due to the turbocharger feedback effect.

The thermal efficiencies of the turbocharged engine from part load to WOT condition at speeds from 1500 rpm to 3000 rpm were determined with both RON 96 gasoline and E85 ethanol blends. At a fixed speed, the efficiencies of the engine using gasoline and E85 were compared. It was determined that the efficiency of the engine is fuel-independent in the performance map as long as the engine was not knock-limited. The engine operated with best efficiencies at around 20 bar brake mean effective pressure (BMEP) at 2500 rpm. The efficiency increase from 1 bar to 6 bar BMEP is about 61%, while the efficiency increase from 6 bar to 11 bar is only about 17%. Above 12 bar, the efficiency increase with increasing load is small.

A general trend of coefficient of variation (COV) of net indicated mean effective pressure (IMEP) to increase with spark retard was established by normalizing spark sweep results over a range of engine speeds and loads. To explore the reason for the COV increase with spark retard,

cycle by cycle variations were analyzed by looking at the COV of in-cylinder pressure traces over a range of CAD. It was found that the shapes of COV of in-cylinder pressure traces do not change with different fuels, engine loads, speeds, or combustion phasing. The peak of COV of in-cylinder pressure was always slightly before CA50 timing where burn rate variations are expected to be large. COV of NIMEP is a strong function of the burn duration and the position of the maximum COV of pressure trace with respect to top dead center.

Knock Limits of a TC SI Engine

Engine experiments were conducted to determine the octane requirements of a turbocharged spark ignition engine. Fourteen fuels, gasoline-ethanol blends and primary reference fuel blends, were tested over the full range of engine loads from 1500 rpm to 3000 rpm. Since octane requirements (or knock limits) depend on many variables, a three-dimensional octane requirement map was generated. The map gives octane requirement information (over the octane range 0-102 RON) for a given engine speed and load, corresponding to a modern DI engine. The knock limited BMEP of 0 RON fuel was about 2 bar: the octane requirement increased greatly from this light load up to 6 bar where the octane requirement was about 75 RON. The rate of increase in RON above this point to full load was more gradual.

To generate the octane requirement map, accurately defining maximum brake torque (MBT) timing was important for determining the octane requirements of the engine at the various speeds and loads examined. Using a new method for accurately determining MBT timing based on the previously known trend between NIMEP and CA50 timing, MBT timings were found to be dependent on engine speed, but essentially independent of the engine loads. Then, knock-limited spark advance boundaries were generated in terms of BMEP, and net and gross IMEP. Knock limits were higher for GIMEP than for BMEP, as mechanical friction and pumping work effects were removed. Also, knock limits increased more with spark retard at higher loads than at lower loads. This was because spark retard reduces peak pressure much more at higher loads than at low loads with the same amount of spark retard.

To examine the effect of intake valve close (IVC) timing on knock limits, knock limited BMEP was determined by changing IVC timings from 10 to 60 crank angle degrees after bottom dead center. Knock limits of E10 fuel at MBT timing increased about 3 bar NIMEP by changing

IVC from 10 to 60 CA aBDC. In addition to the experiments at MIT, Cummins conducted a set of experiments at high compression ratio to determine the effect of compression ratio on the engine efficiency and knock limits. With 13:1 compression ratio, engine efficiency was close to 40% at 10 bar BMEP with knock limited BMEP decreasing substantially with increased compression ratio.

Octane Requirements and Fuel Economy

A passenger vehicle (Toyota Camry) and a medium-duty truck (Ford F-550) were utilized for engine-in-vehicle simulations. The validity of the vehicle simulation tool was checked by comparing the real-world fuel economy and the simulation results on the baseline vehicle. Point-by-point octane requirements were calculated for different driving cycles, downsizing/boosting levels, and spark retard strategies. With a moderate downsizing (30% downsizing in displaced volume), average octane requirements were 66, 58, and 83 for the urban (UDDS), highway (HWFET), and aggressive US06 driving cycles, respectively. Looking at the fuel usage distributions, it was possible to understand how driving cycle characteristics change the octane requirement of a vehicle. In driving cycles, both the vehicle acceleration (driving aggressiveness) and the engine torque requirement prior to the start of the acceleration were important factors in determining the engine octane requirement of the vehicle.

Other than driving cycle features, the engine displaced volume and the extent of boost (or downsizing level) were important factors determining the octane requirement. For 50% downsizing (at constant vehicle acceleration capability), the average octane requirement was increased from 51 to 88 for the UDDS, 41 to 76 for the HWFET, and 71 to 92 for the US06 cycle. Increasing boost and downsizing the engine by 50% increased the average operating BMEP of the engine more than twice. This gave about a 30% increase in the average brake efficiency and a 26% increase in the fuel economy for a passenger vehicle running the UDDS cycle.

We simulated the octane on demand strategy by using a conventional gasoline and ethanol streams, that are mixed on-board to provide the required octane (thus, there is a minimum octane number of the fuel available, that of the base gasoline). With an octane-on-demand system working properly (delivering optimal RON fuel), higher octane requirements imply higher efficiency at the expense of higher ethanol consumption. The ethanol requirement

is a function of the vehicle type (weight), spark retard strategies, average operating loads, compression ratios, and driving aggressiveness. Running a US06 cycle with the 50% downsized engine, the octane requirement increased by 30% from that of the milder UDDS cycle and required that 12% of consumed fuel had to be ethanol (by volume) to suppress knock. Spark retard reduces the ethanol consumption by 66% with up to 10 CAD retard, but reduction in ethanol consumption comes with a cost of 10% reduction in fuel economy. With up to 5 CAD retard, fuel economy does not decrease much, but the ethanol consumption still drops significantly. Therefore, a moderate spark retard strategy should be applied along with OOD applications.

For a medium-duty truck, the fuel economy and the octane requirement change significantly with payload. Adding payload requires the (same) engine to operate at higher loads. With a loading of the average payload (average-loaded vehicle weight, ALVW), the fuel economy decreased about 20%, and the octane requirement increased for all driving cycles. Ethanol consumption increased substantially as well. The benefits of downsizing on fuel economy were higher for a vehicle without any payload and with less aggressive driving cycles.

Increasing compression ratio raised both the average engine brake efficiencies and the fuel economy, but with diminishing returns. The increases in efficiencies were slightly higher for the US06 cycle than the U.S. combined cycle. The efficiency benefits of increasing compression ratio did not change significantly with displaced engine volumes. This was because efficiency benefits are higher at larger displaced volume, but engines with larger displaced volume have lower average operating loads (where efficiency benefits with increasing compression ratio are less). Even though the efficiency increase has diminishing returns with increasing compression ratios, the ethanol fraction increase does not behave this way. For the UDDS cycle with a 50% downsized engine, the ethanol fraction increase was the same (6 percentage point) for both 9.1:1 to 11.5:1 and 11.5:1 to 13.5:1. The benefits of increasing compression ratio decrease above about 11.5:1, since ethanol consumption increases with diminishing return in the engine efficiency.

Fuel Separator Modelling and Systems Comparison

On-board fuel separation system separates high octane components of a regular E10 gasoline into a separate tank. The fuel separation system was modelled using a pore-flow pervaporation model. The model estimates the fuel separation rate for binary mixtures by a pervaporation process, which is driven by the difference between ethanol vapor pressure on the feed side and its partial vapor pressure on the permeate side. Parametric studies were done to analyze the effects of the temperature of the membrane system and the vacuum pressure on the permeate side; the membrane temperature was found to be a dominating parameter. The separation time and separation rates were comparable to the experimental results published by Honda.

For the two-tank system (with an externally filled high octane tank), total fuel consumption decreased with downsizing, but the 50% downsized engine running the US06 cycle resulted in a significant amount of E85 consumption due to the lower volumetric energy content of E85 fuel. However, up to about 5 CAD spark retard reduced the ethanol consumption greatly while not increasing the fuel consumption much. The leveraging ratio decreased with more downsizing and more aggressive driving styles, and refueling frequencies dropped significantly with more spark retard allowed.

For the OBS system, different scenarios were compared, assuming the tank sizes of 15 and 3 gallons for the main and the secondary tanks, respectively. With the 50% downsized engine running at MBT spark timing, the high octane fuel separated from 15 gallons of E10 fuel was used up before the main tank, preventing dual fuel operation over the entire period. Up to 5 CAD spark retard reduced the high octane fuel consumption and allowed a dual fuel operation all the time, as the tank with the high octane fuel is not depleted before the main tank is. Driving range was reduced by 7% and 18% with 5 CAD and 10 CAD spark retard, respectively. The approximate additional cost of the OBS system was about $80-85, while it was $40-45 for two-tank system.

Both systems discussed above are promising and practical options for more effective use of fuel octane in a turbocharged gasoline engine as they give an opportunity to optimize use of high octane ethanol or methanol fuels in various ways. As shown by efficiency and fuel economy benefits (greater than 25%) and by the leveraging effect (displacement of gasoline by small

amount of E85), OOD systems give significant benefits over a conventional single-fuel system. OOD systems with turbo-downsized engines show a synergy in improving engine efficiency with effective knock suppression: but excessive downsizing results in lower leveraging ratios. The octane requirement (or ethanol consumption) of the engine is a function of downsizing, spark-retard strategy, vehicle configuration, and driving cycle (or driving style). To optimize these variables, both systems require a high-octane-fuel management system which enables the engine to operate with the optimal RON fuel at each operating condition (by spark retard or down-speeding) to reduce ethanol consumption with modest reduction in efficiency.

Suggestions for Next Steps

Our study has shown that the fuel economy benefits of using available alcohol fuels, primarily when needed for knock suppression, with standard gasoline as the primary fuel, are substantial. This octane-on-demand approach allows raising the engine's compression ratio, increasing turbocharger boost levels, and downsizing of the engine, while providing the same vehicle acceleration performance. We have examined two approaches to this more effective use of ethanol (or methanol) fuel: a dual-tank system where each tank is filled externally from separate pumps; use of an on-board fuel separator system to separate out the ethanol in the standard E10 gasoline fuel put into the main fuel tank, to create the high octane knock-suppressing fuel stream. The extra costs of these two approaches are estimated to be modest: $40-45 for the two-tank (both external fill) approach, and $80-85 for the on-board fuel separation approach, respectively.

In terms of ease of customer use and fuel supply requirements, the on-board fuel separation approach is more attractive. However, to date, the separator technology is still in the prototype stage. The precise system configuration with the greatest improvement potential needs to be further explored and defined. Also, optimum algorithms for managing the system need to be developed. For both of these dual-fuel approaches, an important next step would be developing and testing the next generation hardware in appropriate vehicles to enable more robust assessments of their potential for reducing petroleum consumption and greenhouse gas emissions from our vehicle fleet.

Especially, it would be beneficial to build a fully-working fuel separation system to assess the system's capability with different base fuel blends. Extensive testing of an actual prototype system would be helpful to further verify the pervaporation model (though we have verified the model at the same temperature and pressure conditions of Honda's prototype system.) Experiments with different fuel blends (e.g., isooctane/n-heptane-ethanol, gasoline-ethanol, gasoline-methanol) using next generation fuel separator system would help us understand how fuel compositions or separation rates change with different fuels.

List of Publications

1. “Performance Maps of Turbocharged SI Engines with Gasoline-Ethanol Blends: Torque, Efficiency, Compression Ratio, Knock Limits, and Octane,” Jo, Y., Lewis, R., Bromberg, L., and Heywood, J.

Published and Presented at 2014 SAE World Congress in Detroit on April 8-10, 2014, SAE Technical Paper 2014- 01-1206, doi: 10.4271/2014-01-1206.

2. “Optimal Use of Ethanol in Dual Fuel Applications: Effects of Engine Downsizing, Spark Retard, and Compression Ratio on Fuel Economy,” Jo, Y., Bromberg, L., and Heywood, J.

Submitted and will be presented at 2016 SAE World Congress in Detroit on April 12-14, 2016: Assigned paper number: 2016-01-0786

3. “Octane Requirement of a Turbocharged Spark Ignition Engine in Various Driving Cycles,” Jo, Y., Bromberg, L., and Heywood, J.

Submitted and will be presented at 2016 SAE World Congress in Detroit on April 12-14, 2016: Assigned paper number: 2016-01-0831

References

[1] U.S. Energy Information Administration, “Monthly Energy Review (January 2014),” U.S. Energy Information Administration Monthly Energy Review, Tables 1.3, 2.1-2.6, Jan. 2014.

[2] U.S. Department of Transportation Bureau of Transportation Statistics, “2015 National Transportation Statistics,” http://www.bts.gov/publications/national_transportation_statistics/, 2015.

[3] PIRA Energy Group, “An Assessment of the Diesel Fuel Market: Demand, Supply, Trade, and Key Drivers,” http://fuelsinstitute.org/ResearchArticles/DieselReport_PIRA.pdf, Sep. 2014.

[4] U.S. Environmental Protection Agency and U.S. Department of Transportation, “2017 and Later Model Year Light-Duty Vehicle Greenhouse Gas Emissions and Corporate Average Fuel Economy Standards.” U.S. Federal Register, 76(231):74854-75420, 1 Dec. 2011.

[5] U.S. Environmental Protection Agency, “Light-Duty Automotive Technology, Carbon Dioxide Emissions, and Fuel Economy Trends: 1975 through 2014,” Oct. 2014, doi: EPA-420-R-14-023a

[6] Heywood, J.B., "Internal Combustion Engine Fundamentals," McGraw-Hill, 1988

[7] Smith, P., Heywood, J., and Cheng, W., "Effects of Compression Ratio on Spark-Ignited Engine Efficiency," SAE Technical Paper 2014-01-2599, 2014, doi: 10.4271/2014-01-2599.

[8] Han, D., Han, S., Han, B., and Kim, W., "Development of 2.0L Turbocharged DISI Engine for Downsizing Application," SAE Technical Paper 2007-01-0259, 2007, doi: 10.4271/2007-01-0259.

[9] Patrick, S. and Cheng, W.K., “Assessing the Loss Mechanisms Associated with Engine Downsizing, Boosting and Compression Ratio Change,” SAE Technical Paper 2013-01-0929, 2013, doi: 10.4271/2013-01-0929.

[10] Jo, Y., Lewis, R., Bromberg, L., and Heywood, J., "Performance Maps of Turbocharged SI Engines with Gasoline-Ethanol Blends: Torque, Efficiency, Compression Ratio, Knock Limits, and Octane," SAE Technical Paper 2014-01-1206, 2014, doi: 10.4271/2014-01-1206.

[11] Gerty, M. and Heywood, J., "An Investigation of Gasoline Engine Knock Limited Performance and the Effects of Hydrogen Enhancement," SAE Technical Paper 2006-01-0228, 2006, doi: 10.4271/2006-01-0228.

[12] Stein, R., House, C., and Leone, T., "Optimal Use of E85 in a Turbocharged Direct Injection Engine," SAE Int. J. Fuels Lubr. 2(1):670-682, 2009, doi: 10.4271/2009-01-1490.

[13] Wardsauto group, “a division of penton media Inc.; World Engines 2013,” http://wardsauto.com/site-files/wardsauto.com/files/datasheets/gated/worlden01_2013_0.xls, accessed Oct. 2015.

[14] Leone, T., Anderson, J., Davis, R., Iqbal, A. et al., “The Effect of Compression Ratio, Fuel Octane Rating, and Ethanol Content on Spark-Ignition Engine Efficiency,” Environmental Science and Technology 49(18):10778–10789, 2015, doi:10.1021/acs.est.5b01420.

[15] Ayala, F., Gerty, M., and Heywood, J., "Effects of Combustion Phasing, Relative Air-fuel Ratio, Compression Ratio, and Load on SI Engine Efficiency," SAE Technical Paper 2006-01-0229, 2006, doi: 10.4271/2006-01-0229.

[16] UCDavis Chemwiki, "Gasoline: A Deeper Look," chemwiki.ucdavis.edu, accessed Dec. 2015

[17] ASTM D2699-15a, Standard Test Method for Research Octane Number of Spark-Ignition Engine Fuel, ASTM International, West Conshohocken, PA, 2015, DOI: 10.1520/D2699-15A

[18] ASTM D2700-14, Standard Test Method for Motor Octane Number of Spark-Ignition Engine Fuel, ASTM International, West Conshohocken, PA, 2014, DOI: 10.1520/D2700-14

[19] Kalghatgi, G.T., “Fuel anti-knock quality – Part I, Engine Studies”, SAE paper# 2001-01-3584, 2001

[20] Kalghatgi, G.T., “Fuel Anti-Knock Quality – Part II. Vehicle Studies – How Relevant is Motor Octane Number (MON) in Modern Engines”, SAE paper# 2001-01-3584, 2001\

[21] Mittal, V., Heywood J.B., Green W.H., “The Underlying Physics and Chemistry behind Fuel Sensitivity”, SAE paper# 2010-01-0617

[22] Bromberg, L., Cohn, D. R., and Heywood, J. B., "Calculations Of Knock Suppression In Highly Turbocharged Gasoline/Ethanol Engines Using Direct Ethanol Injection", MIT Laboratory for Energy and the Environment Report LFEE 2006-001 RP, 2006.

[23] Kasseris, E. and Heywood, J., "Charge Cooling Effects on Knock Limits in SI DI Engines Using Gasoline/Ethanol Blends: Part 2-Effective Octane Numbers," SAE Int. J. Fuels Lubr. 5(2):844-854, 2012, doi: 10.4271/2012-01-1284.

[24] ANFAVEA, “Brazilian Automotive Industry Yearbook,” Brazilian Automotive Industry, 2013.

[25] Stein, R., House, C., and Leone, T., "Optimal Use of E85 in a Turbocharged Direct Injection Engine," SAE Int. J. Fuels Lubr. 2(1):670-682, 2009, doi: 10.4271/2009-01-1490.

[26] Sims, R., Schaeffer, R., Creutzig, F., Cruz-Núñez X. et al., "2014: Transport. In: Climate Change2014: Mitigation of Climate Change. Contribution of Working Group III to the Fifth

Assessment Report of the IntergovernmentalPanel on Climate Change," Cambridge University Press, 2014

[27] Korves, R., “The Potential Role for Corn Ethanol in Meeting the Energy Needs of the United States in 2016-2030,” Global Bioenergy Partnership, Oct. 2008.

[28] Humm, R., Goldsmith, P., Rausch, K., Stein, H., “Land Usage attributed to corn ethanol production in the United States: sensitivity to technological advances in corn grain yield, ethanol conversion, and co-product utilization,” Biotechnology for Biofuels 7(61): 10.1186/1754-6834-7-61.

[29] Kasseris, E. and Heywood, J., "Charge Cooling Effects on Knock Limits in SI DI Engines Using Gasoline/Ethanol Blends: Part 1-Quantifying Charge Cooling," SAE Technical Paper 2012-01-1275, 2012, doi: 10.4271/2012-01-1275.

[30] Kasseris, E. and Heywood, J., "Charge Cooling Effects on Knock Limits in SI DI Engines Using Gasoline/Ethanol Blends: Part 2-Effective Octane Numbers," SAE Int. J. Fuels Lubr. 5(2):844-854, 2012, doi: 10.4271/2012-01-1284.

[31] Bromberg, L., and Cohn, D. R., "Effective Octane and Efficiency Advantages of Direct Injection Alcohol Engines", MIT Laboratory for Energy and the Environment Report LFEE 2008-01 RP, 2008.

[32] Blumberg, P.N., Bromberg, L., Kang, H., and Tai, C., "Simulation of High Efficiency Heavy Duty SI Engines Using Direct Injection of Alcohol for Knock Avoidance" SAE Int. J. Engines 1(1):1186-1195, 2008.

[33] Bromberg, Leslie, Cohn, Daniel R., and Heywood, John B., "Optimized Fuel Management System for Direct Injection Ethanol Enhancement of Gasoline Engines", U.S. patent 7225787 B2, June 5, 2007.

[34] Renewable Fuels Association, “Pocket Guide to Ethanol,” 2013, http://ethanolrfa.org/page/-/PDFs/2013%20Pocket%20Guide.pdf?nocdn=1, Accessed Sep. 2015.

[35] Partridge, R., Weissman, W., Ueda, T., Iwashita, Y. et al., "Onboard Gasoline Separation for Improved Vehicle Efficiency," SAE Int. J. Fuels Lubr. 7(2):366-378, 2014, doi:10.4271/2014-01-1200.2014-01-2614

[36] Kuzuoka, K., Kurotani, T., Chishima, H., and Kudo, H., "Study of High-Compression-Ratio Engine Combined with an Ethanol-Gasoline Fuel Separation System," SAE Int. J. Engines 7(4):1773-1780, 2014, doi: 10.4271/2014-01-2614.

[37] Chang, J., Viollet, Y., Alzubail, A., Abdul-Manan, A. et al., "Octane-on-Demand as an Enabler for Highly Efficient Spark Ignition Engines and Greenhouse Gas Emissions Improvement," SAE Technical Paper 2015-01-1264, 2015, doi:10.4271/2015-01-1264.engine spec reference (in terms of fuel)

[38] Anderson, J., Leone, T., Shelby, M., Wallington, T. et al., "Octane Numbers of Ethanol-Gasoline Blends: Measurements and Novel Estimation Method from Molar Composition," SAE Technical Paper 2012-01-1274, 2012, doi: 10.4271/2012-01-1274.

[39] Stein, R., Polovina, D., Roth, K., Foster, M. et al., "Effect of Heat of Vaporization, Chemical Octane, and Sensitivity on Knock Limit for Ethanol - Gasoline Blends," SAE Int. J. Fuels Lubr. 5(2):823-843, 2012, doi: 10.4271/2012-01-1277.

[40] GM, "Pontiac Debuts 2007 Solstice GXP at LA Auto Show," http://archives.media.gm.com/us/gm/en/news/events/autoshows/06la/brands/pontiac/index.html, Jan. 2006.

[41] McKenzie, J., "The Autoignition Characteristics of Turbocharged Spark Ignition Engines with Exhaust Gas Recirculation." Ph.D. Thesis, M.I.T., June 2015.

[42] Jo, Y., "Turbocharged Engine Operations using Knock Resistant Fuel Blends for Engine Efficiency Improvements." M.S. Thesis, M.I.T., May 2013.

[43] Ozdor, N., Dugler, M., and Sher, E., "Cyclic Variability in Spark Ignition Engines A Literature Survey," SAE Technical Paper 940987, 1994.

[44] Koopmans, L., Backlund, O., and Denbratt, I., "Cycle to Cycle Variations: Their Influence on Cycle Resolved Gas Temperature and Unburned Hydrocarbons from Camless Gasoline Compression Ignition Engine," SAE Technical Paper 2002-01-0110, 2002.

[45] Marriott, C.D., Kong, S.-C., and Reitz, R.D., "Investigation of Hydrocarbon Emissions from a Direct Injection-Gasoline Premixed Charge Compression Ignited Engine," SAE Technical Paper 2002-01-0419, 2002.

[46] Keck, J., Heywood, J., and Noske, G., "Early Flame Development and Burning Rates in Spark Ignition Engines and Their Cyclic Variability," SAE Technical Paper 870164, 1987, doi: 10.4271/870164.

[47] Soltau, J.P., "Cylinder pressure variations in petrol engine", I Mech E conf. Proc, July 1960, pp99-116.

[48] Patterson, D.J., "Cylinder Pressure Variations, A Fundamental Combustion Problem," SAE Technical Paper 660129, 1966.

[49] Barton, R.K., Lestz, S.S., and Meyer, W.E., "An Empirical Model for Correlating Cycle-by-Cycle Cylinder Gas Motion and Combustion Variations of a Spark Ignition Engine." SAE transactions 710163

[50] Rashidi, M., "The nature of Cycle-by-Cycle Variation in the S.I. Engine from High Speed Photographs." Combustion and Flame 42:111-122 (1981)

[51] B.D. Peters and G.L.Borman, "Cyclic Variations and Average Burning Rates in an SI Engine." Paper 700064 presented at SAE Automotive Engineering Congress, Detroit, January 1970.

[52] H.S. Averette, "A Study of Peak Pressure Variations in the Otto Cycle Engine." S.M. Thesis, M.I.T., June 1964.

[53] Zervas, E., “Correlations between cycle-by-cycle variations and combustion parameters of a spark ignition engine”, Applied Thermal Engineering, 24pp 2073-2081, 2004.

[54] Samuel, S., Morrey, D., Whelan, I., and Hassaneen, A., “Combustion Characteristics and Cycle-By-Cycle Variation in a Turbocharged-Intercooled Gasoline Direct-Injected Engine,” SAE Technical Paper 2010-01-0348, doi: 10.4271/2010-01-0348.

[55] Douaud, A. and Eyzat, P., "Four-Octane-Number Method for Predicting the Anti-Knock Behavior of Fuels and Engines," SAE Technical Paper 780080, 1978, doi: 10.4271/780080

[56] Office of Transportation and Air Quality, “EPA Issues New Test Methods for Fuel Economy Window Stickers”, Dec. 2006, doi: EPA420-F-06-069

[57] Office of Transportation and Air Quality, “Final Technical Support Document Fuel Economy Labeling of Motor Vehicle Revisions to Improve Calculation of Fuel Economy Estimates”, Dec. 2006, doi:EPA420-R-06-017

[58] Environmental Protection Agency, “Dynamometer Drive Schedules,” http://www3.epa.gov/nvfel/testing/dynamometer.htm, accessed Oct 2015

[59] Toyota Camry, “2014 Camry Features & Specs,” http://www.toyota.com/camry/features/mechanical/2532/2540/2546/2548, accessed May 2014

[60] Ford, “2014 Chassis Cab Specifications,” http://www.ford.com/commercial-trucks/chassis-cab/specifications/, accessed May 2014

[61] Office of the Federal Register National Archives and Records Administration, “Protection of Environment: Containing a Codification of Documents of General Applicability and Future Effects,” Code of Federal Regulations, 40 C.F.R. 86.129-80, Jul. 2008

[62] Lipnizki, F., “Modelling of pervaporation: models to analyze and predict the mass transport in pervaporation,” Separation & Purification Reviews, doi: 10.1081/SPM-100102985

[63] Pervatech, “Introduction to pervaporation and vapour permeation,” http://pervaporation-membranes.com/home/introduction-to-pervaporation-and-vapor-permeation/, accessed Oct 2015

[64] Okada, T., Matsuura, T., “A new transport model for pervaporation,” Journal of Membrane Science, doi: 10.1016/S0376-7388(00)81179-5

[65] Okada, T., Yoshikawa, M., Matsuura, T., A study on the pervaporation of ethanol/water mixtures on the basis of pore flow model,” Journal of Membrane Science, doi: 10.1016/S0376-7388(00)81180-1

[66] Okada, T., Matsuura, T., “Predictability of transport equations for pervaporation on the basis of pore-flow mechanism,” Journal of Membrane Science, doi: 10.1016/0376-7388(92)80103-Q

[67] M A. Weiss, J. B. Heywood, E. M. Drake, A. Schafer, and F. F. AuYeung, ON THE ROAD IN 2020: A life-cycle analysis of new automobile technologies, Energy Laboratory Report # MIT EL 00-003 (2000)

[68] Light-Duty Vehicle Mass Reduction and Cost Analysis — Midsize Crossover Utility Vehicle, Prepared for EPA by FEV, Report EPA-420-R-12-026 (August 2012)

Acronyms

AKI	Anti-Knock Index
ALVW	Average Loaded Vehicle Weight
ASTM	American Society for Testing and Materials
aTDC	after Top Dead Center
BDC	Bottom Dead Center
BMEP	Brake Mean Effective Pressure
CA50	Crank Angle of 50% burn point
CAD	Crank Angle Degree
CBC	Cycle by Cycle
CD	Cylinder Deactivation
CFR	Cooperative Fuel Research
COV	Coefficient of Variation
CVT	Continuously Variable Transmission
DI	Direct Injection
E0	91 RON gasoline
E10	90% 91 RON gasoline with 10% ethanol
E85	85% ethanol and 15% 91 RON gasoline
ECE	European Urban Driving Cycle
ECU	Engine Control Unit
EGR	Exhaust Gas Recirculation
EPA	Environmental Protection Agency
EUDC	Extra Urban Driving Cycle
FTP	Federal Test Procedure
GDI	Gasoline Direct Injection
GIMEP	Gross Indicated Mean Effective Pressure
HOV	Heat of vaporization
HWFET	Highway Fuel Economy Test Cycle
IVC	Intake Valve Close

KI	Knock Intensity
KLSA	Knock-Limited Spark Advance
KO	Knock Onset
LHV	Lower Heating Value
MAP	Manifold Air Pressure
MBT	Maximum Brake Torque
MET	Maximum Efficiency Timing
MON	Motor Octane Number
MPG	Miles per Gallon
MSE	Mean Squared Error
MY	Model Year
NA	Naturally Aspirated
NEDC	New European Driving Cycle
NIMEP	Net Indicated Mean Effective Pressure
NMHC	Nonmethane Hydrocarbon
NTE	Net Indicated Thermal Efficiency
OBS	On-board fuel Separation
OI	Octane Index
OOD	Octane On Demand
PFI	Port Fuel Injection
PRF	Primary Reference Fuel
PRF0	100% n-heptane
PRF90	90% isooctane and 10% n-heptane
PV	Pressure-volume
RON	Research Octane Numbe**r**
SI	Spark Ignition
TBI	Throttle Body Injection
TDC	Top Deal Center
UDDS	Urban Dynamometer Driving Schedule
US06	US06 Supplemental Federal Test Procedure
VVT	Variable Valve Timing

WOT Wide Open Throttle